OF SYSTEMS

BY YE. B. VOLKOV, T. A. SYRITSYN AND G. YU. MAZIN

21 AUGUST 1979 (FOUO) 1 OF 3

FOR OFFICIAL USE ONLY

JPRS L/8627

21 August 1979

Translation

STATICS OF ROCKET MOTOR SYSTEMS

By

Ye. B. Volkov, T. A. Syritsyn and G. Yu. Mazin

FBIS FOREIGN BROADCAST INFORMATION SERVICE

FOR OFFICIAL USE ONLY

APPROVED FOR RELEASE: 2007/02/08: CIA-RDP82-00850R000100080028-2

NOTE

JPRS publications contain information primarily from foreign newspapers, periodicals and books, but also from news agency transmissions and broadcasts. Materials from foreign-language sources are translated; those from English-language sources are transcribed or reprinted, with the original phrasing and other characteristics retained.

Headlines, editorial reports, and material enclosed in brackets [] are supplied by JPRS. Processing indicators such as [Text] or [Excerpt] in the first line of each item, or following the last line of a brief, indicate how the original information was processed. Where no processing indicator is given, the information was summarized or extracted.

Unfamiliar names rendered phonetically or transliterated are enclosed in parentheses. Words or names preceded by a question mark and enclosed in parentheses were not clear in the original but have been supplied as appropriate in context. Other unattributed parenthetical notes within the body of an item originate with the source. Times within items are as given by source.

The contents of this publication in no way represent the policies, views or attitudes of the U.S. Government.

For further information on report content call (703) 351-2938 (economic); 3468 (political, sociological, military); 2726 (life sciences); 2725 (physical sciences).

APPROVED FOR RELEASE: 2007/02/08: CIA-RDP82-00850R000100080028-2

JPRS L/8627

21 August 1979

STATICS OF ROCKET MOTOR SYSTEMS

Moscow STATIKA I DINAMIKA RAKETNYKH DVIGATEL'NYKH USTANOVOK V DVUKH KNIGAKH ("Statics and Dynamics of Rocket Motor Systems in Two Volumes") in Russian 1978 signed to press 17 Feb 78 pp 2-221

[Volume One ("Statics") of book by Ye. B. Volkov, T. A. Syritsyn and G. Yu. Mazin, Mashinostroyeniye Publishers, 1550 copies, 222 pages]

CONTENTS PAGE

PUBLICATION DATA

English title	: STATICS OF ROCKET MOTOR SYSTEMS
Russian title	: STATIKA I DINAMIKA RAKETNYKH DVIGATEL'NYKH USTANOVOK V DVUKH KNIGAKH
Author (s)	: Ye.B.Volkov, T.A. Syritsyn, G.Yu.Mazin
Editor (s)	:
Publishing House	: Mashinostroyeniye
Place of Publication	: Moscow
Date of Publication	: 1978
Signed to press	: 17 Feb 78
Copies	: 1550
COPYRIGHT	: Izdatel'stvo "Mashinostroyeniye", 1978

PREFACE

One of the most important tasks in rocket-engine theory is the calculation of the parameters of their operating conditions. These parameters are determined by the specific features of the engine design and the characteristics of all engine components. Determination of parameters, especially for engines of complex design, constitutes a fairly difficult task.

Although the rocket engines employed at the present time are highly diversified, their operation is based on a number of identical processes. In connection with this there exists much in common in the characteristics of engines, even of different types, and correspondingly in the methods of calculating these characteristics.

This book is a first attempt to present from a unified viewpoint methods of analysis and calculation of the parameters and characteristics of steady-state operating processes of rocket engines operating on liquid, solid and hybrid fuels. The identical nature of the goals and methods of such an analysis for engines of differing types is illustrated by presentation of the material of its principal sections. At the same time there of course also exist (and this is reflected in the book) features of calculation of parameters which are specific for each type of engine. This is connected with differences in the design and operating conditions of different engines, as well as the fact that methods of calculating parameters were elaborated separately for each type of engine.

Calculation of the parameters and characteristics of a rocket engine is based on the points of theory of calculation of the components and elements comprising an engine. It is assumed that the reader is acquainted with these points, and therefore they are presented in brief and only where this is necessary in order to elucidate the specific features of solving the main problem -- determination of the parameters of an entire engine as a whole.

The quantities and their numerical values characterizing engines are in conformity with the International system of units (SI). Parameters and engine design layouts are based on published foreign materials.

Section III was written by Ye. B. Volkov, Section I by T. A. Syritsyn, and Section II by G. Yu. Mazing.

The authors would like to express their thanks to Doctor of Technical Sciences Professor M. F. Dyunze for his valuable comments made on editing this book, and they would like to express thanks in advance to the readers for critical comments on the substance and method of presentation of the materials.

Please send all comments and remarks in care of the following address: Moscow, B-78, Pervyy Basmannyy pereulok, 3, izdatel'stvo Mashinostroyeniye.

Section I. STATIC CHARACTERISTICS OF LIQUID-PROPELLANT ROCKET MOTORS

Chapter 1. GENERAL DESCRIPTION OF MOTORS

1.1. Classification and Designs of Liquid Propellant Rocket Motors

ZhRD, that is, engines burning liquid rocket fuel, are widely utilized today in rockets and space hardware.

In the general case a ZhRD consists of the following:

a combustion chamber, in which fuel or gas generation products are transformed as a result of chemical reactions into combustion products, which generate a reaction force when escaping from the nozzle;

a supply system, which includes that equipment which feeds the propellant components from the storage tanks to the combustion chamber;

automatic control equipment -- those devices which control engine operation, adjustment and servicing operations.

Liquid-propellant rocket motors or engines are components of the propulsion system.

A propulsion system contains one or several ZhRD, propellant tanks, units for producing tank pressure, fuel and oxidizer lines from tanks to engines, and auxiliary devices.

A detailed classification of motors based on various attributes can be found in [1].

Rocket engines are subdivided into two groups by type of propellant feed: ZhRD with gas pressurization feed, and ZhRD with pumped feed.

In a ZhRD with a gas pressurization system, the fuel components are fed to the combustion chamber by expulsion from the propellant storage tanks by gases the pressure of which exceeds pressure in the combustion chamber.

Figure 1.1 contains a diagram of a ZhRD with a gas pressurization supply system.

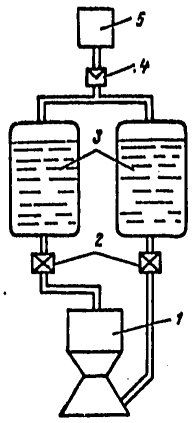

Figure 1.1. Diagram of ZhRD With a Gas Pressurization Supply System

Key:
1. Combustion chamber
2. Shutoff valves
3. Tanks containing propellant components
4. Pressure reducer
5. Compressed-gas tank

The supply system contains a compressed-gas tank or pressure accumulator and automatic control devices ensuring a specified pressure in the tank. The source of gas providing the requisite pressure in the tanks can be compressed-gas tanks -- a gas pressure accumulator (GAD), a liquid-reactant gas generator, (ZhAD), or a gas generator with a solid fuel charge -- a solid-reactant gas generator (PAD). Compressed-gas pressure accumulators are extensively utilized due to their simplicity of design, operating process and high degree of reliability. Propellant is fed from the tanks to the combustion chamber by pressure drop

$$p_б - p_к > 0.$$

The requisite pressure in the tank is determined from the relation

$$p_б = p_к + \sum \Delta p_i - nH\rho,$$

where Δp_i -- hydraulic resistance of the lines, valves, cooling jacket and injectors; $nH\rho$ -- hydrostatic pressure of the column of liquid; n -- calculated axial load factor.

An advantage of this method of propellant feed over a pumped system lies in a comparative design simplicity. But at the same time employment of a gas pressurization supply system results in heavier tanks, since they must stand up to internal pressure exceeding pressure in the combustion chamber $p_б/p_к$=1.3-1.7.

A volume of propellant which is approximately equal to the volume of the tanks is determined by relation

$$V_т = \frac{P\tau_р}{I_у \rho_т}, \qquad (1.1)$$

where P -- engine thrust; $\tau_р$ -- operation time; $I_у$ -- specific thrust impulse; $\rho_т$ -- propellant density.

Consequently, with increase in thrust impulse ($P\tau_р$) there is an increase in volume of propellant, mass of propellant tanks, and the required quantity of gas to drive the combustibles from the tanks into the combustion chamber.

Figure 1.2 shows relation $\tau=\tau(P)$, for which specific engine mass ($m_{д.у} = M_д/P$, $M_д$ -- mass of primed engine) is identical with a gas pressurization and pump-fed system. Therefore motors with a gas pressurization supply system can compete successfully with motors with a pump supply system only with modest thrust impulses.

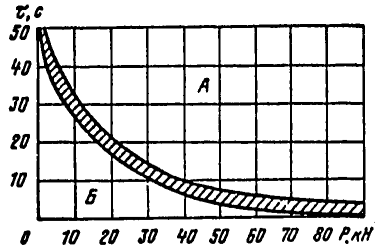

Figure 1.2. Areas of Application of ZhRD With a Pump and Gas Pressurization Fuel Feed System

Key:
A -- pump system
B -- Gas pressurization system

In motors with a gas pressurization supply system, pressure in the combustion chamber does not exceed 2.0-3.0 MPa. At the same time we know that for a given fuel the specific thrust impulse can be increased only by increasing the ratio of nozzle expansion. With limited $p_к$, a value greater than this can be obtained only by reducing $p_а$. In connection with this, motors with a gas pressurization supply system can be employed for operation in a vacuum (when $p_а$ can be reduced) and in cases where large thrust impulses are not required.

Motors with a gas pressurization supply system are employed for the following: course correction and attitude change, docking and undocking spacecraft, and less frequently as propulsion motors for upper rocket stages.

In ZhRD with a pump supply system, combustibles are fed by pumps from the tanks to the combustion chamber. Tank pressure in these motors is insignificant, ensuring tank stability and cavitationless pump operation.

ZhRD with a pump supply system are subdivided into two groups on the basis of utilization of working substance: ZhRD without afterburning of gas generation products in the combustion chamber, and ZhRD with afterburning of generator gas in the combustion chamber.

Figure 1.3 contains a block diagram of a motor without afterburning of generator gas.

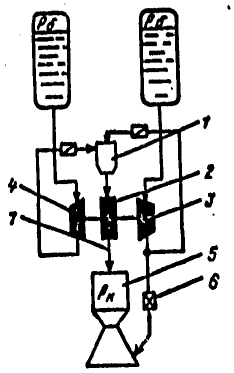

Figure 1.3. Diagram of ZhRD Without Afterburning of Generator Gas

Key:
1. Gas generator
2. Turbine
3. Fuel pump
4. Oxidizer pump
5. Combustion chamber
6. Automatic control devices
7. Exhaust nozzle

In these motors generator gas, after passing through the turbine, is exhausted externally. In view of the fact that the turbines are not cooled, the generator gas temperature is low and the gas which is ejected into the atmosphere past the turbine possesses unexpended energy. With a pressure increase in the combustion chamber, there is an increase in required turbine output and generator gas consumption, which in turn leads to a loss in the specific impulse produced by the combustion chamber and exhaust nozzles. Therefore motors without afterburning of generator gas have an optimal size p_k, exceeding of which results in a decrease in specific impulse. Actual values p_k for motors without generator gas afterburning range between 5.0 and 15 MPa.

ZhRD with afterburning of generator gas make it possible more fully to utilize fuel energy to obtain specific impulse, since in this instance the entire fuel, with an optimal ratio of components, is fed into the combustion chamber.

Motors with afterburning of generator gas are subdivided into three types:

ZhRD with afterburning of oxidizing generator gas;

ZhRD with afterburning of reducing generator gas;

ZhRD with two gas generators.

In the first two arrangements gas generator gas and a liquid component are fed into the combustion chamber, and therefore such motor arrangements are designated G-L.

In motors with two gas generators, gas generator gases are fed into the combustion chamber, and therefore they are designated G-G.

Figure 1.4 contains a block diagram of a G-L motor with oxidizing gas generator.

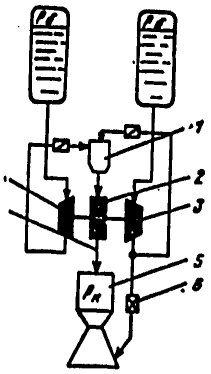

Figure 1.4. Diagram of ZhRD With Afterburning of Oxidizing Generator Gas

Key:

1. Gas generator
2. Turbine
3. Fuel pump
4. Oxidizer pump
5. Pressure chamber
6. Automatic control components
7. Gas line

In motors with an oxidizing gas generator, the entire oxidizer is fed into the gas generator, bypassing the combustion chamber. The greater part of the

fuel is fed into the combustion chamber, with a lesser amount being fed into the gas generator. In motors with afterburning of reducing gas, the entire fuel and a portion of the oxidizer is fed to the gas generator.

Gasification of fuel takes place in the gas generator with $\alpha \gg 1$ or $\alpha \ll 1$. After the generator gas is applied to the turbine, it passes into the combustion chamber, where there occurs fuel mixing with the liquid component and combustion with $\alpha \approx 1$.

Figure 1.5 contains a block diagram of a motor operating on a G-G arrangement.

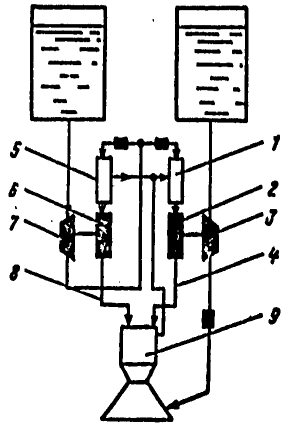

1.5. Diagram of G-G ZhRD

Key:

1. Gas generator for driving turbine
2. Fuel pump-drive turbine
3. Fuel pump
4. Reducing generator gas line
5. Gas generator for driving oxidizer pump turbine
6. Oxidizer pump-drive turbine
7. Oxidizer pump
8. Oxidizing generator gas line
9. Combustion chamber

The propellant components are fed to the combustion chamber by two independent turbopump units, each of which has a gas generator. This arrangement makes it possible to select an optimal pump rpm and to reduce the weight of the supply system.

Motors with afterburning and generator gas, due to the absence of losses in the specific impulse with ejection of generator gas, which possesses considerable energy, make it possible substantially to increase p_k and thus to increase engine economy.

With a pressure increase in the combustion chamber, however, the mass of supply system components increases substantially, and difficulties arise in providing reliable cooling and in obtaining seals.

In addition, motors with afterburning of generator gas are more complex than those without afterburning, due to substantial pressures in the equipment and the presence of a gas feed line between turbine and combustion chamber, and they have a high specific mass. Therefore in selecting a generator gas motor arrangement (motor with or without afterburning), it is essential to proceed from the purpose and efficiency of motor employment on the vehicle to be propelled.

Rocket velocity at the end of the powered segment of flight is determined with the relation

$$v_к = \sum_{i=1}^{n} I_y \ln \mu_{кi} - \Delta v_п, \qquad (1.2)$$

where $\mu_к = M_0/M_к$; $M_0 - M_к = M_т$; M_0 -- rocket launching mass; M_k -- mass of structure; $\Delta v_п$ -- total velocity losses caused by the gravitational attraction of the earth, air resistance and other factors; $\Delta v_п/v_k$=0.18-0.27; i -- number of rocket stages; $M_т$ -- propellant mass.

Equation (1.2) in differential form appears as follows:

$$\frac{dv_к}{v_к} = \frac{dI_y}{I_y} - \frac{dM_к}{M_т} \frac{M_т}{M_0 \ln \frac{M_0}{M_к}}. \qquad (1.3)$$

The engine mass is a component part of the mass of the structure, and therefore equality dM_k=$dM_п$ applies. For a given velocity (distance of flight) v_k=const, equation (1.3) can be written as follows:

$$\frac{dM_д}{M_д} = \frac{M_к \mu_к}{M_д(\mu_к - 1)} \frac{dI_y}{I_y} \ln \mu_к. \qquad (1.4)$$

This last equation determines equivalent change in engine mass and specific thrust impulse.

If the relative change in specific impulse is 0.01, the equivalent change in engine mass is

$$\frac{dM_д}{M_д} = 0{,}01 \frac{M_к \mu_к}{M_д(\mu_к - 1)} \ln \mu_к.$$

For contemporary values of μ_k and $M_k/M_д$ an increase in specific impulse by 1% in influence on v_k or range is equivalent to reducing engine mass by 10-15%.

Thus it is not enough to estimate the degree of ideality of a motor solely on the basis of specific impulse or engine mass; one must examine the aggregate of their influence on a rocket's characteristics.

In the assumption that thrust-to-weight coefficient μ_k is optimal, with equation (1.4) one can determine the equivalent change in engine mass for the first and second rocket stages in relation to stage thrust.

Calculations have shown that for first and second stage motors, there is an increase in the value of the engine mass equivalent with an increase in stage thrust.

For second stage motors, however, the engine mass equivalent is less than for first stage engines. Therefore any measures for first-stage engines which promote an increase in specific impulse are expedient, even with an increase in engine mass.

For rocket upper-stage motors the expediency of such measures should be evaluated taking into account change in mass. Proceeding from the above, we can state that advisable for the first rocket stages, especially if high thrusts are required, is employment of engines with afterburning, since such engines make it possible substantially to boost I_y, in spite of a certain increase in mass in comparison with engines without afterburning.

For rocket upper-stage motors, with small thrust values, specific impulse losses connected with cooling, greater complexity of design and increased mass in comparison with motors without afterburning are not always compensated by gain in specific impulse. In addition, in rocket upper-stage motors high degrees of expansion of gases in the nozzle (high specific thrust impulses) can be obtained for small p_k, which is characteristic of motors without afterburning. Therefore in some instances it is advisable to employ motors without generator gas afterburning for rocket final stages.

Selection of an engine arrangement with generator gas afterburning is determined by the energy potential of the given layout, magnitude of thrust, and other parameters.

Without going into detail for the present on the energy potential of engine layouts, we shall perform a qualitative comparison of different arrangements.

All other conditions being equal, it is desirable to have a high generator gas temperature. At the same time the maximum generator gas temperature is limited by the heat resistance of the material of which the turbine blading components are made, and for oxidizing gas comprises 1,000°K, and for reducing gas 1,300-1,400°K. When high-boiling components are employed as

fuel (NDMG, alcohol, etc), it is advisable to employ oxidizing afterburning. This is due to the fact that generator gas temperature in this arrangement is lower and the gasification products do not contain soot resins, which can foul turbine blading and alter characteristics.

A motor with oxidizing gas afterburning weighs less than with reducing gas afterburning due to the absence of additional cooling manifolds and the small size of controls mounted in the fuel gas generator line.

It is not advisable to employ motors with a reducing gas generator when low-boiling components (hydrogen, etc) are employed as fuel, since in this instance with equal p_k there can be lower pressures beyond the pumps.

If engine shutdown takes place in two stages, and the second stage operates on a gas generator arrangement, in order to obtain high final stage specific thrust impulse it is advisable to employ a reducing arrangement, since $(RT)_B > (RT)_{ok}$.

1.2. Engine Characteristics

1.2.1. Classification of Characteristics

The relationship between thrust and specific thrust impulse and the principal factors which change under operating conditions are called engine characteristics.

The most important factors which change in the process of operation are ambient pressure and consumption of propellant components. During a rocket's flight there occurs change in the altitude at which the engine operates. Ambient pressure changes in conformity with change in altitude. Relation $p_H = p_H(H)$ is based on standard atmosphere figures. Calculations indicate that if one employs International Standard Atmosphere (ISA) tables, one can assume $p_H = 0$ at altitudes greater than 30 km. This assumption produces an error of less than 4%.

The dependence of thrust and specific impulse on ambient pressure, with constant fuel consumption and ratio of propellant components, is called altitude characteristic.

During engine operation there occurs change in operating conditions due to change in consumption of propellant components.

The relationship between thrust and specific impulse on the one hand and propellant consumption on the other, with a specified ratio of propellant components, is called throttle charateristic.

In the general case thrust and specific thrust impulse are dependent not only on consumption and ambient pressure but also on many other factors as well. These relationships will be examined in subsequent chapters.

One differentiates between combustion chamber characteristics and characteristics of the engine as a whole. If in an engine the entire propellant supply is processed into combustion products and is ejected into the environment only through the combustion chamber (motors with a gas pressurization supply system and motors with generator gas afterburning), the altitude and throttle characteristics of the combustion chamber will also be engine characteristics.

Initial relations needed for constructing characteristics include equations of specific thrust impulse

$$I_y = \varphi_I I_{y,n} - \frac{F_a p_H}{\dot{m}} \qquad (1.5)$$

and thrust

$$P = \varphi_I I_{y,n} \dot{m} - F_a p_H, \qquad (1.6)$$

where ϕ_I -- coefficient of completeness of specific thrust impulse; $I_{y,n}$ -- theoretical value of specific thrust impulse in a vacuum;

$I_{y,n} = w_a + \frac{F_a p_a}{\dot{m}}$; F_a -- nozzle throat area; w_a -- velocity of outflow of combustion products from the nozzle.

For F_a=const quantities I_y and ϕ_I can be assumed constant for all conditions, and error will not exceed 3%.

1.2.2. Combustion Chamber Characteristics

Altitude characteristic. The term "altitude characteristic" came about during the operation of the first rockets, which were launched from the ground and reached a certain altitude. At the present time flying vehicles, including rockets, are launched not only from the ground but also under water (the Polaris missile), from a specific altitude in the atmosphere, and from other planets. Therefore, while retaining the traditional term altitude characteristic, we shall examine change in combustion chamber parameters in relation not to altitude of flight but rather ambient pressure. It follows from equations (1.5) and (1.6) that with supersonic flow of gas in a rocket nozzle, when exhaust velocity w_a is independent of external conditions, specific impulse and thrust are linearly dependent on ambient pressure and decrease with an increase in p_H.

Figure 1.6 shows relation $I_y = f_1(p_H)$ and $P = f_2(p_H)$. When pressure at the nozzle exit is less than ambient pressure, a compression wave may form in the nozzle, and the linear relationship between thrust and specific impulse on the one hand and p_H on the other will be disrupted. When the shock wave enters the nozzle the thrust taken from the inner duct of the combustion chamber begins to increase, and intensity of thrust reduction decreases with an increase in p_H. The nature of change in altitude characteristic during nozzle operation with a shock wave is accompanied by a pattern of shock wave movement into the nozzle.

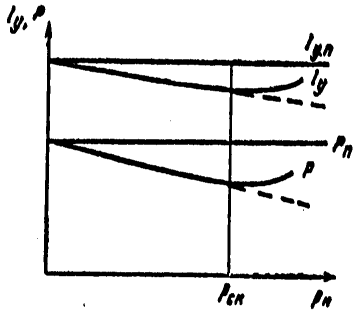

Figure 1.6. Relationship Between Thrust and Specific Thrust Impulse, and Ambient Pressure

In Figure 1.6 the dashed line shows the character of altitude characteristic change with nozzle exhaust without a shock wave, while the solid line shows the altitude characteristic for shock-wave flow with $p_H=p_{ck}$. Shock-wave conditions are observed in first-stage rocket engines, pressure at the nozzle exit of which is fairly low from the condition of obtaining mean maximum specific impulse in the powered segment of flight (p_a=0.5 MPa).

During operation at low altitudes ambient pressure is sufficient for the shock wave to enter deep into the nozzle. It follows from the above that calculation of specific impulse and thrust in a vacuum, based on the results of ground tests, with the presence of a shock wave, cannot be performed with the normal formulas, since in this case one would be determining thrust and specific impulse not in a vacuum but with specific back pressure.

In order to determine the altitude characteristic, engines must be tested on special test beds which make it possible to establish the required degree of vacuum at the nozzle, preventing operation under shock-wave conditions.

It is convenient to examine the altitude characteristic in relative quantities

$$\delta P = \frac{P_n - P}{P_n} = \frac{F_a p_n}{P_n};$$

$$\delta I_y = \frac{I_{y.n} - I_y}{I_{y.n}} = \frac{F_a p_n}{I_{y.n}\dot{m}}.$$

One readily notes that relative changes in thrust and specific impulse are identical. We shall transform relations δP and δI_y by substituting $\dot{m}=p_k F_{kp}/\beta$, and we obtain

$$\delta P = \delta I_y = \frac{f_c \beta}{I_{y.n} p_k} p_n, \qquad (1.7)$$

where

$$f_c = \frac{F_a}{F_{кр}}; \quad \beta = \frac{\sqrt{RT_к}}{b};$$

$$b = \sqrt{n}\left(\frac{2}{n+1}\right)^{\frac{n+1}{2(n-1)}};$$

n -- combustion products expansion polytropic curve indicator. When examining engine characteristics one ignores the relationship between specific pressure impulse β and combustion chamber pressure. This assumption is equivalent to assuming independence of dissociation of combustion products from pressure. This assumption is not rough within a narrow range of change of p_k. The effect of the influence of p_k on β also diminishes due to the fact that with a change in p_k temperature T_k and gas constant R of the combustion products change in opposite directions and approximately to an identical degree, that is, $RT_k \neq f(p_k)$.

Figures 1.7 and 1.8 show relations $\delta P = \delta P(f_c, p_к)$ for a given ambient pressure.

It follows from an analysis of the graphs (figures 1.7 and 1.8) that δP increases for combustion chambers with a greater degree of nozzle expansion, while when f_c=const -- at reduced operating conditions, that is, with reduced pressure values in the combustion chamber.

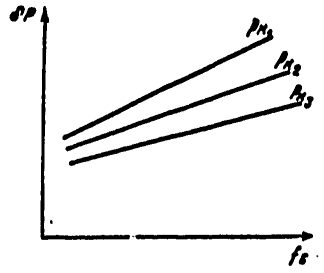

Figure 1.7. Relationship Between δP and Degree of Nozzle Expansion $p_{k1} < p_{k2} < p_{k3}$

Throttle characteristics are plotted in relation to flow rate or pressure in the combustion chamber.

Since $\dot{m} = \frac{F_{кр}}{\beta} p_к$, when F_{kp}=const, $\dot{m}$=cp_k and the type of characteristics $P(p_k)$ and $P(\dot{m})$ is identical, they can be differentiated only by scale.

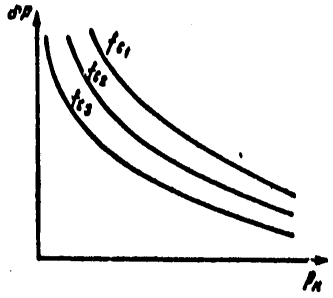

Figure 1.8. Relationship Between δP and Pressure in Combustion Chamber $f_{c_1}>f_{c_2}>f_{c_3}$

Let us examine the throttle characteristics for two conditions of motor utilization $p_H=0$ (vacuum) and p_H at altitude. Thrust in a vacuum is determined by the relation

$$P_п = \varphi \dot{m} w_a + F_a p_a. \qquad (1.8)$$

Thrust at altitude

$$P = P_п - F_a p_н. \qquad (1.9)$$

With a change in p_k, pressure at nozzle exit p_a also changes proportionally, and therefore quantity F_a/F_{kp}, which determines ratio p_a/p_{kp}, remains unchanged. Therefore with an increase in pressure, as was indicated above, RT_k and exhaust velocity w_a do not change. Consequently, following substitution in equation (1.8) of relation $\dot{m}=cp_k$, we obtain

$$P_п = c_p p_к, \qquad (1.10)$$

where

$$c_p = \varphi c w_a + \frac{F_a}{\pi}; \quad \pi = \frac{p_к}{p_a}.$$

It follows from equation (1.10) that thrust in a vacuum is linearly dependent on p_k.

Thrust at arbitrary altitude $P=c_p p_k - F_a p_H$ also changes proportionally to pressure in the combustion chamber, differing from thrust in a vacuum only by constant (for conditions of comparison) negative term $F_a p_H$.

Specific thrust impulse in a vacuum is

$$I_{y.п} = \frac{P_п}{\dot{m}}. \qquad (1.11)$$

After substituting in equation (1.11) relations (1.10) and $\dot{m}=cp_k$, we obtain

$$I_{y.n}=\frac{c_p}{c}=\text{const.}$$

Consequently, specific thrust impulse in a vacuum is independent of pressure in the combustion chamber (flow rate).

Specific thrust impulse

$$I_y=I_{y.n}-\frac{F_a p_H}{cp_k} \qquad (1.12)$$

with a pressure change in the combustion chamber varies in a more complex manner (hyperbolic relation).

The difference between $I_{y.n}$ and I_y is equal to $\frac{F_a p_H}{cp_k}$ and depends on p_k. When $p_k \to 0$ this difference also approaches zero, and when $p_k \to \infty$ the specific thrust impulse asymptotically approaches specific thrust impulse in a vacuum.

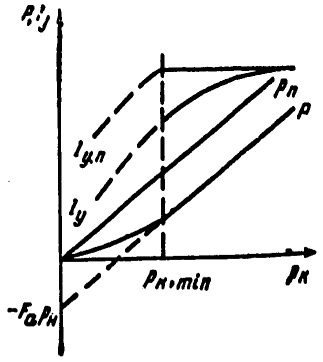

Figure 1.9. Throttle Characteristic Curve of a Combustion Chamber

Figure 1.9 shows a throttle characteristic curve of a combustion chamber.

The tangent of the angle of inclination of straight lines $P(p_k)$ and $P_n(p_k)$ is identical and equal to specific thrust impulse in a vacuum. Point ($p_k=0$, $P=-F_a P_H$) is formal and necessary only in order to plot the characteristic curve.

The combustion chamber when $p_k=0$ does not generate thrust, let alone negative. This is due to the fact that relations (1.5) and (1.6) are correct only for a certain region of change of p_k. Beginning with a certain value $p_{k,\min}$ when $p_k<p_{k,\min}$, supercritical nonimpact gas flow conditions in the nozzle

are replaced by impact conditions, and the above relations are not applicable. $p_{k,\,min}$ depends on ambient pressure and is determined by the approximate ratio [5]

$$p_{k,\,min} = \frac{2p_H}{\lambda_a^2\left(1-\frac{n-1}{n+1}\lambda_a^2\right)}.$$

In addition, as a consequence of a decreased p_k there is a decrease in pressure drop on the injectors, the quality of fuel mixing worsens, and the normal process of combustion is disturbed. All this leads to a situation where with combustion chamber pressures of $0<p_k<p_{k,\,min}$, characteristic curve $P(p_k)$ and $I_y(p_k)$ becomes curvilinear; it is depicted as a dashed line in Figure 1.9.

Dependence P on p_k when $p_k<p_{k,\,min}$ is approximately determined by equation [1]

$$P = n\left(\frac{2}{n+1}\right)^{\frac{n}{n-1}} F_{kp}\left(\sqrt{B^2+\frac{n+1}{n-1}p_k^2}-B\right),$$

where

$$B = \frac{F_a}{F_{kp}(n-1)}\left(\frac{n+1}{2}\right)^{\frac{n}{n-1}} p_H.$$

Actually $I_{y.\Pi}$ is determined by pressure in the combustion chamber, since completeness of combustion and the degree of dissociation of combustion products change somewhat with a change in p_k. As a rule, $I_{y.\Pi}$ increases slightly with an increase in p_k, and therefore relations $P(p_k)$ and $P_\Pi(p_k)$ are not strictly linear.

However, if the range of change of p_k is small, which occurs during engine operation, it is entirely permissible to utilize linear relations.

1.3. Characteristics of an Engine Without Generator Gas Afterburning

The specific thrust impulse of a combustion chamber is determined by relation (1.12).

With a given pressure at nozzle exit p_a=const, with an increase in p_k the specific thrust impulse initially increases intensively due to a decrease in p_a/p_k, while subsequently in the region of large p_k values intensity of growth of $I_{y.k}$ declines. At the extreme, when $p_k\to\infty$, specific thrust impulse approaches its maximum value

$$I_{y,\,max} = \sqrt{\frac{2\varkappa}{\varkappa-1}RT_k},$$

determined by propellant energy.

In a motor without generator gas afterburning, the bulk of the propellant is utilized in the combustion chamber and a smaller portion in the turbine

nozzles. In this case engine thrust contains two components: combustion chamber thrust P_k and turbine nozzle thrust $P_{o.c.}$:

$$P=P_k+P_{o.c.} \tag{1.13}$$

Engine specific thrust impulse

$$I_y=\frac{P}{\dot{m}_\Sigma}=\frac{I_{y.k}\dot{m}_k+I_{y.o.c}\dot{m}_{o.c}}{\dot{m}_\Sigma}, \tag{1.14}$$

where

$$\dot{m}_\Sigma=\dot{m}_k+\dot{m}_{o.c};$$

$I_{y.o.c}$ -- specific thrust impulse of the turbine exhaust nozzle.

Following simple transformations, relation (1.14) can be reduced to the form

$$I_y=I_{y.k}(1-\varepsilon_I), \tag{1.15}$$

where $\varepsilon_I=\frac{\dot{m}_{o.c}}{\dot{m}_\Sigma}\left(1-\frac{I_{y.o.c}}{I_{y.k}}\right)$ — coefficient of losses of specific thrust impulse in the supply system.

For an engine with generator gas afterburning, $\dot{m}_{o.c}=0$, $\varepsilon_I=0$ and $I_y=I_{y.k}$.

Uncooled turbines are employed in ZhRD, and therefore temperature in the gas generator is limited to a value guaranteeing heat resistance of the moving blades, $T_{г}\leq 1300$ K.

In order to obtain such a comparatively low temperature, fuel is fed into the gas generator with a component ratio coefficient differing greatly from stoichiometric. In connection with this, gas containing a considerable energy reserve emerges from the turbine exhaust nozzle.

Consequently the specific thrust impulse of the turbine exhaust nozzles is considerably less than combustion chamber specific impulse $I_{y.o.c}/I_{y.k}=0.3-0.4$. Tne specific impulse of the turbine exhaust nozzles is independent of pressure in the combustion chamber.

Fuel flow rate through the turbine exhaust nozzles is determined by the turbine's required output, and can be determined from an outputs balance equation

$$\dot{m}_{o.c}N_{уд}=\frac{p_{н.ок}\dot{m}_{ок}}{\eta_{н.ок}\rho_{ок}}+\frac{p_{н.г}\dot{m}_г}{\eta_{н.г}\rho_г}, \tag{1.16}$$

where $N_{уд}$ -- turbine specific power.

Gas generator fuel consumption in engines without generator gas afterburning comprises 2-8% of total consumption, and therefore one can assume that

turbine power is determined by the pump output required to feed propellant components only into the combustion chamber.

Then pressure beyond the pumps is determined by the parameters of the combustion chamber oxidizer and fuel systems

$$p_{нj} = p_к + \xi_j \dot{m}_j^2, \qquad (1.17)$$

where ξ_j -- coefficient of hydraulic resistance of the propellant component line from pump to combustion chamber. Substituting (1.17) in (1.16) taking into account

$$\dot{m}_{ок} = \frac{K}{K+1}\dot{m}; \quad \dot{m}_г = \frac{1}{K+1}\dot{m}; \quad K = \frac{\dot{m}_{ок}}{\dot{m}_г} \text{ and } \quad \dot{m} = \frac{F_{кр}}{\beta} p_к,$$

we obtain

$$\frac{\dot{m}_{о.с}}{\dot{m}_\Sigma} = a_1 p_к + a_2 p_к^2, \qquad (1.18)$$

where

$$a_1 = \frac{1}{N_{уд}(K+1)}\left(\frac{K}{\eta_{н.ок}\rho_{ок}} + \frac{1}{\eta_{н.г}\rho_г}\right);$$

$$a_2 = \frac{F_{кр}^2}{N_{уд}(K+1)^2\beta^2}\left(\frac{\xi_{ок}K^2}{\eta_{н.ок}\rho_{ок}} + \frac{\xi_г}{\eta_{н.г}\rho_г}\right).$$

Thus in an engine without generator gas afterburning, with an increase in p_k there is an increase in $I_{y.k}$, but

$$\lim_{p_к \to \infty} \frac{dI_{y.к}}{dp_к} = 0, \quad I_{y.о.с}$$

does not change; ε_I increases due to an increase in required turbine power. As a result of the aggregate influence of p_k and $\dot{m}_{о.с}/\dot{m}_\Sigma$ on I_y, engine specific thrust impulse changes with an increase in combustion chamber pressure following the curve shown in Figure 1.10. For a propulsion system without generator gas afterburning, there occurs an optimal pressure value in the combustion chamber at which one can obtain maximum specific thrust impulse.

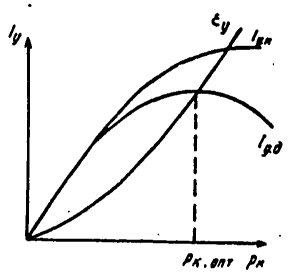

Figure 1.10. Relationship Between Specific Thrust Impulse and Pressure in Combustion Chamber

As a consequence of losses of specific thrust impulse in the supply system, the throttle characteristic of an engine without generator gas afterburning differs from the throttle characteristic of the combustion chamber.

As an illustration we shall examine the throttle characteristic of an engine in a vacuum.

Turbine exhaust nozzle thrust is

$$P_{o.c} = I_{y.o.c}\dot{m}_{o.c}, \qquad (1.19)$$

whereby $I_{y.o.c} \neq f(p_k)$, while fuel flow rate through the turbine nozzles depends on p_k. From (1.18) it is not difficult to show

$$\dot{m}_{o.c} = b_1 p_k^2 + b_2 p_k^3. \qquad (1.20)$$

In conformity with equations (1.10, 1.13, 1.19), a motor's throttle characteristics can be described by relation

$$P = cp_k + b_1 p_k^2 + b_2 p_k^3, \qquad (1.21)$$

which is shown in Figure 1.11.

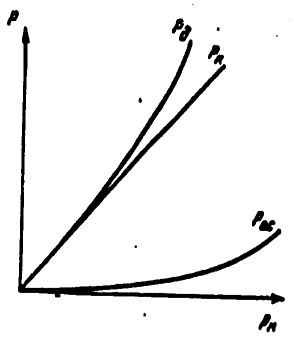

Figure 1.11. Dependence of Thrust of Combustion Chamber, Turbine Nozzles and Engine on Pressure in Combustion Chamber

The relation for specific engine thrust impulse (1.15) can be reduced to the form

$$I_y = I_{y.к}\left(1 - \frac{\dot{m}_{o.c}}{\dot{m}_\Sigma}\right) + \frac{\dot{m}_{o.c}}{\dot{m}_\Sigma} I_{y.o.c}. \qquad (1.22)$$

It follows from an analysis of relation (1.22) that when

$$p_к \to \infty, \frac{\dot{m}_{o.c}}{\dot{m}_\Sigma} \to 1 \text{ and } I_y \to I_{y.o.c}.$$

Figure 1.12 shows relation $I_y=I(p_k)$.

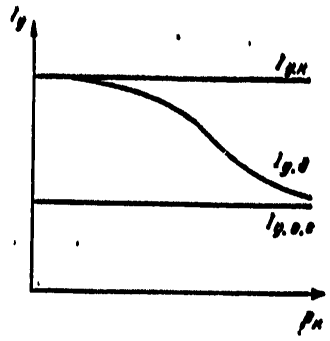

Figure 1.12. Dependence of Specific Thrust Impulse of Combustion Chamber, Turbine Nozzles and Engine on Pressure in Combustion Chamber

Analysis of the throttle characteristics of an engine without generator gas afterburning indicates that the role of turbine nozzles in determining thrust characteristics increases with an increase in pressure in the combustion chamber. Therefore during throttling and control of engines without generator gas afterburning, it is necessary to take into account change in thrust and specific thrust impulse of the turbine nozzles.

1.4. Optimal Pressure in Combustion Chamber of Engine With Gas Pressurization Supply System

Specific thrust impulse increases with an increase in pressure in the combustion chamber; the mass of the supply system increases at the same time. As a criterion of efficiency of an engine with a gas pressurization supply system, one can employ the ratio of total thrust impulse to launch weight $\bar{I}=I_\Sigma/M_0$. If we consider that $M_T=\dot{m}\tau_p$, while $P=\dot{m}I_y$, total thrust impulse is determined by relation

$$I_\Sigma = I_y M_T, \qquad (1.23)$$

where M_T -- mass of fuel on board, not counting reserve.

If we divide equation (1.23) by the launch weight and take into account correlation

$$M_T = M_0 - M_к, \quad \mu_к = M_к/M_0,$$

we obtain

$$\bar{I} = I_y\left(1 - \frac{1}{\mu_к}\right). \qquad (1.24)$$

It follows from equation (1.24) that criterion $\bar{I}$ is equivalent to velocity at the end of the powered segment of flight, since it is determined by the same quantities I_y and μ_k. At the extreme, when

$$\mu_к \to \infty,\ \bar{I} \to I_y,$$

that is, specific thrust impulse is the theoretical limit of criterion $\bar{I}$ with specified propellant. It is convenient to utilize the following criterion for estimating engine efficiency:

$$\eta = I_\Sigma / M_д.$$

In order to investigate relation (1.23) it is necessary to have engine equipment mass equations.

Engine mass

$$M_д = M_{к.д} + M_{с.п} + M_т, \qquad (1.25)$$

where $M_{к.д}$ -- mass of combustion chamber; $M_{с.п}$ -- mass of supply system; $M_т$ -- mass of propellant.

Now

$$M_{с.п} = M_б + M_{а.д} + M_{арм},$$

where $M_б$--- mass of tanks; $M_{а.д}$ -- mass of compressed-gas tank; $M_{арм}$ -- mass of fittings and accessories.

From equation (1.25) we shall determine propellant mass

or

$$M_т = M_д - M_{с.п} - M_{к.д}$$

$$\frac{M_т}{M_д} = 1 - \frac{M_{с.п}}{M_д} - \frac{M_{к.д}}{M_д}. \qquad (1.26)$$

If we multiply the right and left sides of expression (1.25) by I_y, we shall obtain efficiency criterion equation

$$\bar{I} = I_y(1 - m_{с.п} - m_{к.д}), \qquad (1.27)$$

where $m_{с.п}$ and $m_{к.д}$ -- relative masses of supply system and combustion chamber.

The mass of the combustion chamber depends on thrust and pressure in the combustion chamber.

With an increase in pressure in the combustion chamber, with specified pressure at the nozzle exit, combustion chamber volume decreases, while nozzle geometric dimensions increase. At the same time, due to an increase in the load operating on the chamber structure, its mass increases as a consequence of increased wall thickness.

It is difficult to obtain an analytical relationship between combustion chamber mass and $p_к$ with an adequate degree of accuracy. This relationship can be obtained approximately as a result of processing mass data on existing combustion chambers.

One can write the following relationship in general form:

$$M_{к.д} = c_1 + c_2 p_к, \qquad (1.28)$$

where c_1 and c_2 are static coefficients which are determined by engine thrust, all other conditions being equal.

The mass of the tanks also depends on thrust and pressure in the combustion chamber. Spherical tanks are often employed in spacecraft motors, which commonly employ a gas pressurization supply system.

The mass of a spherical tank is determined as follows:

$$M_б = \pi d^2 \delta \rho_м, \qquad (1.29)$$

where d -- tank diameter; δ -- wall thickness; $\rho_м$ -- density of wall material.

Tank wall thickness is

$$\delta = k \frac{p_б d}{4\sigma}, \qquad (1.30)$$

where k -- reserve strength factor; σ -- tensile strength; $p_б = k_1 p_1$,

$$M_б = \frac{\pi d^3 k k_1 p_к \rho_м}{4\sigma}. \qquad (1.31)$$

Expressing tank diameter by volume

$$d = \sqrt[3]{\frac{6V_б}{\pi}}; \quad V_б = \frac{F_{кр}}{\beta \rho_т} p_к \tau_р$$

and substituting value d in expression (1.31), we obtain

$$M_б = c_3 p_к^2 \tau_р, \qquad (1.32)$$

where $c_3 = 1{,}5 k k_1 \frac{F_{кр} \rho_м}{\beta \sigma \rho_т}$.

In like manner we can determine the mass of the compressed-gas tank [14]

$$M_{г.д} = c_4 p_к^2 \tau_р. \qquad (1.33)$$

The mass of fittings and accessories, which include valves, controls, assembly components, lines, and other design components, also depends on p_k, but this relation is small and can be ignored.

Substituting expressions (1.28), (1.32) and (1.33) in equation (1.27), we obtain

$$\bar{I} = f_1(p_к)[1 - f_2(p_к) - f_3(p_к)], \qquad (1.34)$$

where

$$f_1(p_к) = I_у; \quad f_2(p_к) = m_{с.п}; \quad f_3(p_к) = m_{к.д}.$$

If functions $f_1(p_к)$; $f_2(p_к)$; $f_3(p_к)$ are specified analytically, by differentiating equation (1.34) by p_k, we can find $p_{k,опт}$, whereby $\bar{I}$ reaches its maximum value, that is, we can solve equation $d\bar{I}/dp_k=0$ relative to p_k.

Analytical relation (1.34) turns out complex, and it is solved graphically, utilizing semiempirical mass correlations. Since equation (1.34) presupposes an awkward operation -- multiplication of graphic relations, by taking the logarithm of (1.34), we can proceed with plotting logarithmic curves

$$\lg \bar{I} = \lg f_1(p_к) + \lg A,$$

where $A=1-f_2(p_k)-f_3(p_k)$. Quantity A, with p_k changing from zero to infinity, is found within limits $0<A<1$ and lg A is a negative quantity.

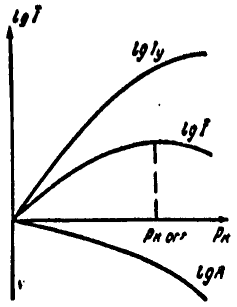

Figure 1.13. Relationship Between Engine Efficiency Indicator and Pressure in Combustion Chamber

Figure 1.13 shows qualitative relation $\lg \bar{I}=f(p_k)$. With an increase in p_k srecific thrust impulse initially increases very intensively and much more than covers losses $\bar{I}$ due to an increase in engine mass. As p_k increases, intensity of growth of I_y decreases, and with a certain value $p_{k,опт}$ growth in I_y fails to compensate for decrease in propellant mass due to increase in engine mass, and I begins to fall off. Consequently only with value $p_{k,опт}$ does there occur maximum engine efficiency I and its equivalent maximum vehicle velocity at the end of the powered segment of flight.

1.5. Limiting Combustion Chamber Pressures in an Engine With Generator Gas Afterburning

1.5.1. Energy Capabilities of Engines

In engines designed for rocket first stages, optimal pressure at nozzle exit p_a with variable external pressure comprises 0.04-0.07 MPa. Therefore in order to increase specific thrust impulse one must have maximum possible

pressure in the combustion chamber. Engine mass increases with an increase in p_k. However, as was indicated above, for first rocket stages increase in engine mass exerts little influence on decrease in rocket terminal velocity and a significant influence on increase in specific thrust impulse. However, the magnitude of pressure in the combustion chamber of engines with generator gas afterburning is limited by the energy capabilities of the engine design.

Engines with generator gas afterburning, in comparison with other ZhRD, are characterized by a deeper interrelationship of equipment (combustion chamber, pumps, turbines and gas generators) parameters, which is realized through an energy balance equation which characterizes equality of utilized and available output in the supply system.

This equation includes all principal engine parameters -- combustion chamber pressure, turbine gas temperature and pressure ratio, hydraulic resistances of lines, etc.

Utilized power includes power expended on driving main, auxiliary and booster pumps, as well as power used to drive propulsion unit power systems.

Available power is power taken from the turbines. In the general case both utilized and available power is determined by pressure developed by the pumps, combustion chamber pressure, temperature and composition of gases in the turbine, turbine pressure ratio, and efficiency of pumps and turbines.

Following is an engine power balance equation:

$$N_т = \sum N_{нj}, \qquad (1.35)$$

where N_T -- turbine available power; N_{Hj} -- consumed power by j pump.

Turbine output

$$N_т = \dot{m}_т \eta_т \frac{\varkappa}{\varkappa - 1} (RT)_{гг} \left[1 - \left(\frac{p_{вых}}{p_{вх}} \right)^{\frac{\varkappa - 1}{\varkappa}} \right], \qquad (1.36)$$

where $p_{вых}$, $p_{вх}$ -- pressures at turbine exit and intake respectively;

$$N_{нj} = \frac{\dot{m}_j (p_{нj} - p_{oj})}{\eta_{нj} \rho_j}. \qquad (1.37)$$

We shall examine engine power capabilities, that is, the conditions of fulfillment of equality (1.35).

With an increase in combustion chamber pressure, pressure beyond the pumps increases, that is, power consumed by the pumps increases. In order to simplify the problem we assume constant fuel flow rate through the combustion chamber. Change in p_k is obtained by change in the nozzle throat area. With variable flow rate through the combustion chamber, the qualitative interrelationship of parameters will remain unchanged.

It follows from equation (1.36) that with a specified λ_T, an increase in turbine output can be obtained by increasing consumption $\dot{m}_T$, quantity $(RT)_{\Gamma\Gamma}$ and turbine pressure ratio $p_{вых}/p_{вх}$. However, quantity $(RT)_{\Gamma\Gamma}$ for a specified propellant, which is determined by allowable gas temperature, selected from the condition of heat resistance of working blades, remains practically constant.

Flow rate through the turbine $\dot{m}_T$ is also a constant quantity for the given engine design, since one of the components goes entirely into the gas generator, while the ratio of components is determined by the allowable gas temperature.

Consequently with an increase in p_k, it is necessary to increase the turbine pressure ratio in order to increase turbine power.

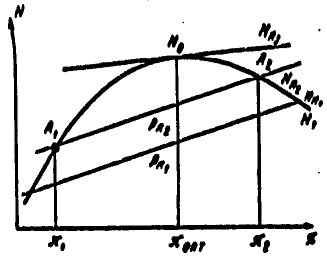

Figure 1.14. Relationship Between Turbine-Pump Unit Power, Combustion Chamber Pressure and Turbine Pressure Ratio

Figure 1.14 shows the character of change in turbine power and pump output at various combustion chamber pressures. Point A_1 of intersection of curve N_{l_1} at p_{k_2} with turbine available power curve N_T gives the value of turbine pressure ratio π_1. With a further increase in p_k, turbine power and pressure ratio increase respectively. However, as is evident from Figure 1.14, an increase in p_k is possible only to a certain limit $p_{k,\,max}$, at which condition $N_T = \sum N_{пл}$ (point N_0) is still fulfilled. When $p_k > p_{k,\,max}$ pressure beyond the pumps increases to such an extent that pump consumed power becomes greater than turbine available power. Thus there exists for an engine with generator gas afterburning a maximum combustion chamber pressure $p_{k,\,max}$.

1.5.2. Maximum Combustion Chamber Pressure in a G-L Engine

In a G-L engine, one of the propellant components is fed from the pump entirely to gasification in the gas generator.

Energy balance equation (1.35) is written in the form

$$\dot{m}_т\eta_т \cdot \frac{\varkappa}{\varkappa-1}(RT)_{гг}\left[1-\left(\frac{p_{вых}}{p_{вх}}\right)^{\frac{\varkappa}{\varkappa-1}}\right] = \frac{\dot{m}_{ок}(p_{н.ок}-p_{о.ок})}{\eta_{н.ок}\rho_{ок}} + \frac{\dot{m}_г(p_{н.г}-p_{о.г})}{\eta_{н.г}\rho_г}. \qquad (1.38)$$

Turbine outlet pressure is determined by combustion chamber pressure

$$p_{вых} = p_к + \Delta p_{тр}, \qquad (1.39)$$

where $\Delta p_{тр}$ -- pressure losses in the gas line between turbine and combustion chamber.

Turbine inlet pressure can be assumed equal to gas generator pressure

$$p_{вх} = p_{гг}. \qquad (1.40)$$

Taking into account relations (139) and (1.40), the turbine pressure ratio is determined as follows:

$$\pi_т = \frac{p_{вх}}{p_{вых}} = \frac{p_{гг}}{p_к + \Delta p_{тр}}. \qquad (1.41)$$

Pressure beyond the pump is determined by pressure in the gas generator

$$p_{нj} = p_{гг} + \Delta p_{гг} = \pi_т(p_к + \Delta p_{тр}) + \Delta p_{гг\,j}, \qquad (1.42)$$

where $\Delta p_{гг\,j}$ -- pressure losses in the lines linking the pumps with the gas generator.

Since gas generator pressure is greater than combustion chamber pressure, it is advisable to install an additional pump to feed the additional component into the gas generator (oxidizer in a reducing arrangement and fuel in an oxidizing arrangement). Obviously the feed pressure of the main pump feeding propellant component into the combustion chamber will be lower than auxiliary pump feed pressure. This will lead to a decrease in pump power requirements, which in turn will make it possible to reduce gas generator pressure. If auxiliary pumps are employed, it is necessary to add to equation (1.38) a term containing the auxiliary pump output.

Taking into account equations (1.39)-(1.42) and in the assumption that

$$\eta_{нj} = \eta_н;\ p_{oj} = p_o;\ \Delta p_{гг\,j} = \Delta p_{гг},$$

equation (1.38) will be rewritten as follows:

$$\dot{m}_т\eta_т \cdot \frac{\varkappa}{\varkappa-1}(RT)_{гг}\left[1-\frac{1}{\pi_т^{\frac{\varkappa-1}{\varkappa}}}\right] = \frac{\pi_т(p_к+\Delta p_{тр})+\Delta p_{гг}-p_o}{\eta_н}\left(\frac{\dot{m}_{ок}}{\rho_{ок}}+\frac{\dot{m}_г}{\rho_г}\right). \qquad (1.43)$$

We shall determine consumption of the propellant components through their relations K:

$$\dot{m}_{ок} = \frac{K_к}{K_к + 1}\dot{m}; \quad \dot{m}_г = \frac{1}{K_к + 1}\dot{m}, \qquad (1.44)$$

where $K_к = \frac{\dot{m}_{ок}}{\dot{m}_г}$ -- ratio of components in the combustion chamber;

$$\dot{m} = \dot{m}_{ок} + \dot{m}_г.$$

For an oxidizing gas generator

$\dot{m}_г = \dot{m}_{ок} + \dot{m}_{г.о}$; since $\dot{m}_{г.о} = \dot{m}_{ок}/_о K_о$, then

$$\dot{m}_т = \dot{m}\frac{(K_о + 1)}{K_о(K_к + 1)}, \qquad (1.45)$$

where $K_о = \dot{m}_{ок}/\dot{m}_{г.о}$ -- ratio of fuel components for an oxidizing gas generator.

For a reducing gas generator

$\dot{m}_т = \dot{m}_г + \dot{m}_{ок.г}$; since $\dot{m}_{ок.г} = \dot{m}_г K_г$, then

$$\dot{m}_т = \frac{K_г + 1}{K_к + 1}\dot{m}, \qquad (1.46)$$

where $K_г = \frac{\dot{m}_{ок.г}}{\dot{m}_г}$ -- ratio of propellant components in a reducing gas generator.

Substituting relations (1.44)-(1.46) in equation (1.43), making transformations and resolving it relative to $p_к$, we obtain

$$p_к = (c + p_о - \Delta p_{гг})\frac{1}{\pi_т} - \frac{c}{\pi_т^{\frac{2\varkappa - 1}{\varkappa}}} - \Delta p_{га}, \qquad (1.47)$$

where

$$c = \bar{R}\frac{\varkappa}{\varkappa - 1}(RT)_{гг}\eta_{ТНА};$$

$\bar{R} = \bar{K}_о = \frac{K_к(K_о + 1)\rho_{ок}\rho_г}{K_о(\rho_г K_к + \rho_{ок})}$ -- reduced density for oxidizing gas generator;

$K = \bar{K}_г = \frac{(K_г + 1)\rho_{ок}\rho_г}{\rho_г K_к + \rho_{ок}}$ -- reduced density for a reducing gas generator.

In a first approximation one can consider that in equation (1.47) combustion chamber pressure is determined only by the turbine pressure ratio.

Maximum pressure in the combustion chamber can be determined from the condition

$$\frac{dp_к}{d\pi_т} = -\frac{c + p_0 - p_{тг}}{\pi_т^2} + c\frac{2к-1}{к}\frac{1}{\pi_т^{\frac{3к-1}{к}}} = 0.$$

From the last equality we obtain pressure differential $\pi_Т$, which ensures maximum combustion chamber pressure

$$\pi_{т,\,опт} = \left(\frac{c}{c + p_0 - p_{тг}}\frac{2к-1}{к}\right)^{\frac{к}{к-1}}. \qquad (1.48)$$

Substituting relation (1.48) in equation (1.47), we obtain

$$p_{к,\,max} = (c + p_0 - p_{тг})^{\frac{2к-1}{к}} - \Delta p_{тр}. \qquad (1.49)$$

1.5.3. Maximum Combustion Chamber Pressure in a G-G Engine

In a G-G propulsion system, fuel and oxidizer are fed from the pumps at specified ratios to the oxidizing and reducing gas generators. The gaseous GG combustion products are utilized to drive the oxidizer system pump turbine and fuel system pump turbine.

Our initial equations are turbopump power balance equations

$$N_{т.о} = N_{н.ок};\quad N_{т.г} = N_{н.г}$$

or in expanded form

$$\dot{m}_{т.о}\eta_{т.о}\cdot\frac{к}{к-1}(RT)_о\left[1 - \frac{1}{\pi_{т.о}^{\frac{к-1}{к}}}\right] = \frac{\dot{m}_{ок}(p_{н.ок} - p_{о.ок})}{\eta_{н.ок}\rho_{ок}}; \qquad (1.50)$$

$$\dot{m}_{т.г}\eta_{т.г}\cdot\frac{к}{к-1}(RT)_г\left[1 - \frac{1}{\pi_{т.г}^{\frac{к-1}{к}}}\right] = \frac{\dot{m}_г(p_{н.г} - p_{о.г})}{\eta_{н.г}\rho_г}. \qquad (1.51)$$

After passing through the pumps, the propellant components are fed to the gas generators, and therefore pressure beyond the pumps is determined by gas generator pressures

and $$p_{нj} = p_{тгj} + \Delta p_{тгj} \qquad (1.52)$$

$$p_{тгj} = \pi_{тj}(p_к + \Delta p_{трj}). \qquad (1.53)$$

The ratio of propellant components in the combustion chamber K_k, in the oxidizing gas generator $K_о$ and in the reducing gas generator $K_г$ are specified.

$$K_о = \frac{\dot{m}_{ок.о}}{\dot{m}_{г.о}};\quad K_г = \frac{\dot{m}_{ок.г}}{\dot{m}_{тг}}. \qquad (1.54)$$

Since oxidizer and fuel pass in their entirety through the gas generators into the combustion chamber,

$$\left.\begin{aligned}\dot{m}_{ок} &= \dot{m}_{ок,\,о} + \dot{m}_{ок,\,г};\\ \dot{m}_{г} &= \dot{m}_{г,\,о} + \dot{m}_{гг}.\end{aligned}\right\} \qquad (1.55)$$

Solving congruently equations (1.54) and (1.55), we obtain propellant component flows into the gas generators

$$\left.\begin{aligned}\dot{m}_{ок,\,о} &= K_о\frac{\dot{m}_{ок}-\dot{m}_{г}K_г}{K_о-K_г};\quad \dot{m}_{г,\,о} = \frac{\dot{m}_{ок}-\dot{m}_{г}K_г}{K_о-K_г};\\ \dot{m}_{ок,\,г} &= K_г\frac{\dot{m}_{г}K_о-\dot{m}_{ок}}{K_о-K_г};\quad \dot{m}_{гг} = \frac{\dot{m}_{г}K_о-\dot{m}_{ок}}{K_о-K_г}.\end{aligned}\right\} \qquad (1.56)$$

From equation (1.56) we find rates of flow of working fluid to each turbine

$$\left.\begin{aligned}\dot{m}_{т,\,о} &= \frac{\dot{m}(K_к-K_г)(K_о+1)}{(K_к+1)(K_о-K_г)};\\ \dot{m}_{т,\,г} &= \frac{\dot{m}(K_о-K_к)(K_г+1)}{(K_к+1)(K_о-K_г)}.\end{aligned}\right\} \qquad (1.57)$$

Substituting relations (1.52), (1.53) and (1.57) in equations (1.50) and (1.51) and resolving them relative to $p_{к}$, we obtain

$$p_{кj} = \frac{c_j-\Delta p_{гг\,j}+p_{0j}}{\pi_{тj}} - \frac{c_j}{\pi_{тj}^{\frac{\varkappa-1}{\varkappa}}} - \Delta p_{тр\,j}, \qquad (1.58)$$

where $j = \overline{о,\,г}$;

$$c_о = \frac{(K_к-K_г)(K_о+1)\,\eta_{т.\,о}\eta_{п.\,ок}\rho_{ок}}{K_к(K_о-K_г)}\cdot\frac{\varkappa}{\varkappa-1}(RT)_о;$$

$$c_г = \frac{(K_о-K_к)(K_г+1)\,\eta_{т.\,г}\eta_{п.\,г}\rho_г}{K_о-K_г}\cdot\frac{\varkappa}{\varkappa-1}(RT)_г.$$

We shall estimate the ratio of parameter c for the oxidizer and fuel line:

$$\bar{c} = \frac{c_о}{c_г} = \frac{(K_к-K_г)(K_о+1)\rho_{ок}(RT)_о}{K_к(K_о-K_г)(K_г+1)\rho_г(RT)_г}.$$

If we consider that $\rho_{ок}/\rho_г = 1{,}8-16$, $K_к > 1$, $K_о > K_г$, , we obtain

$$\bar{c} = 1{,}1-1{,}4.$$

An optimal turbine pressure differential is obtained from the ratio

$$\frac{dp_{кj}}{d\pi_{тj}} = \frac{c_j-\Delta p_{гг\,j}+p_{0j}}{\pi_{тj}^2} + c_j\frac{2\varkappa-1}{\varkappa}\frac{1}{\pi_{тj}^{\frac{3\varkappa-1}{\varkappa}}} = 0. \qquad (1.59)$$

Substituting (1.59) in equation (1.56), we obtain the maximum possible combustion chamber pressures achieved by the oxidizer and fuel circuit.

The smaller of the obtained values is adopted.

1.5.4. Comparison of Engines With Generator Gas Afterburning by Magnitude of Maximum Combustion Chamber Pressure

For all engines maximum combustion chamber pressure is determined by the relation

$$p_{k,\max} = (c + p_0 - \Delta p_{IT})^{\frac{2\varkappa-1}{\varkappa}} \frac{\varkappa-1}{\varkappa} \cdot \frac{1}{c \cdot \frac{\varkappa}{\varkappa-1}\left(\frac{2\varkappa-1}{\varkappa}\right)^{\frac{2\varkappa-1}{\varkappa-1}}} - \Delta p_{rs}. \tag{1.60}$$

It follows from an analysis of the above relation that maximum pressure is determined by parameter

$$c = \overline{K} \cdot \frac{\varkappa}{\varkappa-1}(RT)\eta_{THA},$$

which is characterized by reduced density and efficiency of turbine working fluid and turbopump efficiency, as well as by pressure losses in the engine's hydraulic lines. With identical combustion chamber pressure, the principal parameters of the supply system for an oxidizing and reducing engine setup have a different value. This is due to the fact that for ZhRD propellants oxidizer consumption is always greater than fuel consumption $K_k > 1$, and turbine working fluid consumption in an oxidizing setup is also greater than in a reducing setup. For the majority of propellants (other than propellants utilizing hydrogen as fuel) quantity RT in a reducing setup is greater than in an oxidizing setup due to the high combustion products gas constant value. This increase, however, is not large, and comprises

$$(\dot{RT})_r/(RT)_o^{\cdot} = 1{,}05—1{,}18.$$

The efficiency of a turbine-pump unit is independent of combustion chamber pressure but is determined by engine thrust. With an increase in engine thrust, pump efficiencies increase due to a decrease in hydraulic losses. This is due to the fact that with an increase in thrust there is a decrease in the percentage share of consumption per unit of surface area.

In like manner, with an increase in thrust there is a decrease in pressure losses in the lines, and chiefly due to a decrease in hydraulic losses in the cooling system.

Thus it follows from the above analysis that with an increase in engine thrust, maximum combustion chamber pressure increases, while the magnitude of maximum combustion chamber pressure depends on the engine design.

We shall compare engine designs for a specified thrust. Obviously theoretical limiting-maximum pressure in the combustion chamber will occur when there are no pressure losses in the lines

$$(\Delta p_{\text{тг}} = \Delta p_{\text{тп}} = 0).$$

in this case from equation (1.60) we have

$$p^*_{\text{к, max}} = \frac{\varkappa - 1}{\varkappa} \cdot \left(\frac{2\varkappa - 1}{\varkappa - 1}\right)^{\frac{\varkappa - 1}{2\varkappa - 1}} c, \qquad (1.61)$$

that is, maximum pressure in the combustion chamber is proportional to parameter c, which basically is determined solely by the engine design.

If we substitute in equation (1.61) an expression for c, we obtain

$$p^*_{\text{к, max}} = \left(\frac{2\varkappa - 1}{\varkappa - 1}\right)^{\frac{\varkappa - 1}{2\varkappa - 1}} \overline{K}_j (RT)_j \eta_{\text{ТНА}}, \qquad (1.62)$$

where $\overline{K}_j$ -- reduced density of the working fluid of j gas generator.

For an engine with afterburning of oxidizing generator gas

$$\overline{K}_{\text{о}} = \frac{K_{\text{к}} (K_{\text{о}} + 1) \rho_{\text{ок}} \rho_{\text{г}}}{K_{\text{о}} (\rho_{\text{г}} K_{\text{к}} + \rho_{\text{ок}})}. \qquad (1.63)$$

For an engine with afterburning of reducing generator gas

$$\overline{K}_{\text{г}} = \frac{(K_{\text{г}} + 1) \rho_{\text{ок}} \rho_{\text{г}}}{\rho_{\text{г}} K_{\text{к}} + \rho_{\text{ок}}}. \qquad (1.64)$$

For liquid propellants employed in ZhRD, the propellant component ratios and densities have values K_k=2.5-6.5; K_O=18-27; $K_г$=0.2-0.8; ρ_{ok}=(1100-1700) kg/m^3; $\rho_г$=(71-1000) kg/m^3.

Let us assume that turbine-pump unit efficiencies and adiabatic exponents are identical in the motors being compared.

Then

$$\frac{p^*_{\text{к, max, о}}}{p^*_{\text{к, max, г}}} = \frac{K_{\text{к}} (K_{\text{о}} + 1) (RT)_{\text{о}}}{K_{\text{о}} (K_{\text{г}} + 1) (RT)_{\text{г}}}. \qquad (1.65)$$

It follows from expression (1.65) that for the specified propellant components

$$L_{\text{к}} = p^*_{\text{к, max, о}} / p^*_{\text{к, max, г}} = 1{,}3—1{,}8.$$

For nitrogen techtrochside and NDMG [expansion unknown] propellant

$$K_{\text{к}} = 3{,}0, \; K_{\text{о}} = 20, \; K_{\text{г}} = 0{,}6$$

we have L_k=1.52. Consequently, in engines with afterburning of oxidizing generator gas, maximum allowable combustion chamber pressure is substantially greater than in an engine with reducing gas afterburning.

We shall compare a motor with oxidizing gas afterburning with a G-G motor. In our comparison we shall assume that in a G-G motor maximum combustion chamber pressure is determined by the fuel system.

For a G-G engine fuel system

$$\overline{K}_{\Gamma\Gamma} = \frac{(K_0 - K_k)(K_\Gamma + 1)\rho_\Gamma}{K_0 - K_\Gamma} \quad \text{and}$$

$$\frac{p^*_{к,\,max,\,\Gamma-\Gamma}}{p^*_{к,\,max,\,o}} = \frac{(K_0 - K_к)(K_\Gamma + 1)K_0(\rho_\Gamma K_к + \rho_{ок})(RT)_o}{(K_0 - K_\Gamma)K_к(K_0 + 1)\rho_{ок}(RT)_\Gamma} > 1. \quad (1.66)$$

For a fuel with $K_к = 3{,}0$, $K_0 = 20$, $K_\Gamma = 0{,}6$, $\rho_{ок} = 1450$ кг/м³, $\rho_\Gamma = 780$ кг/м³,

we have $p^*_{к,\,max,\,\Gamma-\Gamma}/p^*_{к,\,max,\,o} = 1{,}48.$

Thus the greatest maximum allowable combustion chamber pressure can be achieved in an engine with two gas generators. Considering actual magnitudes of pressure losses in the lines and efficiencies, maximum combustion chamber pressures will be less than limiting-maximum, but the distribution of their values will not change with a transition from one engine design to another.

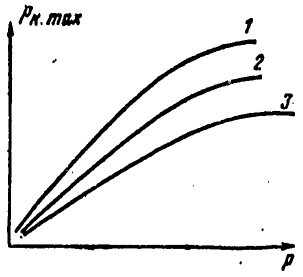

Figure 1.15. Relationship Between Maximum Combustion Chamber Pressure, Engine Thrust and Design

Key:
1. G-G engine
2. G-L engine O
3. G-L engine V

Figure 1.15 shows the character of change in maximum combustion chamber pressure for different engine layouts.

Chapter 2. METHODS OF ANALYSIS AND CALCULATION OF STATIC CHARACTERISTICS

2.1. Disturbances of Operating Conditions. General Description of Disturbing Factors

The characteristics of the working process of a propulsion system in the process of operation differ from those characteristics obtained as a result of design engineering. This is due to the influence of various disturbances. All motors are tuned and adjusted to ensure reproducibility of operating processes. Deviations of operating process parameters from specified values due to operating condition disturbances constitute the input data for adjustment and calculation of control systems.

Disturbing factors which affect the operating process can be arbitrarily divided into external and internal.

External disturbances are independent of the engine layout and design; they are for the most part determined by operating conditions and environmental conditions.

Since a motor is linked to rocket systems only by fuel supply lines, external disturbing influences come for the most part from the propellant lines. Small external disturbances may also enter the engine from the rocket control system due to noise in the electrical circuits of these systems as well as for other reasons.

Internal disturbing factors are determined by engine design, production and testing conditions and process. Characteristics of internal dsiturbances can differ for different engines.

External Disturbances

External disturbances include deviations of characteristics of operating conditions from the standard conditions which were assumed when designing the motor. External disturbing factors include ambient temperature and pressure, density of propellant components, and pressure at pump inlet.

Atmospheric conditions exert practically no influence on engine operation. One exception is ambient pressure and temperature, which directly affect propellant and thrust characteristics.

1. Ambient temperature. In designing an engine one assumes a standard temperature at which the thermophysical characteristics of propellant are determined. As a rule an engine is operated at a temperature differing from standard. Operation of thermostatically-controlled motors is an exception. Change in ambient temperature causes deviations in temperature and enthalpy, density and viscosity of propellant components. Ambient temperature varies within broad limits for different climatic zones, season and time of day.

Table 2.1 contains temperature values for different climatic zones.

Table 2.1

1 Климатическая зона	5 Температура, К		
	T_{max}	T_{min}	Суточные колебания
Арктическая 2	303	253	25
Умеренная 3	308	223	20
Тропическая 4	323	263	40

Key:
1. Climatic zone
2. Arctic
3. Temperate
4. Tropical
5. Temperature
6. Daily variation

2. Density of propellant components. Density of propellant components at standard temperature is determiend by propellant grade and temperature:

$$\rho = \rho_c + \beta (T - \overline{T}),$$

where ρ_c -- density of propellant component at standard temperature; β-- volumetric expansion coefficient; ρ_c -- determined by precision of propellant manufacture. $\rho_T=\beta(T-T)$ is determined by the properties of the propellant and temperature. This quantity can vary within broad limits in the process of operation. Density of propellant components affects the operating process in the supply system and fuel mass in the tanks.

3. Ambient pressure. Ambient pressure varies with altitude. A change in ambient pressure leads to change in engine thrust; in addition, it affects turbine characteristics in a motor without generator gas afterburning in the case of subcritical pressure differential in the turbine nozzles.

4. Pressure at pump inlet. Pressure at pump inlet consists of liquid column pressure p_{ct} and tank absolute pressure above free liquid surface $p_б$.

Figuring in pressure losses Δp in the lines from tank to pumps, we obtain

$$p_0 = p_б + p_{ст} - \Delta p.$$

For a stationary rocket $p_{ст} = \rho H$, , where ρ -- density of propellant components; H -- initial height of liquid column.

Sequential placement of tanks, pumps and combustion chamber is typical of rockets. In spacecraft tanks can be placed at the same level or below pumps, and in this instance $p_{ст} \leq 0$.

During flight of a rocket with an operating engine, liquid column pressure will be variable, due to depletion of propellant components (H decreases), and due to variable axial acceleration j.

In this instance $p_{ст} = Hn\rho$,

where $n = \frac{j}{g} + \sin\varphi$ -- axial G-load factor; φ -- angle of inclination of rocket axis.

Consequently $p_{ст}$, $p_б$ and pump inlet pressure change in the process of engine operation. In addition, during flight there may occur elastic longitudinal oscillations of body and liquid, which will also change p_0.

Internal Disturbances

Internal disturbances constitute deviations of internal engine characteristics from calculated characteristics due to losses and production errors of various kinds.

Following are the principal internal disturbing factors.

1. Design-manufacturing dimensional tolerances of engine components. Structural dimensional tolerances are specified for engine manufacture. One and the same parts of different engine components may differ in size and shape within limits of these tolerances. This leads to variance in characteristics of individual parts of one and the same units and systems manufactured on the basis of identical specifications.

The principal dimensions which affect engine characteristics are nozzle throat area and diameters of pump and turbine rotor wheels.

2. Pump and turbine efficiencies.

3. Hydraulic resistances of lines, etc.

All engine parameters are interlinked, and variance in the characteristics of engine components leads to deviations in engine operating conditions, that is, to deviation from nominal values for thrust, specific thrust impulse and propellant component ratio. As a result there arise additional

disturbances which affect the rocket, and the motor can move out of the specified operating range, which in turn will lead to engine failure.

2.1.1. Statistical Characteristics of Disturbances

Internal and external disturbances are random quantities or functions relative to a specific motor, the conditions and moment of its operation. Disturbances, as random quantities, are characterized by statistical data which are determined on the basis of results of tests or operations. In determining the statistical characteristics of disturbing factors, one must bear in mind that due to the random nonuniformity of operation and test conditions, there frequently occur errors in output results. With a limited volume of practicable information, these errors can lead to incorrect statistical conclusions. In order to avoid such phenomena it is essential to exclude sharply differing observations from consideration. A number of different statistical criteria are utilized for this [15].

This is done most simply and with a sufficient degree of accuracy on the basis of Smirnov's criterion.

We determine arithmetic mean statistics

$$x^* = \frac{1}{n}\sum_{i=1}^{n} x_i, \qquad (2.1)$$

root-mean-square deviation

$$\sigma^* = \sqrt{\frac{1}{n-1}(x_i - x^*)}, \qquad (2.2)$$

where x_i--- quantity measured in the experiment; n -- number of experiments.

We then determine statistics

$$\varepsilon = \frac{|x - x^*|}{\sigma^*},$$

where x -- doubtful result of measurement.

If for a given number of measurements n and selected reliability $P=1-\beta$ quantity ε exceeds critical value ε_β, then one can assume the result of measurement x to be a gross error with a probability greater than P.

Table 2.2.contains values ε_β in relation to number of measurements for two values of β.

Table 2.2.

n	4	8	12	16	20	24	28	32	36	40
ε_β ($\beta = 0{,}1$)	1,689	2,172	2,387	2,523	2,623	2,704	2,762	2,792	2,853	2,904
ε_β ($\beta = 0{,}2$)	1,645	2,041	2,229	2,357	2,441	2,521	2,589	2,609	2,668	2,712

As a result we can determine the numerical characteristics of disturbances: mathematical expectation, and variance.

The results of processing of realizations of disturbing factors indicate that the majority are governed by the normal law of distribution, and only a few, such as design dimensions, by uniform distribution.

There may be functional and stochastic interrelationships between disturbing factors.

For example, a functional relationship effected by the influence of temperature can be established between oxidizer and fuel densities.

If we eliminate temperature factor $(T-\bar{T})$ from component density equations $\rho_{ok}=\rho_{c.ok}+\beta_{ok} \times (T-\bar{T})$ and $\rho_r = \rho_{c.r} + \beta_r (T - \bar{T})$ we obtain a relationship between ρ_{ok} and ρ_r:

$$\rho_{ok} = \rho_{c.ok} + \frac{\beta_{ok}}{\beta_r}(\rho_r - \rho_{c.r}).$$

However, a rigorous functional link between random quantities is rarely achieved, and most frequently such a link cannot be established at all. More frequently there arise statistical relations between random quantities, whereby a change in one quantity results in a change in distribution of the other. In particular, a statistical interrelationship is manifested in the fact that with a change in one quantity there is a change in the mean value of the other, and in this instance the statistical relationship is called a correlation.

A correlation between random quantities x and y is evaluated on the basis of the magnitude of dispersion of values y around conditional mean y_x. Dispersion is characterized by second correlation moment $K_{x, y}$, the value of which can be determined from the data of a set of observations, employing the formula

$$K_{x,y} = \frac{1}{n-1}\sum_{i=1}^{n}(x_i - m_x)(y_i - m_y). \qquad (2.3)$$

A dimensionless correlation value is determined by ratio $r_{x,y} = K_{x,y}/\sigma_x\sigma_y$

which is called a correlation coefficient.

By the magnitude of the correlation coefficient one can judge the degree of statistical relationships between random quantities. When $r_{x, y}=1$ random quantities x and y are linked by a linear functional relation. If $r_{x, y}=0$, random quantities x and y do not have a statistical relationship and influence the system independently.

For system of random quantities $x_1, x_2, \ldots, x_n$, for which statistical characteristics $m_{x1}, m_{x2}, \ldots, m_{xn}$ and $D_{x1}, D_{x2}, \ldots, D_{xn}$, one can determine correlation moments $K_{xi, xj}$ with equation (2.3) and construct a correlation matrix:

$$K = \begin{vmatrix} K_{x_1x_1} & K_{x_1x_2} \dots K_{x_1x_n} \\ K_{x_2x_1} & K_{x_2x_2} \dots K_{x_2x_n} \\ \dots\dots\dots\dots \\ K_{x_nx_1} & K_{x_nx_2} \dots K_{x_nx_n} \end{vmatrix}.$$

The variances of each random quantity are situated on the main diagonal of the matrix, which follows from obvious correlation

$$K_{x_k,x_k} = \frac{1}{n-1}\sum_{i=1}^{n}(x_k - m_x)(x_k - m_x) = D_{x_k}.$$

Proceeding from correlation moments to correlation coefficients, taking into account relation

$$r_{x_k,x_k} = \frac{K_{x_k,x_k}}{\sigma_{x_k}\sigma_{x_k}} = 1$$

and the symmetry of the matrix relative to the diagonal, we can obtain a standardized correlation matrix

$$r_{x_i,x_j} = \begin{vmatrix} 1 & r_{x_1,x_2} \dots r_{x_1,x_n} \\ & 1 \quad \dots r_{x_2,x_n} \\ \dots\dots\dots\dots \\ & & 1 \end{vmatrix}.$$

The statistical relationships between disturbing factors, characterized by correlation coefficients, must be considered during calculation and analysis of precision of engine operation.

2.2. Methods of Analysis and Calculation of the Effect of Disturbances on Engine Characteristics

2.2.1. General Description of Methods

The influence of disturbances on engine operating parameters is established with the aid of static characteristics.

Static characteristics are analytical or graphic relations linking the parameters of a propulsion system under steady-state operating conditions.

Static characteristics can be determined graphically or by analytical methods. Analytical methods presuppose construction of a mathematical engine model in a certain form and elucidation of relationships between

engine characteristics and disturbances. Analytical methods make it possible to obtain the values of any engine parameters of a given design for specific operating conditions and disturbances. The graphic method enables one to plot graphs (nomograms), which graphically characterize interrelationships between operation parameters, but it is not precise enough, and therefore it is employed only for quantitative analysis of the interrelationship of parameters of new engine designs at the preliminary design stage.

Depending on the type of engine mathematical model, the following are designated as analytical methods: direct method, method of small deviations, and statistical method.

2.2.2. Direct Method

Diversified physicochemical processes take place in a motor. On the basis of the general laws of mechanics and theory of motors one constructs equations which link design characteristics and disturbances with the parameters of the operation process. For the majority of engine components these dependences are nonlinear. For example, the mass flow rate of gas from an engine's combustion chamber is determined by the relation

$$\dot{m} = \frac{b(\varkappa)\, p_{\kappa} F_{\kappa p}}{\sqrt{RT_{\kappa}}}.$$

To engine component equations one must add relations which describe the compatibility of engine components to which equations of the consumption and flow rate, pressures and power balance apply. As a result we obtain a system of algebraic equations which is resolved in relation to any engine parameter $y_j = F(y_i, x_i, z_i)$. Since the system has a high order (the number of equations is determined by the engine design) and the majority of equations are nonlinear, even with employment of a computer, solution is very complex and requires considerable time. Therefore this method is employed only for analysis of the static characteristics of individual engine components and for plotting engine throttle and altitude characteristic curves.

2.2.3. Method of Small Deviations

In analyzing static characteristics of an engine, in the final analysis one determines deviations of operation parameters from specified (nominal) values due to the influence of disturbances. Since static characteristics describe engine operation under steady-state conditions, one can make the following assumptions:

deviations of parameters of operation and disturbances are small in comparison with nominal values, that is, $\Delta y_j = y_j - \bar{y}_j \ll \bar{y}_j$;

the principle of superposition applies, that is, one can examine in an isolated manner the influence of individual disturbances and obtain the overall effect by adding together the separate results.

Making these assumptions, we can construct a mathematical engine model by employing the method of small deviations, which in the literature is sometimes called the sensitivity method. Let there be functional relationship $y(x_1, x_2, x_3, \ldots, x_N)$, whereby the nominal (base) value of the function and arguments $\bar{y}(\bar{x}_1, \bar{x}_2, \bar{x}_3, \ldots, \bar{x}_N)$ is known. Then for description of change in function $y(x_1, x_2, \ldots, x_N)$ in the vicinity of nominal values of the arguments we can utilize Taylor's expansion in series. If there exist partial derivative functions

$$\frac{\partial y}{\partial x_i} \text{ up to } (m+1)$$

order of magnitude, then

$$y(x_1, x_2, x_3, \ldots, x_N) - \bar{y}(\bar{x}_1, \bar{x}_2, \ldots, \bar{x}_N) = \frac{\partial y}{\partial x_1}(x_1 - \bar{x}_1) + \ldots + \frac{\partial y}{\partial x_i}(x_i - \bar{x}_i) + \ldots + \frac{\partial y}{\partial x_N}(x_N - \bar{x}_N) + \frac{1}{m!}\left[\frac{\partial}{\partial x_1}(x_1 - \bar{x}_1) + \ldots + \frac{\partial}{\partial x_N}(x_N - \bar{x}_N)\right]^m f(\bar{x}_1, \bar{x}_2, \ldots, \bar{x}_N) + R_m. \quad (2.4)$$

Here

$$\left[\frac{\partial}{\partial x_1}(x_1 - \bar{x}_1) + \ldots + \frac{\partial}{\partial x_N}(x_N - \bar{x}_N)\right]^m f(\bar{x}_1, \bar{x}_2, \ldots, \bar{x}_N) = \sum_{j_1+j_2+\ldots+j_N} \frac{m!}{j_1! \ldots j_i! \ldots j_N!}\left(\frac{\partial^m y}{\partial x_1^{j_1} \partial x_2^{j_2} \ldots \partial x_N^{j_N}}\right)(x_1 - \bar{x}_1)^{j_1} \times \times (x_i - \bar{x}_i)^{j_i} \ldots (x_N - \bar{x}_N)^{j_N}.$$

Summation should be performed for all non-negative integers $j_1, j_2, \ldots, j_N$, which satisfy the condition $j_1+j_2+\ldots+j_N=m$. Partial derivatives are determined with nominal values of $\bar{x}_1, \bar{x}_2, \ldots, \bar{x}_N$. Partial derivatives of (m+1) order enter remainder R_m.

On the basis of the above assumptions we shall perform linearization of relation (2.4), that is, we shall ignore partial derivatives of the second and higher order. We shall then find the full increment of function

$$\Delta y = \frac{\partial y}{\partial x_1}(x_1 - \bar{x}_1) + \cdots + \frac{\partial y}{\partial x_N}(x_N - \bar{x}_N). \quad (2.5)$$

We shall designate $\Delta x_i = x_i - \bar{x}_i$.

As a result relations (2.5) can be rewritten in the form

$$\Delta y = \sum_{i=1}^{N} \frac{\partial y}{\partial x_i} \Delta x_i. \quad (2.6)$$

With linearization of a nonlinear function we obtain error

$$\varepsilon(y) \leqslant \sum_{i=1}^{N} \left|\frac{\partial y}{\partial x_i}\right| |\Delta x_i|,$$

the magnitude of which increases with an increase in the degree of nonlinearity of y (x) and deviation of arguments Δx_i.

Coefficients with argument deviation are called coefficients of sensitivity or coefficients of influence and are designated

$$\bar{a}_i = \frac{\partial y}{\partial x_i} = a_i(\bar{x}, \bar{y}).$$

Thus if the absolute deviation of argument Δx is known, we can easily determine the absolute deviation of function $\Delta y = \bar{a}\Delta x$. In this instance the coefficient of influence possesses dimensionality [y/x]. For a comparative analysis it is more convenient to utilize dimensionless (relative) deviations $\delta y = \Delta y/\bar{y}$; $\delta x = \Delta x/\bar{x}$, and then the coefficients of influence will have zero dimensionality and will be determined with the relation

$$a_i = \frac{\bar{x}_i}{\bar{y}} \bar{a}_i.$$

As a result of employment of the method of small deviations, one can obtain linear equations of the type

$$\delta y = \sum a_i \delta x$$

for all engine components. In this case the engine model is described by a system of linear algebraic equations, which in matrix form appears as AY=BX, where A -- matrix of coefficients with operation parameters; Y -- matrix of engine characteristics; B -- matrix of coefficients with disturbing factors; X -- matrix of disturbing factors.

The latter equation is resolved in relation to any characteristic of engine operation.

2.2.4. Statistical Methods

The above-examined methods make it possible to determine deviations of operation parameters with specified deviations of disturbing factors, that is, to solve a determined problem.

Under actual conditions all disturbing factors are random quantities, as a consequence of which the characteristics of operation will also be random quantities. Methods of mathematical statistics, and specifically probability and regression methods, are being employed to determine the statistical characteristics of operation parameters. In subsequent chapters we shall present the above-listed analytical methods.

Chapter 3. STATIC EQUATIONS OF MOTOR COMPONENTS

3.1. Combustion Chamber and Gas Generator Equation

A principal characteristic of a combustion chamber is the relationship between combustion chamber pressure and rate of consumption of propellant components, characteristics of combustion products and throat area, which has the form

$$p_к = \frac{\beta_к}{F_{кр}}(\dot{m}_{ок} + \dot{m}_г), \qquad (3.1)$$

where β_k -- specific pressure impulse (consumption complex).

The magnitude of the specific pressure impulse depends on composition of the propellant and completeness of combustion, as well as combustion chamber pressure. However, the dependence of β_k on p_k is weak, since with a change in p_k values R and T_k change in opposite directions, while quantity b ($\varkappa$) remains practically constant. Therefore with a specified propellant it is allowable to assume that β_k is dependent only on the ratio of propellant components.

Relation $\beta_k(K)$ can be determined for a given combustion chamber pressure on the basis of results of thermodynamic calculation.

Functional relation (3.1) is written in the form

$$p_к = p_к(\beta_к, F_{кр}, \dot{m}_{ок}, \dot{m}_г).$$

We shall rewrite the last equation in variations

$$\delta p_к = a_{p_к, \dot{m}_{ок}}\delta\dot{m}_{ок} + a_{p_к, \dot{m}_г}\delta\dot{m}_г + a_{p_к, K}\delta K + b_{p_к, F_{кр}}\delta F_{кр}. \qquad (3.2)$$

Coefficients of influence $a_{pk, x}$, $b_{pk, x}$ are obtained from equation (3.1) by means of differentiation

$$a_{p_к, \dot{m}_l} = \frac{\bar{\dot{m}}_l}{\bar{p}_к}\frac{\partial p_к}{\partial \dot{m}_l}; \quad \frac{\partial p_к}{\partial \dot{m}_l} = \frac{\bar{p}_к}{\bar{\dot{m}}},$$

where $\bar{\dot{m}} = \bar{\dot{m}}_{ок} + \bar{\dot{m}}_г$.

Solving congruently written relations taking into account ratios

$$\frac{\dot{m}_{ok}}{\dot{m}} = \frac{\bar{K}}{\bar{K}+1}; \quad \frac{\dot{m}_r}{\dot{m}} = \frac{1}{\bar{K}+1},$$

we obtain

$$a_{p_k,\ \dot{m}_{ok}} = \frac{\bar{K}}{\bar{K}+1}; \quad a_{p_k,\ \dot{m}_r} = \frac{1}{\bar{K}+1}; \quad b_{p_k,\ p_{kp}} = -1.$$

The coefficient of influence for propellant component ratio is determined as follows. The specific pressure impulse is determined by the ratio of propellant components.

This relation can be determined from the results of thermodynamic calculations.

$$\frac{\partial p_k}{\partial \bar{K}} = \operatorname{tg}\alpha = a_p,$$

where α -- angle of inclination of the tangent to curve $\beta_k = f(K)$ at point $\bar{K}$, β_k.

$$a_{p_k,\ K} = \frac{\bar{K}}{\beta_k} a_p, \qquad (3.3)$$

since

$$\frac{\partial p_k}{\partial p_k} = \frac{p_k}{\beta_k}.$$

Based on the results of thermodynamic calculation, relation $\beta_k = \beta(K)$ can be approximated by a polynomial of the type

$$\beta_k = c_2 K^2 + c_1 K + c_0, \qquad (3.4)$$

where c_0, c_1, c_2 -- propellant constants.

In this case

$$a_{p_k,\ K} = \frac{\bar{K}}{\beta_k}(2c_2\bar{K} + c_1).$$

Relative coefficients of influence characterize the degree of interrelationship of combustion chamber characteristics. The magnitudes of the coefficients of influence are determined by nominal combustion chamber parameters and propellant properties.

For NDMG and AT propellant, for example, in relation to combustion chamber pressure the correlation of propellant components varies as follows:

$$K = 2.12\text{-}2.95; \quad \beta_k = (1700\text{-}1750)\ c, \quad \alpha_p = 0.001.$$

In conformity with the above figures, the coefficients of influence are characterized by the following quantities:

$$a_{p_к,\dot{m}_{ок}} = 0{,}68—0{,}75;\quad a_{p_к,\dot{m}_г} = 0{,}32—0{,}25;\quad a_{p_к,K} = (1{,}2 — 1{,}7)\cdot 10^{-5}.$$

The gas generator equation is written analogously to the combustion chamber equation.

When analyzing coefficients of influence one must bear in mind the following. The magnitude of the coefficients of influence of any engine component reflects the mutual influence of parameters only under conditions of isolated operation of that component. Components are interrelated in engine operation, and the interaction between parameters will be different, which will determine other values of coefficients of influence.

3.2. Pump Equations

Pump operation is characterized by head and output. In place of head, in calculating static characteristics one employs pressure at pump outlet. In this case pump characteristics have the following form:

$$p_н = p_н(\dot{m},\ n,\ \rho,\ p_0,\ D);$$
$$N_н = N_н(\dot{m},\ n,\ \rho,\ p_0,\ D,\ \eta), \qquad (3.5)$$

where D -- geometric characteristic; η -- efficiency.

In variations, equations (3.5) are written as follows:

$$\delta p_н = \sum a_{p_н,\ y_j}\delta y_j + \sum b_{p_н,\ x_i}\delta x_i; \qquad (3.6)$$

$$\delta N_н = \sum a_{N_н,\ y_j}\delta y_j + \sum b_{N_н x_i}\delta_{x_i}, \qquad (3.7)$$

where $y_j = \overline{\dot{m},\ n},\ x_i = \overline{\rho,\ D,\ \eta}$.

Coefficients of influence are determined with pump equations [3]:

$$p_н = A\rho n^2 - Bn\dot{m} - c\frac{\dot{m}^2}{\rho} + p_0; \qquad (3.8)$$

$$N_н = \frac{(p_н - p_0)\dot{m}}{\eta_н \rho}, \qquad (3.9)$$

where

$$A = \frac{1}{q_н}\left(\frac{\pi}{60}\right)^2(D_2^2 - D_1^2);$$

$$B = \frac{1}{60q_н}\left(\frac{1}{b_2 k_2 \operatorname{tg}\beta_2} - \frac{1}{b_1 k_1 \operatorname{tg}\beta_1}\right);$$

$$C = \xi + \frac{1}{2q_н}\left(\frac{1}{F^2_{вых}} - \frac{1}{F^2_{вх}}\right);$$

$q_л$ -- coefficient taking into account pressure decrease due to a finite number of blades ($q_л$=1.1-1.3); ξ -- a coefficient which takes into account pressure losses in overcoming hydraulic resistance in the pump blading; D_2, D_1, b_2, b_1, β_2, β_1 -- geometric characteristics of pump blading.

Following differentiation of equations (3.8) and (3.9) and simple transformations taking into consideration inequalities $p_H \gg p_0$, we obtain expressions for coefficients of influence

$$a_{p_H, n} = \frac{2A\bar{\rho}\bar{n}^2 - B\bar{n}\bar{m}}{\bar{p}_H}; \quad a_{p_H, \dot{m}} = -\frac{B\bar{n}\bar{m} + \frac{2C\bar{m}^2}{\bar{\rho}}}{\bar{p}_H};$$

$$b_{p_H, \rho} = \frac{A\bar{\rho}\bar{n}^2 + \frac{C\bar{m}^2}{\bar{\rho}}}{\bar{p}_H}; \quad b_{p_H, p_0} = \frac{\bar{p}_0}{\bar{p}_H}; \quad b_{p_H, D} = \frac{\bar{D}}{\bar{p}_H}\frac{\partial p_H}{\partial D};$$

$$a_{N, n} = a_{p_H, n}; \quad a_{N, \dot{m}} = 1 + a_{p_H, \dot{m}};$$

$$b_{N, \rho} = b_{p_H, \rho} - 1; \quad b_{N, p_0} = 0;$$

$$b_{N, D} = b_{p_H, D}; \quad b_{N, \eta} = -1.$$

Coefficients of influence in pump equations can be determined from the pump flow rate characteristic and similarity relations.

From the pump pressure-flow rate characteristic, which can be obtained as a result of tests on pumps, we have

$$a_{p_H, \dot{m}} = \frac{\bar{m}}{\bar{p}_H} \operatorname{tg}\alpha_H, \qquad (3.10)$$

where α_H -- angle of inclination of the tangent to the pump characteristic curve at point $\bar{m}$, $\bar{p}_H$.

We know from general pump theory a correlation which determines similar conditions [3]:

$$p_H = \left(\frac{n}{\bar{n}}\right)^2 \frac{\rho}{\bar{\rho}} \left(\frac{D_2}{\bar{D}_2}\right)^2 p_H \left(\frac{\dot{m}}{\bar{n}} n \frac{\bar{\rho}}{\rho} \frac{\bar{D}_2^2}{D_2^2}\right). \qquad (3.11)$$

Differentiating equation (3.11) taking into account relation (3.10), we have

$$a_{p_H, n} = 2 - \frac{\bar{m}}{\bar{p}_H} \operatorname{tg}\alpha_H;$$

$$b_{p_H, \rho} = 1 - \frac{\bar{m}}{\bar{p}_H} \operatorname{tg}\alpha_H;$$

$$b_{p_H, D_2} = 2 - 3\frac{\bar{m}}{\bar{p}_H} \operatorname{tg}\alpha_H.$$

3.3. Turbine Equations

Turbines employed in ZhRD as pump-drive turbines are usually impulse turbines with velocity stages or pressure turbines. Most frequently impulse turbines are employed in engines without generator gas afterburning, and pressure turbines in engines with afterburning of generator gas.

The principal relation describing turbine operation is a turbine power equation. Power is determined by gas flow rate (pressure), adiabatic work performed by gas expansion in the turbine, and efficiency, that is,

$$N_т = \dot{m}_т L_{ад} \eta_т. \qquad (3.12)$$

Following linearization of relation (3.12) we obtain a turbine equation written in variations

$$\delta N_т = \delta \dot{m}_т + \delta L_{ад} + \delta \eta_т. \qquad (3.13)$$

We shall determine variables $\delta \dot{m}_т$, $\delta L_{ад}$ and $\delta \eta_т$, which enter equations (3.13); for this we shall utilize relation (3.10).

The rate of gas flow through a turbine depends on the type type of gas flow in the blading and is determined by turbine type. For supercritical flow conditions (impulse turbines) the rate of gas flow through the turbine is determined by relation

$$\dot{m}_т = \frac{b(\varkappa) p_{тг} F_c}{\sqrt{RT_т}},$$

and variation of flow rate $\delta \dot{m}_т = \delta p_{тг} - 0{,}5\delta RT_т + \delta F_c$. The capability of gas to perform work $RT_т$ is determined by the ratio of propellant components in the gas generator K and is practically independent of pressure. Relation $RT_т = f(K)$ is determined as a result of thermodynamic calculation and can be described by the correlation

$$\delta \overline{RT}_т = \frac{\overline{K}}{\overline{RT}_т} \frac{\partial RT_т}{\partial K}.$$

Substituting the last correlation in the equation for $\delta \dot{m}_т$, we obtain

$$\delta \dot{m}_т = \delta p_{тг} - a_{\dot{m}_т, K} \delta K + \delta F_c, \qquad (3.14)$$

where

$$a_{\dot{m}_т, K} = 0{,}5 \frac{\overline{K}}{\overline{RT}_т} \frac{\partial RT_т}{\partial K}.$$

For subcritical flow, characteristic of pressure or reaction turbines, gas flow rate through the turbine is determined by relation

$$\dot{m}_т = F_c \sqrt{\frac{2\varkappa}{\varkappa - 1} \frac{p_{тг}^2}{RT_т} \left[\left(\frac{p_{1т}}{p_{тг}} \right)^{\frac{2}{\varkappa}} - \left(\frac{p_{1т}}{p_{тг}} \right)^{\frac{\varkappa+1}{\varkappa}} \right]}, \qquad (3.15)$$

where F_c -- nozzle throat area, p_{1T} -- pressure at turbine nozzle exit. Pressure at turbine inlet p_{1T} depends on the degree of turbine reaction

$$p_{1T} = p_{TT}\left[\rho - (1-\rho)\left(\frac{p_{2T}}{p_{TT}}\right)^{\frac{\varkappa-1}{\varkappa}}\right]^{\frac{\varkappa}{\varkappa-1}}, \qquad (3.16)$$

where ρ -- degree of turbine reaction; p_{2T} -- gas pressure at turbine outlet.

Degree of turbine reaction is determined by a semiempirical relation of type [5]

$$\rho = a + b\left(\frac{u}{c_1}\right) + c\left(\frac{u}{c_1}\right)^2, \qquad (3.17)$$

where a, b, c -- experimental constants; u -- turbine blade tip speed;

$$u = \frac{\pi d_T}{60};$$

c_1 -- gas velocity at nozzle exit. Variation of gas flow rate through the turbine is obtained from equation (3.15)

$$\delta\dot{m}_T = \delta F_c + \delta p_{TT} - a_{\dot{m}_T, K}\delta K + \alpha_T(\delta p_{1T} - \delta p_{TT}), \qquad (3.18)$$

where

$$\alpha_T = \frac{2\left(\frac{\bar{p}_{1T}}{\bar{p}_{TT}}\right)^{\frac{1}{\varkappa}} - (\varkappa+1)\left(\frac{\bar{p}_{1T}}{\bar{p}_{TT}}\right)^{\frac{\varkappa+1}{\varkappa}}}{2\varkappa\left[\left(\frac{\bar{p}_{1T}}{\bar{p}_{TT}}\right)^{\frac{2}{\varkappa}} - \left(\frac{\bar{p}_{1T}}{\bar{p}_{TT}}\right)^{\frac{\varkappa+1}{\varkappa}}\right]}.$$

Following linearization of equations (3.16) and (3.17) and their common solution, we obtain

$$\delta p_{1T} = a_1(\delta n - \delta c_1) + a_2\delta p_{2T} + a_3\delta p_{TT}, \qquad (3.19)$$

$$a_1 = \frac{\varkappa}{\varkappa+1}\frac{\bar{b}\bar{\rho}\left[1 - \left(\frac{\bar{p}_{2T}}{\bar{p}_{1T}}\right)^{\frac{\varkappa-1}{\varkappa}}\right]}{\bar{C}};$$

where

$$a_2 = \frac{(1-\bar{\rho})\left(\frac{\bar{p}_{2T}}{\bar{p}_{TT}}\right)^{\frac{\varkappa-1}{\varkappa}}}{\bar{C}}; \quad a_3 = \frac{\bar{\rho}}{\bar{C}};$$

$$\bar{b} = \frac{1}{\bar{\rho}}\left[b\left(\frac{\bar{u}}{\bar{c}_1}\right) + 2C\left(\frac{\bar{u}}{c_1}\right)^2\right];$$

$$\bar{C} = \bar{\rho} + (1 - \bar{\rho}) \left(\frac{\bar{p}_{ST}}{\bar{p}_{TT}} \right)^{\frac{\varkappa - 1}{\varkappa}}.$$

Adiabatic work by gas in the turbine

$$L_{aA} = \frac{\varkappa}{\varkappa - 1} RT_T \left[1 - \left(\frac{p_{ST}}{p_{TT}} \right)^{\frac{\varkappa - 1}{\varkappa}} \right] \quad \text{or} \quad L_{aA} = \frac{c_1^2}{2}. \tag{3.20}$$

Following linearization of equation (3.20) we obtain

$$\delta L_{aA} = 2\delta c_1 = a_{L,K} \delta K - \beta_T (\delta p_{ST} - \delta p_{TT}), \tag{3.21}$$

where

$$a_{L,K} = 2a_{\dot{m}_T,K}; \quad \beta_T = \frac{(\varkappa - 1) \left(\frac{\bar{p}_{ST}}{\bar{p}_{TT}} \right)^{\frac{\varkappa - 1}{\varkappa}}}{2\varkappa \left[1 - \left(\frac{\bar{p}_{ST}}{\bar{p}_{TT}} \right)^{\frac{\varkappa - 1}{\varkappa}} \right]}.$$

Turbine efficiency is determined by parameter u/c_1 that is, $\eta_T = f(u/c_1)$.

A variation of turbine efficiency can be presented in the form

$$\delta\eta_T = \psi_\eta (\delta n - \delta c_1), \tag{3.22}$$

where

$$\psi_\eta = \frac{\bar{u}/c_1}{\bar{\eta}_T} \frac{\partial \eta_T}{\partial \left(\frac{u}{c_1} \right)}.$$

Substituting relations (3.18), (3.19), (3.21) and (3.22) in original equation (3.13), we obtain reaction turbine power variation equation

$$\delta N_T = \delta F_c + a_{N_T, p_{TT}} \delta p_{TT} + a_{N_T, p_{ST}} \delta p_{2T} + a_{N_T, n} \delta n + a_{N_T, K} \delta K, \tag{3.23}$$

where

$$a_{N_T, p_{TT}} = 1 - \alpha_T (1 - a_3) - \beta_T \left(\frac{\alpha_T a_1 - \psi_\eta}{2} - 1 \right);$$

$$a_{N_T, p_{ST}} = \beta_T \left(\frac{\alpha_T a_1 - \psi_\eta}{2} - 1 \right) + \alpha_T a_2;$$

$$a_{N_T, n} = \alpha_T a_1 + \psi_\eta;$$

$$a_{N_T, K} = a_{\dot{m}_T, K} (1 - \alpha_T a_1).$$

For an impulse turbine, characteristic of which are critical or supercritical flow conditions, a turbine power variation can be obtained from equation (3.23). In this case condition

$$\alpha_T = 0, \beta_T = 0,$$

applies, and the coefficients of influence in equation (3.23) will be determined by the relations:

$$a_{N_T,\, p_{\Gamma\Gamma}} = 1;\ a_{N_T,\, n} = \psi_n;$$

$$a_{N_T,\, p_{\Gamma T}} = 0;\ a_{N_T,\, K} = a_{\dot{m}_T,\, K}.$$

3.4. Supply Line Equations

ZhRD equipment (pumps, turbines, gas generators, combustion chambers) contain ducts through which liquid or gas flows, and engine components are linked by hydraulic or gas lines. Therefore the principal stages of operating processes, which determine the characteristics of an engine as a whole, take place both in flow ducts and lines. Let us examine the static characteristics of hydraulic and gas lines.

3.4.1. Hydraulic Lines

Hydraulic lines link the pumps with combustion chamber and gas generator (pressure lines) and propellant tanks with pumps (suction lines). Dependences of pressure differential, that is, hydraulic resistance, on rate of flow and density of propellant and geometric dimensions of the line constitute the static characteristics of all lines. In the general form a static characteristic of a line is described by functional relation

$$\Delta p = \Delta p\,(\dot{m},\ \rho,\ D).$$

Pressure losses Δp in the line are formed of line and local losses.

Line losses are determined by hydraulic losses, caused primarily by friction by the conveyed liquid against the wall of the line, and are characterized by the relation

$$\Delta p_{Tl} = \lambda_l \frac{l_l}{d_{el}} \frac{\rho w_l^2}{2}, \qquad (3.24)$$

where λ_l -- coefficient taking into account liquid friction against the line walls; w_l -- velocity of liquid movement; l, d_e -- line length and equivalent diameter respectively.

Pressure losses for overcoming local resistances are proportional to dynamic pressure

$$\Delta p_{M,\, l} = \varepsilon_l \frac{\rho w_l^2}{2}, \qquad (3.25)$$

where ε -- coefficient of local resistances.

Local resistances in hydraulic lines can be constant and variable.

Engine lines consist of a number of sections, which differ from one another in geometric dimensions, and may contain several different local constant and variable hydraulic resistances.

Total losses for the entire line are determined by the sum of all components

$$\Delta p_\tau = \sum_{i=1}^{n} \Delta p_{\tau, i}; \quad \Delta p_M = \sum_{i=1}^{n} \Delta p_{M, i}. \qquad (3.26)$$

Velocity of the conveyed liquid in i section of the line is determined by equation of discontinuity

$$w_i = \frac{\dot{m}}{\rho F_i}.$$

Substituting the last relation in equation (3.26), we obtain

$$\Delta p_\tau = R \frac{\dot{m}^2}{\rho}; \quad \Delta p_M = \xi \frac{\dot{m}^2}{\rho}, \qquad (3.27)$$

where $R = \frac{1}{2} \sum_{i=1}^{n} \lambda_i \frac{l_i}{F_i^2 d_{ei}}$ -- total coefficient of line losses;

$\xi = \frac{1}{2} \sum_{i=1}^{n} \frac{\varepsilon_i}{F_i}$ -- total coefficient of local losses.

If we designate pressure at line inlet p_1, and outlet p_2, the line equation will be written in the form

$$\Delta p = p_1 - p_2 = (R + \xi) \frac{\dot{m}^2}{\rho}. \qquad (3.28)$$

Following linearization and transformations, we obtain a line equation in the form

$$\delta \Delta p = 2\delta \dot{m} - \delta \rho + b_{\Delta p, R} \delta R + b_{\Delta p, \xi} \delta \xi, \qquad (3.29)$$

where

$$b_{\Delta p, R} = 1 - \frac{\Delta \bar{p}_\tau}{\Delta \bar{p}}; \quad b_{\Delta p, \xi} = 1 - \frac{\Delta \bar{p}_M}{\Delta \bar{p}}.$$

In a number of cases, for analysis of characteristics it is necessary to have variations not of pressure differential but pressure at line outlet. For these cases the line equation is written in the form

$$\delta p_2 = a_{p_2, p_1} \delta p_1 - a_{p_2, \dot{m}} \delta \dot{m} + b_{p_2, \rho} \delta \rho - b_{p_2, R} \delta R - b_{p_2, \xi} \delta \xi, \quad (3.30)$$

where

$$a_{p_2, p_1} = \frac{\bar{p}_1}{\bar{p}_2}; \quad a_{p_2, \dot{m}} = 2 \frac{\Delta \bar{p}}{\bar{p}_2}; \quad b_{p_2, \rho} = \frac{\Delta \bar{p}}{\bar{p}_2};$$

$$b_{p_2, R} = \frac{\Delta \bar{p}_\tau}{\bar{p}_2}; \quad b_{p_2, \xi} = \frac{\Delta \bar{p}_M}{\bar{p}_2}.$$

3.4.2. Gas Lines

In propulsion systems with generator gas afterburning, the combustion chamber is connected to the turbine by a gas line which has gas resistances on the injectors and other elements.

A gas line equation, similar to a hydraulic line equation, is written in the form

$$p_{gT} - p_K = \xi_r \frac{\dot{m}^2}{\rho_{rr}}, \qquad (3.31)$$

where ξ_r -- resistance coefficient; ρ_{rr} -- average gas density in the line.

Average gas density can be determined from the relation

$$\rho_{rr} = \frac{p_{gT} + p_K}{R_{gT}T_{gT} + RT_K}, \qquad (3.32)$$

where T_{2T} -- gas temperature beyond the turbine.

Gas temperature beyond the turbine differs from temperature in the gas generator due to the work performed by the gas in the turbine. In order to determine gas temperature drop in the turbine, we shall utilize known relation

$$c_p(T_{rr} - T_{gT}) = \frac{c_1}{2}\eta_T. \qquad (3.33)$$

From equation (3.31) we have

$$\delta\Delta p_{rв} = \delta\xi_r + 2\delta\dot{m} - \delta p_{rr}, \qquad (3.34)$$

where

$$\Delta p_{rв} = p_{gT} - p_K \text{ и } \delta\Delta p_{rв} = \frac{\bar{p}_{gT}}{\Delta\bar{p}_{rв}}\delta p_{gT} - \frac{\bar{p}_K}{\Delta\bar{p}_{rв}}\delta p_K.$$

Accepting assumption $R_{2T}=R_K=R$ from equation (3.32) we obtain

$$\delta\rho_{rr} = \delta\Delta p_{rв} - \frac{\bar{T}_{gT}}{\bar{T}_{gT}+\bar{T}_K}\delta T_{gT} - \frac{\bar{T}_K}{\bar{T}_{gT}+\bar{T}_K}\delta T_K. \qquad (3.35)$$

From equation (3.33), assuming c_p=const, we obtain

$$\frac{\bar{T}_{rr}}{\bar{T}_{rr}-\bar{T}_{gT}}\delta T_{rr} - \frac{\bar{T}_{gT}}{\bar{T}_{rr}-\bar{T}_{gT}}\delta T_{gT} = 2\delta c_1 + \delta\eta_T. \qquad (3.36)$$

Following common solution of equations (3.34)-(3.36) and taking into account relations (3.21) and (3.22), we finally obtain gas line equations:

$$\delta\Delta p_{rв} = \delta\xi_r + \delta\dot{m} + a_{\Delta p_{rв}, K'}\delta K' + a_{\Delta p_{rв}, K''}\delta K'' - a_{\Delta p_{rв}, n}\delta n; \qquad (3.37)$$

$$a_{\Delta p_{rв}, K'} = \frac{\bar{T}_K}{2(\bar{T}_{gT}+\bar{T}_K)}\psi_{T_{rr}};\ \psi_{T_{rr}} = \frac{\bar{K}''}{\bar{T}_{rr}}\frac{\partial T_{rr}}{\partial K''};$$

$$a_{\Delta p_{rв}, K''} = \frac{\bar{T}_{rr}}{2(\bar{T}_{gT}+\bar{T}_K)}\psi_{T_K};\ \psi_{T_K} = \frac{\bar{K}'}{\bar{T}_K}\frac{\partial T_K}{\partial K'};$$

$$a_{\Delta p_{гв}, n} = \frac{\overline{T}_{гг} - \overline{T}_{вг}}{2(\overline{T}_{вг} + \overline{T}_{н})} \psi_{\eta};$$

K', K'' -- ratio of propellant components in the combustion chamber and gas generator respectively.

3.5. Pressure Accumulator Equations

In propulsion systems with gas pressurization supply systems, the propellant components are forced from the tanks by pressure accumulators. The most common are gas pressure accumulators and solid fuel pressure accumulators (GAD and PAD). In both cases pressure in the tanks, by means of which the pressure force is generated, is determined by the characteristics of the accumulators.

3.5.1. Gas Pressure Accumulator

Gas is fed from a tank under high pressure into a gas pressure reducer, in which pressure is reduced to the required level, and from which it is fed into the tank to force out propellant. Thus pressure above the surface of the propellant in the tank will be determined primarily by precision of reducer performance and the characteristics of the gas accumulator. Initial gas pressure in the tanks is determined by the conditions of tank filling. Final pressure in the compressed gas tank should be greater than supply pressure $p_б$ by the magnitude of minimum pressure drop in the reducer $\Delta p_р$, requisite to ensure normal reducer operation. $\Delta p_р$ is determined by reducer design and depends on supply pressure. At high supply pressures

$$\Delta p_р = l_{p_р}, \text{ where } p_р \text{ -- reducer outlet pressure,}$$
$$l = 0.25 \ldots 0.4.$$

Taking into account gas orificing and its expansion in the tank in the process of pressurization, the gas pressure accumulator operation equation has the form

$$(p_б + l_{p_р}) V_{газ} = p_{г.н} V_{газ} c_1 - \frac{c_1}{c_2} p_б V_б, \qquad (3.38)$$

where $V_{газ}$ -- volume of compressed gas tanks; $p_{г.н}$ -- initial gas pressure in compressed gas tank; $V_б$ -- volume of propellant tank;

$$c_1 = \left(\frac{p_{г.к}}{p_{г.н}}\right)^{\frac{\varkappa - 1}{\varkappa}}; \quad c_2 = \frac{T_{б.к}}{T_{г.н}}.$$

The values of coefficients c_1 and c_2 are determined by the polytropic curve index and pressure differential $p_{г.к}/p_{г.н}$ and are indicated in Table 3.1.

Table 3.1.

$\frac{p_{г.н}}{p_{г.к}}$	10	7	4	2
c_1	0,55	0,60	0,70	0,82
c_2	0,75	0,80	0,87	0,90

Equation (3.38) is resolved in relation to tank pressure:

$$p_б = b_1 p_{р.н} - b_2 p_р, \tag{3.39}$$

where

$$b_1 = \frac{c_1}{1 + \frac{c_1}{c_2}\frac{V_б}{V_{газ}}}; \quad b_2 = \frac{1}{1 + \frac{c_1}{c_2}\frac{V_б}{V_г}}.$$

Pressure at reducer outlet is determined by reducer design and pressure at reducer inlet. The value of maximum pressure deviation at reducer outlet from nominal (initial value) $\Delta p_р = p_р - p_{р0}$ is stated in the data supplied by the reducer manufacturer. Tank pressure variation with a gas pressure accumulator has the form

$$\delta p_б = b_{p_б, p_{р.н}} \delta p_{р.н} - b_{p_б, p_р} \delta p_р, \tag{3.40}$$

where

$$b_{p_б, p_{р.н}} = \frac{b_1 \bar{p}_{р.н}}{\bar{p}_б}; \quad b_{p_б, p_р} = \frac{b_2 \bar{p}_р}{\bar{p}_б}.$$

3.5.2. Solid Fuel Pressure Accumulator

With employment of a solid fuel or cartridge pressure accumulator, fuel is forced from the tanks by solid fuel combustion products. Utilizing equation of state and balance of arrival of solid propellant gases into the propellant tank and rate of flow from the propellant tanks, one can obtain a tank pressure equation [1]:

$$p_б = \frac{F_п u \rho_п f_0}{V_б \psi},$$

where $F_п$ -- propellant charge combustion surface; u -- rate of cartridge combustion; $\rho_п$ -- density of solid propellant; f_0 -- reduced solid propellant force; ψ -- coefficient of solid propellant gas energy losses in the tanks.

The last equation, written in variations, has the form

$$\delta p_б = \delta F_п + \delta u + \delta \rho_п + \delta f_0 - \delta V_б - \delta \psi. \tag{3.41}$$

3.6. Thrust Characteristics

Thrust and specific thrust impulse are propulsion system output characteristics, which determine its economy and ballistic capabilities.

Propulsion system thrust is determined by the relation $P = \dot{m} I_y$.

In variations the last equation is written in the form

$$\delta P = \delta \dot{m} + \delta I_y. \qquad (3.42)$$

Specific thrust impulse, as we know from theory of engines, is determined by the quality of organization of the operation process, ratio of propellant components, combustion chamber pressure, and degree of expansion of gases:

$$I_y = I_y(\rho_k, K, \pi_a),$$

where

$$\pi_a = \frac{p_a}{p_k}.$$

In variations specific thrust impulse is written in the form

$$\delta I_y = a_{I,K}\delta K + a_{I,p_k}\delta p_k + a_{I,\pi_a}\delta\pi_a, \qquad (3.43)$$

where coefficients of influence $a_{I,x}$ are obtained from relation

$$a_{I,x} = \frac{\bar{x}}{\bar{I}_y}\frac{\partial I_y}{\partial x};$$

$\frac{\partial I_y}{\partial x}$-- are determined from the results of thermodynamic calculation [1].

Equation (3.43) is valid for an engine with generator gas afterburning. For an engine without generator gas afterburning specific thrust impulse is determined by relation (1.15)

$$I_y = I_{y,a}(1 - \varepsilon_I), \qquad (3.44)$$

where

$$\varepsilon_I = \frac{\dot{m}_{o.c}}{\dot{m}_\Sigma}\left(1 - \frac{I_{y.o.c}}{I_{y.a}}\right).$$

Designating $\dot{m}_{o.c}/\dot{m} = \bar{q}$, we obtain engine specific thrust impulse variation

$$\delta I_y = a_{I,\ I_a}\delta I_{y.a} + a_{I,\bar{q}}\delta\bar{q} + a_{I,\ I_{o.c}}\delta I_{y.o.c}, \qquad (3.45)$$

where

$$a_{I,\ I_a} = \frac{\bar{I}_{y.a}}{\bar{I}_y}(1 - \bar{q});$$

$$a_{I,\bar{q}} = \frac{\bar{q}}{\bar{I}_y}(\bar{I}_{y.a} - \bar{I}_{y.o.c});$$

$$a_{I,\ I_{o.c}} = \frac{\bar{I}_{y.o.c}}{\bar{I}_y}\bar{q}.$$

A thrust equation for an engine without generator gas afterburning is

$$P=P_k+P_{o.c}.$$

A variation of the engine thrust equation

$$\delta P = a_{P,\ P_K}\delta P_K + a_{P,\ P_{o.c}}\delta P_{o.c}, \qquad (3.46)$$

where

$$a_{P,\ P_K}=\frac{\overline{P}_K}{\overline{P}};\quad a_{P,\ P_{o.c}}=\frac{\overline{P}_{o.c}}{\overline{P}}.$$

Chapter 4. ENGINE STATIC CHARACTERISTICS (DETERMINED PROBLEM)

4.1. General Solution

At the stage of designing a propulsion system it is necessary to evaluate the effect of disturbances on operating parameters in order to elaborate engineering-design measures to ensure the desired precision and reliability.

Static characteristics make it possible to establish the mutual influence of components during their concurrent operation with specific design characteristics of motors, propellant components, and ambient conditions.

Input data for obtaining static characteristics are the following:

propulsion system design and nominal (by specifications) engine operation parameter values;

composition and characteristics of disturbing factors;

propulsion system component equations written in variations.

In the general case the method of calculating static characteristics consists in the following. For a concrete propulsion system design one formulates pump and turbine outputs, pressures and flow rates balance equations. After substituting component and line equations in these balance relations, one obtains a system of equations which is written in standard form:

$$\left\{\sum_{j=1}^{N} a_{j,i}\delta y_j = \sum_{K=1}^{M} b_{j,K}\delta x_K\right\}, \qquad (4.1)$$

where δy_j -- variations of operating process parameters; δx_K -- variations of disturbing factors; j -- number of equation in the system, i=1, L; j=1, N; K=1, M.

System of equations (4.1) can be rewritten in matrix form

$$A|\delta y| = B|\delta x|, \qquad (4.2)$$

where $A = \begin{vmatrix} a_{11} & a_{12} & a_{13} & \dots & a_{1N} \\ a_{21} & a_{22} & a_{23} & \dots & a_{2N} \\ \dots & \dots & \dots & \dots & \dots \\ a_{L1} & a_{L2} & a_{L3} & \dots & a_{LN} \end{vmatrix}$ -- matrix of equation coefficients on its left side;

$B = \begin{vmatrix} b_{11} & b_{12} & \dots & b_{1M} \\ b_{21} & b_{22} & \dots & b_{2M} \\ \dots & \dots & \dots & \dots \\ b_{L1} & b_{L2} & \dots & b_{LM} \end{vmatrix}$ -- matrix of equation coefficients on its right side;

$\delta y = \begin{vmatrix} \delta y_1 \\ \delta y_2 \\ \dots \\ \delta y_N \end{vmatrix}$; $\delta x = \begin{vmatrix} \delta x_1 \\ \delta x_2 \\ \dots \\ \delta x_M \end{vmatrix}$ -- matrices of variations of propulsion system characteristics and disturbance variations.

Equation (4.2) is resolved relative to any operating process characteristic

$$|\delta y| = A^{-1}B|\delta x|. \qquad (4.3)$$

System of equations (4.1) can be formulated for propulsion systems in such a manner that matrix A is quadratic [1=N]. In this case equation (4.3) is resolved in determinants

$$\delta y_j = \sum_{K=1}^{M} C_{j,K}\delta x_K, \qquad (4.4)$$

where $C_{j,k}$ -- coefficient of influence of x_k disturbance on operating process parameter y_j, which is defined as follows:

$$C_{j,K} = \frac{\Delta_{j,K}}{\Delta};$$

Δ -- determinant of matrix A; $\Delta_{j,k}$ -- additional determinant obtained by substituting in matrix A, in place of the column corresponding to y_j parameter, the column from matrix B, corresponding to x_k disturbance.

4.2. Model of Propulsion System With Gas Pressurization Supply System

Figure 1.1 contains a diagram of a propulsion system.

Balance equations for this engine layout have the following form:

oxidizer system equation

$$p_{6.ok} = p_k + \Delta p_{ok} - n\rho_{ok}H_{ok}; \qquad (4.5)$$

fuel system equation

$$p_{6.r} = p_k + \Delta p_r - n\rho_r H_r, \qquad (4.6)$$

where $n\rho_j H_j$ -- static pressure of propellant component column; n -- calculated coefficient of rocket axial G-loading.

Since H_j and n change in flight, static pressure is also a variable quantity. When calculating deviations of propulsion system characteristics, for definiteness one assumes static pressure for the initial or final moment of engine operation.

Assume the propulsion system has a gas pressure accumulator; then following linearization of equations (4.5, 4.6) and substitution of relations (3.40), (3.29) and (3.2), we obtain a system written in standard form:

$$\left.\begin{aligned}
&\delta p_к - a_{p_к,\dot m_{ок}}\delta\dot m_{ок} - a_{p_к,\dot m_г}\delta\dot m_г = -\delta F_{кр};\\
&\bar p_к\delta p_к + 2\Delta\bar p_{ок}\delta\dot m_{ок} = \bar p_{б.ок}b_{p_{б.ок},p_{г.н}}\delta p_{г.н} -\\
&\quad -\bar p_{б.ок}b_{p_{б.ок}p_р}\delta p_р - (\Delta\bar p_{ок}+\Delta\bar p_{ст})\delta\rho_{ок} -\\
&\quad -\Delta\bar p_{ок}b_{\Delta p_{ок},\xi_{ок}}\delta\xi_{ок};\\
&\bar p_к\delta p_к + 2\Delta\bar p_г\delta\dot m_г = \bar p_{б.г}b_{p_{б.г},p_{г.н}}\delta p_{г.н} -\\
&\quad -\bar p_{б.г}b_{p_{б.г},p_р}\delta p_р - (\Delta\bar p_г+\Delta\bar p_{ст})\delta\rho_г -\\
&\quad -\Delta\bar p_г b_{\Delta p_г,\xi_г}\delta\xi_г.
\end{aligned}\right\} \qquad (4.7)$$

Matrix |A| of Coefficients With Operation Characteristics

$\delta p_к$	$\delta\dot m_{ок}$	$\delta\dot m_г$
1	$-a_{p_к,\dot m_{ок}}$	$-a_{p_к,\dot m_г}$
$\bar p_к$	$2\Delta\bar p_{ок}$	0
$\bar p_к$	0	$2\Delta\bar p_г$

Matrix |B| of Coefficients During Disturbances

$\delta F_{кр}$	$\delta\rho_{ок}$	$\delta\rho_г$	$\delta\rho_р$	$\delta\xi_{ок}$	$\delta\xi_г$
-1	0	0	0	0	0
0	$\Delta\bar p_{ок}+\Delta\bar p_{ст}$	0	$-\bar p_{б.ок}b_{p_{б.ок},p_р}$	$-\Delta\bar p_{ок}b_{\Delta p_{ок},\xi_{ок}}$	0
0	0	$\Delta\bar p_г+\Delta\bar p_{ст}$	$-\bar p_{б.г}b_{p_{б.г},p_р}$	0	$-\Delta\bar p_г b_{\Delta p_г,\xi_г}$

The main system determinant is

$$\Delta = |A| = 4\,\Delta\bar{p}_{ок}\Delta\bar{p}_{г} + 2\bar{p}_{к}\left(\Delta\bar{p}_{г}a_{p_к,\dot{m}_{ок}} + \Delta\bar{p}_{ок}a_{p_к,\dot{m}_{г}}\right). \qquad (4.8)$$

As an example we shall obtain additional determinants for disturbances $\delta\rho_{ок}$, $\delta\rho_{г}$, $\delta F_{кр}$;

$$\Delta_{p_к,F_{кр}} = -4\,\Delta\bar{p}_{ок}\,\Delta\bar{p}_{г};$$
$$\Delta_{p_к,\rho_{ок}} = 2\,\Delta\bar{p}_{ок}\,\Delta\bar{p}_{г}a_{p_к,\dot{m}_{ок}};$$
$$\Delta_{p_к,\rho_{г}} = 2\,\Delta\bar{p}_{ок}\,\Delta p_{г}a_{p_к,\dot{m}_{г}};$$
$$\Delta_{\dot{m}_{ок},F_{кр}} = 2\bar{p}_{к}\,\Delta\bar{p}_{г};$$
$$\Delta_{\dot{m}_{ок},\rho_{ок}} = \Delta\bar{p}_{ок}\left(2\,\Delta\bar{p}_{г} + \bar{p}_{к}a_{p_к,\dot{m}_{г}}\right);$$
$$\Delta_{\dot{m}_{ок},\rho_{г}} = -\,\Delta\bar{p}_{г}\bar{p}_{к}a_{p_к,\dot{m}_{г}};$$
$$\Delta_{\dot{m}_{г},F_{кр}} = 2\bar{p}_{к}\,\Delta\bar{p}_{ок};$$
$$\Delta_{\dot{m}_{г},\rho_{ок}} = -\,\bar{p}_{к}\,\Delta\bar{p}_{ок}a_{p_к,\dot{m}_{ок}};$$
$$\Delta_{\dot{m}_{г},\rho_{г}} = \Delta\bar{p}_{г}\left(2\,\Delta\bar{p}_{ок} + \bar{p}_{к}a_{p_к,\dot{m}_{г}}\right).$$

In conformity with relation (4.4), propulsion system equations in variations will be written in the form

$$\left.\begin{aligned}
\delta p_{к} &= C_{p_к,F_{кр}}\delta F_{кр} + C_{p_к,\rho_{ок}}\delta\rho_{ок} + C_{p_к,\rho_{г}}\delta\rho_{г};\\
\delta\dot{m}_{ок} &= C_{\dot{m}_{ок},F_{кр}}\delta F_{кр} + C_{\dot{m}_{ок},\rho_{ок}}\delta\rho_{ок} + C_{\dot{m}_{ок},\rho_{г}}\delta\rho_{г};\\
\delta\dot{m}_{г} &= C_{\dot{m}_{г},F_{кр}}\delta F_{кр} + C_{\dot{m}_{г},\rho_{ок}}\delta\rho_{ок} + C_{\dot{m}_{г},\rho_{г}}\delta\rho_{г};\\
\delta K &= \delta\dot{m}_{ок} - \delta\dot{m}_{г}.
\end{aligned}\right\} \qquad (4.9)$$

Coefficients of influence $C_{j,i}$ are determined with equation (4.4) and depend on nominal engine parameters.

For combustion chamber pressure, for example, coefficients of influence are determined by relations

$$\left.\begin{aligned}
C_{p_к,F_{кр}} &= -\frac{1}{1 + 0{,}5\bar{p}_{к}\left(\dfrac{\bar{K}}{(\bar{K}+1)\,\Delta\bar{p}_{ок}} + \dfrac{1}{(\bar{K}+1)\,\Delta\bar{p}_{г}}\right)};\\
C_{p_к,\rho_{ок}} &= \frac{1}{\dfrac{2\,(\bar{K}+1)}{\bar{K}} + \bar{p}_{к}\left(\dfrac{1}{\Delta\bar{p}_{ок}} + \dfrac{1}{\bar{K}\,\Delta\bar{p}_{г}}\right)};\\
C_{p_к,\rho_{г}} &= \frac{1}{2\,(\bar{K}+1) + \bar{p}_{к}\left(\dfrac{\bar{K}}{\Delta\bar{p}_{ок}} + \dfrac{1}{\Delta\bar{p}_{г}}\right)}.
\end{aligned}\right\} \qquad (4.10)$$

As follows from the relations, coefficients of influence are determined by the values of nominal pressures in the combustion chamber, pressure differential and ratio of propellant components. The character of change in coefficients of influence with change in nominal combustion chamber pressure (ratio of propellant components and pressure differentials are assumed constant) is indicated in Figure 4.1.

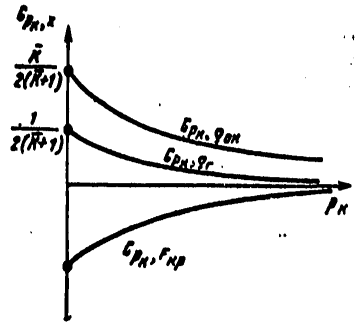

Figure 4.1. Relationship Between Coefficients of Influence and Combustion Chamber Pressure

Thus with an increase in nominal combustion chamber pressure, the influence of disturbances and in particular change in nozzle throat area and density of propellant components diminishes.

As an example we shall specify the numerical values of coefficients of influence for the propulsion system of the second stage of an (Eybl Stor) rocket with a gas pressurization supply system [3].

The propulsion system has the following nominal parameters:

propellant	NDMG + HNO_3
combustion chamber pressure p_k, Mn/m^2	1.42
ratio of propellant components K	2.8
pressure in fuel tank $p_{б.г}$, Mn/m^2	2.6
pressure in oxidizer tank, $p_{б.ок}$, Mn/m^2	1.96

The quantities in the determinants have the following values:

$$\Delta\bar{p}_{ок} = \bar{p}_{б.ок} - \bar{p}_к = 1{,}96 - 1{,}42 = 0{,}54 \text{ Мн/м}^2;$$
$$\Delta\bar{p}_г = \bar{p}_{б.г} - \bar{p}_к = 2{,}6 - 1{,}42 = 1{,}18 \text{ Мн/м}^2.$$

$$a_{p_к},\ \dot{m}_{ок} = \frac{\bar{K}}{\bar{K}+1} = \frac{2{,}8}{2{,}8+1} = 0{,}72;$$

$$a_{p_K,\ \dot{m}_\Gamma} = \frac{1}{K+1} = \frac{1}{2{,}8+1} = 0{,}28;$$

$$\Delta = 4\Delta\bar{p}_{OK}\Delta\bar{p}_\Gamma + 2\bar{p}_K\left(\Delta\bar{p}_\Gamma a_{p_K,\ \dot{m}_{OK}} + \Delta\bar{p}_{OK}a_{p_K,\ \dot{m}_\Gamma}\right) =$$

$$= 4\cdot 0{,}54\cdot 1{,}18 + 2\cdot 1{,}42\ (1{,}18\cdot 0{,}72 + 0{,}54\cdot 0{,}28) = 5{,}39;$$

$$\Delta_{p_K,\ F_{KP}} = -4\Delta\bar{p}_{OK}\Delta\bar{p}_\Gamma = -4\cdot 0{,}54\cdot 1{,}18 = -2{,}55;$$

$$\Delta_{p_K,\ \rho_{OK}} = 2\Delta\bar{p}_{OK}\Delta\bar{p}_\Gamma a_{p_K,\ \dot{m}_{OK}} = 2\cdot 0{,}54\cdot 1{,}18\cdot 0{,}72 = 0{,}92;$$

$$\Delta_{p_K,\ \rho_\Gamma} = 2\Delta\bar{p}_{OK}\Delta\bar{p}_\Gamma a_{p_K,\ \dot{m}_\Gamma} = 2\cdot 0{,}54\cdot 1{,}18\cdot 0{,}28 = 0{,}36;$$

$$\Delta_{\dot{m}_{OK},\ F_{KP}} = 2\Delta\bar{p}_\Gamma\bar{p}_K = 2\cdot 1{,}18\cdot 1{,}42 = 3{,}34;$$

$$\Delta_{\dot{m}_{OK},\ \rho_{OK}} = \Delta\bar{p}_{OK}\left(2\Delta\bar{p}_\Gamma + \bar{p}_K a_{p_K,\ \dot{m}_\Gamma}\right) =$$

$$= 0{,}54\ (2\cdot 1{,}18 + 1{,}42\cdot 0{,}28) = 1{,}49;$$

$$\Delta_{\dot{m}_{OK},\ \rho_\Gamma} = -\Delta\bar{p}_\Gamma\bar{p}_K a_{p_K,\ \dot{m}_\Gamma} = -1{,}18\cdot 1{,}42\cdot 0{,}28 = -0{,}47;$$

$$\Delta_{\dot{m}_\Gamma,\ F_{KP}} = 2\Delta\bar{p}_{OK}\bar{p}_K = 2\cdot 0{,}54\cdot 1{,}42 = 1{,}53;$$

$$\Delta_{\dot{m}_\Gamma,\ \rho_{OK}} = -\Delta\bar{p}_{OK}\bar{p}_K a_{p_K,\ \dot{m}_{OK}} = -0{,}54\cdot 1{,}42\cdot 0{,}72 = -0{,}55;$$

$$\Delta_{\dot{m}_\Gamma,\ \rho_\Gamma} = \Delta\bar{p}_\Gamma\left(2\Delta\bar{p}_{OK} + \bar{p}_K a_{p_K,\ \dot{m}_\Gamma}\right) = 1{,}18\ (2\cdot 0{,}54 + 1{,}42\cdot 0{,}28) = 1{,}75.$$

Coefficients of influence $C_{j,\ i}$ are contained in Table 4.1.

Table 4.1

Coefficient	δF_{KP}	$\delta\rho_{OK}$	$\delta\rho_\Gamma$
δp_K	—0,47	0,172	0,067
$\delta\dot{m}_{OK}$	0,62	0,28	—0,087
$\delta\dot{m}_\Gamma$	0,28	—0,095	0,33

4.3. Model of Engine Without Generator Gas Afterburning

Figure 1.3 contains a diagram of an engine without generator gas afterburning. For an engine of this design, balance equations (of compatibility of components) written in variations, are the following. The equation of balance of outputs is

$$\bar{N}_T\delta N_T = \sum_1^2 \bar{N}_{H,\ j}\delta N_{H,\ j}, \qquad (4.11)$$

where $j = \overline{OK,\ \Gamma}$.

Equations of balance of pressures in oxidizer and fuel lines from pumps to combustion chamber:

$$\left.\begin{aligned}\bar{p}_{\text{н. ок}}\delta p_{\text{н. ок}} &= \bar{p}_{\text{тг}}\delta p_{\text{к}} + \Delta\bar{p}'_{\text{ок}}\delta\Delta p'_{\text{ок}};\\ p_{\text{н. т}}\delta p_{\text{н. т}} &= \bar{p}_{\text{тг}}\delta p_{\text{к}} + \Delta\bar{p}'_{\text{т}}\delta\Delta p'_{\text{т}}.\end{aligned}\right\} \qquad (4.12)$$

Equations of balance of pressures in gas generator lines:

$$\left.\begin{aligned}\bar{p}_{\text{н. ок}}\delta p_{\text{н. ок}} &= \bar{p}_{\text{тг}}\delta p_{\text{тг}} + \Delta\bar{p}''_{\text{ок}}\delta\Delta p''_{\text{ок}};\\ \bar{p}_{\text{н. т}}\delta p_{\text{н. т}} &= \bar{p}_{\text{тг}}\delta p_{\text{тг}} + \Delta\bar{p}''_{\text{т}}\delta\Delta p''_{\text{т}}.\end{aligned}\right\} \qquad (4.13)$$

Equations of balance of flow rates:

$$\left.\begin{aligned}\bar{\dot{m}}_{\text{ок}}\delta\dot{m}_{\text{ок}} &= \bar{\dot{m}}'_{\text{ок}}\delta\dot{m}'_{\text{ок}} + \bar{\dot{m}}''_{\text{ок}}\delta\dot{m}''_{\text{ок}};\\ \bar{\dot{m}}_{\text{т}}\delta\dot{m}_{\text{т}} &= \bar{\dot{m}}'_{\text{т}}\delta\dot{m}'_{\text{т}} + \bar{\dot{m}}''_{\text{т}}\delta\dot{m}''_{\text{т}}.\end{aligned}\right\} \qquad (4.14)$$

Substituting in equations (4.11)-(4.13) equation (4.14) and equations of components (3.2), (3.6), and (3.29), following simple transformations we obtain a system of five equations, which in matrix form appears as follows:

$$A\,|\delta y| = B\,|\delta x|,$$

where

$$|\delta y| = \begin{vmatrix}\delta\dot{m}'_{\text{ок}}\\ \delta\dot{m}'_{\text{т}}\\ \delta\dot{m}''_{\text{ок}}\\ \delta\dot{m}''_{\text{т}}\\ \delta n\end{vmatrix}; \quad |\delta x| = \begin{vmatrix}\delta\rho_{\text{ок}}\\ \delta\rho_{\text{т}}\\ \delta\eta_{\text{н. ок}}\\ \delta\eta_{\text{н. т}}\\ \cdot\\ \cdot\\ \cdot\\ \delta F_{\text{с}}\\ \delta F_{\text{кр}}\end{vmatrix}.$$

The elements of matrix |A| are contained in Table 4.2, and the elements of matrix |B| are in Table 4.3.

(See Table 4.2 and Table 4.3 on the following two pages).

4.4. Motor With Generator Gas Afterburning (G-L)

Figure 1.4 contains a diagram of a motor with afterburning of (oxidizing) generator gas.

Equation of output balance:

$$\bar{N}_{\text{т}}\delta N_{\text{т}} = \sum_{1}^{2}\bar{N}_{\text{н}j}\delta N_{\text{н}j}. \qquad (4.15)$$

Table 4.2.

$\delta \dot{m}'_{ок}$	$\delta \dot{m}'_{г}$	$\delta \dot{m}''_{ок}$	$\delta \dot{m}''_{г}$	$\delta \pi$
$-\bar{N}_{к.ок}\sigma_{ок}$	$-\bar{N}_{к.г}\bar{\rho}_{г.к}$	$\bar{N}_{т}\left(\frac{\partial}{\partial \rho_{тт}}, \dot{m}''_{ок} + \frac{\partial}{\partial N_{т}}, K'\right) - \bar{N}_{к.ок}\sigma_{ок.г}$	$\bar{N}_{т}\left(\frac{\partial}{\partial \rho_{тт}}, \dot{m}''_{г}\right) - \frac{\partial}{\partial N_{т}}, K') - \bar{N}_{к.г}\sigma_{тт}$	$\bar{N}_{т}\psi_{т} - \bar{N}_{к.ок}\sigma_{Nк.ок.к} - \bar{N}_{к.г}\sigma_{Nк.г.к}$
$\bar{\dot{m}}'_{ок}\operatorname{tg}\alpha_{к.ок} - 2\Delta\bar{\dot{\rho}}''_{ок} - \bar{\rho}_{к}\frac{\partial}{\rho_{к}}, \dot{m}''_{ок}$	$\bar{\dot{m}}'_{г}\operatorname{tg}\alpha_{к.г} - \bar{\rho}_{к}\frac{\partial}{\rho_{к}}, \dot{m}'_{г}$	$\bar{\dot{m}}''_{ок}\operatorname{tg}\alpha_{к.ок}$	$\bar{\dot{m}}''_{г}\operatorname{tg}\alpha_{к.г}$	$\bar{\rho}_{к.ок}\sigma_{\rho к.ок.к}$
$\bar{\dot{m}}'_{ок}\operatorname{tg}\alpha_{к.ок} - \bar{\rho}_{к}\frac{\partial}{\rho_{к}}, \dot{m}''_{ок}$	$\bar{\dot{m}}'_{г}\operatorname{tg}\alpha_{к.г} - 2\Delta\bar{\dot{\rho}}''_{г} - \bar{\rho}_{к}\frac{\partial}{\rho_{к}}, \dot{m}'_{г}$	$\bar{\dot{m}}''_{ок}\operatorname{tg}\alpha_{к.ок}$	$\bar{\dot{m}}''_{г}\operatorname{tg}\alpha_{к.г}$	$\bar{\rho}_{к.г}\sigma_{\rho к.г.к}$
$\bar{\dot{m}}'_{ок}\operatorname{tg}\alpha_{к.ок} - 2\Delta\bar{\dot{\rho}}''_{ок} - \bar{\rho}_{тт}\sigma_{\rho тт}, \dot{m}''_{ок}$	0	$\bar{\dot{m}}''_{ок}\operatorname{tg}\alpha_{к.ок} - \bar{\rho}_{тт}\sigma_{\rho тт}, \dot{m}''_{ок} - 2\Delta\bar{\dot{\rho}}''_{ок}$	$-\bar{\rho}_{тт}\frac{\partial}{\partial \rho_{тт}}, \dot{m}''_{г}$	$\bar{\rho}_{к.ок}\sigma_{\rho к.ок.к}$
0	$\bar{\dot{m}}'_{г}\operatorname{tg}\alpha_{к.г}$	$-\bar{\rho}_{тт}\frac{\partial}{\partial \rho_{тт}}, \dot{m}''_{ок}$	$\bar{\dot{m}}''_{г}\operatorname{tg}\alpha_{к.г} - \bar{\rho}_{тт}\frac{\partial}{\partial \rho_{тт}}, \dot{m}''_{г} - 2\Delta\bar{\dot{\rho}}''_{г}$	$\bar{\rho}_{к.г}\sigma_{\rho к.г.к}$

Table 4.3.

δp_{ok}	δp_r	$\delta n_{н.ok}$	$\delta n_{н.r}$	$\delta p_{o.ok}$	$\delta p_{o.r}$	δD_{ok}	δD_r	$\delta E'_{ok}$	$\delta E'_r$	$\delta E''_{ok}$	$\delta E''_r$	δF_c	$\delta F_{кр}$
$\bar{N}_{н.ok}{}^{b}N_{н.o}, \rho_{ok}$	$\bar{N}_{н.r}{}^{b}N_{н.r}, \rho_r$	$-\bar{N}_{н.ok}$	0	0	0	$\bar{N}_{н.ok}{}^{b}N_{н.o}, D_o$	$N_{н.r}{}^{b}N_{н.r}, D_r$	0	0	0	0	0	0
$-\bar{p}_{н.ok}{}^{b}\rho_{н.ok}, \rho_{ok}, -\Delta\bar{p}'_{ok}$	0	0	$-\bar{N}_{н.r}$	$-\bar{p}_{o.ok}$	0	$\bar{p}_{н.ok}{}^{b}\rho_{н.ok}, D_{ok}$	0	$\Delta\bar{p}'_{ok}$	0	0	0	0	$-\bar{p}_к$
0	$-\bar{p}_{н.r}{}^{b}\rho_{н.r}, \rho_r, -\Delta\bar{p}'_r$	0	0	0	$-\bar{p}_{o.r}$	.0	$-\bar{p}_{н.r}{}^{b}\rho_{н.r}, D_r$	0	$\Delta\bar{p}'_r$	0	0	0	$-\bar{p}_к$
$-\bar{p}_{н.ok}{}^{b}\rho_{н.ok}, \rho_{ok}, -\Delta\bar{p}'_{ok}$	0	0	0	$-\bar{p}_{o.ok}$	0	$-\bar{p}_{н.ok}{}^{b}\rho_{н.ok}, D_{ok}$	0	0	0	$\Delta\bar{p}''_{ok}$	0	0	0
0	$-\bar{p}_{н.r}{}^{b}\rho_{н.r}, \rho_r, -\Delta\bar{p}'_r$	0	0	0	$-\bar{p}_{o.r}$	0	$-\bar{p}_{н.r}{}^{b}\rho_{н.r}, D_r$	0	0	0	$\Delta\bar{p}''_r$	0	0

Equations of balance of gas generator line pressures:

$$\left.\begin{aligned}\bar{p}_{н.ок}\delta p_{н.ок} &= \bar{p}_{гг}\delta p_{гг} + \Delta\bar{p}''_{ок}\delta\Delta p''_{ок};\\ \bar{p}_{н.г}\delta p_{н.г} &= \bar{p}_{гг}\delta p_{гг} + \Delta\bar{p}''_{г}\delta\Delta p''_{г}.\end{aligned}\right\} \qquad (4.16)$$

Equations of combustion chamber line pressure balance:

$$\bar{p}_{н.г}\delta p_{н.г} = \bar{p}_{к}\delta p_{к} + \Delta\bar{p}'_{г}\delta\Delta p'_{г}; \qquad (4.17)$$

$$\bar{p}_{вт}\delta p_{вт} = \bar{p}_{к}\delta p_{к} + \Delta\bar{p}_{гв}\delta\Delta p_{гв}. \qquad (4.18)$$

Equation of fuel flow rate balance:

$$\bar{\dot{m}}_{г}\delta\dot{m}_{г} = \bar{\dot{m}}'_{г}\delta\dot{m}'_{г} + \bar{\dot{m}}''_{г}\delta\dot{m}''_{г}. \qquad (4.19)$$

After substituting equation (4.18) in (4.15), utilizing the relation for components (Ch. 3), system (4.15)-(4.19) reduces to a system of four equations, for which the matrix elements have the form

$$|\delta y| = \begin{vmatrix}\delta\dot{m}_{ок}\\ \delta\dot{m}'_{г}\\ \delta\dot{m}''_{г}\\ \delta n\end{vmatrix}; \quad |\delta x| = \begin{vmatrix}\delta p_{ок}\\ \delta p_{г}\\ \delta\eta_{н.ок}\\ \cdot\\ \cdot\\ \cdot\\ \delta F_{с}\\ \delta F_{кр}\end{vmatrix}.$$

The elements of matrices |A| and |B| are contained in tables 4.4 and 4.5.

$$Z_1 = a_{N_т,\, p_{гг}} a_{p_{гг},\, \dot{m}_{ок}} + \frac{a_{N_т,\, p_{вт}}}{\bar{p}_{вт}}\left[\bar{p}_{к}a_{p_к,\, \dot{m}_{ок}} + \right.$$
$$\left. + \Delta\bar{p}_{гв}\left(a_{p_{гг},\, \dot{m}_{ок}} + a_{\Delta p_{гв},\, K^*}\right)\right] + a_{N_т,\, K^*};$$
$$Z_2 = \frac{a_{N_т,\, p_{вт}}}{\bar{p}_{вт}}\left(\bar{p}_{к}a_{p_к,\, \dot{m}'_г} - \Delta\bar{p}_{гв}a_{\Delta p_{гв},\, K^*}\right);$$
$$Z_3 = a_{N_т,\, p_{гг}} a_{p_{гг},\, \dot{m}''_г} + a_{N_т,\, p_{вт}}\frac{\Delta\bar{p}_{гв}}{\bar{p}_{вт}}\left(a_{p_{гг},\, \dot{m}''_г} - a_{\Delta p_{гв},\, K^*}\right);$$
$$Z_4 = a_{N_т,\, n} + \frac{\Delta\bar{p}_{гв}}{\bar{p}_{вт}}a_{N_т,\, p_{вт}}a_{\Delta p_{гв},\, n};$$
$$q_{г.к} = \frac{\bar{\dot{m}}'_г}{\bar{\dot{m}}_г}; \quad q_{г.г} = \frac{\bar{\dot{m}}''_г}{\bar{\dot{m}}_г}.$$

Table 4.4

$\delta\dot{m}_{ок}$	$\delta\dot{m}'_{г}$	$\delta\dot{m}''_{г}$	δn
$Z_1\bar{N}_т - \bar{N}_{н.ок}$	$Z_2\bar{N}_т - \bar{N}_{н.г}$	$Z_3\bar{N}_т$	$Z_4\bar{N}_т - \sum \bar{N}_{нi}a_{Ni,n}$
$\bar{p}_{н.ок}a_{\rho_{н.о}}, \dot{m}_{ок} - \bar{p}_{гг}a_{\rho_{гг}}, \dot{m}_{ок} - 2\Delta\bar{p}''_{ок}$	0	$-\bar{p}_{гг}a_{\rho_{гг}}, \dot{m}''_{г}$	$\bar{p}_{н.ок}a_{\rho_{н.ок}}, n$
$-\bar{p}_{гг}a_{\rho_{гг}}, \dot{m}_{ок}$	$\bar{p}_{н.г}a_{\rho_{н.г}}, \dot{m}'_{г}$	$-\bar{p}_{гг}a_{\rho гг}, \dot{m}''_{г} - 2\Delta\bar{p}_{гг}$	$\bar{p}_{н.г}a_{\rho_{н.i}}, n$
$-\bar{p}_{к}a_{\rho_{к}}, \dot{m}_{ок}$	$\bar{p}_{н.г}a_{\rho_{н.г}}, \dot{m}_{г} - \bar{p}_{к}a_{\rho_{к}}, \dot{m}'_{г} - 2\Delta\bar{p}'_{г}q_{г.к}$	$2\Delta\bar{p}''_{г}q_{гг}$	$\bar{p}_{н.г}a_{\rho_{н.г}}, n$

4.5. Motor With Generator Gas Afterburning (G-G)

Figure 1.5 contains an engine diagram.

We shall designate the parameters of an oxidizing gas generator -- Z^{o} and reducing gas generator -- $Z^{г}$.

Output balance equation

$$\delta N^{o}_{т} = \delta N_{н.ок}; \tag{4.20}$$

$$\delta N^{г}_{т} = \delta N_{н.г}. \tag{4.21}$$

Gas generator line pressure balance equation

$$\bar{p}_{н.ок}\,\delta p_{н.ок} = \bar{p}^{o}_{гг}\,\delta p^{o}_{гг} + \Delta\bar{p}^{o}_{ок}\,\delta\,\Delta p^{o}_{ок}; \tag{4.22}$$

$$\bar{p}_{н.ок}\,\delta p_{н.ок} = \bar{p}^{г}_{гг}\,\delta p^{г}_{гг} + \Delta\bar{p}^{г}_{ок}\,\delta\,\Delta p^{г}_{ок}; \tag{4.23}$$

$$\bar{p}_{н.г}\,\delta p_{н.г} = \delta p^{o}_{гг}\,\delta p^{o}_{гг} + \Delta\bar{p}^{o}_{г}\,\delta\,\Delta p^{o}_{г}; \tag{4.24}$$

$$\bar{p}_{н.г}\,\delta p_{н.г} = \delta p^{г}_{гг}\,\delta p^{г}_{гг} + \Delta\bar{p}^{г}_{г}\,\delta\,\Delta p^{г}_{г}. \tag{4.25}$$

Table 4.5.

$\delta p_{ок}$	δp_r	$\delta\eta_{ш.ок}$	$\delta\eta_{ш.г}$	$\delta p_{о.ок}$	$\delta p_{о.г}$	$\delta D_{ок}$	δD_r	$\delta\xi'_r$	$\delta\xi_{ок}$	$\delta\xi''_r$	δF_c	$\delta F_{кр}$
$\overline{N}_{ш.ок}b_{N_{ш}.о}p_{ок}$	$\overline{N}_{ш.г}b_{N_{ш}.г}p_r$	$-\overline{N}_{ш.ок}$	0	0	0	$\overline{N}_{ш.ок}b_{N_{ш}.о}D_о$	$\overline{N}_{ш.г}b_{N_{ш}.г}D$	0	0	0	$-\overline{N}_г$	0
$-\overline{p}_{ш.ок}b_{p_{ш}.ок}p_{ок}$	0	0	0	$-\overline{p}_{о.ок}$	D	$\overline{p}_{ш.ок}b_{p_{ш}.ок}D$	0	0	$\Delta\overline{p}_{ок}b_{\Delta p_о}\xi_о$	$\Delta\overline{p}''_r b_{\Delta p''_r}\xi''_r$	0	0
0	$-\overline{p}_{ш.г}b_{p_{ш}.г}p_r - -\Delta p''_r$	0	0	0	$-\overline{p}_{о.г}$	0	$\overline{p}_{ш.г}b_{p_{ш}.г}D$	0	0	0	0	$-\overline{p}_{кл}$
0	$-\overline{p}_{ш.г}b_{p_{ш}.г}p_r - -\Delta p''_r$	0	0	0	$-\overline{p}_{о.г}$	0	0	0	$\Delta\overline{p}'_r b_{p'_r}\xi'_r$	0	0	0

Combustion chamber gas duct balance equation

$$p^{\circ}_{2T}\,\delta p^{\circ}_{2T} = \bar{p}_{K}\,\delta p_{K} + \Delta\bar{p}^{\circ}_{rB}\,\delta\,\Delta p^{\circ}_{rB}; \tag{4.26}$$

$$p^{r}_{2T}\,\delta p^{r}_{2T} = \bar{p}_{K}\,\delta p_{K} + \Delta\bar{p}^{r}_{rB}\,\delta\,\Delta p^{r}_{rB}. \tag{4.27}$$

Flow rate balance equations

$$\dot{m}_{OK}\,\delta\dot{m}_{OK} = \bar{\bar{m}}^{\circ}_{OK}\,\delta\dot{m}^{\circ}_{OK} + \bar{\bar{m}}^{r}_{OK}\,\delta\dot{m}^{r}_{OK}; \tag{4.28}$$

$$\bar{\bar{m}}_{r}\,\delta\dot{m}_{r} = \bar{\bar{m}}^{\circ}_{r}\,\delta\dot{m}^{\circ}_{r} + \bar{\bar{m}}^{r}_{r}\,\delta\dot{m}^{r}_{r}. \tag{4.29}$$

System (4.20)-(4.29) reduces to a system of six equations, the matrix elements of which have the form

$$|\delta y| = \begin{vmatrix} \delta\dot{m}^{\circ}_{OK} \\ \delta\dot{m}^{r}_{OK} \\ \delta\dot{m}^{\circ}_{r} \\ \delta\dot{m}^{r}_{r} \\ \delta n^{r} \\ \delta n^{\circ} \end{vmatrix}.$$

The elements of matrices |A| and |B| are contained in tables 4.6 and 4.7.

Table 4.6.

$\delta\dot{m}^{\circ}_{OK}$	$\delta\dot{m}^{r}_{OK}$	$\delta\dot{m}^{\circ}_{r}$	$\delta\dot{m}^{r}_{r}$	δn°	δn^{r}
a_{11}	a_{12}	a_{13}	a_{14}	a_{15}	0
a_{21}	a_{22}	a_{23}	a_{24}	0	a_{26}
a_{31}	a_{32}	a_{33}	0	a_{35}	0
a_{41}	a_{42}	0	a_{44}	a_{45}	0
a_{51}	0	a_{53}	a_{54}	0	a_{56}
0	a_{62}	a_{63}	a_{64}	0	a_{66}

Table 4.7.

$\delta\varepsilon_r^r$	$\delta\varepsilon_c^r$	$\delta\varepsilon_c^0$	$\delta\varepsilon_r^0$	$\delta\varepsilon_{ok}^0$	δF_{sp}	$\delta n_{z.r}$	$\delta n_{z.ok}$	$\delta\rho_{o.r}$	$\delta\rho_{o.ok}$	$\delta\rho_r$	$\delta\rho_{ok}$
0	0	—1	0	0	$-\frac{\bar{\rho}_{ok}}{\bar{\rho}_{2r}^2} a_{N_r^0}^0 \rho_{2r}^0$	0	—1	0	0	0	$b_{N_{z.ok}}, \rho_{ok}$
0	1	0	0	0	$-\frac{\bar{\rho}_{ok}}{\bar{\rho}_{2r}^2} a_{N_r^r}^r \rho_{2r}^r$	0	0	0	0	$b_{N_{z.r}}, \rho_r$	0
0	0	0	0	$\Delta\bar{\rho}_{ok}^0 b_{\Delta\rho_{ok}^0}, \xi_{ok}^0$	0	0	0	0	$-\bar{\rho}_{z.ok} b_{\rho_{z.ok}}, \rho_0$	0	$-\Delta\bar{\rho}_{ok}^0 -$ $-\bar{\rho}_{z.ok} b_{\rho_{z.ok}}, \rho_0$
0	0	0	$\Delta\bar{\rho}_{ok}^r b_{\Delta\rho_{ok}^r}, \xi_r^0$	0	0	0	0	0	$-\bar{\rho}_{z.ok} b_{\rho_{z.ok}}, \rho_0$	0	$-\bar{\rho}_{z.ok} b_{\rho_{z.o}}, \rho -$ $-\Delta\bar{\rho}_{ok}^r$
0	0	0	$\Delta\bar{\rho}_r^0 b_{\Delta\rho_r^0}, \xi_r^0$	0	0	0	0	$-\bar{\rho}_{z.r} b_{\rho_{z.r}}, \rho_{o.r}$	0	$-\bar{\rho}_{z.r} b_{\rho_{z.r}}, \rho_r -$ $-\Delta\bar{\rho}_r^0$	0
$\Delta\bar{\rho}_r^r b_{\Delta\rho_r^r}, \xi_r^r$	0	0	0	0	0	0	0	$-\bar{\rho}_{z.r} b_{\rho_{z.r}}, \rho_{o.r}$	0	$-\bar{\rho}_{z.r} b_{\rho_{z.r}}, \rho_r -$ $-\Delta\bar{\rho}_r^r$	0

$$a_{11} = a_{N_т^0,\ p_{гг}^0 a_{p_{гг}^0,\ \dot{m}_{ок}^0}} + \bar{q}_0^0 \left(\frac{\bar{p}_к}{\bar{p}_{2т}^0} a_{N_т^0,\ p_{2т}^0 a_{p_к,\ \dot{m}_{ок}}} - a_{N_{н.\,ок}^0,\ \dot{m}_{ок}} \right) +$$

$$+ \frac{K^0}{K^0+1} \frac{\Delta\bar{p}_{гв}^0}{\bar{p}_{2т}^0} a_{N_т^0,\ p_{2т}^0} \left(1 + a_{\Delta p_{гв}^0,\ k}\right) + a_{N_т^0, K^0};$$

$$a_{12} = \bar{q}_0^г \left[\frac{a_{N_т^0,\ p_{2т}^0}}{\bar{p}_{2т}^0} \left(a_{p_к,\ \dot{m}_{ок}} \bar{p}_к + \Delta\bar{p}_{гв}^0 \right) - a_{N_{н.\,ок},\ \dot{m}_{ок}} \right];$$

$$a_{13} = a_{N_т^0,\ p_{гг}^0 a_{p_{гг}^0,\ \dot{m}_г^0}} + \frac{a_{N_т^0,\ p_{2т}^0}}{\bar{p}_{2т}^0} \left[\bar{q}_г^0 \left(\bar{p}_к a_{p_к,\ \dot{m}_г} - \Delta p_{гв}^0 \right) + \right.$$

$$\left. + \Delta\bar{p}_{гв}^0 \left(\frac{1}{K^0+1} - a_{\Delta p_{гв}^0,\ k^0} \right) \right];$$

$$a_{14} = a_{N_т^0,\ p_{2т}^0} \frac{\bar{q}_г^г}{\bar{p}_{2т}^0} \left(\bar{p}_к a_{p_к,\ \dot{m}_г} - \Delta\bar{p}_{гв}^0 a_{\Delta p_{гв}^0,\ K^0} \right);$$

$$a_{15} = a_{N_т^0,\ n^0} - a_{N_{н.\,ок},\ n^0} - \frac{\Delta\bar{p}_{гв}^0}{\bar{p}_{2т}^0} a_{\Delta p_{гв}^0,\ n^0};$$

$$a_{16} = 0,$$

$$a_{21} = \frac{a_{N_т^г,\ p_{2т}^г}}{\bar{p}_{2т}^г} \bar{q}_0^0 \left(\bar{p}_к a_{p_к,\ \dot{m}_{ок}} + \Delta\bar{p}_{гв}^г a_{\Delta p_{гв}^г,\ K} \right);$$

$$a_{22} = a_{N_т^г,\ p_{гг}^г a_{p_{гг}^г,\ \dot{m}_{ок}^г}} + a_{N_т^г,\ p_{2т}^г} \frac{\bar{q}_0^г}{\bar{p}_{2т}^г} \times$$

$$\times \left[\bar{p}_к a_{p_к,\ \dot{m}_{ок}} + \Delta\bar{p}_{гв}^г \left(1 + a_{\Delta p_{гв}^г,\ K} \right) \right] + a_{N_т^г,\ K^г};$$

$$a_{23} = \bar{q}_г^0 \left[\frac{a_{N_т^г,\ p_{2т}^г}}{\bar{p}_{2т}^г} \left(\bar{p}_к a_{p_к,\ \dot{m}_г} - \Delta\bar{p}_{гв}^г \right) - a_{N_т^г,\ \dot{m}_г^г} \right];$$

$$a_{24} = a_{N_т^г,\ p_{гг}^г a_{p_{гг}^г,\ \dot{m}_г^г}} + a_{N_т^г,\ p_{2т}^г} \frac{\bar{q}_г^г}{\bar{p}_{2т}^г} \times$$

$$\times \left[\bar{p}_к a_{p_к,\ \dot{m}_г} + \Delta\bar{p}_{гв}^г \left(1 + a_{\Delta p_{гв}^г,\ K} \right) \right] - a_{N_т^г,\ K^г} - a_{N_{н.\,г},\ \dot{m}_г^г \bar{q}_г^г};$$

$$a_{31} = \bar{p}_{н.\,ок} a_{p_{н.\,ок},\ \dot{m}_{ок}} \bar{q}_0^0 - \bar{p}_{гг}^0 a_{p_{гг}^0,\ \dot{m}_{ок}^0} - 2\Delta\bar{p}_{ок}^0;$$

$$a_{32} = \bar{p}_{н.\,ок} \bar{q}_0^г a_{p_{н.\,ок},\ \dot{m}_{ок}};$$

$$a_{33} = -\bar{p}_{гг}^0 a_{p_{гг}^0,\ \dot{m}_г^0};$$

$$a_{35} = \bar{p}_{н.\,ок} a_{p_{н.\,ок},\ n^0};$$

$$a_{41} = \bar{p}_{н.\,ок} \bar{q}_0^0 a_{p_{н.\,ос},\ \dot{m}_{ок}};$$

$$a_{42} = a_{41} - \bar{p}_{гг}^г a_{p_{гг}^г,\ \dot{m}_{ок}^г} - 2\Delta\bar{p}_{ок}^г;$$

$$a_{44} = -\bar{p}_{гг}^г a_{p_{гг}^г,\ \dot{m}_г^г};$$

$$a_{45} = a_{35};\ a_{51} = -a_{p_{гг}^0,\ \dot{m}_{ок}^0} \bar{p}_{гг}^0;$$

$$a_{63} = \bar{p}_{\text{м. г}} a_{\rho_{\text{м. г}}, \dot{m}_{\text{г}} \bar{q}^{\text{о}}_{\text{г}}} - a_{61} - 2\Delta\bar{p}^{\text{о}}_{\text{г}};$$

$$a_{64} = \bar{p}_{\text{м. г}} a_{\rho_{\text{м. г}}, \dot{m}_{\text{г}} \bar{q}^{\text{г}}_{\text{г}}};$$

$$a_{66} = \bar{p}_{\text{м. г}} a_{\rho_{\text{м. г}}, n^{\text{г}}};$$

$$a_{62} = -\bar{p}^{\text{г}}_{\text{гг}} a_{\rho^{\text{г}}_{\text{гг}}, \dot{m}^{\text{г}}_{\text{ок}}};$$

$$a_{63} = \bar{p}_{\text{м. г}} a_{\rho_{\text{м. г}}, \dot{m}_{\text{г}} \bar{q}^{\text{о}}_{\text{г}}};$$

$$a_{64} = \bar{p}_{\text{м. г}} a_{\rho_{\text{м. г}}, \dot{m}_{\text{г}} \bar{q}^{\text{г}}_{\text{г}}} - \bar{p}^{\text{г}}_{\text{гг}} a_{\rho_{\text{гг}}, \dot{m}^{\text{г}}_{\text{г}}} - 2\Delta\bar{p}^{\text{г}}_{\text{г}},$$

$$a_{66} = \bar{p}_{\text{м. г}} a_{\rho_{\text{м. г}}, n^{\text{г}}}.$$

4.6. Synthesized Engine Charateristics

As a result of solution of matrix equations for a specific engine, we obtain equations of the type

$$\delta y_j = \sum C_{y_j x_i} \delta x_i,$$

which link an operating parameter variation with deviations of disturbing factors from standard or nominal values.

Table 4.8 is constructed for a motor, and depicts the degree of sensitivity of operating parameters to various disturbances.

Table 4.8.

δx_i / δy_j	$\delta\rho_{\text{ок}}$	$\delta\rho_{\text{г}}$	$\delta F_{\text{кр}}$	...	$\delta\eta$
$\delta p_{\text{к}}$	$C_{p_{\text{к}}, \rho_{\text{ок}}}$	$C_{p_{\text{к}}, \rho_{\text{г}}}$	$C_{p_{\text{к}}, F_{\text{кр}}}$	...	$C_{p_{\text{к}}, \eta}$
δp	$C_{p, \rho_{\text{ок}}}$	$C_{p, \rho_{\text{г}}}$	$C_{p, F_{\text{кр}}}$	...	$C_{p, \eta}$
δI_y	$C_{I, \rho_{\text{ок}}}$	$C_{I, \rho_{\text{г}}}$	$C_{I, F_{\text{кр}}}$	...	$C_{I, \eta}$
.	.	.	.	.	.
.	.	.	.	.	.
δn	$C_{n, \rho_{\text{ок}}}$	$C_{n, \rho_{\text{г}}}$	$C_{n, F_{\text{кр}}}$	...	$C_{n, \eta}$

For a specific engine design, coefficients of influence C_{y_j, x_i} are the essence of the number, since they are determined only by the nominal operating parameters.

Table 4.8 enables one to determine for specified values of disturbing factors δx_i the values of operating parameters and to obtain input data for tuning and adjusting a propulsion system and for designing control systems, as well as elaboration of operating processes, for example, conditions of thermostatic control.

The value of an operating parameter for variation δy_j is determined from relation

$$y_l = \bar{y}_l (1 + \delta y_l).$$

In addition, the calculation results contained in Table 4.8 enable one to estimate the sensitivity of any operating parameter to a given disturbance and to elaborate measures for compensation for the strongest disturbances.

Engine equations written in variations make it possible to synthesize dimensional circuits of components and engine for the purpose of optimal distribution of tolerances on geometric dimensions of components.

In general manufacturing tolerances for the fabrication of engine structural components are selected from a number of conflicting conditions.

Following are the principal demands imposed on tolerances: design compatibility of components, producibility, cost (the smaller the tolerance, the greater the cost of manufacture), and precision. In general one can specify in a motor a small number of geometric dimensions of components which significantly affect the value of the principal operating parameters p_K, P, I_y, K, which determine economy, precision and operational reliability. These dimensions include nozzle throat area F_{kp}, pump impeller diameter D_H and turbine rotor wheel diameter D_T, diameters of hydraulic resistances (adjusting disks, jets $D_{ш}$), plus several others.

For analysis of tolerances as determining parameters, one can select combustion chamber pressure or specific thrust impulse. Utilizing Table 4.8, one can write an accuracy equation for any of the specified parameters:

$$\delta y = \sum C_{y, x_l} \delta x_l, \qquad (4.30)$$

where

$$x_l = \overline{F_{кр}, D_н, D_т, D_ш}.$$

In calculating tolerances one can make the following assumptions regarding the law of summation of particular deviations δx_i, which can be selected from examination of three cases. The worst case is where change in all components only increases full deviation of the operating parameter from the desired value.

A statistical case is where changes in δx_i are viewed as random quantities, and δy is a random quantity. This case will be examined in general form in the following chapter. And finally, one can consider a composite case.

When calculating the worst case, we rewrite equation (4.30) in the form

$$\delta y \leqslant \varepsilon = \sum_{i=1}^{n} |C_i| d_i, \qquad (4.31)$$

where δ -- maximum allowable deviation; d_i -- maximum deviation of dimension.

This method is utilized when the number of examined dimensions dx_i is small.

One can determine d_i as follows from equation (4.31). Maximum allowable deviation δ and sensitivity C_i are known. Let the absolute values of particular deviations $|C_i|d_i$ be identical for all elements, that is, we assume uniform distribution of particular deviations.

From the ratio of maximum allowable deviation δ to the number of elements n, we determine particular deviations

$$\frac{\delta}{n} = |C_i| d_i. \qquad (4.32)$$

From this we calculate component tolerance

$$d_i = \frac{\delta}{n} \frac{1}{|C_i|}. \qquad (4.33)$$

Thus if the corresponding sensitivity is small, the dimension of a component will have a greater tolerance, and vice versa.

4.7. Maximum Propulsion System Running Time

The principal external factor influencing propulsion system characteristics is temperature of propellant components. This is due to the fact that propellant characteristics (density, viscosity, enthalpy) are dependent on temperature, and a change in these characteristics leads to deviations in flow rates, thrust, and other engine characteristics.

It is convenient to characterize the influence of temperature of propellant components on propulsion system parameters by maximum running time, that is, propulsion system running time to total exhaustion (depletion) of one of the propellant components.

As a consequence of the fact that the dependence of physicochemical characteristics on temperature differs for oxidizer and fuel, maximum propulsion system running time for oxidizer and fuel differs in magnitude and is determined by evident relationships:

$$\tau_{ок} = \frac{M_{ок}}{\dot{m}_{ок}}; \quad \tau_г = \frac{M_г}{\dot{m}_г}, \qquad (4.34)$$

where M_{ok}, $M_г$ -- masses of propellant components in a rocket's tanks.

In view of the fact that propellant mass and flow rate are dependent on temperature, maximum propulsion system running time, all other conditions being equal, is also determined by the temperature of the propellant components.

In a linear approximation, we shall determine variation of maximum time with the equation

$$\left.\begin{aligned}\delta\tau_{ок} &= \delta M_{ок} - \delta\dot{m}_{ок};\\ \delta\tau_{г} &= \delta M_{г} - \delta\dot{m}_{г},\end{aligned}\right\} \qquad (4.35)$$

where

$$\delta y = \frac{y-\bar{y}}{\bar{y}}; \quad y = \overline{\tau_{ок},\ \tau_{г},\ M_{ок},\ M_{г},\ \dot{m}_{ок},\ \dot{m}_{г}}.$$

Variations of flow rates of propellant components are determined in solving the problem of influence of external and internal factors (Table 4.8):

$$\left.\begin{aligned}\delta\dot{m}_{ок} &= C_{\dot{m}_{ок},\ \rho_{ок}}\delta\rho_{ок} + C_{\dot{m}_{ок},\ \rho_{г}}\delta\rho_{г};\\ \delta\dot{m}_{г} &= C_{\dot{m}_{г},\ \rho_{ок}}\delta\rho_{ок} + C_{\dot{m}_{г},\ \rho_{г}}\delta\rho_{г}.\end{aligned}\right\} \qquad (4.36)$$

The dependence of density of propellant components on temperature is determined by the relation

$$\rho_j = \bar{\rho}_j + \beta_j (T_j - \bar{T}_j), \qquad (4.37)$$

where $j = \overline{ок,\ г}$; β_j -- temperature coefficient; $\bar{T}_j$ -- standard (nominal) temperature of propellant component.

Table 4.9 contains the characteristics of several propellant components.

Table 4.9.

1 Название компонента	2 Химическая формула	μ	3 ρ, $\frac{кг}{м^3}$ при 288 K	β, $\frac{кг}{м^3 K}$
Азотная кислота 4	HNO_3	63	1520	—1,66
Четырехокись азота 5	N_2O_4	92	1470	—1,98
Тетранитрометан 6	$C(NO_2)_4$	196	1650	—1,7
Кислород 7	O_2	32	1140 (90 K)	—4,4
Перекись водорода 8	H_2O_2	34	1460	—1,6
Фтор 9	F_2	38	1510 (90 K)	—3,2
Керосин 10	$C_{17\cdot21}H_{19\cdot29}$	100 17(усл.)	834	—1,15
Водород 11	H_2	2	710	—4,3
Спирт (этил) 12	C_2H_5OH	46	789	—1,32
НДМГ 13	$(CH_3)_2N_2H_2$	60	785	—1,0
Гидрозингидрат 14	$(NH_2)_2H_2O$	50	1030	—1,1
Гидразин 15	N_2H_4	32	1010	—1,2
Спирт метиловый 16		32	791	—1,14

Key to Table 4.9 on preceding page:

1. Component
2. Chemical formula
3. $\frac{kg}{m^3}$ at
4. Nitric acid
5. Nitrogen tetroxide
6. Tetranitromethane
7. Oxygen
8. Hydrogen peroxide
9. Fluorine
10. Kerosene
11. Hydrogen
12. Alcohol (ethyl)
13. NDMG
14. Hydrazine hydrate
15. Hydrazine
16. Methyl alcohol
17. Conditional

For noncryogenic propellant components, when separate thermostatic control is not employed, the following condition is met:

$$T_{ок} = T_г$$

and in this case

$$\delta\rho_l = a_{\rho_l,\ T}\delta T, \tag{4.38}$$

where

$$a_{\rho_l,\ T} = \beta_l \frac{\overline{T}_l}{\overline{\rho}_l}.$$

Equation (4.36), taking into account (4.38), is written in the form

$$\left.\begin{aligned} \delta\dot{m}_{ок} &= B_{ок}\delta T; \\ \delta\dot{m}_г &= B_г\delta T, \end{aligned}\right\} \tag{4.39}$$

where

$$\left.\begin{aligned} B_{ок} &= \left(C_{\dot{m}_{ок},\ \rho_{ок}} \frac{\beta_{ок}}{\overline{\rho}_{ок}} + C_{\dot{m}_{ок},\ \rho_г} \frac{\beta_г}{\overline{\rho}_г}\right)\overline{T}; \\ B_г &= \left(C_{\dot{m}_г,\ \rho_{ок}} \frac{\beta_{ок}}{\overline{\rho}_{ок}} + C_{\dot{m}_г,\ \rho_г} \frac{\beta_г}{\overline{\rho}_г}\right)T. \end{aligned}\right\} \tag{4.40}$$

We shall evaluate the signs and relationship between coefficients B_j. The following qualitative relations occur for noncryogenic propellant components:

$$\rho_{ок} > \rho_г; \quad \frac{\rho_{ок}}{\rho_г} = 1{,}8 \div 2{,}2; \quad \beta_{ок} < 0; \quad \beta_г < 0;$$

$$|\beta_{ок}| > |\beta_г|; \quad \frac{\beta_{ок}}{\beta_г} = 1 \div 1{,}5;$$

$$C_{\dot{m}_l,\ \rho_l} > 0; \quad C_{\dot{m}_l,\ \rho_l} < 0;$$

$$|C_{\dot{m}_{ок},\ \rho_{ок}}| > |C_{\dot{m}_{ок},\ \rho_г}|;$$

$$|C_{\dot{m}_г,\ \rho_{ок}}| < |C_{\dot{m}_г,\ \rho_г}|;$$

$$\frac{C_{\dot{m}_{ок},\ \rho_{ок}}}{C_{\dot{m}_{ок},\ \rho_{г}}} = 2{,}2 \div 25;$$

$$\frac{C_{\dot{m}_{г},\ \rho_{г}}}{C_{\dot{m}_{г},\ \rho_{ок}}} = 2{,}5 \div 18.$$

On the basis of the above relations, it follows from equations (4.40) that

$$B'_{ок} < 0; \quad B_{г} < 0 \qquad \text{and} \qquad |B_{ок}| < |B_{г}|.$$

Thus with an increase in the temperature of propellant components propellant flow rates decrease, whereby the degree of change in oxidizer flow rate is less than that of the fuel. Variation of mass fueling of propellant components depends on the method of fueling.

a) Fueling by volume.

With fueling by volume, the mass of the fueled propellant is

$$M = V\rho, \tag{4.41}$$

where V--- volume of propellant pumped on board.

Since with fueling by volume the volume of propellant pumped on board depends on the temperature, taking (4.38) into account, equation (4.41) has the form

$$\left.\begin{aligned} \delta M^{V}_{ок} &= L_{ок}\delta T; \\ \delta M^{V}_{г} &= L_{г}\delta T, \end{aligned}\right\} \tag{4.42}$$

where

$$L_{j} = \beta_{j}\frac{\overline{T}}{\overline{\rho}_{j}}.$$

It follows from the correlation of quantities β_j and ρ_j that

$$L_{j} < 0; \quad |L_{ок}| < |L_{г}|.$$

Substituting (4.42) and (4.39) in equation (4.35) we obtain variations of maximum time for fueling by volume

$$\left.\begin{aligned} \delta\tau^{V}_{ок} &= (L_{ок} - B_{ок})\delta T; \\ \delta\tau^{V}_{г} &= (L_{г} - B_{г})\delta T. \end{aligned}\right\} \tag{4.43}$$

Since $B_j < 0$ and $L_j < 0$, the sign of the coefficient with δT is determined by the correlation between L_j and B_j. Results of propellant calculations indicate that for motors there occurs relation

$$|L_{j}| > |B_{j}| \qquad \text{and} \qquad |L_{ок} - B_{ок}| < 0; \quad |L_{г} - B_{г}| < 0.$$

It follows from this that with fueling by volume, with an increase in temperature of the propellant components, maximum running time for oxidizer and fuel diminishes.

b) Fueling by mass.

With fueling by mass, the mass of the propellant pumped on board is independent of temperature, that is,

$$\delta M_{ок}^{M} = \delta M_{г}^{M} = 0.$$

In this case it follows from equations (4.35) and (4.39) that

$$\left.\begin{aligned} \delta\tau_{ок}^{M} &= -B_{ок}\delta T; \\ \delta T_{г}^{M} &= -B_{г}\delta T. \end{aligned}\right\} \qquad (4.44)$$

Since $|B_{ок}| < |B_{г}|$ and $B_{ок} < 0;\ B_{г} < 0,$ with an increase in the temperature of propellant components, with fueling by mass the maximum running time increases, whereby for fuel this increase is greater than for oxidizer.

Figure 4.2 shows qualitative relation $\tau_j = f(T)$ for both types of fueling.

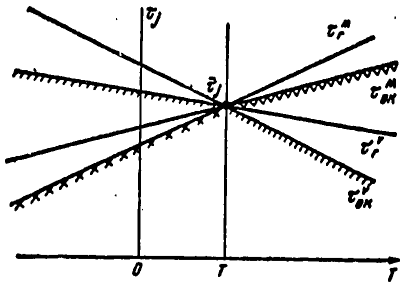

Figure 4.2. Dependence of Maximum Running Time on Propellant Temperature

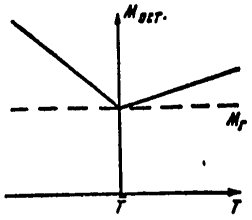

Figure 4.3. Dependence of Fuel Remainder on Temperature

It follows from an analysis of Figure 4.2 that when $T > \bar{T}$ maximum propulsion system running time is determined by the oxidizer supply, while when $T < \bar{T}$ it is determined by the fuel supply.

This means that when the engine is shut down under conditions $T \neq \bar{T}$, unconsumed components remain on board the rocket.

The mass of the unconsumed propellant depends on temperature and is estimated by quantity

$$M_{oc\tau} = |\tau_{ok} - \tau_r| \dot{m}_j, \qquad (4.45)$$

where j=ok when $T < \bar{T}$, j=r when $T > \bar{T}$.

Relation (4.45) is shown in Figure 4.3, where M_r -- guaranteed fuel reserves. The engine is shut down by an automatic preset range control unit. Guaranteed reserves are ensured in order to eliminate the possibility of premature engine shutdown due to exhaustion of one of the propellant components.

Guaranteed fuel reserve refers to the minimal quantity of propellant above standard which ensures, with a specified probability under all operating conditions, engine shutdown by the automatic preset range control unit.

In order to reduce fuel residue M_{ocT}, and consequently passive rocket mass, control systems are employed, which under all conditions ensure simultaneous tank emptying, that is, condition

$$\tau_{ok} - \tau_r = 0$$

and $M_{ocT}=0$.is fulfilled.

Chapter 5. STATISTICAL ANALYSIS OF PRECISION OF MOTOR OPERATION

5.1. Laws of Distribution of Operation Parameters

For analysis and calculation of precision and reliability of engine operation, it is essential to know the laws of distribution of operation parameters and their statistical characteristics.

In practice one very frequently encounters normal distribution. This is due to the fact that it is the maximum distribution toward which other distributions approach. In addition, it follows from Lyapunov's theorem that distribution of a sum of a sufficiently large number of independent or slightly-dependent random quantities with random distributions approaches normal distribution.

Density of normal distribution is described by relation

$$\varphi(y) = \frac{1}{\sigma_y \sqrt{2\pi}} \exp\left(-\frac{y - m_y}{2\sigma_y}\right).$$

Therefore when processing statistical realizations one first of all tests the assumption of normal distribution. Testing of distribution is a task of statistical verification of hypotheses, that is, testing of the adequacy of empirical laws of distribution of samples obtained durings tests to theoretical normal distribution. The procedure of testing the law of distribution is as follows.

Actual data on the aggregate of operation parameter values are determined as a result of tests and engine operation. If we designate the magnitude of measurement of operation parameter y_j, then for the aggregate of all measurements we can construct variation series $\{y_j\}$, for which sequence $y_1 \leqslant y_2 \leqslant \ldots \leqslant y_n$ is valid. For formalization of calculations, we make the series denser by breaking it down into separate intervals, and in each interval all values are replaced by one, corresponding to the middle of the interval.

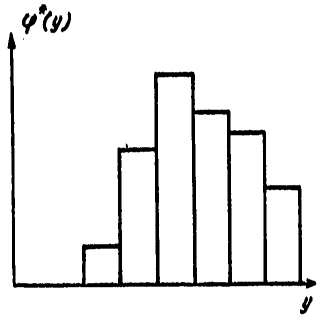

Figure 5.1. Histogram of Distribution

Interval length is determined by relation [18]

$$\Delta y = \frac{y_{max} - y_{min}}{1 + 3{,}2 \log N}.$$

For each interval one calculates frequency

$$P^*_j = \frac{m_j}{N},$$

where m_j -- number of measurements falling within interval j; N -- number of all measurements.

As a result of this processing we determine an empirical distribution function comprising accumulated frequencies in intervals

$$F^*(\bar{y}_j) = \sum_{i=1} P^*_j,$$

and for each interval

$$\bar{y}_j = \frac{1}{2}(y_j + y_{j+1}).$$

On the distribution function we plot a histogram (Figure 5.1) or empirical distribution density

$$\varphi^*(\bar{y}_j) = \frac{F^*(\bar{y}_j)}{\Delta y}.$$

Adequacy of empirical distribution to normal is tested on the basis of statistical criteria which have been well elaborated in mathematical statistics. The Pearson criterion is most convenient for calculations [28].

Criterion χ^2 is based on statistical distribution

$$\chi^2 = \sum (m_j - NP^*_j)/NP^*_j \qquad (5.1)$$

in the assumption that part P^*_j of incidence of random quantity y_j in certain interval $[L_{j-1}, L_j]$ is determined directly by sample $\{y_j\}$, while estimate of probability of occurrence of event $P^*=P[L_{j-1} < y < L_j]$ can be calculated with the aid of law of distribution $F(y, a_1, a_2)$, which is known with an accuracy up to a certain group of parameters a_1, a_2.

If we utilize as estimates of parameters a_i estimates on results of measurements y_j, then when $N \to \infty$ statistics (5.1) possess χ^2 distribution with degrees of freedom k=1-3.

When an assumption of normal distribution is made with respect to sample $\{y_j\}$, in order to verify advanced hypothesis $F(y)=B(m_y, \sigma_y)$ one must perform the following estimates:

figure an estimate of mathematical expectation and standard deviation of experimental sample $\{y_j\}$

$$m_y^* = \frac{1}{N}\sum y_j; \quad \sigma_y^{*2} = \frac{1}{N-1}\sum (y_j - m_y^*)^2$$

with the aid of distribution tables [18] of Laplace functions $\Phi(y)$ and find probability P_j of appearance of the value of a random quantity at each interval;

determine the number of degrees of freedom k=1-3, where l -- number of intervals in the sample;

choose level of significance β, that is, probability of erroneous rejection of a correct hypothesis of distribution. For solving this problem we assume β =0.05-0.1;

determine empirical statistic

$$\chi_э^2 = \sum \frac{m_j - NP_j^*}{NP_j^*}$$

and according to the tables in [15] calculate quantity $P(\chi^2 > \chi_э^2)$.

If table value $P(\chi^2) > \beta$, then the hypothesis of normal distribution of $\{y_j\}$ is correct.

In addition to testing by criterion χ^2 one estimates the degree of difference of actual distribution from normal.

The degree of deviation of actual distribution from normal is determined by moments of a higher order.

If distribution of $\{y_j\}$ is normal, then the following relations are valid:

mean absolute deviation

$$\delta = \frac{E(|y - m_y|)}{\sigma_y} = 0{,}7978;$$

coefficient of asymmetry

$$\gamma = \frac{E(|y - m_y|^3)}{\sigma_y^3} = 0;$$

coefficient of excess

$$\lambda = \frac{E(|y - m_y|^4)}{\sigma_y^4} = 0.$$

In order to determine the degree of deviation of actual from normal distribution, one must calculate statistics

$$\left.\begin{aligned} \delta^* &= \frac{1}{N\sigma_y^*} \sum |y_j - m_y^*|; \\ \gamma^* = \frac{1}{N\sigma_y^{*3}} \sum |y_j - m_y^*|^3; \quad \lambda &= \frac{1}{N\sigma_y^{*4}} \sum |y_j - m_y^*|^4. \end{aligned}\right\} \quad (5.2)$$

Comparing calculated statistics (5.2) with the critical values contained in Table 5.1 [28], we can determine in which characteristics actual distributions differ from normal.

Table 5.1.

N	Critical Value					
	δ		γ		λ	
	$\beta = 0{,}5$	$\beta = 0{,}1$	$\beta = 0{,}05$	$\beta = 0{,}1$	$\beta = 0{,}05$	$\beta = 0{,}1$
10	0,907	0,89	0,862	1,135	—	—
20	0,90	0,877	0,721	1,116	—	—
30	0,882	0,862	0,661	0,982	—	—
40	0,870	0,852	0,587	0,869	—	—
50	0,865	0,848	0,533	0,787	4,92	4,01
60	0,859	0,843	0,492	0,723	—	—
70	0,854	0,840	0,459	0,673	—	—
80	0,852	0,838	0,432	0,631	—	—
90	0,848	0,835	0,409	0,596	—	—
100	0,846	0,834	0,389	0,547	4,70	3,77

Figures 5.2 and 5.3 contain histograms of combustion chamber pressure for controllable and uncontrollable motors without generator gas afterburning. The histograms are constructed in coordinates

$$\Delta z = \frac{\Delta p_к}{\bar{\sigma}_{p_к}}; \quad \bar{\sigma}_{p_к} = \frac{\sigma_{p_к}}{m_{p_к}},$$

and normal distribution curve

$$\varphi(\Delta z) = \frac{1}{\sqrt{2\pi}} e^{-\frac{\Delta z^2}{2}}.$$

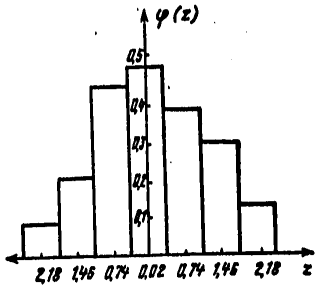

Figure 5.2. Histogram of Combustion Chamber Pressure Distribution for a Controllable Motor

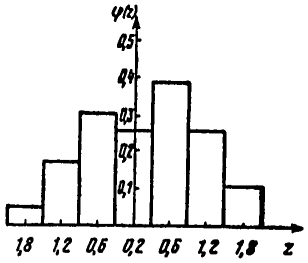

Figure 5.3. Histogram of Combustion Chamber Pressure Distribution for an Uncontrollable Motor

Statistical characteristics of normal distribution of parameters are determined by many factors. However, processing of statistical data indicates that root-mean-square deviations for different motors vary within narrow limits and only differ substantially for controllable and noncontrollable motors.

Table 5.2 contains results of processing of statistical data of distribution of operation parameters of motors without generator gas afterburning.

Table 5.2

Параметр рабочего процесса 1	Тип двигателя 2	$\bar{\sigma}^*$	γ^*	λ^*
Давление в камере двигателя, $p_к$ 3	4 Регулируемый	0,21—0,57	—0,123	—0,607
	5 Нерегулируемый	2,12—4,0	—	—
Тяга P 6	4 Регулируемый	0,32—0,8	—0,3	—0,45
	5 Нерегулируемый	2,43—4,76	—0,2	—0,5
Соотношение компонентов в камере двигателя, K 7	4 Регулируемый (СОБ)	2,52—2,69	—0,15	—0,72
	5 Нерегулируемый	1,22—1,53	—0,28	—0,82

Key:
1. Operation parameter
2. Type of motor
3. Combustion chamber pressure
4. Controllable
5. Noncontrollable
6. Thrust
7. Ratio of propellant components in combustion chamber

The table contains root-mean-square deviations relative to mathematical expectations

$$\bar{\sigma}^* = \frac{\sigma^*}{m}[\%].$$

It follows from an analysis of the figures in Table 5.2 that operation parameters are distributed according to the normal law with slight negative excess. As could be expected, there occurs a considerable increase in precision of operation of controllable motors; root-mean-square deviations of thrust and combustion chamber pressure in controllable motors are an order of magnitude less than in noncontrollable.

5.2. Statistical Characteristics of Precision

Under operating conditions all disturbing factors are random quantities pertaining to employment of a specific motor and moment in time.

Statistical characteristics can be obtained for disturbing factors: mathematical expectation m_{x_i}, root-mean-aquare deviation σ_{x_i}, and correlation coefficients $r_{x_i s_i}$ (Ch. 2). If these characteristics are not known, mathematical expectation is assumed equal to the nominal value of the disturbing factor, and root-mean-square deviation is determined on the magnitude of the maximum deviation. For the normal law of distribution,

root-mean-square deviation is linked with maximum deviation $\Delta x_{пр}$ by relation $\sigma_x = \Delta x_{пр}/2{,}7$, and for uniform distribution $\sigma_x = \Delta x_{пр}/2{,}45$.

Calculation of the statistical characteristics of engine precision presupposes determination of operation parameters which will occur under all operating conditions, that is, with specified statistical characteristics of disturbing factors.

Statistical characteristics are calculated with the following simplifying premises: operation characteristics are random functions with the normal law of distribution at each and every point in time and are linearly dependent on disturbing factors.

Let engine characteristics y_j be determined by a functional relation of the type

$$y_j = y(y_1, y_2, \ldots, y_N; x_1, x_2, \ldots, x_k),$$

where y_j -- operation characteristics j=1, $\bar{N}$; x_i -- disturbing factors i=1, $\bar{K}$.

Then, possessing mean values m_{y_j} and m_{x_i} of quantities y_j and x_i, one can obtain value

$$y_j = m_{y_j} + \left(\frac{\partial y_j}{\partial z_i}\right)(z_j - m_{z_i}), \qquad (5.3)$$

where $z=\overline{y, x}$, while derivatives are taken at point m_{y_j}, m_{x_i}. In the general case the mean function value may not coincide with the function value from the mean argument value; this is evident from relation [6]:

$$m = m[\varphi(t_1, t_2, \ldots, t_N)] = \varphi(m_1, m_2, \ldots, m_N) + \Delta,$$

where m_i -- mean value of random quantities t_i; Δ -- correction for nonlinearity of function φ.

However, when linear functions are examined, Δ =0. According to the indicated observation,

$$m_{y_j} = f(\bar{y}_1, \bar{y}_2, \ldots, \bar{y}_N; \bar{x}_1, \bar{x}_2, \ldots, \bar{x}_k). \qquad (5.4)$$

Linearizing the equations, from relation (5.3) we obtain

$$\sum_{j=1}^{N} a_{ij}\delta y_j = \sum_{i=1}^{k} b_{ij}\delta x_i, \qquad (5.5)$$

where

$$\delta y_j = \frac{y_j - m_y}{m_y}; \quad \delta x_i = \frac{x_i - m_x}{m_x}.$$

The solution of equation (5.5) is contained in Section 4.1 (4.4)

$$\delta y_j = \sum_{i=1}^{k} C_{ij}\delta x_i. \qquad (5.6)$$

Proceeding in equation (5.6) from relative deviations to standard deviations and utilizing the theorem on summation of standard deviations, we obtain

$$\tilde{\sigma}_{y_j} = \sqrt{\sum_{i=1}^{k} C_{ij}^2 \tilde{\sigma}_{x_i}^2 + 2 \sum_{k \neq z} C_{j,\,k} C_{jz} r_{x_k,\,x_z} \bar{\sigma}_{x_k} \tilde{\sigma}_{x_z}}, \qquad (5.7)$$

where $\bar{\sigma} = \sigma/m$.

The coefficient of correlation between operation parameters is determined by relation

$$r_{y_j,\,y_k} = \frac{1}{\sigma_{y_j} \sigma_{y_k}} \left[\sum C_{ji} \sigma_{k,\,i} \sigma_{x_i}^2 + \right.$$

$$\left. + \sum_{s \neq t} (C_{ji} C_{ks} + C_{js} C_{ki}) \sigma_{x_s} \sigma_{x_i} r_{x_s,\,x_i} \right], \qquad (5.8)$$

where the symbol $\sum_{s \neq t}$ signifies that the sum is composed of combinations $(C_{ji} C_{ks} + C_{js} C_{ki})$, taken from set C_{ji}, for which there is a correlation between disturbing factors.

In a case where disturbing factors are not correlated ($r_{x_i,\,x_k} = 0$), equations (5.7) and (5.8) will assume the form

$$\left.\begin{aligned} \sigma_{y_j} &= \sqrt{\sum_{i=1}^{k} C_{ij}^2 \left(\frac{m_{y_j}}{m_{x_i}}\right)^2 \sigma_{x_i}^2}; \\ r_{y_j,\,y_k} &= \frac{1}{\sigma_{y_j} \sigma_{y_k}} \sum_{i=1}^{k} C_{ji} C_{ki} \sigma_{x_i}^2. \end{aligned}\right\} \qquad (5.9)$$

The value of the operation parameters which a motor will have under any and all operating conditions will be determined as follows:

$$y_j = m_{y_j} \pm 3\sigma_{y_j}. \qquad (5.10)$$

Thus, depending on available information on disturbing factors and the stated objective, two problems can be solved:

determination of the values of operation parameters for concrete conditions of operation and for a specified motor [formula (4.4)];

determination of the probability values of the parameters, that is, values of operation parameters under any conditions of motor operation [formula (5.10)].

For comparison of the above-examined calculation methods, Table 5.3 contains results of calculation of external and internal factors on the operation parameters of a coded engine.

Table 5.3

Вид расчета (1)	$\dot{m}_{ок}$	$\dot{m}_{г}$	$p_{к}$	n
Расчет по уравнению (4.4) δ_{yj} (2)	0,2	0,32	0,15	0,03
(3) Расчет при $r_{x_l x_k} = 0$, уравнение (5.9) $\tilde{\sigma}_{yj}$ (4)	0,092	0,5	0,06	0,042
Расчет с учетом корреляционной матрицы (табл. 2.3), уравнение (5.7) $\tilde{\sigma}_{yj}$ (5)	0,04	0,42	0,032	0,02
Результаты обработки данных испытаний $\tilde{\sigma}_{tj}$ (6)	0,06	0,04	0,02	0,01

Key:
1. Type of calculation
2. Calculation on equation (4.4)
3. Calculation with
4. Equation
5. Calculation taking into account correlation matrix (Table 2.3), equation
6. Results of processing test data

It follows from an analysis of the table that calculations taking into account correlations between disturbing factors ensure the least error in comparison with experimental data.

5.3. Conditions of Engine Efficiency

5.3.1. General

In the general case engine failure is a consequence of disturbance of specific conditions, which are determined by the demands imposed on operation parameters and characteristics. The conditions of efficiency are conditions of failure-free operation expressed in the form of inequalities. All efficiency conditions can be subdivided into two groups: internal and external.

Internal efficiency conditions are those fulfillment of which is essential for an engine to operate; they include balance equations for flow rates, outputs and pressures. External conditions of efficiency include specifications for operation parameters, proceeding from the requirements of economy, controllability, and reliability.

In general form conditions of efficiency are written as follows: $y_1 < y_j < y_2$ or in normal form $y_j - y_1 > 0$; $y_2 - y_1 > 0$; $\psi_1(y_j) = y_j - y_1$ and $\psi_2(y_j) = y_2 - y_j$ are called functions of efficiency.

One can list a large number of efficiency functions for motors. Only a few quantities among efficiency functions are determined, without random components. These quantities are characteristics determined by topological design properties (number of turbine blades, pumps, number of injectors, physical constants, etc).

The overwhelming majority of parameters (y_j) in efficiency functions are random quantities or functions, and therefore functions of efficiency are random.

In the general case operation parameters y_j can be viewed as a load acting on the structure, and allowable limits of change $y_j = Y$ -- as strength or carrying capacity. Both y_j and Y are functions of disturbing factors x_i and time τ.

In this case functions of efficiency will be written in the form

$$y_j(\tau, x_1, x_2, \ldots, x_k) < Y_j(\tau_1, x_1, x_2, \ldots, x_k)$$

or

$$\psi_j(\cdot) = y_j(\cdot) - Y_j(\cdot) < \gamma_j,$$

where $j = \overline{1, N}$ -- number of functions of efficiency; γ_j -- allowable level of efficiency;

$\gamma_j = 0$ or a finite quantity; $(\cdot) = (\tau_1, x_1, x_2, \ldots, x_k)$.

Conditions of efficiency will be disrupted when $\psi_j > 0$.

The probability that all conditions of efficiency will be met, that is, failure will not occur, is determined by the equation

$$P(\cdot) = \text{Bep}\begin{Bmatrix} \psi_1(\cdot) < \gamma_1 \\ \psi_2(\cdot) < \gamma_2 \\ \cdots \\ \psi_N(\cdot) < \gamma_N \end{Bmatrix} = \frac{1}{\sqrt{(2\pi)^N D}\prod_1^N \sigma_{\psi_j}} \int_{-\infty}^{\gamma_1}\int_{-\infty}^{\gamma_2}\cdots\int_{-\infty}^{\gamma_k} \times$$

$$\times \int_{-\infty}^{\gamma_N} \exp\left\{-\frac{1}{2D}\sum_{i=j}^{N} D_{ij}\frac{[\psi_j(\cdot)-\gamma_j][\psi_i(\cdot)-\gamma_i]}{\sigma_{\psi_j}\sigma_{\psi_i}}\right\} d\psi_1 \ldots d\psi_N; \quad (5.11)$$

$$D = \|r_{\psi_i, \psi_j}\|.$$

Determination of the probability of fulfillment of conditions of efficiency presupposes calculation of multivariate integrals of distribution.

An approximate solution of equation (5.11) is contained in [6], consisting in the following.

One determines the probability of fulfillment of each individual condition of efficiency $P_j(\psi_j > 0)$.

The probability of fulfillment of all conditions of efficiency in the aggregate is determined with equation

$$P(\psi > 0) = \prod_{j=1}^{N} P_j + \left[P_{j,m} - \prod_{j=1}^{N} P_j \right] K_N, \qquad (5.12)$$

where $P_{j,m} = \min_{1<j<N} P_j$ -- the minimal of values P_j;

$$K_N = \frac{2}{\pi c} \sum \arcsin r_{i,j};$$

$$c = \frac{N(N-1)}{2},$$

where N -- number of conditions of efficiency; $r_{i,j}$ -- coefficient of correlation between conditions of efficiency.

Obviously if conditions of efficiency are independent

$(r_{i,j}=0)$, then $K_N=0$ and $P(\psi>0) = \prod_{j=1}^{N} P_j$.

If $r_{i,j}=1$, conditions of efficiency are written linearly, then $P(\psi>0)=P_{j,m}$.

5.3.2. Conditions of Engine Efficiency. Parametric Reliability

Parametric reliability is defined as the probability that engine parameters will fall within limits prescribed by technical specifications.

Parametric reliability in design can be determined not for all operation parameters, but only for those which determine the economy and efficiency of an engine design. These parameters include, first and foremost, specific thrust impulse, combustion chamber and gas generator pressure, ratio of propellant components in the gas generator, combustion chamber and gas generator wall temperature. In conformity with this, one can write the following efficiency functions:

$$\psi_{I_y} = I_y - I_{y.д} > 0; \quad \psi_K = K_д - K > 0;$$
$$\psi_{p_к} = p_{к.д} - p_к > 0; \quad \psi_{p_{гг}} = p_{гг.д} - p_{гг} > 0;$$
$$\psi_{T_{ст}} = T_{ст.д} - T_{ст} > 0,$$

where subscript д designates allowable parameter values prescribed by technical specifications.

All the enumerated parameters are random quantities for a specified point in time.

In analyzing statistical characteristics, σ_{y_j} and m_{y_j} are determined for them.

Allowable parameter values are prescribed by technical specifications, and therefore they can be considered determined, that is, $\sigma_{y_{jд}}=0$. In the general case, when y_j and $y_{jд}$ are random quantities, and under the condition that they have normal laws of distribution, the probability of fulfillment of ψ_j condition of efficiency will be determined by the equation

$$P(\psi_j > 0) = \int_0^{\infty} \varphi(\psi_j)\, d\psi = 0{,}5 + \Phi(z_j), \qquad (5.13)$$

where $\Phi(\psi_j)$ -- distribution function of ψ_j; $\Phi(z_j)$ -- Laplace function;

$$\Phi(-z) = -\Phi(z); \quad z_j = m_{\psi_j}/\sigma_{\psi_j}.$$

Since an efficiency function is a superposition of two normal functions $\Phi(y_j)$ and $\Phi(y_{jд})$, then

$$\left.\begin{aligned} m_{\psi_j} &= m_{y_{jд}} - m_{y_j}; \\ \sigma_{\psi_j} &= \sqrt{\sigma_{y_j}^2 + \sigma_{y_{jд}}^2 - 2r_{y_j, y_{jд}}\sigma_{y_j}\sigma_{y_{jд}}}, \end{aligned}\right\} \qquad (5.14)$$

where $j = \overline{p_к,\ p_{тг},\ K,\ T_{ст},\ I_y}$.

If there is no correlation between y_j and $y_{jд}$ $(r_{y_j, y_{jд}} = 0)$, then

$$\sigma_{\psi_j} = \sqrt{\sigma_{y_j}^2 + \sigma_{y_{jд}}^2}.$$

Obvious consequences follow from relation (5.13):

a) when $m_{y_j} = m_{y_{jд}}$; $\Phi(z_j) = 0$ and $P(\psi_j > 0) = 0{,}5$;

b) when $m_{y_j} < m_{y_{jд}}$; $\Phi(z_j) > 0$ and $P(\Psi_j > 0) > 0{,}5$;

c) when $m_{y_j} > m_{y_{jд}}$; $\Phi(z_j) < 0$ and $P(\Psi_j > 0) < 0{,}5$.

5.3.3. Condition of Reliable Combustion Chamber Cooling

As an example we shall examine the condition of combustion chamber wall temperature efficiency.

In the general case the combustion chamber of a ZhRD consists of two concentric shells. A propellant component moves between the outer and inner shell, absorbing heat from the inner shell, which is heated by combustion products.

With unsatisfactory cooling, the inner wall of the combustion chamber can burn through, with subsequent failure.

A condition of reliable cooling is

$$Q_a = Q_n - Q_{oT} < Q_{kr}, \qquad (5.15)$$

where Q_a -- quantity of heat accumulated by the system during operation; Q_{st} -- quantity of heat conducted to the wall; Q_{oT} -- quantity of heat removed by liquid coolant from the wall; Q_{kr} -- allowable (critical) quantity of heat accumulated by the wall material.

Quantities Q_j in the general case are random functions of the wall coordinates and operating time. In addition, Q_j depends on other random arguments.

For example, Q_{st} depends on rate of flow, ratio of propellant components and other factors. Q_{oT} depends on rate of flow and thermophysical properties of the cooling propellant component and its flow conditions in the coolant jacket; Q_{kr} is determined by the mechanical properties of the material.

We can demonstrate that condition (5.15) is equivalent to the following $T < T_{kr}$, or

$$\psi_T = T_{kr}(\tau, x, y, z) - T(x, y, z) > 0, \qquad (5.16)$$

where $T(\cdot)$ -- inner shell heating temperature; $T_{kr}(\cdot)$ -- shell critical temperature.

The process of heat exchange in the combustion chamber takes place as follows. Heat from the combustion products is conveyed to the walls as a result of convective and radiant heat exchange, spreads in the walls due to heat conductivity, and is further conveyed to the liquid coolant.

Gas wall temperature T is the principal characteristic on which one judges cooling system efficiency.

Total specific heat flow under steady-state operating conditions, transferred to the liquid [5]:

$$q_\Sigma = \frac{T_r - T_ж}{\frac{1}{\alpha_r} + \frac{1}{\alpha_ж} + \frac{\delta}{\lambda}} = q_\Sigma(x),$$

where

$$T_ж = T_{вх} + \int_x^x q_\Sigma \frac{\pi D}{c_ж \dot{m}_ж} dx = T_{вх} + \Delta T = T_ж(x)$$

temperature of liquid;

$$\alpha_r = 4c_p \dot{m}^{0,82} D^{-1,82} = \alpha_r(x)$$

coefficient of heat transfer from gases to wall;

$$\alpha_ж = 27c_ж \left(\frac{\eta}{D_э}\right)_ж^{0,2} (\rho w)_ж^{0,8} = \alpha_ж(x)$$

coefficient of heat transfer from wall to liquid; δ, λ -- wall thickness and coefficient of heat conductivity of material; $D_э$ -- equivalent diameter;

$$T_r = T_0 + \varepsilon_r c_0 T_r^4/\alpha_r,$$

T_r -- calculated temperature, taking into account heat transfer by radiation; T_0 -- gas stagnation temperature; x -- coordinate coinciding with combustion chamber generatrix, figured from induction manifold.

For steady-state operating conditions and specified combustion chamber geometry, T_0 is independent of x, and wall temperature changes insignificantly lengthwise.

Therefore change in convective heat flow along combustion chamber length is determined chiefly by chamber diameter ($D^{-1.82}$) and reaches maximum value in the nozzle throat area.

Wall temperature depends on thickness, and it can be determined as follows:

$$T_r = T_{r.п} - (T_{r.п} - T_{ж.п})\frac{z}{\delta} = T(x, z), \qquad (5.17)$$

where $0 < z < \delta$ -- wall thickness coordinate; $T_{ж.п} = T_ж + \frac{q_Σ}{\alpha_ж}$ -- wall surface temperature on coolant side;

$T_{r.п} = T_{ж.п} + \frac{q_Σ \delta}{\lambda}$ -- wall surface temperature on gas side.

Allowable wall temperature value $T_д$ is approximately determined

$$T_д = T_{r.д} - \chi(T_{r.д} - T_{ж.д}), \qquad (5.18)$$

where $T_{r.д}$ and $T_{ж.д}$ -- allowable wall temperature value on the gas and coolant side respectively; χ -- delta function, $\chi = 0$ when $z=0$; $\chi = 1$ when $z=\delta$. Quantity $T_{ж.д}$ is determined by temperature of thermal decomposition or coolant liquid film boiling temperature. Probability of reliable combustion chamber wall cooling is determined by inequality

$$P(\psi_T > 0) = P\{T_д(z) - T(x, z) > 0\}. \qquad (5.19)$$

Determination of $P(\psi_T > 0)$ is performed as follows.

Several points must be selected on the combustion chamber surface. However, since a maximum heat flow takes place in the nozzle throat area, one can limit examination to checking reliable cooling of just this area. On the z axis (wall thickness) one should examine two points: z=0 and z= δ .

In this case (5.19) breaks down into two:

$$\left.\begin{aligned} P_1 &= P[T_д(0) - T(x_{кр}, 0) > 0] = P(\psi_{T_1} > 0); \\ P_2 &= P[T_д(\delta) - T(x_{кр}, \delta) > 0] = P(\psi_{T_2} > 0). \end{aligned}\right\} \qquad (5.20)$$

The sought value $P(\psi_i > 0)$ is determined by formula (5.12), which for N=2 assumes the form

$$P(\psi_T > 0) = P_1 \cdot P_2 + (P_{1,m} - P_1 P_2) \frac{2}{\pi} \arcsin r_{\psi_{T_1}, \psi_{T_2}}. \qquad (5.21)$$

For normal distribution

$$P_j = P(\psi_{T_j} > 0) = 0{,}5 + \Phi(z_j), \qquad (5.22)$$

Where $\Phi(z_j)$ -- Laplace function;

$$z_j = \frac{\bar{T}_{дj} - \bar{T}_j}{\sqrt{\sigma^2_{T_{дj}} + \sigma^2_{T_j}}}; \qquad (5.23)$$

$$\left.\begin{aligned} \bar{T}_{дj} &= \bar{T}_{г.д} \\ \sigma^2_{T_{дj}} &= \sigma^2_{T_{г.д}} \end{aligned}\right\} \text{when } z=0; \quad \left.\begin{aligned} \bar{T}_{дj} &= \bar{T}_{х.д} \\ \sigma^2_{T_{дj}} &= \sigma^2_{T_{х.д}} \end{aligned}\right\} \text{when } z=\delta;$$

$\bar{T}_{г.д}$, $\bar{T}_{х.д}$, $\sigma_{T_{г.д}}$, $\sigma_{T_{х.д}}$ -- are determined from reference or experimental data. $\bar{T}_j$ and σ_{T_j} are determined from heat exchange equations with fixed values x_i and z_i.

$$\bar{T}_j = T(x, z) = \bar{T}_{х.п\,j} + \frac{q_{\Sigma_j}(\delta - z)}{\bar{\lambda}}; \qquad (5.24)$$

$$\sigma^2_{T_j} = \sigma^2_{T_{х.п}} + \left(\frac{\bar{\delta} - z}{\bar{\lambda}}\right)^2 \sigma^2_{q_\Sigma} + \left(\frac{q_\Sigma}{\bar{\lambda}}\right)^2 \sigma^2_\lambda + \left[\frac{q_\Sigma}{\bar{\lambda}}(\bar{\delta} - z)\right]^2 \sigma^2_\delta$$

where

$$q_\Sigma = \frac{\bar{T}_г + \bar{T}_ж}{\frac{1}{\bar{\alpha}_г} + \frac{1}{\bar{\alpha}_ж} + \frac{\bar{\delta}}{\bar{\lambda}}};$$

$$\sigma^2_{q_\Sigma} = \frac{1}{\bar{\alpha}^2}(\sigma^2_{T_г} + \sigma^2_{T_ж}) + \frac{1}{\bar{\alpha}^2} q^2_\Sigma \left(\frac{\sigma^2_{\alpha_г}}{\bar{\alpha}^4_г} + \frac{\sigma^2_\delta}{\bar{\lambda}^2} + \frac{\bar{\delta}^2}{\bar{\lambda}^4}\sigma^2_\lambda + \frac{1}{\bar{\alpha}^4_ж}\sigma^2_{\alpha_ж}\right);$$

$$\tilde{\alpha} = \frac{1}{\frac{1}{\bar{\alpha}_r} + \frac{1}{\bar{\alpha}_ж} + \frac{\delta}{\bar{\lambda}}};$$

$$\bar{T}_r = \bar{T}_0 + e_r c_0 \bar{T}_r^4/\bar{\alpha}_r; \quad \bar{T}_ж = \bar{T}_{вх} + \Delta\bar{T};$$

$$\sigma^2_{\bar{T}_r} = \sigma^2_{T_0} + \frac{e_r c_0 \bar{T}_r^4}{\bar{\alpha}_r}\left(16\frac{\sigma^2_{T_r}}{\bar{T}_r^2} + \frac{\sigma^2_{\alpha_r}}{\bar{\alpha}_r^2}\right);$$

$$\sigma^2_{T_ж} = \sigma^2_{T_{вх}} + \sigma^2_{\Delta T}.$$

The quantities in the above relations contain mean values T_j and standard deviation $\sigma^2_{T_j}$. Some of them are primary and are obtained from reference data, while others in turn constitute functions of random arguments $\dot{m}$, T_0, w, etc.

The correlation coefficient between functions ψ_{T_1} and ψ_{T_2} is determined from relation

$$r_{\psi T_1, \psi T_2} = \frac{\sigma_{T_1}\sigma_{T_2} r_{T_1 T_2} + \sigma_{T_{1Д}}\sigma_{T_{2Д}} r_{T_{1Д}, T_{2Д}}}{\sqrt{\sigma^2_{T_1} + \sigma^2_{T_2}}\sqrt{\sigma^2_{T_{1Д}} + \sigma^2_{T_{2Д}}}}. \qquad (5.25)$$

To determine quantities $r_{T_1 T_2}$ and $r_{T_{1Д}, T_{2Д}}$ we employ expressions for T and $T_Д$.

$$r_{T_j, T_l} = \frac{1}{\sigma_{T_j}\sigma_{T_l}}(a_1\sigma^2_{T_0} + a_2\sigma^2_{\delta} + \cdots),$$

where

$$a_1 = \left(\frac{\partial T_j}{\partial T_0}\right)\left(\frac{\partial T_l}{\partial T_0}\right) = \frac{(\delta - z)^2}{\bar{\lambda}^{-2}\bar{\alpha}_l\bar{\alpha}_j};$$

$$a_2 = \left(\frac{\partial T_l}{\partial \delta}\right)\left(\frac{\partial T_j}{\partial \delta}\right), \text{ etc.}$$

5.4. Regression Analysis of Precision

The methods of analysis of statistical characteristics presented in the preceding sections do not always make it possible to establish an analytical relationship between engine parameters.

For example, it is extremely difficult to establish an analytical relationship between specific thrust impulse, combustion chamber pressure, and propellant component ratio. In such cases it is sufficient to link system input (k, p_k) with its output I_k, without examining the intermediate physical processes. For this one employs a method of regression analysis,

based on description of surface of system "Output" response to "Input" in certain vector space. Let us assume we must determine the dependence of index y (operation parameter) on several factors $\{x_i\}$. The type of function $y=y\{x_i\}$ is not known in advance. The function is represented by a series

$$y = b_0 + \sum b_i x_i + \sum b_{ij} x_i x_j + \sum b_{ii} x_i^2 + \cdots, \qquad (5.26)$$

where b_i, b_{ij} -- coefficients of regression, determining the degree of influence of factor x_i and their interaction $x_i x_j$ on output index y.

Determination of regression coefficients b_i, b_{ij} -- is the principal problem which is solved in regression analysis. Coefficients of regression are determined on the basis of experimental results. The method of regression analysis is widely employed for experimental establishment of interrelationships between characteristics of complex systems. There exist a number of restrictions on their employment, however, the principal of which are the following.

1. Results of measurements should follow the normal law of distribution.

2. Error standard deviations should be constant.

For motors operating under steady-state conditions, the above-enumerated conditions are met.

Most frequently multiple linear regression is employed in analyzing motor static characteristics.

Let us assume that a priori data enable us to state that the input regression equation has the form

$$y = b_0 + b_1 x_1 + b_2 x_2 + \cdots + b_k x_k. \qquad (5.27)$$

The adequacy of equation (5.27) to actual operation is determined from the results of the experiment shown in the Table 5.4.

Table 5.4.

y	x_1	x_2	x_3	x_4	. . .	x_k	n
y_1	x_{11}	x_{21}	x_{31}	x_{41}	. . .	x_{k1}	n_1
y_2	x_{12}	x_{22}	x_{32}	x_{42}	. . .	x_{k2}	n_2
. . .	. . .	. . .	. . .	. . .	. . .	. . .	. . .
y_N	x_{1N}	x_{2N}	x_{3N}	x_{4N}	. . .	x_{kN}	n_N

To solve the adequacy problem we must determine statistical estimates of coefficients b_i according to results of observations (Table 5.4).

In conformity with Table 5.4, we construct a system of equations

$$\left.\begin{aligned} b_0x_{01}+b_1x_{11}+b_2x_{21}+\cdots+b_kx_{k1}&=y_1;\\ b_0x_{02}+b_1x_{12}+b_2x_{22}+\cdots+b_kx_{k2}&=y_2;\\ \cdots\cdots\cdots\cdots\cdots\cdots\cdots&\\ b_0x_{0N}+b_1x_{1N}+b_2x_{2N}+\cdots+b_kx_{kN}&=y_N, \end{aligned}\right\} \qquad (5.28)$$

where $x_{01}=1$.

Estimates of coefficients b_i are performed utilizing the method of least squares. In conformity with this method, to obtain an optimal approximation of regression equation (5.27) to experimental data (Table 5.4), the following condition must be met:

$$S=\sum_{i=1}^{N} n(y-b_0x_0-b_1x_1-\cdots-b_kx_k)^2=\min.$$

To meet this condition one should equate to zero partial derivatives by b_i, as a result of which one obtains system of equations

$$\left.\begin{aligned} \frac{\partial S}{\partial b_0}&=-2\sum n[y-(b_0+b_1x_1+\cdots+b_kx_k)]=0;\\ \frac{\partial S}{\partial b_1}&=-2\sum n[y-(b_0+b_1x_1+\cdots+bx_k)x_1]=0;\\ \cdots\cdots\cdots\cdots\cdots\cdots\cdots&\\ \frac{\partial S}{\partial b_k}&=-2\sum n[y-(b_0+b_1x_1+\cdots+bx_k)x_k]=0. \end{aligned}\right\} \qquad (5.29)$$

From system of equations (5.29) it is not difficult to obtain a system of equations with reference to b_i:

$$\left.\begin{aligned} b_0\sum n+b_1\sum nx_1+b_2\sum nx_2+\cdots+b_k\sum nx_k&=\sum ny;\\ b_0\sum nx_1+b_1\sum nx_1^2+b_2\sum nx_1x_2+\cdots+b_k\sum nx_1x_k&=\\ =\sum nx_1y;&\\ \cdots\cdots\cdots\cdots\cdots\cdots\cdots\cdots\cdots&\\ b_0\sum nx_k+b_1\sum nx_1x_k+b_2\sum nx_2x_k+\cdots+b_k\sum nx_k^2&=\\ =\sum nx_ky.& \end{aligned}\right\} \qquad (5.30)$$

From the first equation of system (5.30) follows

$$b_0=\bar{y}-b_1\bar{x}_1-b_2\bar{x}_2-\cdots-b_k\bar{x}_k, \qquad (5.31)$$

where $$\bar{y} = \frac{\sum ny}{\sum n}; \quad \bar{x}_l = \frac{\sum nx_l}{\sum n};$$

taking (5.31) into account, regression equation (5.27) can be written

$$y = \bar{y} + b_1(x_1 - \bar{x}_1) + b_2(x_2 - \bar{x}_2) + \cdots + b_k(x_k - \bar{x}_k). \quad (5.32)$$

If we designate $\Delta y = y - \bar{y}$, $\Delta x = x - \bar{x}$, equation (5.32) will assume the form

$$\Delta y = b_1 \Delta x_1 + b_2 \Delta x_2 + \cdots + b_k \Delta x_k. \quad (5.33)$$

Taking into account the relations of (5.31), system (5.30) is reduced to the form

$$\left.\begin{array}{c} b_1 \sum n \Delta x_1^2 + b_2 \sum n \Delta x_1 \Delta x_2 + \cdots + \\ + b_k \sum n \Delta x_1 \Delta x_k = \sum n \Delta x_1 \Delta y; \\ b_1 \sum n \Delta x_1 \Delta x_2 + b_2 \sum n \Delta x_2^2 + \cdots + \\ + b_k \sum n \Delta x_2 \Delta x_k = \sum n \Delta x_2 \Delta y; \\ \cdots\cdots\cdots\cdots\cdots\cdots \\ b_1 \sum n \Delta x_1 \Delta x_k + b_2 \sum n \Delta x_2 \Delta x_k + \cdots + \\ + b_k \sum n \Delta x_k^2 = \sum n \Delta x_k \Delta y. \end{array}\right\} \quad (5.34)$$

We shall insert into system (5.34) paired correlation coefficients

$$r_{x_l, x_j} = \frac{\sum n \Delta x_l \Delta x_j}{N \sigma_{x_l} \sigma_{x_j}}; \quad r_{y, x_l} = \frac{\sum n \Delta x_l \Delta y}{N \sigma_{x_l} \sigma_y},$$

where

$$l = \overline{1, k}, \; j = \overline{1, k}, \; j \neq l, \; N = \sum n,$$

we obtain

$$\left.\begin{array}{c} b_1 \sigma_{x_1}^2 + b_2 \sigma_{x_1} \sigma_{x_2} r_{x_1, x_2} + \cdots + b_k \sigma_{x_1} \sigma_{x_k} r_{x_1, x_k} = \\ = r_{x, y} \sigma_{x_1} \sigma_y; \\ b_1 \sigma_{x_1} \sigma_{x_2} r_{x_1, x_2} + b_2 \sigma_{x_2}^2 + \cdots + b_k \sigma_{x_2} \sigma_{x_k} r_{x_2, x_k} = \\ = r_{x_2, y} \sigma_{x_2} \sigma_y; \\ \cdots\cdots\cdots\cdots\cdots\cdots \\ b_1 \sigma_{x_1} \sigma_{x_k} r_{x_1, x_k} + b_2 \sigma_{x_2} \sigma_{x_k} r_{x_2, x_k} + \cdots + b_k \sigma_{x_k}^2 = \\ = r_{x_k, y} \sigma_{x_k} \sigma_y. \end{array}\right\} \quad (5.35)$$

Coefficients b_i of system (5.35) are determined by the ratio

$$b_i = \frac{\Delta_i}{\Delta}, \tag{5.36}$$

where

$$\Delta = \begin{vmatrix} \sigma_{x_1}^2 & \sigma_{x_1}\sigma_{x_2}r_{x_1, x_2} \dots \sigma_{x_1}\sigma_{x_k}r_{x_1, x_k} \\ & \sigma_{x_2}^2 \quad \dots \sigma_{x_2}\sigma_{x_k}r_{x_2, x_k} \\ \dots & \dots \\ & \sigma_{x_k}^2 \end{vmatrix};$$

Δ_i -- additional determinant.

Coefficients of regression b_i depend on correlation coefficients r_{y, x_i} and root-mean-square deviations. The adequacy of regression equation (5.27) or (5.33) is tested by Fisher's criterion [28]

$$F = \frac{\sigma_a^2}{\sigma_y^2}, \tag{5.37}$$

where

$$\sigma_a^2 = \frac{\sum^N (y_j - m_y)^2}{N-1}.$$

If value F, obtained with formula (5.37), is less than critical value F_{kp}, with a specified confidence coefficient, the regression equation is adequate to a real process.

Values F_{kp} are contained in Table 5.5: $k_1=N-1$; $k_2=k_1-1$ when $\beta=0.1$.

We shall examine the method of calculating regression coefficients with a concrete example. Let us assume that as a result of tests we have obtained an experimental field (p_k, T) of combustion chamber pressures and propellant component temperature as indicated in Figure 5.4.

Table 5.5.

k_2	k_1							
	1	2	3	4	5	7	10	15
1	161,0	199	216,7	224	230	237	242	246
2	18,5	19,0	19,1	19,2	19,3	19,3	19,4	19,4
3	10,1	9,5	9,3	9,1	9,0	8,9	8,8	8,7
4	7,7	6,9	6,6	6,4	6,2	6,1	5,9	5,8
5	6,6	5,8	5,4	5,2	5,0	4,9	4,3	4,6
7	5,6	4,7	4,3	4,1	3,9	3,8	3,6	3,5
10	4,9	4,1	3,7	3,5	3,3	3,1	3,0	2,8
15	4,5	3,7	3,3	3,0	2,9	2,7	2,7	2,4

A regression equation is sought in the form

$$p_к = b_0' + b_1 T.$$

To reduce the volume of calculations it is convenient to break down the axes of pressures and temperature into intervals Δp_k and ΔT and to present the results in dimensionless quantities p'_k and T'.

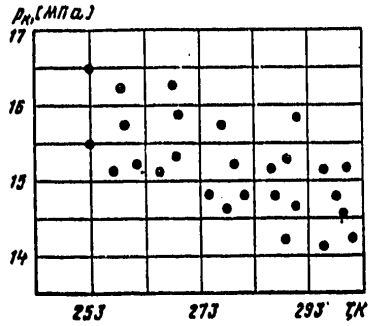

Figure 5.4. Experimental Relation $p_k = p_k$ (T)

One selects base values $p_{k.o}$, T_0, for which one adopts nominal quantities or midpoints of measurement intervals. Let $p_{k.o}$=15.25 MPa, T=5 K. The value of interval h_{pk}=0.5 MPa, h_T=10 K. Then dimensionless quantities p'_k and T' are expressed with integers 0, 1, 2... m.

Experiment results are contained in Table 5.6.

The number of experimental points in the intervals is indicated at the intersection of the lines and columns.

Mean dimensionless quantities

$$\bar{p}'_к = \frac{\sum n_{p_к} p'_к}{N} = \frac{2}{38} = 0{,}053; \quad \bar{T}' = \frac{\sum n_T T'}{N} = \frac{7}{38} = 0{,}184.$$

Mean dimensional $\bar{p}_к = p_{к.o} + \bar{p}'_к h_{p_к} = 15{,}25 + 0{,}053 \cdot 0{,}5 =$

$= 15{,}28$ МПа, $\bar{T} = T_0 + \bar{T}' h_T = 5 + 0{,}184 \cdot 10 = 23{,}4$ K.

Root-mean-square deviations of dimensionless variables

$$\sigma_{p'_к} = \sqrt{\frac{\sum n_{p_к} (p'_к)^2}{N} - (\bar{p}'_к)^2} = \sqrt{\frac{48}{38} - 0{,}053^2} = 1{,}12;$$

$$\sigma_{T'} = \sqrt{\frac{\sum n_T (T')^2}{N} - (\overline{T}')^2} = \sqrt{\frac{77}{38} - 0{,}183^2} = 1{,}4;$$

$$\sigma_{p_K} = h_{p_K}\sigma_{p_K'} = 1{,}12 \cdot 0{,}5 = 0{,}56 \text{ МПа};$$

$$\sigma_T = h_T\sigma_{T'} = 10 \cdot 1{,}4 = 14 \text{ K}.$$

Table 5.6.

p_K'	Δp_K	T'					n_{p_K}	$n_{p_K} p_K'$	$n_{p_K} (p_K')^2$
		−2	−1	0	1	2			
		ΔT							
		(−20)+(−10)	(−10)+0	0—10 [5]	10—20	20—30			
−2	14—14,5	0	0	0	1	2	3	−6	12
−1	14,5—15	0	0	3	3	3	9	9	9
0	15—15,5 [15, 25]!	2	3	1	5	3	14	0	0
1	15,5—16	2	2	2	1	0	7	7	7
2	16—16,5	3	1	0	1	0	5	10	20
	n_T	7	6	6	11	8	N=38	$\sum$=2	$\sum$=48
	$n_T T'$	−14	−6	0	11	16	$\sum$ 7		
	$n_T (T')^2$	28	6	0	11	32	$\sum$ 77		
	$n_T, p_K' T'$	−16	−4	0	−2	−14	$\sum$ 36		

Correlation coefficient

$$r_{p_K', T'} = \frac{\sum n_{p_K, T} p_K' T' - N\overline{p}_K'\overline{T}'}{N\sigma_{p_K'}\sigma_{T'}} = \frac{-36 - 38 \cdot 0{,}53 \cdot 0{,}184}{38 - 1{,}12 \cdot 1{,}4} = -0{,}61.$$

From system (5.35) coefficient b_1 is determined as follows:

$$b_1 = r_{p_K', T'} \frac{\sigma_{p_K}}{\sigma_T} = -0{,}61 \frac{0{,}56}{14} = -0{,}024.$$

In conformity with (5.32) we have $p_k=\bar{p}_k + b_1 (T-\bar{T})$ or

$$p_к = 15{,}28 - 0{,}024\,(T - 23{,}4) = 15{,}84 - 0{,}024T. \qquad (5.38)$$

As was to be expected, the dependence of combustion chamber pressure on fuel temperature is slight.

We shall verify the adequacy of equation (5.38) to an actual process according to Fisher's criterion

$$\sigma_a^2 = \frac{\sum_1^5 (p_{кj} - \bar{p}_к)^2}{5-1} = \frac{0{,}85}{4} = 0{,}212;$$

$$F = \frac{\sigma_a^2}{\sigma_{p_к}^2} = \frac{0{,}212}{0{,}56} = 0{,}37.$$

From Table 5.5, when $k_1=k_2=4$ we find $F_{kp}=6.4$. Since $F < F_{kp}$, the regression equation is adequate to an actual process.

Chapter 6. TUNING AND ADJUSTING MOTORS

6.1. Tasks and Methods of Tuning and Adjusting

As a result of the operation of internal disturbing factors there occurs deviation of the operation parameters of a concrete motor from nominal values, that is, reproducibility of operating conditions is disturbed.

Variants of operation process parameters leads to an increase in the field of rocket trajectory dispersion, decreased accuracy and range. In addition, an increase in parameters spread also leads to narrowing of the area of stable operation and complicates rocket control as a consequence of the occurrence of additional disturbing factors.

To compensate for the influence of internal disturbing factors and to increase rocket accuracy and range, engines are tuned and adjusted to nominal rating, that is, nominal values of the principal engine operation parameters are secured by selecting the requisite characteristics of components (controllers, throttles, reducers, jets, etc) contained in the propellant component line.

Tuning and adjustment designates a complex of calculation-experimental work ensuring securement of specified operation parameters by means of one-time influence on several engine characteristics. Tuning and adjustment should optimally ensure meeting tactical-technical requirements placed on an engine in respect to principal parameters.

Since engine operation is characterized by a substantial number of parameters, tuning and adjustment ensure acquisition of specified values only of those parameters which affect a motor's economy, efficiency, and controllability.

The concrete tasks of tuning and adjustment are determined by the specific peculiarities of the design and by the motor's specific purpose and operating conditions.

For example, if an engine is designed for a booster, its tuning and adjustment do not involve any particular labor, since in this instance tough demands are not imposed on precision of engine operation.

If an engine is designed for ballistic missiles, which should be highly accurate in hitting the target, high demands are imposed on tuning and adjustment. This is primarily for two reasons.

A high degree of variance in ratio of propellant components results in decreased economy (specific thrust impulse) and increased guaranteed fuel residue in the tanks, and consequently an increase in mass at launch.

With a large variance of total propellant consumption (thrust), rocket control is made difficult as a consequence of the occurrence of additional disturbances affecting the control system.

The economy of an engine is characterized by specific thrust impulse, which for a given design and specified propellant is determined primarily by combustion chamber pressure and ratio of propellant components.

Thus securement of the following condition constitutes the first and basic task of tuning and adjustment:

$$p_{kj} = \bar{p}_k; \quad K'_j = \bar{K}',$$

where j -- engine number.

The conditions of efficiency depend on engine design; there is a large number of possible engine layouts. In a motor with a pumped supply system, turbine efficiency is secured with tuning and adjustment. This is due to the fact that gas with a high temperature and pressure is acting on the turbine blades.

Since the turbine blades are not cooled, they can burn out with a gas temperature and pressure deviation from the specified values. The temperature of the gas passing through the turbine blades is determined by the ratio of propellant components in the gas generator.

Therefore the second task of tuning and adjustment is that of fulfilling condition

$$K''_j = \bar{K}''.$$

In multiple combustion chamber propulsion systems there occurs a thrust spread relative to the axis of the rocket (eccentricity of thrust) due to a spread of operation parameters. As a result the rocket becomes difficult o control in the flight trajectory. Therefore the third task of tuning nd adjustment is securement of the following condition:

$$P_j = \bar{P},$$

where j -- number of combustion chamber.

In addition to the above-enumerated tasks, in certain cases there may be other particular tuning and adjustment tasks, such as ensuring a specified turbine shaft rpm, specified pressure in the tanks, etc.

Depending on the features of propulsion system design, conditions of tuning and adjustment can be as follows:

$$а)\ \delta\dot{m}'_{ок} = \delta\dot{m}'_{т} = 0,\ \delta K'' = 0;$$

$$б)\ \delta K' = 0,\ \delta p_{к} = 0.$$

In the first variant combustion chamber pressure is not directly adjusted. However, due to securement of nominal rates of flow, it is close to rated pressure. The method of adjustment is selected taking into account the features of the propulsion system, its specific purpose and the adopted testing system. It can be individual and statistical, depending on the method of obtaining input data for tuning and adjustment.

Input data for individual tuning and adjustment are results of shop tests on all engine components and assemblies, as well as propulsion system tests.

Input data for statistical adjustment are the results of tests on preceding engines, averaged over the full number of tests.

Tuning and adjustment is broken down by process cycle into "KTI+KVI" adjustment and adjustment with KVI.

The first type of tuning and adjustment includes the performance of process monitoring tests (KTI) of each motor on test beds, and selective monitoring tests (KVI) of a motor selected at random from a batch, which is tested to determine that principal characteristics are in conformity with the requirements of technical specifications.

"KTI+KVI" tuning and adjustment is individual as a rule and contains the following stages:

motor tuning and adjustment for performing KTI;

process monitoring tests;

tuning adjustment;

selective monitoring tests.

Tuning and adjustment with KVI can be both individual and statistical.

6.2. Individual Tuning and Adjustment

6.2.1. Input Data for Tuning and Adjustment

Input data for tuning and adjustment include specified (nominal) operation parameters and component shop test results.

Nominal values are specified for those parameters to be adjusted.

These parameters include the following:

combustion chamber pressure $\bar{p}_k$;

propellant component rates of flow into combustion chamber $\bar{\dot{m}}_j$;

ratio of propellant components in gas generator $\bar{K}''$.

In addition to the above-enumerated parameters, external disturbances are also specified for ensuring identical conditions for tuning and adjusting all motors: pressures at pump inlet $\bar{p}_{o.ок}$, $\bar{p}_{o.г}$ and propellant component densities $\bar{\rho}_{ok}$ and $\bar{\rho}_г$.

Following manufacture, each component is subjected to independent (shop) tests, during which individual characteristics are determined.

1. Hydraulic characteristics. Testing determines pressure losses:

a) in lines from pumps to combustion chamber $\Delta p'_{ок}$, $\Delta p'_г$;

b) in combustion chamber cooling jacket $\Delta p_г$;

c) in lines from pumps to gas generator $\Delta p''_{ок}$, $\Delta p''_г$;

d) valve hydraulic resistances $\Delta p_{к.ок}$; $\Delta p_{к.г}$.

The values of all indicated losses are determined from the results of running a liquid through, usually water, and liquid flow rate during this test is specified from the condition of equality of hydraulic resistances with water and the actual propellant component, and is determined with the formula

$$\dot{m}_в = \bar{\dot{m}}_к \sqrt{\frac{\rho_в}{\rho_к}},$$

where $\dot{m}_B$, $\dot{m}_k$ -- flow rates of water and propellant component respectively; ρ_B, ρ_k -- density of water and component respectively.

2. Pressure-flow rate characteristics of pumps at nominal angular velocities $p_H = p_H(\dot{m}, \bar{n})$.

As a result of pump testing, one determines coefficients A, B, C in pressure characteristic equation $p_H = An^2 + Bn\dot{m} + C\dot{m}^2 + p_0$ or quantity tg α_H, as well as efficiency η_H.

3. Turbine characteristics r_1 and r_2 in power equation

$$N_т = p_{тг} n \left(r_1 - \frac{r_{gn}}{\sqrt{RT_{тг}}} \right).$$

6.2.2. Individual Tuning and Adjustment of a Motor Without Generator Gas Afterburning

As a consequence of the fact that in a motor without generator gas afterburning there is no direct link between combustion chamber and turbine driving generator, adjustment of combustion chamber and gas generator can be performed sequentially.

In this case adjustment prior to KTI is broken down into two stages:

adjustment of engine parameter for fulfilling condition

$$\delta \dot{m}_{ок} = \delta \dot{m}_г = 0$$

by placing throttle disks in the combustion chamber lines;

turbine-pump adjustment ($\delta K'' = 0$) by adjusting control devices or installing jets in the gas generator lines.

Combustion Chamber Tuning and Adjustment

To fulfill condition $\delta \dot{m}_{ок} = \delta \dot{m}_г = 0$ it is essential that the pressures generated by the pumps have the following values:

$$\left.\begin{aligned} p^*_{н.ок} &= \bar{p}_к + \sum \Delta p_{i\,ок} - \bar{p}_{о.ок}; \\ p^*_{н.г} &= \bar{p}_к + \sum \Delta p_{iг} - \bar{p}_{о.г}, \end{aligned}\right\} \qquad (6.1)$$

where $\sum \Delta p_{i,j} = \Delta p'_j + \Delta p_{к,j} + \Delta p_{р,j}$ — total losses from pumps to combustion chamber.

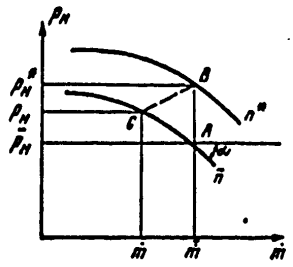

Figure 6.1. Similar Pump Conditions

As a consequence of the influence of various internal disturbing factors on the pumps, the required pressures at the pump outlets (6.1) will not coincide with nominal values; otherwise there would be no need for adjustment.

Thus the required pressures p^*_{Hj} can be obtained for nominal flow rates with differing rpm.

The required rpms n^*_{ok} and n^*_T can be determined by two methods.

1. Equations of similarity. We know from theory of pumps that the following relations are valid for similar conditions:

$$p^*_H = p_H (n^*/\bar{n})^2; \qquad (6.2)$$

$$\dot{m}^* = \dot{m} (n^*/\bar{n}). \qquad (6.3)$$

Line of similar conditions BC is contained in Figure 6.1. For transition along curve n*=const to the point of nominal conditions, one can utilize linear approximation

$$p_H = \bar{p}_H + (\dot{m} - \bar{\dot{m}}) \operatorname{tg} \alpha_H, \qquad (6.4)$$

where

$$\operatorname{tg} \alpha_H = \left| \frac{\partial p_H}{\partial \dot{m}} \right|_{\substack{n=\bar{n} \\ \dot{m}=\bar{\dot{m}}}}.$$

Substituting equation (6.4) in relation (6.2), taking into account (6.3), we obtain

$$p^*_H = \left[\bar{p}_H + \left(1 - \frac{\bar{n}}{n^*} \right) \operatorname{tg} \alpha_H \cdot \bar{\dot{m}} \right] \left(\frac{n^*}{\bar{n}} \right)^2. \qquad (6.5)$$

In a linear approximation, in the vicinity of point A one can write

$$\Delta p_H = \left(\frac{\partial p^*_H}{\partial n} \right) \Delta n,$$

where

$$\Delta p_H = \bar{p}_H - p^*_H; \quad \Delta n = \bar{n} - n^*;$$

$\frac{\partial p^*_H}{\partial n}$ -- is determined from equation (6.5) for nominal conditions, that is, when $\bar{n}$=n*;

$\frac{\partial p^*_H}{\partial n} = \frac{1}{\bar{n}} [2\bar{p}_H + \bar{\dot{m}} \operatorname{tg} \alpha_H]$, thus,

$$n^* = \bar{n} \left(1 - \frac{\bar{p}_H - p^*_H}{2\bar{p}_H + \bar{\dot{m}} \operatorname{tg} \alpha_H} \right). \qquad (6.6)$$

From formula (6.6) one determines required n^*_{ok} and $n^*_г$, ensuring $p^*_{н.ok}$ and $p^*_{н,г}$.

2. Pump characteristic. If the equation for pressure at pump outlet is specified, the required rpm can be determined from obvious equation

$$p^*_{нj} = \bar{p}_к + \sum \Delta p_{l,\ j} - \bar{p}_{0j} = A_j n^{*2}_j + B_j n^*_j \bar{m}_j + c_j \bar{m}^2_j + \bar{p}_{0j}. \quad (6.7)$$

Resolving equation (6.7) relative to n^*_j, we obtain

$$n^*_j = \frac{-B_j \bar{m}_j \pm \sqrt{(B_j \bar{m}_j)^2 - 4\left(C_j \bar{m}^2_j - \bar{p}_к - \sum \Delta p_{lj} - 2\bar{p}_{0j}\right) A_j}}{2A_j}, \quad (6.8)$$

where $j = \overline{ок,\ г}$.

As a consequence of the fact that the characteristics of the lines and pumps are different, as was already noted, $n^*_г \neq n^*_{ok}$. At the same time condition $n^*_{ok} = zn^*_т$ should be met in the turbopump unit, where z -- reduction gear ratio (in a turbopump unit without a reduction figure z=1). The greater of quantities n^*_{ok} and $n^*_г$ is selected. Assume that $n^*_{ok} > n^*_г$. Then the pressure produced by the oxidizer pump will be equal to the required $p^*_{н.ok}$, and pressure at the fuel pump outlet will be greater than required $p^*_{н.г}$ ($p^*_{н.г}$ (Figure 6.2), and rate of flow will be greater than nominal.

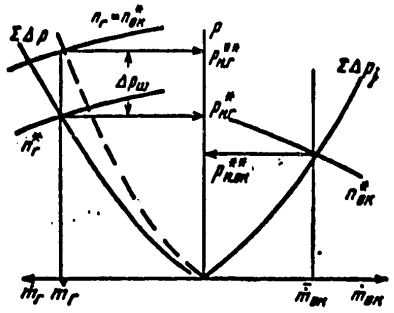

Figure 6.2. Graphic Determination of $\Delta p_ш$

In order to obtain nominal fuel flow rate it is necessary to throttle down the fuel pump, that is, place a hydraulic resistance, a throttle disk, in the line beyond the pump.

The excessive pressure (throttle effect) which is absorbed by the throttle disk is determined as

$$\Delta p_ш = p^{**}_{н.г} - p^*_{н.г}, \quad (6.9)$$

where $p^*_{н.г}$ -- is calculated with equation (6.11), while $p^{**}_{н.г}$ -- equation (6.7) with $n=n^*_{ок}$.

The diameter of the throttle disk of the throttled pump is determined from the relation

$$d_ш = 2\sqrt{\frac{\bar{m}}{\pi k \mu \sqrt{2\rho \Delta p_ш}}}, \qquad (6.10)$$

where k -- coefficient of thermal expansion; μ -- coefficient of flow rate.

Coefficients k and μ are determined experimentally.

After installing the throttle disk, the combustion chamber together with lines and pumps are adjusted to nominal $\bar{p}_k$ and $\bar{k}'$. The motor, however, has not yet been adjusted. Required $\bar{p}_k$ and $\bar{k}'$ should be secured by corresponding turbopump and gas generator operating conditions.

Adjusting Turbopump and Gas Generator

Under steady-state conditions operations for tuning and adjusting combustion chamber parameters to nominal values should be performed with observance of a basic requirement -- balance of turbine and pump outputs, that is,

$$N_т = \sum N_{нj}. \qquad (6.11)$$

Oxidizer and fuel pump output are determined on the basis of the results of combustion chamber tuning and adjustment and pump tests

$$N_{нj} = \frac{p^*_{нj}\bar{m}_j}{\bar{\rho}_j \bar{\eta}_{нj}}. \qquad (6.12)$$

Turbine power is determined by the relation

$$N_т = p_{гг} n^* \left(r_1 - \frac{r_2 n^*}{\sqrt{RT_{гг}}}\right), \qquad (6.13)$$

where r_1 and r_2 -- are determined from turbine tests.

Substituting (6.12) and (6.13) in equation (6.11), we obtain required gas generator pressure ensuring nominal rates of flow into the combustion chamber

$$p^*_{гг} = \left(\frac{p^*_{н.ок}\bar{m}_{ок}}{\bar{\rho}_{ок}\bar{\eta}_{н.ок}} + \frac{p^*_{н.г}\bar{m}_г}{\rho_г \eta_{н.г}}\right) \frac{1}{n^* \left(r_1 - \frac{r_2 n^*}{\sqrt{RT_{гг}}}\right)}. \qquad (6.14)$$

Requisite pressure drops in the gas generator lines are determined from pressure balance equation

$$\Delta p^{**}_{ок} = p^{*}_{н.\,ок} - p^{*}_{гг};$$
$$\Delta p^{**}_{г} = p^{*}_{н.\,г} - p^{*}_{гг}. \qquad (6.15)$$

Jets (throttle resistances) are placed in the gas generator line for adjustment purposes, with pressure drop on the jets determined by the relations

$$\Delta p_{ж.\,ок} = \Delta p^{**}_{ок} - \Delta p^{*}_{ок};$$
$$\Delta p_{ж.\,г} = \Delta p^{**}_{г} - \Delta p^{*}_{г},$$

where $\Delta p^{*}_{ок}$, $\Delta p^{*}_{г}$ -- gas generator line hydraulic resistances, determined by tests.

Engine tuning and adjustment to specified parameter values is completed with placement of jets in the gas generator line.

6.2.3. Tuning and Adjustment of a Motor with Generator Gas Afterburning

In motors with afterburning of generator gas there is a direct link between operating processes in the combustion chamber and in the gas generator.

Therefore the separate method of combustion chamber and gas generator adjustment is not applicable here. A characteristic condition of motor tuning and adjustment for motors with generator gas afterburning is

$$\delta p_k = 0, \quad \delta K = 0.$$

One can influence operation in such motors by means of changing the hydraulic resistance of three lines: the combustion chamber fuel oxidizer line (depending on afterburning arrangement) and two gas generator lines. Since a control (RKS control) is placed in one of the gas generator lines, the control element is adjusted instead of placing a throttle disk (jet).

As a result of solving the problem of influence of external and internal factors, we have knowledge of correlations which determine the link between adjusted parameters, disturbances and line hydraulic resistances, for which we take coefficients of hydraulic resistances of the throttle disks and controls:

$$\delta K = \sum_{i=1} C_{k,\,x_i}\delta x_i + C_{k,\,\xi_{ок}}\delta\xi_{ок.\,ш} + C_{k,\,\xi_{ш.\,г}}\delta\xi_{ш.\,г} + C_{k,\,\xi_{р.\,о}}\delta\xi_{р.\,о};$$
$$\delta p_к = \sum_{i=1} C_{p_к,\,x_i}\delta x_i + C_{p_к,\,\xi_{ок.\,ш}}\delta\xi_{ок.\,ш} + C_{p_к,\,\xi_{ш.\,г}}\delta\xi_{ш.\,г} + C_{p_к,\,\xi_{р.\,о}}\delta\xi_{р.\,о}, \qquad (6.16)$$

where $\xi_{ш.\ i}$ -- coefficients of line hydraulic resistance.

Since we have two adjustment conditions $(\delta p_к = 0,\ \delta K = 0)$ and three possible actions $\delta\xi_{ок.\ ш},\ \delta\xi_{ш.\ г},\ \delta\xi_{р.\ о}$, one of the lines is not throttled.

As a rule one adopts as unthrottled line the line of that component which is fed entirely to the gas generator.

For oxidizing afterburning, for example, the oxidizer line is not throttled $(\delta\xi_{ок.\ ш} = 0)$, and for a reducing arrangement -- the fuel line $(\delta\xi_{ш.\ г} = 0)$.

Fulfilling in system (6.16) adjustment condition ($\delta p_к = 0$, $\delta K = 0$) and assuming, for example, $\delta\xi_{ок.\ ш} = 0$, we determine unknown $\delta\xi_{ш.\ г}$ and $\delta\xi_{р.\ о}$.

$$\left.\begin{aligned}\delta\xi_{ш.\ г} &= \frac{b_{p_к}C_{K.\ \xi_{р.\ о}} - b_K C_{p_к.\ \xi_{р.\ о}}}{\Delta};\\ \delta\xi_{р.\ о} &= \frac{b_K C_{p_к.\ \xi_{ш.\ г}} - b_{p_к}C_{K.\ \xi_{р.\ о}}}{\Delta},\end{aligned}\right\} \qquad (6.17)$$

where

$$\Delta = C_{K.\ \xi_{ш.\ г}}C_{p_к.\ \xi_{р.\ о}} - C_{p_к.\ \xi_{ш.\ г}}C_{K.\ \xi_{ш.\ о}};$$

$$b_K = \sum_{i=1} C_{K.\ x_i}\delta x_i;\quad b_{p_к} = \sum_{i=1} C_{p_к.\ x_i}\delta x_i.$$

From coefficients of hydraulic resistances it is not difficult to proceed to throttle disk pressure drops

$$\xi_{ш.\ г} = \bar{\xi}_{ш.\ г}(1 + \delta\xi_{ш.\ г});$$

$$\Delta p_{ш.\ г} = \xi_{ш.\ г}\frac{\bar{\dot{m}}_г^2}{\bar{\rho}_г}.$$

6.2.4. Process Monitoring Tests and Tuning Adjustment

In order to check engine efficiency and to ensure that operation parameters meet the requirements of technical specifications, each tuned and adjusted motor is subjected to process monitoring tests.

KTI involves measuring a number of operation parameters, including those for which tuning and adjustment were performed.

When the values of the adjusted parameters (p_k and K) are not within the limits specified by technical specifications, the motor is retuned in order to ensure nominal values during operation or KVI. Tuning adjustment following KTI is also necessary because motors which have been subjected to process monitoring tests are taken down; some of the components are replaced with new ones, which leads to change in characteristics.

Following are input data for engine tuning and adjustment:

measured values of adjustment parameters p_k, K;

measurement of pressure losses in motor lines with replacement of components $\Delta\Delta p_{ок}$, $\Delta\Delta p_г$;

values of required losses on disks and jets obtained during initial adjustment $\Delta p_{ш.г}$.

For definiteness we shall examine retuning and readjustment of a motor with afterburning of oxidizing generator gas. In this case the following are retuning input data:

$$p_{к.н};\quad K_н;\quad \Delta\Delta p_{ок};\quad \Delta\Delta p_г;\quad \Delta p_{ш.г};\quad \Delta p_{р.о}.$$

The following system of equations is written relative to the parameters to be adjusted

$$\left.\begin{aligned}(\bar{p}_к - p_{к.н}) &= a_{p_к,\,\Delta p_{р.о}}(\Delta p_{р.о.к} - \Delta p_{р.о}) + \\ &+ a_{p_к,\,p_{ш.г}}(\Delta p_{ш.г.к} - \Delta p_{ш.г}) + \\ &+ a_{p_к,\,\Delta p_{о.к}}\Delta\Delta p_{ок} + a_{p_к,\,\Delta p_г}\Delta\Delta p_г; \\ (\bar{K} - K_н) &= a_{K,\,\Delta p_{р.о}}(\Delta p_{р.о.к} - \Delta p_{р.о}) + \\ &+ a_{K,\,p_{ш.г}}(\Delta p_{ш.г.к} - \Delta p_{ш.г}) + \\ &+ a_{K,\,\Delta p_{ок}}\Delta\Delta p_{ок} + a_{K,\,\Delta p_г}\Delta\Delta p_г,\end{aligned}\right\} \qquad (6.18)$$

where $\Delta p_{р.о.к}$, $\Delta p_{ш.г.к}$ -- new values of pressure losses in the control element and on the throttle disk.

System (6.18) is resolved in relation to $\Delta p_{ш.г.к}$ and $\Delta p_{р.о.к}$:

$$\left.\begin{aligned}a_{p_к,\,\Delta p_{р.о}}\cdot\Delta p_{р.о.к} + a_{p_к,\,p_{ш.г}}\Delta p_{ш.г.к} &= d_{p_к}; \\ a_{K,\,\Delta p_{р.о}}\Delta p_{р.о.к} + a_{K,\,p_{ш.г}}\Delta p_{ш.г.к} &= d_K,\end{aligned}\right\} \qquad (6.19)$$

where

$$a_{p_к} = (\bar{p}_к - p_{к.н}) + a_{p_к,\,\Delta p_{р.о}}\Delta p_{р.о} + \\ + a_{p_к,\,p_{ш.г}}\Delta p_{ш.г} - a_{p_к,\,\Delta p_{ок}}\Delta\Delta p_{ок} - a_{p_к,\,\Delta p_г}\Delta\Delta p_г;$$

$$d_K = (\bar{K} - \bar{K}_н) + a_{K,\,\Delta p_{р.о}}\Delta p_{р.о} + a_{K,\,\Delta p_{ш.г}}\Delta p_{ш.г} - a_{K,\,\Delta p_{ок}}\Delta\Delta p_{ок}.$$

Values d_{p_k}, d_k are determined by nominal parameters and results of measurements during KTI.

We finally have from system (6.19)

$$\left.\begin{aligned}\Delta p_{p.o.k} &= \frac{d_k - a_3 d_{p_k}}{a_{p_k,\,\Delta p_{p.o}} a_3 - a_{k,\,\Delta p_{p.o}}};\\ \Delta p_{w.r.k} &= \frac{d_{p_k} - a_4 d_k}{a_4 a_{k,\,p_{w.r}} - a_{p_k,\,p_{w.r}}},\end{aligned}\right\} \qquad (6.20)$$

where

$$a_3 = \frac{a_{K,\,p_{w.r}}}{a_{p_k,\,p_{w.r}}};\quad a_4 = \frac{a_{p_k,\,\Delta p_{p.o}}}{a_{k,\,\Delta p_{p.o}}}.$$

Selective monitoring tests (KVI) are performed following motor readjustment. One randomly selected motor from a batch is subjected to KVI. If tests on this motor indicate that operation parameters are within the limits specified by technical specifications, the entire batch is accepted; otherwise it is rejected.

6.3. Statistical Tuning and Adjustment

Analysis of results of tuning and adjustment indicates that with stable production and a tested engine design, pressure differentials and dimensions of the throttling cross section of throttle disks and jets lie within very narrow limits for all motors of a given type. Therefore one can tune and adjust motors in batches with disks of identical dimensions, constituting a mathematical expectation from all preceding motors. In addition, this method of tuning and adjustment does not require performance of KTI, and therefore it is comparatively simple, economical, and is the only possible method of adjusting motors which cannot be taken down.

For application of the statistical method, it is necessary to adjust the first N motors according to the individual tuning and adjustment method. The number of motors N tuned and adjusted individually depends on stability of production and degree of finished development of design. The moment of transition from individual to statistical tuning and adjustment is determined as follows.

For N tuned and adjusted motors one determines the mathematical expectation of throttle disk area or coefficient of hydraulic resistance

$$M[F_{wj}] = \frac{\sum_1^N F_{wj}}{N} \quad \text{or} \quad M[\xi_{wj}] = \frac{\sum_1^N \xi_{wj}}{N}. \qquad (6.21)$$

Individual tuning and adjustment is performed for N+1 motors, as a result of which one determines $\xi_{ш}$, Tp, and the motor is tested (KVI or KTI).

As a result of the tests one determines deviations of adjusted parameters from those specified by technical specifications $\delta p_{к.н}$, $\delta K_{н}$. Two equations can be written for $\delta K_{н}$, $\delta p_{к}$:

$$\delta p_{к.н} = \sum C_{p_к, x_i} \delta x_i + \sum C_{p_к, \xi_{ш}} \delta \xi_{ш.тр}; \qquad (6.22)$$

$$\delta K_{н} = \sum C_{K, x_i} \delta x_i + \sum C_{K, \xi_{ш}} \delta \xi_{ш.тр}. \qquad (6.23)$$

In like manner one writes equations for $\delta p_{к.с}$ and $\delta K_{с}$, which will be, with statistical tuning and adjustment,

$$\delta p_{к.с} = \sum C_{p_к, x_i} \delta x_i + \sum C_{p_к, \xi_{ш}} M[\delta \xi_{ш}]; \qquad (6.24)$$

$$\delta K_{с} = \sum C_{K, x_i} \delta x_i + \sum C_{K, \xi_{ш}} M[\delta \xi_{ш}]. \qquad (6.25)$$

The first term of equations (6.22)-(6.25) is an unknown quantity and determines the discrepancy between the required and expected (following statistical tuning and adjustment) value of the parameter to be adjusted.

If we eliminate terms $\Sigma C_j \times \delta x$, from equations (6.22), (6.24) and (6.25), we obtain

$$\delta p_{к.с} = \delta p_{к.н} + \sum C_{p_к, \xi_{ш}} [M[\delta \xi_{ш}] - \delta \xi_{ш.тр}]; \qquad (6.26)$$

$$\delta K_{с} = \delta K_{н} + \sum C_{K, \xi_{ш}} [M[\delta \xi_{ш}] - \delta \xi_{ш.тр}]. \qquad (6.27)$$

If values $\delta p_{к.с}$ and $\delta K_{с}$ do not go beyond the limit established by the technical specifications, all motors following N+1 can be tuned and adjusted by the statistical method.

In the process of manufacture, accuracy of tuning and adjustment is verified with KVI, and when necessary it is adjusted as indicated above.

6.4. Comparison of Methods of Tuning and Adjustment

Two methods of tuning and adjustment are examined: KTI + KVT and KVI.

With the first method all engines are subjected to selective monitoring tests. After these tests tuning adjustment is performed: each motor is disassembled, components are inspected for defects, discovered defects are corrected, defective components and single-use parts are replaced, components are treated, and the motor is reassembled for performance of KVI and delivery to the customer.

Thus with KTI not only precision of tuning and adjustment is tested but also the efficiency of each motor; hidden defects are spotted, which are corrected

at the manufacturing stage, which in the final analysis leads to increased reliability. This is especially important at early stages of development and manufacture of newly-designed motors.

The method of tuning and adjustment with KTI is highly precise. However, alongside advantages, this procedure of tuning and adjustment also possesses some shortcomings. They include the following:

initiation of motor wear even before it goes into service;

considerable economic expenditures on testing, disassembly and assembly of each motor;

impossibility of taking down undisassemblable motors, etc.

Proceeding from the above, one can conclude that it is advisable to perform tuning and adjustment with KTI on newly-designed motors at early stages of manufacture. This method of tuning and adjustment makes it possible to obtain a fairly large volume of statistical material essential for evaluating reliability, to spot latent defects at early stages of manufacture in each motor and to correct them.

In the process of engine improvement and stabilization of production one can eliminate KTI and perform tuning and adjustment with KVT (statistical tuning and adjustment).

Let us perform an economic comparison of both methods of tuning and adjustment.

KTI + KVI Tuning and Adjustment Program

All motors without exception are subjected to KTI. From a batch of n* units, one motor is subjected to KVI with subsequent inspection for defects and destruction or utilization other than designated. The size of batch n* depends on the stage of production and experience of the manufacturer. At early stages of production the batch size is smaller than for production in full swing.

Tuning and Adjustment Program With KVI

Out of a batch of n motors one is subjected to KVI with subsequent inspection for defects and destruction. The size of batch n is determined by the same factors as for n*. It is also obvious that at early stages of production $n < n^*$. In the process of improving production the size of batch n increases and approaches n*.

Let us introduce the following designations:

N -- volume of motor series, number of units;

n^* -- volume of batch for KVI with tuning and adjustment with KTI;

n -- volume of batch for KVI;

c_T -- cost of KTI on one motor;

c_B -- cost of KVI for one motor;

c_n -- cost of disassembly, inspection for defects and assembly of motor following KTI;

c -- cost of engine manufacture.

Cost of motor tuning and adjustment on KVI + KTI:

$$c_{КТИ} = (c_{ТИ} + c_{П}) N + (c_{ВИ} + c_{Д}) \frac{N}{n^*}. \quad (6.28)$$

Cost of tuning and adjustment on KVI program:

$$c_{КВИ} = (c_{ВИ} + c_{Д}) \frac{N}{n}. \quad (6.29)$$

Relative cost:

$$\bar{c} = \frac{c_{КТИ}}{c_{КВИ}} = n\left(c + \frac{1}{n^*}\right), \quad (6.30)$$

where

$$c = \frac{c_{ТИ} + c_{П}}{c_{ВИ} + c_{Д}}.$$

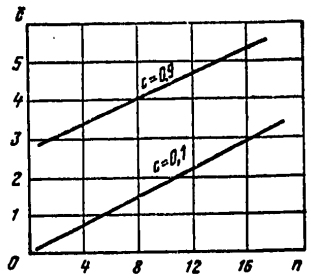

Figure 6.3. Relationship Between Cost of Tuning and Adjustment and Size of Sample

Let us estimate quantity c. With KVI a motor is tested for service life and conformity between principal characteristics and the requirements of technical specifications. Motor operation and accuracy of tuning and adjustment are checked from KTI results. Consequently the cost of performing KVI is greater than the cost of KTI due to a difference in operation time

and propellant flow rate, $c_{BM} > c_{TM}$. For an approximate analysis one can assume $c_{TM} \approx c_{BM}$.

The cost of motor disassembly is less than the cost of manufacture. However, with increase in complexity of motor design and with employment of aggressive propellant components, the cost of disassembly approaches the cost of manufacture.

For motors for which one can perform KTI without disassembly, $c_{\text{д}} = 0$. Quantity c can vary within limits $0.15 < c < 1$.

Figure 6.3 shows relation $\bar{c} = f(c, n)$ when $n = 20$.

It follows from an analysis of Figure 6.3 that with an increase in volume of sample n (as the plant gains experience and know-how), tuning and adjustment with KTI is economically disadvantageous, since $c_{KTM} > c_{KBM}$.

The volume of sample n, whereby outlays on both programs are identical, is determined from equation (6.30), if we assume condition $\bar{c} = 1$,

$$n = \frac{n^*}{cn^* + 1}.$$

Section II. STATIC CHARACTERISTICS OF SOLID-PROPELLANT ROCKET MOTORS

Chapter 7. OPERATING CHARACTERISTICS OF SOLID-PROPELLANT ROCKET MOTORS

7.1. Solid Rocket Propellants and Principal Designs of Solid-Propellant Rocket Motors

At the present time two principal types of solid rocket propellants (TRT) are employed in rocket hardware: ballistite, and composite.

Ballistite propellants are chemically based on organic compounds containing the oxygen-rich nitro- or nitrate groups. Thus in a ballistite propellant both the fuel |C| and |H| and oxidizer |O| are contained within the structure of the same molecule. One of the main components of ballistite propellant, which determine its mechanical structure, is nitrocellulose -- a product of nitration of cellulose. A second mandatory component is a solvent (plasticizer). Nitrocellulose forms, together with the solvent, a plastic, from which various-shaped charges are made by the continuous molding method.

Low-volatility solvents are employed in rocket propellants: nitroglycerin, dinitrate diethylene glycol, and dinitrotoluene [22]. Propellants based on these solvents are designated ballistite propellants. The above-listed solvents, just as nitrocellulose, are active propellant components. Among the solvents, the highest energy characteristics are possessed by nitroglycerin, which for this reason is employed considerably more frequently than the others. In addition to these two principal components, additives are added to a ballistite propellant, which ensure the propellant's stability during storage, stability of combustion, which increase or retard rate of combustion, as well as additives to aid in the manufacturing process.

Composite solid propellants constitute a mechanical mixture (aggregate), consisting chiefly of finely-ground mineral oxidizer and an organic fuel-binder. Most frequently ammonium perchlorate is used as oxidizer in modern TRT [22], while potassium perchlorate and ammonium nitrate are used less frequently. Polyurethane, polybutadiene and other polymers are employed as fuel-binder. Light metals are frequently added to composite propellant in order to improve its energy characteristics -- magnesium, aluminum [22]. Composite propellant constitutes a viscous mass after mixing the components. Composite propellant charges are made by free casting or injection molding

methods. Binder polymerization takes place during heating, with the formation of a solid propellant block.

Modified ballistite TRT with mechanical inclusions of mineral oxidizer, explosives with a positive oxygen balance and metallic fuel occupy an intermediate position between the two principal types of TRT.

All solid rocket propellants burn in parallel layers in such a manner that the burning surface (combustion front) occupies at each succeeding point in time a position equidistant from the proceeding position.

Since linear burning rate, that is, rate of movement of the combustion front into the charge, comprises several mm/s for modern TRT, less frequently in the order of 20 to 30 mm/s, in order to ensure the desired gas generation one must employ charges with radial burning, the burning surface of which is distributed along the entire length of the motor.

Considerably less frequently one employs charges which burn from the end, coated on the lateral surface with a noncombustible material (Figure 7.1).

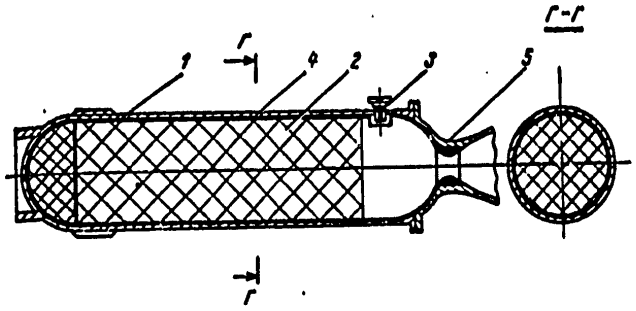

Figure 7.1. Solid-Propellant Rocket Motor With End-Burning Charge

Key:
1. Case
2. Charge
3. Igniter
4. Coating
5. Nozzle

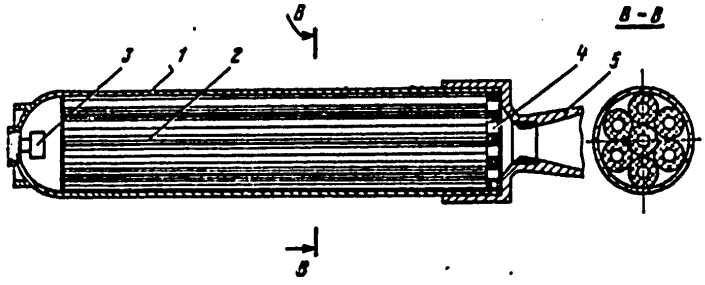

Figure 7.2. Solid-Propellant Rocket Motor With Insert Charge

Key to Figure 7.2 on preceding page:

1. Case
2. Charge
3. Igniter
4. Diaphragm
5. Nozzle

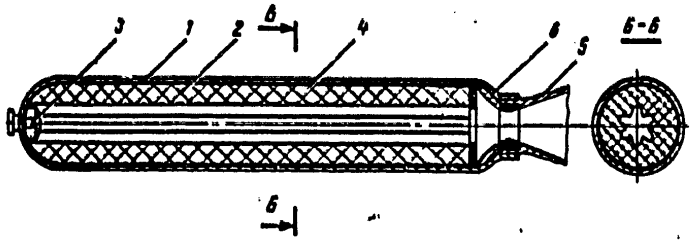

Figure 7.3. Solid-Propellant Rocket Motor With Case-Bonded Charge

Key:

1. Case
2. Charge
3. Igniter
4. Adhesion layer
5. Nozzle
6. Insulation

There are two basic designs for solid-propellant rocket motors with radial burning:

solid-propellant rocket motors with free filling, that is, with an inserted charge (Figure 7.2);

solid-propellant rocket motors with a case-bonded charge (Figure 7.3).

The first of these is typical for solid-propellant motors with ballistite propellant, and the second -- of composite-propellant motors.

In a solid-propellant rocket motor with free filling, the charge consists of separate grains placed in the combustion chamber with a gap. Following are disadvantages of this arrangement:

low coefficient of combustion chamber propellant filling;

contact between burning gas and motor case along its entire inner surface, which requires either a thick-walled case or thick insulation;

the necessity of employing special devices to secure the charge in the chamber and to prevent charge components from ejecting during combustion.

The above-listed drawbacks result in poor mass characteristics of an RDTT [solid-propellant rocket motor] with an inserted charge, which limits the

area of its utilization to instances where the decisive role is played by simplicity of design, low cost of manufacture and simplicity of operation. This arrangement is extensively employed in unguided rocket projectiles and in booster rockets of various designation.

When fueling an RDTT with composite propellant, strong adhesion of charge to motor case can be secured during charging. In such a motor the charge burns along the internal cavity surface, and the case material is protected from the combustion products by the entire thickness of the propellant charge. Contact between the hot gases and case occurs at the very end or in the final stage of charge burning.

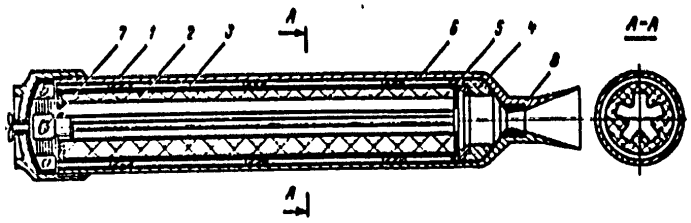

Figure 7.4. Solid-Propellant Rocket Motor With Coated Insert Charge

Key:
1. Case
2. Charge
3. Coating
4. Support
5. Obturator
6. Insulation
7. Igniter
8. Nozzle

Advantages of this design include the following:

high coefficient of chamber propellant filling;

reliable protection of the motor case surface by the entire thickness of the charge, which makes it possible for the case to be thin-walled, utilizing lightweight high-strength materials (titanium, plastics, aluminum alloys);

absence of special devices for securing the charge in the motor.

Disadvantages of this arrangement include relative complexity of loading, as well as complexity of charge inspection (flaw detection) during maintenance. However, in view of the significant advantages, and particularly due to good mass characteristics, this arrangement is widely employed in rockets and has become the basis for large-diameter rockets with considerable engine burning time.

An intermediate position is occupied by an arrangement with a free-inserted coated charge (Figure 7.4). Rubber obturator 5, against which the charge

rests, prevents gas from passing through the annular gap between charge and engine case. As a consequence of this a stagnant zone forms in the annular gap, which is filled with gases through a slot on the front face of the charge in the initial period of engine operation. Heat exchange in the stagnant zone takes place with low intensity, as a consequence of which thermal protection of the case along the length of the charge can be secured with a comparatively thin insulation coating.

RDTT operation breaks down into a principal, operating period and transition period. The transition periods include the following: burn initiation, pressure drop following charge burnup or as a result of burn interruption, and transition from one mode to another for a dual-mode engine. Transition periods comprise a small percentage of total RDTT operating time. During the principal period RDTT working parameters change comparatively slowly and smoothly in conformity with change in charge burning surface and flow passage cross sectional area as a consequence of propellant burnup. The processes taking place in an RDTT during this period can be viewed as quasi-steady-state. In this volume we shall examine only the quasi-steady-state period of RDTT operation.

The principal factors determining the working parameters and thrust characteristics of an RDTT during this period are the following:

propellant composition, which determines its energy characteristics;

law governing propellant burning;

shape of charge, area of its burning surface, and the law governing its change on a time axis;

nozzle throat area;

features of engine gas-dynamic route, which determine the character of chamber internal gas flows.

The methods of calculating operation parameters and static characteristics of an RDTT also change in conformity with the specific features of an engine's gas-dynamic path.

The first method is utilized for a motor with an end-burning charge, as well as for motors with radial burning charges with insignificant pressure drops along the charge. In these cases it is possible to consider pressure and other gas physical parameters constant for total engine ullage, that is, to solve a problem stated zero-dimensionally.

The second method is used when a substantial pressure drop is established along the charge and it is necessary to take into consideration changes in thermodynamic parameters lengthwise along the motor, examining one-dimensional gas flow.

Some studies recommended more rigorous solutions taking into account two- and three-dimensionality of gas flow in RDTT [23, 24], but these solutions are unwieldy and are little suited for analysis of static characteristics of RDTT.

Solution of the problem stated one-dimensionally breaks down in turn into two variants.

The first variant encompasses radial burning charges with lengthwise constant flow passage cross sectional area.

The second variant covers charges with lengthwise variable cross sectional area. In practice one most frequently observes step-wise change in flow-passage cross sectional area at the boundary of two sections of a charge of differing geometry, such as in a slot charge at the boundary of the slot and cylindrical section; also included here are multitier and multisection charges with intermediate spaces.

We should note that the results of one-dimensional and zero-dimensional solutions converge with an increase in motor flow passage cross sectional areas as a result of charge burnup. Therefore the above solution variants can stand side by side in performing calculations for one and the same engine.

7.2. Empirical Law of Rate of Combustion of Solid Rocket Propellants Under Static Conditions

Linear velocity of burning of a solid rocket propellant is defined as the velocity of displacement of the burning surface into the charge. Since rocket propellants burn in parallel layers, the direction of burning velocity always coincides with the normal to the burning surface.

Linear burning velocities of modern rocket propellants under RDTT conditions range from 0.3-0.5 mm/s to 40-50 mm/s [26]. High burning velocities are desirable for charges in uncontrolled rocket projectiles and for rocket boosters, as well as end-burning charges for sustainer engine. Low burning velocities are necessary for ensuring extended operating time for sustainer engines with internally and radially burning charges, as well as for solid-propellant gas generators (pressure accumulators) with extended operating time.

Propellant burning rate $\underline{u}$ is determined by its physicochemical characteristics, combustion chamber pressure p_k, rate of gas flow across the burning surface, initial charge temperature T_H, as well as G loads acting on the charge during burning.

The composition of the propellant and the process of its manufacture exert considerable influence on the rate of burning. For nitroglycerin ballistite propellants quantity $\underline{u}$ increases with an increase in nitroglycerin content.

The conditions of the molding process exert certain influence. For composite propellants u is determined by the type of oxidizer and grain size. The rate of burning can be changed substantially by catalysts added in small quantities to the propellant.

Of the best-known oxidizers, the greatest burning rate is produced by potassium perchlorate, and the slowest by ammonium nitrate [26].

At the present time there do not exist rigorous theoretical methods for calculating the burning rate of TRT. Establishment of such methods is made difficult by the complexity of the burning mechanism of solid rocket propellants, its multiple-stage character, and by the participation of a large number of physical and chemical factors. Therefore in calculating the operation parameters of an RDTT one utilizes an experimental law of TRT burning, that is, an experimental relationship between the linear rate of burning and principal determining parameters in the form

$$u = u_{10} f_1(p) f_2(v) f_3(T_н), \qquad (7.1)$$

where functions f_1, f_2 and f_3 are usually assumed independent of one another. We shall designate $u_1 = u_{10} f_2(v) f_3(T_H)$.

Let us examine the relationship between burning rate and pressure $u = f_1(p)$.

For ballistite propellants, in the low pressure range (to $30\text{-}40 \cdot 10^5$ Pa), the relationship between burning rate and pressure is expressed by the formula

$$u = u_1 p^{\nu}, \qquad (7.2)$$

which in interior ballistics is called the exponential law of combustion. With an increase in pressure the exponential relationship transitions to a linear relationship

$$u = u_1 (1 + b\bar{p}). \qquad (7.3)$$

The linear combustion law is valid for pressures from 4×10^6 to 2×10^7 Pa. In the pressure interval from 3×10^6 to 15×10^6 Pa one can utilize both the exponential and linear relations with approximately equal accuracy. We shall subsequently designate quantity u_{10}, determined by propellant composition, unit burning rate. The law of combustion of composite propellants is usually expressed by formulas of the same type as for ballistite propellants. Taken for separate pressure intervals, they approximate an experimental curve with acceptable accuracy.

The value of exponent ν for modern rocket propellants varies between 0.1 and 0.85. Higher values of ν are characteristic of ballistite propellants. For composite propellants the burning rate is dependent on pressure to a lesser degree.

Summerfield, on the basis of a simple physical model of combustion of composite propellants, proposed the following relation for determining their burning rate:

$$\frac{1}{u} = \frac{a}{p} + \frac{b}{p^{1/3}}. \qquad (7.4)$$

In this equation a and b are constants which are independent of pressure, expressing the relationship between burning rate and various physicochemical parameters.

In practice coefficients a and b are determined from experiment, and Summerfield's law is transformed in practice into an empirical relation, which for pure composite compositions (without metallic additives) can be utilized for calculating burning rate across a broad range of pressures from 1×10^5 to 1×10^7 Pa. For calculating RDTT operations, it is expedient to present Summerfield's relation in the form

$$u = \frac{p}{a + bp^{2/3}}. \qquad (7.4a)$$

We should point to one of the possible deviations from the above-examined laws of combustion, the so-called "plateau" effect observed during combustion of propellants with the addition of various lead compounds. Within a certain range of pressures the burning rate for such propellants is independent of pressure ($\nu \to 0$).

The burning rate of a propellant increases during gas flow along the burning surface of a charge. The increase in propellant burning rate is caused by increased flow of heat from gas to propellant with increased turbulence of gas flow in the vicinity of the burning surface. In the literature this phenomenon is called erosion or turbulent burning. A number of investigators point to the existence of a certain threshold rate of flow, beginning with which the erosion effect occurs.

Consideration of this phenomenon in calculating RDTT operation is performed by means of a correlation function which constitutes the ratio of rates of propellant burning with a gas flow and in a calm environment:

$$f_2(v) = \frac{u_{1v}}{u_{10}}.$$

At the present time this relation is usually presented in the form

$$f_2(v) = 1 + k_v (v - v_{np}) \qquad (7.5)$$

or in a function of dimensionless velocity of flow

$$f_2(v) = 1 + k_\lambda (\lambda - \lambda_{np}), \qquad (7.6)$$

where v_{np}, λ_{np} -- so-called threshold velocity of flow; k_v, k_λ -- coefficient of erosion; when

$$\left.\begin{array}{l}\lambda < \lambda_{np} \\ v < v_{np}\end{array}\right\} f_8(v) = 1.$$

The burning rate of the majority of solid propellants depends to a substantial degree on the initial temperature of the charge. The following formulas are most frequently utilized to express this relation:

$$\frac{u_{1T}}{u_{1N}} = \frac{B}{B-(T_H - T_{HN})}; \qquad (7.7)$$

$$\frac{u_{1T}}{u_{1N}} = e^{D(T_H - T_{HN})}, \qquad (7.8)$$

where T_H -- charge temperature for which a burning rate is determined; T_{HN} -- temperature adopted as standard; u_{1T} and u_{1N} -- unit burning rates at specified and standard temperature respectively. B and D -- physicochemical constants which are individual characteristics of a given kind of fuel.

Formulas (7.7) and (7.8), in spite of an external difference, are mathematically identical expressions under the condition that one and the same value T_N is used in both relations. The relationship between the constants is established as follows:

$$D = \frac{1}{B}.$$

For rocket propellants known from the literature, constant D ranges from 0.001 to 0.004 [26]. The upper value applies to postwar ballistite propellants with a high temperature relation, while the lower value applies to composite propellants.

TRT burning rate is also affected by stressed state of the charge and G loads to which a rocket is subjected in flight. However, since these factors are of a random character, we shall examine their influence together with the influence of other factors disturbing RDTT operation conditions.

7.3. Law of Change of Propellant Burning Surface on a Time Axis

The burning surface of a charge is a second important factor in gas formation in an RDTT. Depending on the nature of change in burning surface on a time axis, we distinguish charges of progressive shape (surface increases during burning), degressive shape and charges with a constant burning surface (neutral charge). The ratio of burning surface S to the initial value of this surface S_0 is called the charge progressiveness characteristic φ.

Selection of charge shape should ensure the character of change in pressure and consequently engine thrust on a time axis in conformity with the required flight program.

If flight conditions do not require changes in engine thrust across a broad range, a charge with a constant burning surface is preferable. In practice such charges are employed considerably more frequently than the others.

Solid rocket propellants burn in parallel layers, which in most cases makes it possible, guided by elementary geometric considerations, to calculate in advance change in burning surface as a function of the percentage of the burned portion of the charge

$$\psi = \omega_{cr}/\omega,$$

that is, to determine relation $\sigma(\psi)$.

We shall note that this is possible only with a uniform field of propellant burning rates, that is, when the linear burning rate is identical for all points in a charge.

Complete charge burning time is determined by thickness of the burning web e_1, which constitutes its smallest linear dimension in the principal direction of burning.

Sometimes in place of relation $\sigma(\psi)$ one utilizes equivalent relation $\sigma(z)$, where $z=e/e_1$ -- relative thickness of the burned charge layer corresponding to given value ψ.

As is indicated by studies, dependence ψ on z can be expressed for all charge shapes by a polynomial of the type

$$\psi = k_1 z (1 + k_2 z + k_3 z^2 + \cdots), \qquad (7.9)$$

where coefficients k_1, k_2, k_3, etc reflect the geometric properties of a given charge.

Obviously with rigorous observance of constancy of burning surface $\sigma = 1$, $\psi = z$. In actuality, however, some variability of surface during burning is observed for the majority of charges which are considered neutral.

Let us examine some general patterns of behavior of charge surface during burning.

In the general case the perimeter of the burning surface Π_σ in a cross or meridional section of a charge consists of areas of smooth curves and points where they intersect -- surface fractures. Figure 7.5 contains typical variants of change in surface shape during burning of various charge elements. If two adjacent surface sections, intersecting, form an angle of less than 180°, in the process of burning the angle shifts together with the burning surface but remains constant. If that same angle is greater than 180°, the apex of the angle rounds off in the process of burning.

For example, the conical surface of an end-burning charge inevitably degenerates during burning into a spherical surface. In order to preserve the angle of conicity it is necessary to place along the axis of the charge a rod of propellant with a higher burning rate $u_2 > u_1$, which satisfies condition

$$\sin\alpha = \frac{u_1}{u_2}$$

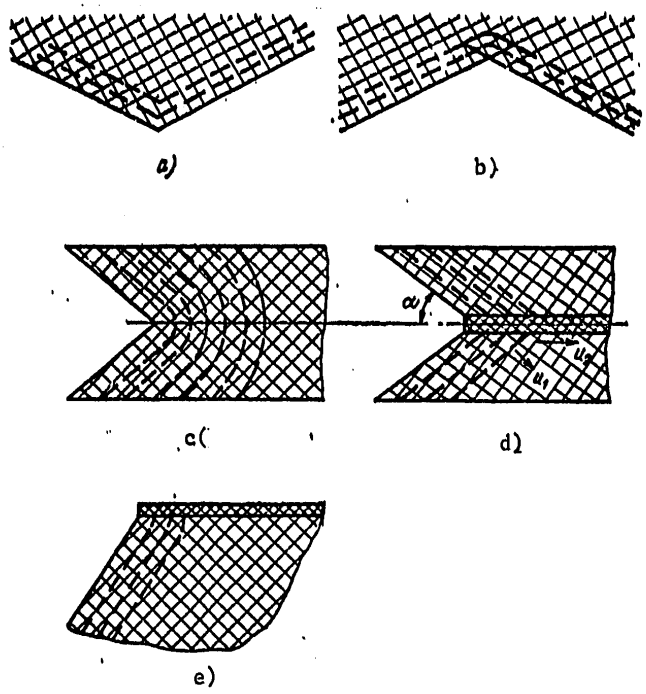

Figure 7.5. Characteristic Variants of Change in Perimeter of Burning for Various Charge Elements

Key:

a. External angle burning
b. Internal angle burning
c. Development of cone-shaped crater in end burning charge
d. Retention of cone-shaped crater with utilization of a lead rod ($u_2 > u_1$);
e. Burning of a corner with coated face

(Figure 7.5 d). A similar rounding off of the angle apex will be observed by the points of intersection of the burning surface with the inhibitory coating (Figure 7.5 e).

In order to determine the behavior of a more complex charge contour, we shall examine a certain fracture-free elementary region of a curvilinear section (Figure 7.6). We shall assume axis x is the principal direction of combustion propagation.

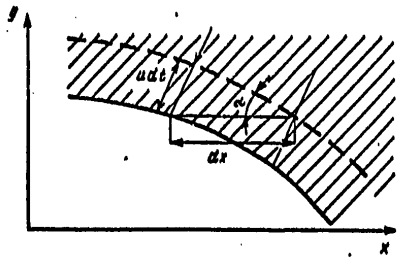

Figure 7.6. Combustion of a Curvilinear Charge Section

During time dt the combustion front will move in direction x by amount $dx=u/\sin\alpha\cdot dt$, where $\alpha=\operatorname{arctg}\frac{dy}{dx}$, and therefore the axial velocity of surface element displacement is equal to

$$u_x=\frac{dx}{dt}=u\frac{\sqrt{1+(dy/dx)^2}}{dy/dx}. \qquad (7.10)$$

If the principal direction of propagation of combustion coincides with axis y, then

$$dy/dt=u\sqrt{1+(dy/dx)^2} \qquad (7.10a)$$

It is obvious that with axial burning constancy of rates dx/dt for all points will constitute a condition of charge state stability, for otherwise the section shape will deform in the process of burning.

Relations (7.10) and (7.10a) assume special importance when calculating change in charge surface with a nonuniform field of burning rates. Field nonuniformity may be caused by changes in initial temperature or propellant chemical composition within the charge. The current position of the charge surface is no longer determined thereby by initial geometry of the charge and its changes according to the law of combustion in parallel layers. In a nonuniform field of velocities there may occur distortion of rectilinear profiles, sharpening of angles greater than 180° and blunting of angles less than 180°. These changes can be taken into consideration on the basis of differential relations (7.10) and (7.10a) with utilization of local burning rate u.

In some cases, with deformation of the initial profile in an inhomogeneous field of propellant burning rates, a new stable profile may form. Profile stability is secured, for example, by the fact that change in burning rate on the y coordinate (with axial burning) is compensated by corresponding change in angle α. This case will be examined in greater detail in Chapter 10.

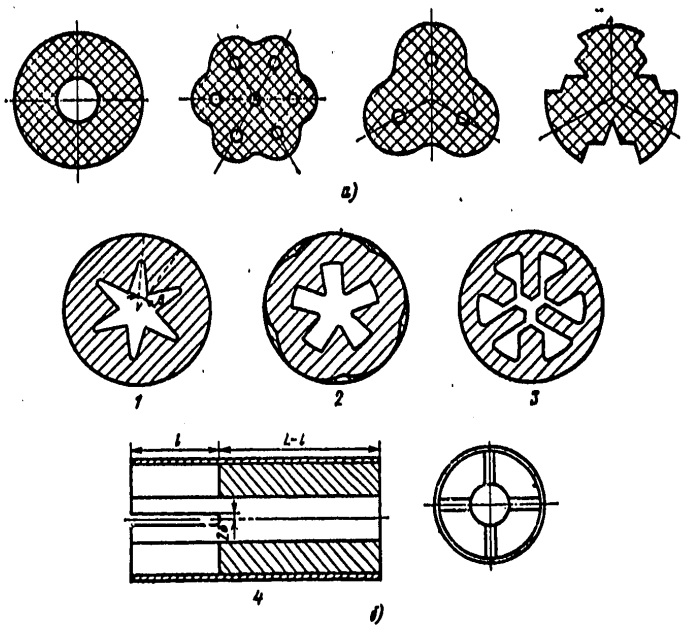

Figure 7.7 Shapes of RDTT Charges

Key:
- a. Shapes of insert charge propellant elements (grains)
- b. Shapes of case-bonded charges
- 1, 2. Star
- 3. Wagon wheel
- 4. Slotted charge

For the majority of radial burning charge shapes, the required progression characteristic is achieved by selection of a ratio of degressively and progressively burning antagonistic surface elements.

Antagonistic elements can be represented in each charge section, such as in a star, or placed along the length of the charge, constituting essentially separate charges with a differing character of combustion (slotted charge).

The most typical charge shapes are presented in Figure 7.7.

7.4. Determination of Operating Parameters and Characteristics of Solid-Propellant Rocket Motors With Zero-Dimensional Statement of the Problem

With steady-state operation the motor material balance equation is written in the form

$$\dot{m}_c = \dot{m}_1 + \dot{m}_2, \qquad (7.11)$$

where $\dot{m}_1$ -- per-second arrival of mass of gases due to propellant burning, volatilization of charge coating material and case insulation coating; $\dot{m}_c$ -- per-second flow rate of gases through the nozzle; m_2 -- mass consumption of gas filling the space evacuated during charge burnup.

In estimating term $\dot{m}_1$ we shall proceed from the assumption that its quantity is entirely determined by gas yield from burning of rocket propellant . Change in gas yield due to thermal destruction of the charge coating and combustion chamber installation plays a role of adjustment to the principal quantity, which we shall examine separately. With this assumption and with utilization of the exponential law of combustion

$$\dot{m}_1 = \rho_T u_1 p_k^{\nu} S, \qquad (7.12)$$

where ρ_T -- density of rocket propellant; S -- burning surface; p_k -- steady-state pressure in the chamber.

Per-second gas flow through the nozzle is expressed by formula

$$\dot{m}_c = \frac{\varphi_c A p_k F_{kp}}{\sqrt{\chi R T_k}}. \qquad (7.13)$$

Here φ_c -- coefficient of nozzle flow rate; F_{kp} -- nozzle throat area;

$$A = \left(\frac{2}{k+1}\right)^{\frac{1}{k-1}} \sqrt{\frac{2k}{k+1}};$$

RT_k -- thermodynamic value of rocket propellant force; χ -- coefficient of losses, taking into account decrease in propellant force due to thermal losses and chemical incompleteness of combustion.

The quantity of gases used to fill area vacated during combustion per unit of time ΔW_{cek} with steady-state pressure p_k, is determined as

$$\dot{m}_2 = \frac{p_k \Delta W_{cek}}{\chi R T_k}.$$

Equation (7.11), with substitution of expressions for $\dot{m}_1$, $\dot{m}_2$ and $\dot{m}_c$, assumes the form

$$\rho_T u_1 p_k^{\nu} S \left(1 - \frac{p_k}{\rho_T \chi R T_k}\right) = \frac{\varphi_c A p_k F_{kp}}{\sqrt{\chi R T_k}}. \qquad (7.14)$$

We shall estimate the second term in the parentheses, assuming

$$p_k = 40 \cdot 10^5 \text{ Па}, \ \chi R T_k = 10^7 \text{ Дж}, \ \rho_T \sim 1600 \ \text{kg/m}^3.$$

We shall obtain $\frac{p_k}{\rho_T \chi R T_k} = 0{,}003$, , that is, 0.3% with respect to 1.

Ignoring this quantity, solving equation (7.14) relative to p_k, we find

$$p_к = \left(\frac{\rho_т u_j S \sqrt{\chi RT_к}}{\varphi_c A F_{кр}}\right)^{\frac{1}{1-\nu}}. \qquad (7.15)$$

Utilizing the above relations, we shall examine the conditions of static stability of RDTT operation. Figure 7.8a shows change in quantities $\dot{m}_c$ and $\dot{m}_1$ for the case $\nu < 1$; Figure 7.8b shows change in the same characteristics for the case $\nu > 1$. The point of intersection of curves $\dot{m}_c$ and $\dot{m}_1$ corresponds to steady-state pressure in the engine. If for any reason engine pressure rises above steady-state, in the case of $\nu < 1$, flow rate will be greater than gas arrival and pressure will drop until it becomes equal to $p_{k.уст}$. When pressure drops below $p_{k.уст}$, gas arrival exceeds flow rate and pressure will rise until it reaches the level $p_{k.уст}$. Thus when $\nu < 1$ RDTT operation is statically stable. When $\nu > 1$ any insignificant engine pressure deviation from $p_{k.уст}$ leads to further movement away from the point of equilibrium process, either in the direction of unlimited pressure increase on in the direction of a pressure drop to zero.

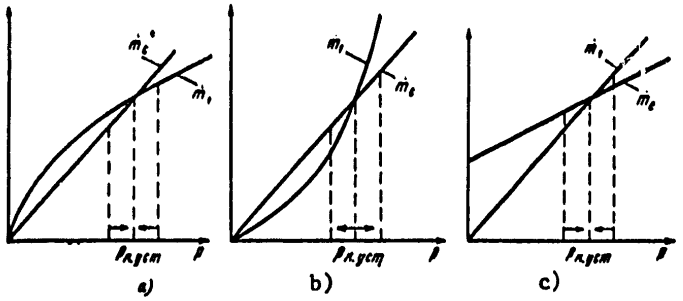

Figure 7.8. Conditions of Static Pressure Stability in a Solid-Propellant Rocket Motor

Key:

a. For the exponential combustion law when $\nu < 1$
b. For the exponential combustion law when $\nu > 1$
c. For binomial linear combustion law

The magnitude of steady-state pressure with the linear binomial combustion law is determined by relation

$$p_к = \frac{1}{\frac{\varphi_c A F_{кр}}{\rho_т S u_{1в} \sqrt{\chi RT_к}} - \tilde{b}}.$$

In this case the condition of static pressure stability (see Figure 7.8c) is expressed by inequality

$$\rho_T S u_{10} \tilde{b} < \frac{\varphi_c A F_{kp}}{\sqrt{\chi R T_k}}.$$

For Summerfield's law $p_{k.ycT}$ is determined by the formula

$$p_k = \left(\frac{\rho_T S \sqrt{\chi R T_k}}{\varphi_c A b F_{kp}} - \frac{a}{b}\right)^{1/2}.$$

If we proceed from the general relation for a burning propellant surface $S=S_0\sigma(\psi)$, p_k should change on a time axis in conformity with change in characteristic $\sigma(\psi)$. Utilizing the latter, one can obtain for the principal period of motor operation relation $p_k(\psi)$. In order to transition to relation $p_k(t)$ one must utilize a gas arrival equation. For the exponential combustion law

$$\frac{d\psi}{dt} = \frac{\rho_T S_0 \sigma(\psi) u_1 p^{\nu}}{\omega}. \qquad (7.16)$$

From this we obtain a working formula for conversion

$$\Delta t = \frac{\omega}{\rho_T S_0 \bar{\sigma} u_1 \bar{p}_k^{\nu}} \Delta\psi, \qquad (7.17)$$

where $\bar{p}_k$, $\bar{\sigma}$ -- mean pressure and regular burning rate characteristic values in interval $\Delta\psi$; Δt -- corresponding $\Delta\psi$ time interval.

Knowing the magnitude of engine pressure in steady-state operation, one can calculate such engine output parameters as rate of gas flow through the nozzle, thrust and specific thrust.

Rate of gas flow is calculated with formula (7.13).

To determine engine thrust one can utilize relation

$$P = \dot{m}_c v_a + p_a F_a - p_H F_a.$$

We shall convert it into formulas which we shall utilize in subsequent derivations. for this we shall replace the first two terms on the right side with a monomial, which includes one of the known gas-dynamic functions.

Utilizing function $f(\lambda)$, the equation can be rewritten in the form

$$P = \sigma_c p_k F_a f(\lambda_a) - p_H F_a; \qquad (7.18)$$

$$f(\lambda) = (1+\lambda^2)\left(1 - \frac{k-1}{k+1}\lambda^2\right)^{\frac{1}{k-1}},$$

where σ_c -- a coefficient characterizing losses of total pressure in the RDTT nozzle. Utilizing function $Z(\lambda)$, we obtain

$$P = \frac{k+1}{k} \chi_c \dot{m}_c a_{kp} Z(\lambda_a) - p_n F_a, \qquad (7.19)$$

where $a_{kp} = \sqrt{\frac{2k}{k+1} \chi R T_к}$ -- critical velocity; χ_c -- a coefficient characterizing nozzle losses.

$$Z(\lambda) = \frac{1}{2}\left(\lambda + \frac{1}{\lambda}\right).$$

Substituting in formula (7.19) expanded expressions for $\dot{m}_c$ and a_{kp}, we obtain

$$P = 2\left(\frac{2}{k+1}\right)^{\frac{1}{k-1}} \varphi_c p_к F_{кр} Z(\lambda_a) - p_n F_a. \qquad (7.19a)$$

The principal virtue of relations (7.18) and (7.19), alongside their simplicity, is the fact that with their utilization calculations are simplified by employing tabular gas-dynamic functions f (λ_a) and Z (λ_a). It is not difficult to find argument λ_a from gas-dynamic tables according to ratio $F_{kp}/F_a = q(\lambda_a)$, where q ($\lambda_a$) is also a tabular gas-dynamic function.

We shall utilize relation (7.19) to obtain a formula for specific thrust impulse. Dividing both parts of the equality by $\dot{m}_c$ and substituting an expanded expression for $\dot{m}_c$ in the last term, we obtain

$$I_y = \sqrt{\frac{k+1}{2k}} \sqrt{\chi R T_к} \left[2\chi_c Z(\lambda_a) - \left(\frac{k+1}{2}\right)^{\frac{1}{k-1}} \frac{F_a}{\varphi_c F_{кр}} \frac{p_n}{p_к}\right]. \qquad (7.20)$$

In view of the triviality of the second term in the brackets, in calculating RDTT specific impulse nozzle loss coefficient χ_c is usually applied to the entire brackets.

Nozzle loss coefficient χ_c characterizes the distinction of the actual process taking place in the nozzle from the ideal process on which derivation of the above obtained relations is based and which presupposes one-dimensional isentropic flow of an ideal gas in the nozzle. Usually this coefficient is presented in the form of a product:

$$\chi_c = \prod \chi_{c_i}, \qquad (7.21)$$

where χ_{ci} -- factors resulting from individual types of losses.

The principal types of nozzle losses include the following:

1. Dispersion losses, connected with nonuniformity of nozzle flow, that is, with the presence of a radial velocity component at the nozzle exit;

2. two-phase losses with condensed particles in the combustion products;

3. friction losses;

4. thermal losses connected with heat dissipation into the nozzle walls.

Dispersion losses are easily determined by calculation.

For conical nozzles coefficient of losses of this type is equal to

$$\chi_{a_1} = \cos^2 \frac{\alpha_1}{2},$$

where α_1 -- half-angle of nozzle opening.

For shaped nozzles

$$\chi_{a_1} = \frac{1}{2}\left(1 + \cos \frac{\alpha_0 + \alpha_1}{2}\right),$$

where α_0, α_1 -- nozzle opening half-angles at the beginning of the bell mouth and in the exit section respectively.

Calculation determination of the remaining types of losses involves a number of difficulties. This applies in particular to two-phase losses, which for RDTT with metallized propellants are the principal type of specific impulse losses. This is due to inadequate study of the mechanism of interaction between condensed particles and gas, the nature of the processes of particle coagulation and fractionation and, chiefly, to a lack of reliable data on dimensions of condensed particles and the spectrum of their distribution. Two-phase losses increase in direct proportion to the mass percentage of condensate in combustion products and decrease with an increase in nozzle size in proportion to the square of the diameter of the particles. The magnitude of these losses for a nozzle of medium size, with average particle size of 2-4 microns in the combustion chamber, ranges from 2 to 4%.

Thermal losses for large engines with an insulated nozzle surface do not exceed fractions of a percent. For small motors with uninsulated nozzles the magnitude of thermal losses increases to several percent.

Friction losses depend substantially on the state of the nozzle surface. The development of surface roughness during nozzle heat erosion is accompanied by an increase in these losses, which may comprise 1-2%.

Study [19] lists standard values of nozzle specific impulse losses for an RDTT burning aluminized propellant, obtained on the basis of experiments with a motor with a thrust of 230 kg:

Table 7.1.

1 Категория потерь	2 Средняя величина потерь, %
Потери из-за запаздывания конденсированной фазы 3	2,5
Рекомбинационные потери 4	1,0
Потери на трение 5	1,0
Потери на конденсацию 6	0,3
Потери на скачки уплотнения 7	0,2
Полные потери 8	5,0

Key:

1. Category of losses
2. Average magnitude of losses
3. Losses due to condensed phase delay
4. Recombination losses
5. Friction losses
6. Condensation losses
7. Shock wave losses
8. Total losses

When utilizing a flush nozzle additional losses occur, the magnitude of which is determined primarily by the degree of nozzle penetration into the combustion chamber and content of metal additive in the propellant. According to [8], with a degree of penetration from 20 to 60% these losses comprise approximately 0.4% for a composite propellant with 5% aluminum; they increase to 1-1.2% for propellant with 21% aluminum.

7.5 Determination of Operating Parameters of Solid-Propellant Rocket Motors With One-Dimensional Statement of the Problem (Charges With Lengthwise-Constant Flow Passage Cross-Sectional Area)

An increase in the coefficient of combustion chamber propellant filling for the purpose of improving a motor's mass characteristic α leads to a situation where at the initial stage of charge combustion the rate of gas flow along its surface increases sharply. This is accompanied by erosion effect, that is, an increase in rate of propellant burning, resulting in a pressure increase in the motor. In addition, there occurs a substantial pressure drop along the charge. In other words, with the adopted working pressure in the motor (pressure at nozzle inlet) there is an increase in pressure at the forward face, from which in this instance one must proceed in performing motor case strength calculations.

Under these conditions, the previously-examined zero-dimensional solution becomes unsound. The following problem solution in a one-dimensional statement is suitable to an equal degree for charges of various shapes: a charge of cylindrical single-cavity grains, including a single-grain variant, for a star charge and its modifications, charges of telescopic and cross shape, a "wagon wheel" charge, etc, under the condition that the chamber flow passage cross sectional area remains constant lengthwise on the charge. With

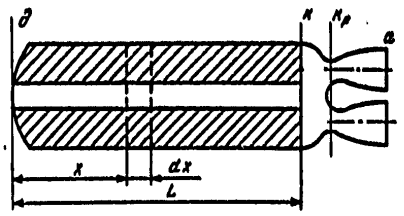

Figure 7.9. Calculation Diagram of Charge With Lengthwise-Constant Flow Passage Cross Sectional Area

this condition the diversity of charge shapes can be reduced to the diagram contained in Figure 7.9. For simplicity of calculations, we shall first examine a charge with a blind forward end. Subsequently it will be shown in (7.6) how end burning can be considered with this arrangement.

We shall examine change in thermodynamic parameters along the motor's gas path, proceeding from the forward end to the nozzle.

1. Region "d-k," bounded by the charge ends

We shall assume that gas temperature remains constant within the engine cavity, equal to the temperature of propellant combustion. Change in parameters of gas flow in section "d-k" will be determined by two equations: quantity of movement and continuity.

The quantity of movement equation for a constant section cavity assumes the form

$$\dot{m}v + pF = \text{const} = I_p. \quad \dot{m}v+pF=\text{const}=I_p \ .$$

In the initial channel section when v=0 $I_p=p_д F_k$.

For any section

$$\dot{m}v + pF = \frac{pF}{r(\lambda)} = \text{const}, \qquad (7.22)$$

where

$$r(\lambda) = \frac{1 - \frac{k-1}{k+1}\lambda^2}{1+\lambda^2} \qquad (7.23)$$

gas-dynamic function;

$\lambda = \frac{v}{a_{кр}}$ -- dimensionless velocity.

Equation (7.22) does not consider the forces of gas friction on the charge surface. Estimation of this factor in the region of Reynolds numbers characteristic for flow along a charge (Re $\sim 10^5$-10^6), indicates that these losses comprise at the initial stage of combustion not more than 2-5% of pressure drop along the charge caused by gas flow. It follows from the equation of quantity of movement that static pressure along the cavity changes as

$$p = p_к r(\lambda). \qquad (7.24)$$

To derive a continuity equation we shall specify an elementary burning region of extent dx (see Figure 7.9). Change in flow rate through the cavity cross section in region dx is equal to gas arrival in this section:

$$d\dot{m} = \rho_т \Pi_т u_{10} f_1(p) f_2(v)\, dx. \qquad (7.25)$$

We shall present a general expression for gas flow rate in the form

$$\dot{m} = \rho_т v F = \frac{p}{\chi R T_к} Fv.$$

Taking into consideration relation (7.24), we obtain

$$\dot{m} = \frac{p_к}{\chi R T_к} F a_{кр} \lambda r(\lambda). \qquad (7.26)$$

Differentiating (7.26) and substituting the result in (7.25), we obtain

$$\frac{p_к}{\chi R T_к} F a_{кр} \left\{ r(\lambda) + \lambda \frac{d}{d\lambda}[r(\lambda)] \right\} d\lambda = \rho_т \Pi_т u_{10} f_1(p) f_2(v)\, dx. \qquad (7.27)$$

We shall designate the braces on the left side of the equality by $\varphi(\lambda)$. Substituting on the right side of the equality expressions for t_1 (p) in conformity with (7.2) and f_2 (p) in conformity with (7.6), dividing the variables and integrating, we obtain:

for the erosion burning section

$$\int_{\lambda_{пр}}^{\lambda} \frac{\varphi(\lambda)\, d\lambda}{[r(\lambda)]^{\nu}[1 + k_\lambda(\lambda - \lambda_{пр})]} = \frac{\rho_т \Pi_т u_{10} \chi R T_к}{F_к a_{кр} \rho_к^{1-\nu}}(x - x_{пр}), \qquad (7.28)$$

where $x_{пр}$ — coordinate of the section in which dimensionless velocity reaches a value $\lambda_{пр}$;

for a nonerosion combustion section

$$\int_0^{\lambda_{пр}} \frac{\varphi(\lambda)\, d\lambda}{[r(\lambda)]^{\nu}} = \frac{\rho_т \Pi_т u_{10} \chi R T_к}{F_к a_{кр} \rho_к^{1-\nu}} x_{пр}. \qquad (7.29)$$

Combining equations (7.28) and (7.29) and substituting an expression for a_{kp} on the right-hand side, we obtain

$$\Phi(\lambda) = \frac{\rho_1 u_1 S_\phi}{F_\kappa \rho_\kappa^{1-\nu}} \sqrt{\frac{k+1}{2k} \chi R T_\kappa}, \qquad (7.30)$$

where

$$\Phi(\lambda) = \int_{\lambda_{np}}^{\lambda} \frac{\varphi(\lambda)\, d\lambda}{[r(\lambda)]^\nu [1 + k_\lambda (\lambda - \lambda_{np})]} + \int_0^{\lambda_{np}} \frac{\varphi(\lambda)\, d\lambda}{[r(\lambda)]^\nu};$$

$S_\phi = \pi_p x$ -- charge lateral burning surface.

Figure 7.10 contains a graph of function $\Phi(\lambda)$ for $\lambda_{\kappa p}$=0.15; k_λ=1.0-5.0 and ν=0.3-0.7.

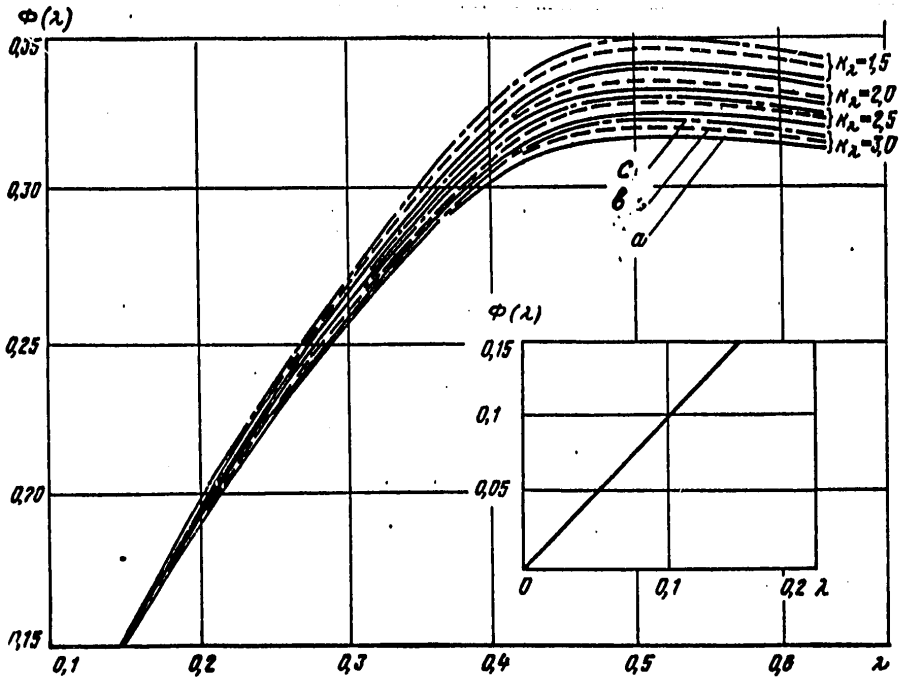

Figure 7.10. Graphs of Function $\Phi(\lambda)$ With $\lambda_{\kappa p}$=0.15

Key:

a. ν=0.3
b. ν=0.5
c. ν=0.7

We shall note that the complex $S_{\text{кр}}/F_k$ constitutes U. A. Pobedonostsev's criterion for a finite charge section.

The obtained relations make it possible to determine all parameters of interest to us in section "д-к" (see Figure 7.9).

The pressure drop along the charge is determined as

$$\Delta p_{д.к} = p_д - p_к = p_д [1 - r(\lambda_к)]. \qquad (7.31)$$

We shall note that when $\lambda \leqslant 0.5$, a simplified expression can be used to compute gas-dynamic function r (λ):

$$r(\lambda) = 1 - \lambda^2. \qquad (7.32)$$

With values $\lambda < 0{,}4$, $k = 1{,}11-1{,}25$, the error of such an approximation remains less than 1%, and only when λ =0.5-0.55 does it increase to 3-6%.

Utilizing expression (7.32), we obtain

$$\Delta p_{д.к} = p_д \lambda_к^2.$$

Gas flow rate in a finite charge section is expressed as

$$\dot{m}_к = \frac{AF_к q(\lambda_к) p_{ок}}{\sqrt{RT_к \chi}}.$$

Since complete flow pressure in this section is equal to $p_{ок} = p_к/\pi(\lambda_к)$, the formula for gas flow rate assumes the form

$$\dot{m}_к = \frac{AF_к y(\lambda_к) p_к}{\sqrt{\chi RT_к}}, \qquad (7.33)$$

where q (λ_k) and y (λ_k) -- tabular gas-dynamic functions.

The rate of propellant burning along the charge changes due to decrease in static pressure and increase in gas velocity. At short distances from the forward end and with short charges, when $\lambda > \lambda_{кр}$ there is no erosion effect and the burning rate decreases in conformity with the drop in pressure. However, when $\lambda > \lambda_{кр}$ erosion effect becomes the predominant factor, and burning rate increases. It is expedient to utilize for solving a number of problems burning rate averaged along the charge length. We shall designate with K_u the ratio of this average burning rate to the rate of end burning of the same propellant. Then generation of gases along the length of the charge, equal to flow rate in section k, can be represented as

$$\dot{m}_к = \rho_т u_{10} p_к^\nu S_б K_u. \qquad (7.34)$$

Equalizing the right sides of equations (7.33) and (7.34) and substituting value $S\sigma/F_k$ from (7.30), we obtain

$$K_u = \left(\frac{2}{k+1}\right)^{\frac{1}{k-1}} \frac{\psi(\lambda_K)[r(\lambda_K)]^{1-\nu}}{\Phi(\lambda_K)}. \qquad (7.35)$$

2. Region "k-kp," between charge end and nozzle throat area

Significant hydraulic losses can occur in this area, connected with dissipation of the mechanical energy of gas flow preceding from the charge cavity into the prenozzle space. These losses are determined on the basis of the general relationships of hydraulics as

$$\Delta p_c = \xi \frac{\rho_r v_K^2}{2},$$

where ξ -- coefficient of hydraulic losses, determined experimentally.

Having determined gas density from the state equation through static pressure in the charge cavity exit section, and velocity in this section through $\lambda_k a_{kp}$, we obtain

$$\Delta p_c = \frac{\xi k}{k+1} p_K \lambda_K^2. \qquad (7.36)$$

Coefficient of restoration of full pressure in the prenozzle space σ_c is determined as

$$\sigma_c = \frac{p_{0K} - \Delta p_c}{p_{0K}} = 1 - \frac{\Delta p_c}{p_{0K}},$$

or, substituting (7.36), we obtain

$$\sigma_c = 1 - \frac{\xi k}{k+1} \pi(\lambda_K) \lambda_K^2. \qquad (7.37)$$

A continuity equation for area "k-kp" is written in the form

$$\dot{m}_c = \dot{m}_K + \dot{m}_T,$$

where $\dot{m}_c$ -- total gas flow through the nozzle; $\dot{m}_T$ -- arrival of gases from the charge end facing the nozzle.

In expanded form

$$\dot{m}_c = \rho_r S_6 \mu_{10} p_K^{\nu} K_u + \rho_r S_T \mu_{10} p_T^{\nu},$$

where p_T -- gas pressure at end surface.

Considering that generation of gases from the end surface usually comprises a small percentage of total gas generated, one can, without introducing significant error in calculation of $\dot{m}_c$, assume $p_T = p_k$. Then, designating $S_T/S_\sigma = \bar{S}$ we obtain

$$\dot{m}_c = \rho_T u_{10} S_6 p_K^{\nu} (K_u + \bar{S}). \qquad (7.38)$$

Gas flow through the nozzle can be expressed just as

$$\dot{m}_c = \frac{A \sigma_c \varphi_c F_{KP} p_{0K}}{\sqrt{\chi R T_K}}. \qquad (7.39)$$

Equating the right-hand parts of equations (7.38) and (7.39), we obtain

$$p_K = \left[\frac{\rho_T S_6 (K_u + \bar{S}) u_{10} \sqrt{\chi R T_K}\, \pi(\lambda_K)}{A \sigma_c \varphi_c F_{KP}} \right]^{\frac{1}{1-\nu}}. \qquad (7.40)$$

The obtained relation essentially comprises a modification of formula (7.15) for pressure in the case of a zero-dimensional variant, but taking into account in integral form change in rate of burning and pressure through the engine.

An expression for p_k can also be obtained taking into account (7.24) from relation (7.30):

$$p_K = \left[\frac{\rho_T u_{10} S_6}{F_K \Phi(\lambda_K)} \sqrt{\frac{k+1}{2k} \chi R T_K} \right]^{\frac{1}{1-\nu}} r(\lambda_K). \qquad (7.41)$$

One can obtain from equalities (7.40) and (7.41) a relation linking dimensionless velocity in the exit section of the charge cavity with the correlation between cavity and nozzle throat areas.

$$\frac{F_K}{F_{KP}} = \frac{\sigma_c \varphi_c}{q(\lambda_K)\left(1 + \frac{\bar{S}}{K_u}\right)}. \qquad (7.42)$$

In the process of engine operation area F_k increases as a consequence of propellant burnup, and the percentage share of erosion combustion in total gas generation continuously decreases, becoming zero when $\lambda_k \leqslant \lambda_p$. At the same time there occurs equalization of pressure along the length of the combustion chamber. Relation (7.15) becomes applicable thereby. This relation can be utilized to determine mean indicated pressure $\bar{p}_k$ in the engine, substituting in it time-averaged values S_{cp} and $u_{1\,cp}$. Then one can determine from formulas (7.15) and (7.30) the maximum amount average engine pressure $p_{\text{ф}\,\max}/\bar{p}_k$ on a time axis is exceeded, where $p_{\text{ф}\,\max}$ -- maximum pressure in the forward part of the motor after it enters quasi-steady-state mode. Charge geometric parameters at the moment of attainment of $p_{\text{ф}\,\max}$ can be assumed equal to their initial value. If we assume

$$u_{1\,cp} \sim u_{10},$$

we obtain from formulas (7.15), (7.30) and (7.42)

$$\frac{p_{A\max}}{p_к} = \left[\frac{1+\bar{S}/K_н}{1+\bar{S}}\,\frac{\lambda_к\left(1-\frac{k-1}{k+1}\lambda_к^2\right)^{\frac{1}{k-1}}}{\sigma_c\Phi(\lambda)}\right]^{\frac{1}{1-\nu}}. \qquad (7.43)$$

In determining engine thrust corresponding to the moment of attainment of $p_{A\max}$, one can proceed from relation (7.19a), bearing in mind that one must substitute in this relation full pressure at nozzle inlet.

$$P = 2\left(\frac{2}{k+1}\right)^{\frac{1}{k-1}}\frac{\varphi_c\sigma_c p_к F_{кр}}{\pi(\lambda_к)}Z(\lambda_н) - p_н F_a.$$

7.6. Determination of Operating Parameters of Solid-Propellant Rocket Motors With Charges With Step-Wise Change in Flow Passage Cross-Sectional Area

Charges with flow passage cross sectional area changing step-wise along the length of the engine are in widespread use. They can be subdivided to two basic groups:

monoblock charges consisting of two sections with differing geometry;

sectional charges, consisting of several sections (tiers) divided by intermediate spaces.

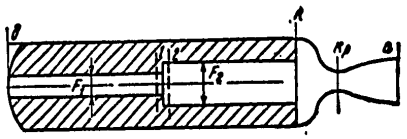

Figure 7.11. Diagram of Charge With Step-Wise Change in Flow Passage Cross-Sectional Area

A slotted charge consisting of a cylindrical and slotted section can serve as an example of charges of the first group. An example of a sectional charge is the propellant charge powering the Titan-3C booster, consisting of five short elements with a cylindrical cavity, burning on the surface of the ends and cavity.

We shall first examine an RDTT with a charge consisting of sections with differing geometry. Figure 7.11 contains a diagram of such a charge.

We shall examine here a charge consisting of two sections, although the relations obtained below can also apply to more complex variants. The charge cavity cross sectional area changes abruptly at the boundary of the

sections, but it remains constant in each. We shall designate in the vicinity of the boundary two test sections 1 and 2, in the upper and lower sections. From the continuity equations written for these sections we have

$$q(\lambda_2) = q(\lambda_1)\frac{p_{01}}{p_{02}}\frac{F_1}{F_2}. \qquad (7.44)$$

Relative losses of total pressure during sudden expansion (compression) are determined as

$$\frac{\Delta p_0}{p_{01}} = \xi\frac{k}{k+1}\lambda^2\pi(\lambda),$$

where ξ -- coefficient of hydraulic losses equal to [29] $\xi_{сж} = \frac{1}{2}\left(1-\frac{F_2}{F_1}\right)$ -- during compression;

$$\xi_{расш} = \frac{F_2}{F_1} - 1 \quad \text{-- during expansion.}$$

Consequently,

$$q(\lambda_2) = q(\lambda_1)\frac{F_1}{F_2}\left[1-\xi\frac{k}{k+1}\lambda_1^2\pi(\lambda_1)\right] \qquad (7.45)$$

and dimensionless velocity at the beginning of the second section λ_2 is a function of λ_1 and the ratio of areas F_1/F_2.

An equation of quantity of gas movement for section "1-k" can be written in the form

$$\dot{m}_к v_к + p_к F_2) = (\dot{m}_1 v_1 + p_1 F_1) + p_1(F_2 - F_1),$$

where $\dot{m}_1$ and $\dot{m}_к$ -- mass gas flow rates in sections 1 and k.

Expressing complete impulse flow through function r (λ), we obtain

$$\frac{p_к F_2}{r(\lambda_к)} = \frac{p_1 F_1}{r(\lambda_1)} + p_1 F_1\left(\frac{F_2}{F_1} - 1\right).$$

For a random section in area "1-k" one can write

$$\frac{p}{r(\lambda)} = p_1\frac{F_1}{F_2}\left[\frac{1}{r(\lambda_1)} + \frac{F_2}{F_1} - 1\right]. \qquad (7.46)$$

We shall designate

$$Б = p_1\frac{F_1}{F_2}\left[\frac{1}{r(\lambda_1)} + \frac{F_2}{F_1} - 1\right]. \qquad (7.47)$$

Then static pressure in any section of area "2-k" will be determined as

$$p = Br(\lambda). \qquad (7.48)$$

Relation (7.48) is analogous to (7.24), but in place of $p_{дн}$ it contains combined parameter B.

In order to obtain a relation for gas arrival in section "2-k," we shall utilize equation (7.27), substituting in it static pressure determined by formula (7.48).

Dividing the variables and integrating the left-hand side from λ_2 to λ_k, and the right-hand side from x_2 to x_k, we obtain

$$\Phi(\lambda_k) - \Phi(\lambda_2) = \frac{\rho_T u_{10} S_0}{F_0 B^{1-\nu}} \sqrt{\frac{k+1}{2k} \chi R T_к}. \qquad (7.49)$$

Relation (7.49) differs from the previously derived (7.30) in that the difference of values of functions $\Phi(\lambda)$ enters the left-hand side, and parameter B -- in place of $p_{дн}$ -- into the right-hand side.

Gas flow rate in section k is determined from relation (7.33). Hydraulic losses in the prenozzle space are calculated as in 7.5. It is more convenient to perform calculation of engine parameters in the following sequence.

1. Specifying pressure at forward end $p_{дн}$, one determines λ_1 and p_1 on the basis of relations (7.30) and (7.24).

2. With formula (7.47) we calculate parameter B, and then find λ_k and p_k with (7.45) and (7.48), (7.49).

3. We determine flow rates $\dot{m}_k$ and $\dot{m}_T$, and then $\dot{m}_c$ as well.

4. With λ_k we calculate the coefficient of losses of complete pressure in the prenozzle space.

5. On the basis of total flow and pressure p_k, we obtain the required nozzle throat area.

Nomograms can be constructed on the basis of such calculations for propellant with specified characteristics, enabling one to solve a direct problem -- to determine engine pressure on the basis of specified engine and charge geometry.

The specific features of calculating the operating parameters of a section charge reduce to figuring hydraulic losses in the spaces between sections and figuring initial velocity at section inlet when calculating gas generation in the section cavity.

With a large intermediate space and narrow cavity in the above-lying section (tier), calculation of hydraulic losses is performed on the basis

of relation (7.36). If the sections are separated by narrow transverse slots, the following relation is recommended in [29] for determining losses of complete pressure in the slot:

$$\Delta p_0/p_0 = -\frac{2k}{k+1}\lambda\Delta\lambda,$$

where $\Delta\lambda$ -- difference of dimensionless velocities at slot inlet and outlet.

If flow rate at section cavity inlet $\dot{m}_{Bx}$ is known, initial velocity λ_{0x} is obtained from the condition

$$y(\lambda_{0x}) = \frac{\dot{m}_{0x}p_{0x}\sqrt{\chi RT_к}}{A\varphi_{0x}P_к}, \qquad (7.50)$$

where φ_{Bx} -- coefficient of stream narrowing at cavity inlet.

With this initial condition, change in static pressure, according to equation (7.22), follows the relation

$$p = \frac{p_{0x}}{\tau(\lambda_{0x})}\tau(\lambda). \qquad (7.51)$$

Consequently the relation (7.49) in this case assumes the form

$$\Phi(\lambda_к) - \Phi(\lambda_{0x}) = \frac{p_т u_{1e} S_б}{F_к \tilde{p}^{\frac{1}{1-\nu}}}\sqrt{\frac{k+1}{2k}\chi RT_к}, \qquad (7.52)$$

where

$$\tilde{p} = \frac{p_{0x}}{\tau(\lambda_{0x})}.$$

Obviously relations (7.50), (7.51) and (7.52) must be followed in solving the problem examined in 7.5 with a burning forward end. If $\lambda_{Bx} < \lambda_{gp}$ the value of function $\phi(\lambda_{Bx})$ can be calculated with the relation

$$\Phi(\lambda) = \frac{3}{\nu}\lambda - \frac{3-\nu}{2\nu\sqrt{\nu}}\ln\frac{1/\sqrt{\nu}+\lambda}{1/\sqrt{\nu}-\lambda}.$$

Chapter 8. DEVIATIONS OF OPERATING PARAMETERS OF SOLID-PROPELLANT ROCKET MOTORS IN THE VICINITY OF SPECIFIED CONDITIONS

8.1. Relations for Deviations of Operating Parameters of Solid-Propellant Rocket Motors in Vicinity of Specified Conditions for a Zero-Dimensional Variant

We shall utilize formula (7.15) to derive relations for deviation of RDTT operating parameters. Taking its logarithm, differentiating it, and subsequently replacing differentials with finite parameter increments, we obtain

$$\frac{\Delta p_к}{p_к} = \frac{1}{1-\nu}\left[\frac{\Delta u_1}{u_1} + \frac{\Delta S}{S} + \frac{\Delta \rho_т}{\rho_т} + \frac{1}{2}\frac{\Delta \chi}{\chi} + \right.$$
$$\left. + \frac{1}{2}\frac{\Delta (RT_к)}{RT_к} - \frac{\Delta \varphi_c}{\varphi_c} - \frac{\Delta F_{кр}}{F_{кр}}\right].$$

For simplifying calculations and subsequent conclusions it is expedient to proceed to relative deviations of parameters $\delta x_1 = \Delta x_1 / x_1$.

The relation for relative engine pressure deviation assumes the form

$$\delta p_к = \frac{1}{1-\nu}\left[\delta u_1 + \delta S + \delta \rho_т + \frac{1}{2}\delta \chi + \frac{1}{2}\delta (RT_к) - \delta \varphi_c - \delta F_{кр}\right]. \tag{8.1}$$

Examining variations of quantities u_1 and $RT_к$ we shall distinguish components, one of which results from variants in the characteristics of the propellant proper, while the other is determined by change in initial charge temperature. We shall examine small deviations of initial charge temperature from its expected value, whereby one determines nominal engine characteristics. Change in RDTT thrust parameters within a broad range of temperatures, as well as methods of engine tuning and adjustment making it possible to reduce this change to a minimum, will be examined in Chapter 10. The charge temperature deviations examined in this derivation play the role of errors in determining expected charge temperature both during engine tuning and adjustment and for a motor without tuning and adjustment. It is assumed thereby that temperature is constant throughout the entire volume of the charge. Consequently,

$$\delta u_1 = \delta \tilde{u}_1 + \frac{\partial u_1}{\partial T_н} \frac{T_н}{u_1} \delta T_н; \qquad (8.2)$$

$$\delta RT_к = \delta (\widetilde{RT}_к) + \frac{\partial (RT_к)}{\partial T_н} \frac{T_н}{RT_к} \delta T_н. \qquad (8.3)$$

Here the symbol ~ denotes variation components resulting from variance of characteristics of the propellant proper, as a consequence of random changes in chemical composition, deviations in the manufacturing process, changes in properties during storage, etc. Substituting (8.2) and (8.3) in (8.1) and utilizing relations (10.1) and (10.2) (see Chapter 10) for determining derivatives, we obtain

$$\delta p_к = \frac{1}{1-\nu} \left[\delta \tilde{u}_1 + \delta S + \delta \rho_т + \frac{1}{2} \delta \chi - \right.$$

$$\left. - \delta \varphi_c - \delta F_{кр} + \frac{1}{2} \delta (\widetilde{RT}_к) + (m + D) T_н \delta T_н \right]. \qquad (8.4)$$

Proceeding in like manner with equation (7.13), we obtain

$$\delta \dot{m}_c = \delta p_к + \delta F_{кр} - \delta \varphi_c - \frac{1}{2} \delta \chi - \frac{1}{2} \delta (\widetilde{RT}_к) - m T_н \delta T_н.$$

Substituting here the value of $\delta p_к$ from the preceding formula, we obtain

$$\delta \dot{m}_c = \frac{1}{1-\nu} \left[\delta \tilde{u}_1 + \delta S + \delta \rho_т - \frac{\nu}{2} \delta \chi - \nu \delta F_{кр} - \right.$$

$$\left. - \nu \delta \varphi_c + \frac{\nu}{2} \delta (\widetilde{RT}_к) + (\nu m + D) T_н \delta T_н \right]. \qquad (8.5)$$

To determine thrust variation we shall utilize equation (7.19a), rewriting it in the form

$$P + F_a p_н = 2 \left(\frac{2}{k+1} \right)^{\frac{1}{k-1}} \chi_c \varphi_c p_к F_{кр} Z (\lambda_a),$$

where χ_c -- a coefficient characterizing losses in the supersonic portion of the nozzle.

Sequentially taking the logarithm and differentiating this equation, we obtain

$$\frac{\Delta P + p_н \Delta F_a}{P + p_н F_a} = \frac{\Delta \chi_c}{\chi_c} + \frac{\Delta \varphi_c}{\varphi_c} + \frac{\Delta p_к}{p_к} + \frac{\Delta F_{кр}}{F_{кр}} + \frac{\partial Z}{\partial \left(\frac{F_{кр}}{F_a} \right)} \frac{\Delta \left(\frac{F_{кр}}{F_a} \right)}{Z (\lambda_a)}.$$

Ratio F_{kp}/F_a is equal to the value of gas-dynamic function $q(\lambda_a)$, as a consequence of which the last term can be rewritten as

$$\frac{\partial Z(\lambda_a)}{\partial q(\lambda_a)} \frac{\Delta q(\lambda_a)}{Z(\lambda_a)}.$$

In order to obtain the simplest analytical solution, we shall employ an approximating relation which links the numerical values of functions $q(\lambda)$ and $Z(\lambda)$ in the range of velocities λ_a of interest to us. It is evident from the graphs $Z=f(q)$, plotted for the supersonic flow region with various values of k that within a fairly broad range of change in λ_a one can resort to a linear approximation

$$Z(\lambda) = a - bq(\lambda). \tag{8.6}$$

For example, when k=1.25 in the range λ=1.7-2.4, if we assume a=1.425 and b=0.50, the error of approximation does not exceed 1.6%.

Utilizing relation (8.6) and proceeding to relative quantities, we obtain

$$\delta P = \left(1 + \frac{p_H F_a}{P}\right)\left\{\delta\varphi_c + \delta\chi_c + \delta p_k + \delta F_{kp} - \right.$$
$$\left. - \frac{b}{\frac{a}{q(\lambda_a)} - b}\delta[q(\lambda_a)]\right\} - \frac{p_H F_a}{P}\delta F_a. \tag{8.7}$$

We shall introduce designation $\frac{p_H F_a}{P} = \gamma_p$.

Substituting in (8.7) an expression for δp_k, we obtain

$$\delta P = \frac{1+\gamma_p}{1-\nu}\left\{\delta\tilde{u}_1 + \delta\rho_\tau + \delta S + \frac{1}{2}\delta\chi + \right.$$
$$+ \frac{1}{2}\delta(\overline{RT}_k) - \nu\delta\varphi_c + (D+m)T_k\delta T_H - \nu\delta F_{kp} -$$
$$\left. - \frac{b(1-\nu)}{\frac{a}{q(\lambda_a)} - b}\delta[q(\lambda_a)]\right\} - \gamma_p\delta F_a + (1+\gamma_p)\delta\chi_c. \tag{8.8}$$

In order to obtain an expression for δI_y it is necessary to subtract (8.5) from (8.8):

$$\delta I_y = \delta P - \delta\dot{m}_c = \frac{\gamma_p}{1-\nu}(\delta\tilde{u}_1 + \delta S + \delta\rho_\tau) +$$
$$+ \frac{1+\gamma_p-\nu}{2(1-\nu)}[\delta\chi + \delta(\overline{RT}_k)] - \frac{\nu\gamma_p}{1-\nu}(\delta\varphi_c + \delta F_{kp}) -$$
$$- (1+\gamma_p)\frac{b}{\frac{a}{q(\lambda_a)} - b}\delta[q(\lambda_a)] - \gamma_p\delta F_a +$$
$$+ \frac{(m+D)\gamma_p + m(1-\nu)}{1-\nu}T_H\delta T_H + (1+\gamma_p)\delta\chi_c. \tag{8.9}$$

$\delta\chi_c$ in turn can be represented in the form of a sum of variations of individual types of losses in the supersonic portion of the nozzle:

$$\delta\chi_c = \sum_{i}^{n} \delta\chi_{c_i}. \qquad (8.10)$$

Of these, only dispersion losses can be expressed by simple analytical relations:

$\delta\chi_{c_1} = \operatorname{tg}\frac{\alpha}{2} \cdot \alpha\delta\alpha$ -- in the case of a conical nozzle;

$\delta\chi_{c_1} = \frac{1}{2}\operatorname{tg}\frac{\alpha_0+\alpha_1}{4}(\alpha_1\delta\alpha_1 + \alpha_0\delta\alpha_0)$ -- in the case of a shaped nozzle.

Calculated determination of variations of other types of losses in the supersonic portion of the nozzle encounters substantial difficulties.

It is stated in [19] that different kinds of losses of specific impulse, as losses due to two-phase flow, due to recombination processes, heat dissipation into the nozzle walls and losses in the boundary layer can be connected with engine pressure and with nozzle dimensions as follows:

$$\chi_{c_i} \sim \frac{1}{(p_к R_{кр})^{0,2}},$$

where R_{kp} -- radius of critical section.

Consequently, the relative variance of these losses with specified conditions of flow in the nozzle can in a first approximation be considered as

$$\delta\chi_{c_i} = -0,1\,(\delta F_{кр} + 2\delta p_к).$$

Coefficients of system of equations (8.1)-(8.10) are figured for a specific motor on the basis of its known characteristics. For specified external and internal disturbances δx_i, one can determine from a solution to the system of equations deviations of engine operating parameters δy_j from their nominal values, and one can obtain coefficients of influence $\frac{\partial y_j}{\partial x_i}$ as deviations of individual engine operating parameters by a unit of deviation of each of the disturbing factors x_i. Maximum deviations of principal operating parameters are determined with the following formulas:

$$\delta p_{к.пр} = \sqrt{\sum^{i}\left(\frac{\partial p_к}{\partial x_i}\delta x_i\right)^2};$$

$$\delta \dot{m}_{с.пр} = \sqrt{\sum^{i}\left(\frac{\partial \dot{m}_с}{\partial x_i}\delta x_i\right)^2};$$

$$\delta P_{пр} = \sqrt{\sum^{i}\left(\frac{\partial P}{\partial x_i}\delta x_i\right)^2};$$

$$\delta I_{у.пр} = \sqrt{\sum^{i}\left(\frac{\partial I_у}{\partial x_i}\delta x_i\right)^2}.$$

$\delta\tilde{u}_1$, δS, $\delta\rho_т$, $\delta(RT_к)$, $\delta\chi$, $\delta\varphi_c$, $\delta F_{кр}$, constitute disturbances δx_i entering into the formulas for $\delta p_{к.пр}$ and $\delta \dot{m}_{c.пр}$. Disturbances δF_a, $\delta\chi_c$, $\delta[q(\lambda_a)]$ above and beyond the ones enumerated above, also enter into the formula for $\delta P_{пр}$ and $\delta I_{y.пр}$. Derivatives

$$\frac{\partial p_к}{\partial x_i}, \quad \frac{\partial \dot{m}_c}{\partial x_i}, \quad \frac{\partial P}{\partial x_i}, \quad \frac{\partial I_y}{\partial x_i}$$

constitute coefficients of influence determined from the solution of system (8.1)-(8.10) relative to the specified disturbing factors.

8.2. Relations for Deviations in Operating Parameters of Solid-Propellant Rocket Motors in the Environs of Specified Conditions in the Case of a One-Dimensional Solution

Analytical determination of deviations of RDTT operating parameters in the environs of specified (nominal) conditions in the given case are based on solution of a system of linearized equations obtained as a result of transformation of relations (see 7.5).

As in the preceding paragraph, we shall present deviations of operating parameters and charging parameters of RDTT in relative quantities. Dimensionless coefficients with relative deviations (variations) are given in the designations previously adopted in Chapter 1.

Logarithmically varying equation (7.30), which links pressure at the forward end of the engine with charging parameters and combined gas-dynamic function $\Phi(\lambda)$ and proceeding to relative deviations, we obtain

$$\delta p_к = \frac{1}{1-\nu}\left[\delta\rho_т + \delta u_{10} + \delta S_6 - \delta F_к + \frac{1}{2}\delta\chi + \right.$$

$$\left. + \frac{1}{2}\delta(RT_к) - \frac{\lambda_к}{\Phi(\lambda_к)}\frac{d}{d\lambda}[\Phi(\lambda)]\,\delta\lambda_к\right].$$

We shall present this relation in the following form:

$$a_3^{p_к}\delta p_к + b_3^{\rho}\delta\rho_т + b_3^{u}\delta u_{10} + b_3^{S}\delta S_6 + \text{where}$$

$$+ b_3^{F}\delta F_к + b_3^{\chi}\delta\chi + b_3^{RT}\delta(RT_к) + a_3^{\lambda}\delta\lambda_к = 0, \qquad (8.11)$$

$$a_3^{p_к} = -1; \quad b_3^{\rho} = b_3^{u} = b_3^{S} = \frac{1}{1-\nu};$$

$$b_3^{F} = -\frac{1}{1-\nu}; \quad b_3^{\chi} = b_3^{RT} = \frac{1}{2}\frac{1}{1-\nu};$$

$$a_3^{\lambda} = -\frac{\lambda_к}{\Phi(\lambda_к)}\frac{d}{d\lambda}[\Phi(\lambda)]\frac{1}{1-\nu}.$$

A relative change in pressure drop along the charge can be presented in the form

$$\delta \Delta p_{д.к} = \frac{\Delta p_д}{\Delta p_{д.к}} - \frac{\Delta p_к}{\Delta p_{д.к}}.$$

Utilizing relations (7.24) and (7.31), we obtain

$$\delta \Delta p_{д.к} = \frac{1}{1 - r(\lambda_к)} \delta p_{д.к} - \frac{r(\lambda_к)}{1 - r(\lambda_к)} \delta p_к$$

or

$$a^{\Delta p}_{д.к} \delta \Delta p_{д.к} + a^{p_д}_{д.к} \delta p_д + a^{p_к}_{д.к} \delta p_к = 0, \qquad (8.12)$$

where

$$a^{\Delta p}_{д.к} = -1; \quad a^{p_д}_{д.к} = \frac{1}{1 - r(\lambda_к)};$$

$$a^{p_к}_{д.к} = -\frac{r(\lambda_к)}{1 - r(\lambda_к)}.$$

In like manner we obtain from equation (7.31)

$$\delta \Delta p_{д.к} = \delta p_д - \frac{\lambda_к}{1 - r(\lambda_к)} \frac{d}{d\lambda} [r(\lambda_к)] \delta \lambda_к$$

or

$$a^{\Delta p_к}_к \delta \Delta p_{д.к} + a^{p_д}_к \delta p_д + a^к_\lambda \delta \lambda = 0, \qquad (8.13)$$

where

$$a^{\Delta p}_к = 1; \quad a^{p_д}_к = 1; \quad a^\lambda_к = -\frac{\lambda}{1 - r(\lambda_к)} \frac{d}{d\lambda} [r(\lambda_к)].$$

Logarithmicly varying the equation of gas flow through the nozzle and proceeding to relative deviations, we obtain

$$\delta \dot{m}_c = \delta \varphi_c + \delta \sigma_c + \delta p_к + \delta F_{кр} - \frac{1}{2} \delta \chi - \frac{1}{2} \delta (RT_к) -$$

$$- \frac{d}{d\lambda} [\pi(\lambda)] \frac{\lambda_к}{\pi(\lambda_к)} \delta \lambda_к$$

or

$$a^{\dot{m}_c}_к \delta \dot{m}_c + b^\varphi_{к.c} \delta \varphi_c + a^\sigma_{к.c} \delta \sigma_c + a^p_{к.c} \delta p_к + b^F_{к.c} \delta F_{пр} +$$

$$+ b^\chi_{к.c} \delta \chi + b^{RT}_{к.c} \delta (RT_к) + a^\lambda_{к.c} \delta \lambda = 0, \qquad (8.14)$$

where

$$a^{\dot{m}_c}_{к.c} = -1; \quad b^\varphi_{к.c} = a^\sigma_{к.c} = a^p_{к.c} = b^F_{к.c} = 1;$$

$$b^\chi_{к.c} = b^{RT}_{к.c} = -\frac{1}{2};$$

$$a^\lambda_{к.c} = -\frac{d}{d\lambda} [\pi(\lambda)] \frac{\lambda}{\pi(\lambda)}.$$

Differentiating an expression for σ_c, after transformations we obtain

$$\delta\sigma_c = -\frac{2+\frac{d}{d\lambda}[\pi(\lambda)]\frac{\lambda}{\pi(\lambda)}}{\frac{k+1}{\xi k}\frac{1}{\lambda^2\pi(\lambda)}-1}\delta\lambda. \qquad (8.15)$$

Logarithmically varying the gas flow equation for the charge cavity exit section and proceeding to relative deviations, we obtain

$$\delta\dot{m}_к = \delta F_к + \delta p_к - \frac{1}{2}\delta\chi - \frac{1}{2}\delta(RT_к) + \frac{\lambda}{y(\lambda)}\frac{d}{d\lambda}[y(\lambda)]\delta\lambda$$

or

$$a^{\dot{m}}_к\delta\dot{m}_к + b^F_к\delta F_к + a^p_к\delta p_к + b^\chi_к\delta\chi + b^{RT}_к\delta(RT_к) + b^\lambda_к\delta\lambda = 0, \qquad (8.16)$$

where

$$a^{\dot{m}}_к = -1;\quad b^F_к = a^p_к = 1;\quad b^\chi_к = b^{RT}_к = -\frac{1}{2};$$

$$b^\lambda_к = \frac{\lambda_к}{y(\lambda_к)}\frac{d}{d\lambda}[y(\lambda)].$$

In like manner, transforming the equation of gas generation from the charge end surface, we obtain

$$\delta\dot{m}_т = \delta\rho_т + \delta S_т + \delta u_{10} + \nu\delta p_к$$

or

$$a^{\dot{m}}_т\delta\dot{m}_т + b^\rho_т\delta\rho_т + b^{S_т}_т\delta S_т + b^u_т\delta u_{10} + a^p_т\delta p_к = 0, \qquad (8.17)$$

where

$$a^{\dot{m}}_т = -1;\quad b^\rho_т = b^S_т = b^u_т = 1;\quad a^p_т = \nu.$$

We can transform as follows the last equation -- sums of gas generated from the end surface and cavity surface:

$$\delta\dot{m}_c = \delta\dot{m}_т\frac{\dot{m}_т}{\dot{m}_c} + \delta\dot{m}_к\frac{\dot{m}_к}{\dot{m}_c}.$$

Since

$$\dot{m}_к = \rho_т u_{10} S_B p^\nu_к K_u;$$

$$\dot{m}_т = \rho_т u_{10} S_т p^\nu_к;$$

$$\dot{m}_c = \rho_т u_{10} S_B p^\nu_к\left(K_u + \frac{S_т}{S_B}\right),$$

we obtain

$$\frac{\dot{m}_к}{\dot{m}_c} = \frac{K_u}{K_u+\bar{S}};\quad \frac{\dot{m}_т}{\dot{m}_c} = \bar{S}\frac{1}{K_u+\bar{S}},$$

where

$$\bar{S} = S_т/S_B.$$

In final form we obtain

$$a_c^{\dot{m}_c}\delta\dot{m}_c + a_c^{\dot{m}_T}\delta\dot{m}_T + a_c^{\dot{m}_K}\delta\dot{m}_K = 0, \qquad (8.18)$$

where

$$a_c^{\dot{m}_c} = -1; \quad a_c^{\dot{m}_T} = \frac{\overline{S}}{K_u + \overline{S}}; \quad a_c^{\dot{m}_K} = \frac{K_u}{K_u + \overline{S}}.$$

We have obtained a closed system of eight equations. Following are unknowns in this system:

$$\delta\lambda, \delta p_k, \delta\Delta p_{д.к}, \delta\sigma_c, \delta\dot{m}_T, \delta\dot{m}_K, \delta\dot{m}_c.$$

External and internal disturbances are manifested in the form

$$\delta u_{10}, \delta\rho_T, \delta F_K, \delta F_{кр}, \delta\chi, \delta(RT_K), \delta S_B, \delta S_T, \delta\varphi_c.$$

The obtained system of equations makes it possible for the specified disturbances to find deviations of the principal parameters of the in-chamber process and gas flow through the nozzle.

In order to obtain thrust variations we must utilize equation (7.43), transforming it as was done in 8.1.

We shall obtain the following:

$$\delta P = (1+\gamma_p)\left\{\delta\varphi_c + \delta\sigma_c + \delta p_K + \delta F_{кр} - \frac{\lambda_K}{\pi(\lambda_K)}\frac{d}{d\lambda}[\pi(\lambda)]\,\delta\lambda_K\right\} -$$

$$-\gamma_p\delta F_a.$$

Value δp_k is placed here from the solution of system of equations (8.11)-(8.18).

Variations of specific thrust impulse are obtained as

$$\delta I_y = \delta P - \delta\dot{m}_c.$$

For brevity of presentation in deriving a system of equations, we have not examined the individual variation components u_{10} and RT_k, which can be introduced into the equations as was shown on 8.1.

We shall note that the relationship between variations δp_k and the disturbances producing them can be established by another method, logarithmically varying equation (7.40).

Table 8.1 contains coefficients of influence calculated for RDTT with the following characteristics:

$$\nu = 0{,}3; \ \lambda_K = 0{,}3; \ k_\lambda = 2{,}0; \ \lambda_{пр} = 0{,}15; \ k = 1{,}2; \ \overline{S} = 0{,}05.$$

Table 8.1.

Возмущение 1	2 Отклонения параметров на единицу отклонения возмущающего фактора			
	$\delta p_{\text{д}}$	$\delta p_{\text{к}}$	$\delta h_{\text{к}}$	$\delta \dot{m}_{\text{с}}$
δu_{10}	1,429	1,429	0	1,429
$\delta \rho_{\text{т}}$	1,429	1,429	0	1,429
$\delta (\chi R T_{\text{к}})$	0,714	0,714	0	0,214
$\delta F_{\text{к}}$	—0,410	—2,363	—1,065	—2,370
$\delta F_{\text{кр}}$	—1,019	—0,934	—1,065	—1,941
δS_{δ}	1,384	—1,460	1,047	1,470
$\delta \varphi_{\text{с}}$	—1,020	—0,935	—1,065	—1,941
$\delta S_{\text{т}}$	0,045	0,041	0,047	0,041

Key:
1. Disturbance
2. Deviations of parameters per unit of deviation of the disturbing factor

The following conclusions can be drawn from the calculation results:

1. Disturbances δu_{10}, $\delta \rho_{\text{т}}$ and $\delta (\chi RT_{\text{к}})$, do not influence quantity $\lambda_{\text{к}}$, produce in the case under examination the same relative deviations δp and $\delta \dot{m}_{\text{с}}$ as in the case of a zero-dimensional solution. Coefficients of influence for pressure prove to be equal to $1/1-\nu$ for $\delta \rho_{\text{т}}$ and δu_{10}, and for $\delta (\chi RT_{\text{к}})$ comprise $-\frac{1}{2}\frac{1}{1-\nu}$ for pressure and $\frac{1}{2}\left(\frac{1}{1-\nu}-1\right)$ for rate of flow.

2. A different character of influence is observed for disturbances connected with change in $\lambda_{\text{к}}$. Influence $\delta F_{\text{к}}$, $\delta F_{\text{кр}}$ and δS_{δ} is manifested most strongly.

An additional relationship between coefficients of influence is seen from the numerical results of all calculations, including those contained in Table 8.2:

$$-\frac{\partial p_{\text{к}}}{\partial F_{\text{кр}}} = \frac{1}{1-\nu} - \frac{\partial p_{\text{к}}}{\partial F_{\text{к}}}.$$

This relation can be obtained analytically if one logarithmically varies formula (7.40).

Table 8.2.

1 Возмущение	Отклонение $\delta p_д$ на единицу отклонения возмущающего фактора 2		
	$\bar{S}=0,05$	$\bar{S}=0,1$	$\bar{S}=0,3$
$\delta F_к$	—1,202	—1,183	—0,877
$\delta F_{кр}$	—0,227	—0,246	—0,552
$\delta S_б$	1,420	1,411	1,325
$\delta S_т$	0,008	0,018	0,104

Key:
1. Disturbance
2. Deviation $\delta p_д$ per unit of disturbing factor deviation

3. The influence of disturbances δF_k, δF_{kp} and $\delta S_б$ increases with a decrease in characteristic $\bar{S}$, that is, with a decrease in the role of end burning in the process of gas formation. This is evident from Table 8.2, which contains the results of calculations for variants differing by quantity $\bar{S}$, but with common values of the remaining characteristics:

$$\nu = 0,3;\ \lambda_к = 0,5;\ k_\lambda = 2,0;\ \lambda_{пр} = 0,15;\ k = 1,2.$$

At the same time the influence of deviation $\delta S_т$ increases.

4. The influence of deviations δF_k and $\delta S_б$ on quantity $\delta p_д$ increases substantially with an increase in λ_k, which can be seen from the figures in tables 8.1 and 8.2, obtained for λ_k=0.3 and λ_k=0.5. The influence of deviations δF_{kp} and $\delta S_т$ decreases with an increase in λ_k.

5. The value of erosion coefficient k_λ influences in the same direction as λ_k. Table 8.3 contains results of calculations for variants differing in their values with common characteristics

$$\nu = 0,3;\ \lambda_к = 0,3;\ \lambda_{пр} = 0,15;\ k = 1,2;\ \bar{S} = 0.05.$$

Table 8.3.

1 Возмущение	Отклонение $\delta p_д$ на единицу отклонения возмущающего фактора 2		
	$k_\lambda=1,5$	$k_\lambda=2,0$	$k_\lambda=2,5$
$\delta F_к$	0,360	0,410	0,454
$\delta F_{кр}$	1,069	1,019	0,975
$\delta S_б$	1,381	1,384	1,386
$\delta S_т$	0,047	0,045	0,042

Key:
1. Disturbance
2. Deviation $\delta p_д$ per unit of disturbing factor deviation

8.3. Selection of Optimal p_k and λ_k Values

Selection of optimal RDTT design parameters and operating conditions in engine design and engineering has the ultimate objective of obtaining the least launch mass value m_0 for a vehicle with a specified payload $m_{п.н}$ and performance data (range, speed and altitude).

The initial mass of a rocket with RDTT is determined in general form as

$$m_0 = \frac{m_{п.н}}{1-\mu_к(1+\alpha)-\bar{k}}, \qquad (8.19)$$

where $\mu_k = \omega_к/m_0$ -- relative fuel reserve; α -- coefficient of engine mass perfection; $\bar{k}$ -- a coefficient taking into account the mass of connecting assemblies, lines, aerodynamic elements and auxiliary devices.

Consequently, determination of the condition of minimum value of m_0 boils down to examination for the extremum of product $\mu_k(1+\alpha)$, which is the function of a large number of ballistic, gas-dynamic and structural parameters. Performance of this task develops into a multilevel investigation which goes far beyond the limits of the topic under investigation. Within the framework of our presentation we shall limit ourselves to a brief analysis of the influence of two parameters on the mass characteristics of the vehicle -- engine operating pressure p_k and quantity λ_k, which constitutes one of the most important characteristics of loading conditions. With this approach the condition of the extremum is written in the form

$$\left.\begin{aligned} \frac{\partial\alpha}{\partial p_к}\mu_к + \frac{\partial\mu_к}{\partial p_к}(1+\alpha) = 0; \\ \frac{\partial\alpha}{\partial\lambda_к} = 0. \end{aligned}\right\} \qquad (8.20)$$

We shall examine derivative $\frac{\partial\mu_к}{\partial p_к}$:

$$\frac{\partial\mu_к}{\partial p_к} = \frac{\partial\mu_к}{\partial I_y}\frac{\partial I_y}{\partial p_к},$$

where the first factor of the right side characterizes change in required fuel reserve with change in specific impulse I_y when v_k=const. Taking into account gravitational losses, which for vertically-launched rockets comprise the bulk of velocity losses in the powered segment of flight,

$$\frac{\partial\mu_к}{\partial I_{(v_к=\text{const})}} = \frac{1}{I_y}\frac{\ln(1-\mu_к)-\frac{a+b\mu_к}{\eta}}{\frac{1}{1-\mu_к}-\frac{b}{\eta}}, \qquad (8.21)$$

where η -- initial thrust-weight ratio

$$\eta = \frac{P_S}{gm_0};$$

a and b -- coefficients of approximation, dependent on the control program, that is, on the type of function $\theta=\theta(\mu)$. For example, for function $\theta(\mu)$ in [27], a=0.10, b=0.689.

If in the first approximation we proceed from Tsiolkovskiy's formula, then

$$\frac{d\mu_к}{dI_y} = -\frac{1-\mu_к}{I_y}\ln(1-\mu_к),$$

which also follows from relation (8.21), when $\eta=\infty$.

Derivative $\partial I_y/\partial p_к$ expresses the relationship between specific impulse and combustion chamber pressure, which was examined in general form in Chapter 3. according to the approximation dependence of RDTT specific impulse on pressure obtained in [4] for standard composite propellants when $p_к=(30-70)\cdot10^5$ Pa,

$$\frac{\partial I_y}{\partial p_к} = 0{,}76 - 0{,}006p_к.$$

Let us examine the relationship to pressure of engine mass perfection coefficient $\alpha=m_{к.д}/\omega$. Without going into a detailed analysis of the components of engine structure mass $m_{к.д}$, we shall represent it as the sum of two terms:

$$m_{к.д} = m_{н.э} + m_{п.э},$$

where $m_{н.э}$ -- mass of the structure's load-bearing elements, for which the forces of engine internal pressure are the principal type of load; $m_{п.э}$ -- mass of structure elements indifferent to internal pressure (heat shielding components, nozzle inserts, diaphragms, etc). Quantity $m_{п.э}$ is determined chiefly by the mass of the cylindrical engine case and end plates. Mass of the cylindrical case is

$$m_{у.к} = \pi D_н^2 \rho_к k_L L \bar{\Delta}_к,$$

where $D_н$ -- engine bore; $\rho_к$ -- density of material; L -- length of charge; k_L -- coefficient taking into account difference in charge and thrust chamber lengths; $\bar{\Delta}_к$ -- relative wall thickness, equal to

$$\bar{\Delta}_к = \frac{p'_m}{2\sigma_в}.$$

Here p'_m -- calculated pressure; $\sigma_в$ -- ultimate strength of case material.

The mass of two end plates of elliptical shape without insulation and nozzle cutouts with a semiaxis ratio of 1:2 is determined with the following formula [4]:

$$m_д = \frac{5}{8}\pi D_н^3 \rho_к \bar{\Delta}_д,$$

where $\bar{\Delta}_д$ -- relative thickness of end plate wall.

Henceforth we shall assume $\bar{\Delta}_д = \bar{\Delta}_к$. Consequently mass $m_{н.э}$ can be presented in a first approximation as

$$m_{н.э} = k_{mн}\pi D_н^3 \rho_к \bar{\Delta}_к \left(k_L \bar{L} + \frac{5}{8}\right),$$

where $\bar{L}$ -- charge length in gauges; $k_{mн}$ -- coefficient taking into account mass of additional elements also contained in $m_{н.э}$ (fasteners, threaded connections, etc).

Derivative $\frac{d\alpha}{dp}$ with specified charge mass and length is determined as

$$\frac{d\alpha}{dp} = \frac{1}{\omega}\frac{dm_{н.э}}{dp} = k_{mн}\frac{\pi D_н^3}{\omega}\rho_к \left(k_L \bar{L} + \frac{5}{8}\right)\frac{1}{2\sigma_в} k_p, \quad (8.22)$$

where $k_p = p'_m/p_к$ -- coefficient of calculated pressure exceeding engine working pressure.

Let us examine the structure of coefficient k_p:

$$k_p = \eta_p (1 + \delta p_д)\frac{p_{д\,max}}{p_к}\frac{p_{кT}}{p_{кN}}. \quad (8.23)$$

Factor $p_{кT}/p_{кN}$ characterizes change in $p_к$ with change in initial charge temperature in the specified temperature range of engine utilization: $T_{HN} \div T_{HT}$. Calculation of ratio $p_{кT}/p_{кN}$ is examined in Chapter 10. Ratio $(p_{д\,max}/p_к)$ is figured with formula (7.43).

Factor $(1+\delta p_д)$ takes into account maximum variance of quantity $p_д$ in the environs of its nominal value. Maximum variance $\delta p_{д.п} p$ with the assumption that the principal disturbances engendering it are of a random nature and are governed by the law of normal distribution:

$$\delta p_{д.\,пр} = \sqrt{\left(\frac{\partial p_д}{\partial u_{10}}\delta u_{10}\right)^2 + \left(\frac{\partial p_д}{\partial \rho_т}\delta \rho_т\right)^2 + \left(\frac{\partial p_д}{\partial F_к}\delta F_к\right)^2 + \left(\frac{\partial p_д}{\partial \chi}\delta\chi\right)^2 + \left[\frac{\partial p_д}{\partial (RT_к)}\delta(RT_к)\right]^2 + \left(\frac{\partial p_д}{\partial S_в}\delta S_в\right)^2 + \left(\frac{\partial p_д}{\partial S_т}\delta S_т\right)^2 + \left(\frac{\partial p_д}{\partial \varphi_c}\delta\varphi_c\right)^2}. \quad (8.24)$$

Here δu_{10}, $\delta \rho_т$, etc -- values of disturbances; $\frac{\partial p_д}{\partial u_{10}}$, $\frac{\partial p_д}{\partial \rho_т}$, etc -- coefficients of influence of disturbances on quantity $p_д$, determined from solution of (8.11)-(6.18) as numbers indicating deviation $\delta p_д$, caused by a single disturbance of a given type. η_p is a reserve strength factor adopted on the basis of experience in engine development or determined for specified reliability taking into account normal distribution of wall thickness, material strength characteristic, and quantity $p_д$.

In selecting an engine working pressure from extremum conditions $p_{k}(1+\alpha)$, it is also necessary to consider possibilities of abnormal burning and engine operation instability when p_k drops below a certain limit determined experimentally for each propellant -- $p_{k\min}$. This condition can be presented in the form

$$p_к(1-\delta p_{к.\,пр}) > p_{к\,\min}, \qquad (8.25)$$

where $\delta p_{k.\,пр}$ -- maximum spread of p_k around its nominal value with the lowest utilization temperature $T_{н\,\min}$.

Quantity $\delta p_{k.\,пр}$, according to 8.1, is calculated with the formula

$$\delta p_{к.\,пр} = \frac{1}{1-\nu} \times \cdot$$

$$\times \sqrt{(\delta u_1)^2 + (\delta S)^2 + (\delta \rho_т)^2 + \frac{1}{4}(\delta\chi)^2 + \frac{1}{4}[\delta(RT_к)]^2 + (\delta\varphi_c)^2 + (\delta F_{кр})^2}. \qquad (8.26)$$

In case the value of p_k obtained from the condition of the optimum fails to satisfy condition (8.25), in spite of the condition of optimization it is necessary to proceed from a higher value of p_k, which should ensure reliability of engine operation at the lower pressure limit.

Probability of normal engine operation at the lower working pressure limit is determined as

$$\text{Вер}(p_к - p_{к\,\min} > 0) = \Phi(Z),$$

where $\Phi(Z)$ -- Gauss probability integral;

$$Z = \frac{p_к - p_{к\,\min}}{\sigma_{p\,\min}};$$

$$\sigma_{p\,\min} = \sqrt{\sigma^2_{p_к} + \sigma^2_{p_{эксп}}}.$$

Here $\sigma_{p\,\min}$ -- root-mean-square deviation of p_k, calculated on the basis of solution (8.1); $\sigma_{p\,эксп}$ -- root-mean-square error with which allowable value $p_{k\,\min}$ is determined experimentally.

It follows from the above-examined relations that static characteristics play an important role in selection of optimal engine pressure.

The second equation of system (8.20) establishes in general form a link between coefficient α and gas-dynamic parameter λ_k. Velocity coefficient λ_k influences quantity α in two directions:

according to relation (7.43), coefficient λ_k, with specified value p_k, determines ratio $p_{кам}/p_k$, and consequently calculated value p'_m as well, that is, an increase in λ_k should lead to a heavier structure and increase in α;

according to relation (7.30), quantity λ_k, with specified value $p_{\text{д}}$, determines charge flow passage cross sectional area F_k, and consequently the coefficient of engine propellant filling.

Selection of a higher value λ_k leads to a decrease in F_k, and consequently to a decrease in α.

Following these conclusions, derivative $\frac{\partial \alpha}{\partial \pi_к}$ can be written in the form

$$\frac{\partial \alpha}{\partial \lambda_к} = \frac{\partial \alpha}{\partial (p_{дm}/p_к)} \frac{\partial}{\partial \lambda_к}\left(\frac{p_{дm}}{p_к}\right) + \frac{\partial \alpha}{\partial \varepsilon}\frac{\partial \varepsilon}{\partial \lambda_к}. \qquad (8.27)$$

Here $\varepsilon = S_T/F_{кам}$ coefficient of propellant filling of thrust chamber cross sectional area $F_{кам}$.

This coefficient can be presented in the form

$$\varepsilon = 1 - \frac{F_к}{F_{кам}}.$$

Hence

$$\frac{\partial \varepsilon}{\partial \lambda_к} = -\frac{1}{F_{кам}}\frac{1}{\partial \lambda_к / \partial F_к}.$$

Derivative $\partial \pi_к / \partial F_к$ is determined from solution (8.2).

Derivative $\partial\alpha/\partial\varepsilon$ is determined on the basis of analysis of masses and dimensions of RDTT structural elements.

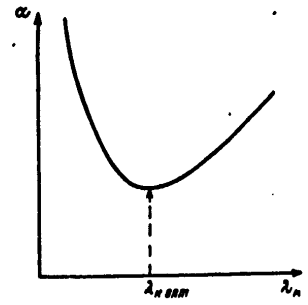

Figure 8.1. Dependence of Coefficient of RDTT Mass Perfection on λ_k

Solution of equation (8.27) enables one to establish an optimal value $\lambda_{k.o\ T}$, which with the adopted level p_k ensures minimum α (Figure 8.1). In the region lying to the left of $\alpha_{k.o\ T}$, the influence of low density of engine propellant filling predominates with low values of λ_k and correspondingly high F_k. In the region to the right of $\lambda_{k.o\ T}$ the factor of more heavily weighting the structure due to an increase in the ratio $p_{дm}/\bar{p}_k$ with an increase in λ_k predominates. At the point of the optimum, the influence of these oppositely-acting factors balances, securing α_{min}.

We shall note that in place of argument λ_k one can utilize Pobedonostsev's criterion $\varkappa = S_\phi/F_k$, since according to (7.30), there exists an unambiguous correspondence between $\varkappa$ and λ_k. This will lead to change in the form of notation of the above-examined relations, without altering their substance.

Linked to optimal values p_k and λ_k is such an important RDTT characteristic as ultimate operating time $\tau_{\text{пр}}$, which is defined as the fuel burnup time by the thickness of the burning web. Nominal value $\tau_{\text{пр}}$ is determined as

$$\tau_{np} = \frac{e_1}{\int_0^1 u_1(Z)\,[p(Z)]^\nu\,dZ},$$

where $Z = e/e_1$ -- relative thickness of burned propellant layer.

Here functions p (Z) and u_1 (Z) take into consideration changes in pressure and unit burning rate, corresponding to current value Z. Erosion effect at the initiation of burning, as well as change in u_1 in web thickness, due to nonuniformity of temperature field, is taken into account by function u_1 (Z).

Variation of ultimate engine operating time is determined as

$$\delta\tau_{np} = \delta e_1 - \delta u_1 - \nu\delta\bar{p}_k,$$

where δe_1 -- relative deviation of thickness of burning web, caused by manufacturing errors; δu_1 -- variation of unit burning rate; $\delta \bar{p}_k$ -- variation of mean indicated engine pressure.

Chapter 9. FACTORS DISTURBING OPERATING CONDITIONS OF SOLID-PROPELLANT ROCKET MOTORS

9.1. General Survey of Disturbing Factors

Factors causing disturbance of RDTT operating conditions and deviation of operating parameters from specified figures are extremely diversified in their nature and manifestation. Some are connected with variance in loading parameters and random processes during engine operation. Others constitute factors not taken into account in deriving principal relations for calculating RDTT operating characteristics. The influence of these factors in comparison with the main factors entering into calculated relations is small, and from methodological considerations should be figured in the form of corrections, that is, disturbances of calculated operating conditions.

Disturbing factors are divided into external and internal, based on mode of manifestation.

External disturbing factors include the following:

deviations of charge initial temperature, caused by changes in ambient temperature and accompanied by changes in rate of fuel burning, its energy characteristic RT_k and density ρ_T:

external load factors which alter the conditions of charge burning and which disrupt its continuity.

Following are internal disturbing factors:

deviation of charge geometry within the limits of process allowances in its manufacture;

variance in propellant burning rates and energy characteristics, caused by deviations in its composition and manufacturing process from standards;

deviations of nozzle throat area and dimensions of exhaust bell mouth from nominal value within the limits of nozzle and nozzle insert manufacturing tolerances;

defects in charge mechanical structure (cracks, pores), occurring during charge manufacture or during storage and transport.

The above-enumerated internal disturbing factors are connected with errors of manufacture and manufacturing process deviations. In addition internal disturbing factors are in operation which are caused by phenomena attending the RDTT operating process. These factors include the following:

change in nozzle throat area as a consequence of heat erosion or, on the contrary, as a consequence of slagging (obliteration) by condensed propellant combustion products;

variance in heat losses due to variability of processes of heat transfer from combustion products to the engine's interior surface;

variance in completeness of propellant combustion as a consequence of instability of combustion conditions, as well as mechanical ejection of incompletely-burned charge particles;

change in flow rate of propellant combustion products and their thermodynamic characteristics due to mass removal of insulation and non-propellant motor components.

The above is a list of the principal factors causing deviation in RDTT operating parameters from their calculated (standard) values.

One should bear in mind that the influence of one and the same disturbing factor can be manifested in several directions, causing various disturbances which in turn determine variance of RDTT operating characteristics. For example, change in initial charge temperature gives rise to disturbances

$$\delta u_1,\ \delta S_T,\ \delta(RT_k),\ \delta p_T \quad \text{, etc.}$$

The enumerated factors are far from equivalent in degree of effect on RDTT operating conditions. We should emphasize first of all the temperature factor, which significantly exceeds all other factors in its consequences, a fact which makes it necessary to devote a separate chapter to examination of this factor. Sections in this chapter deal with the most significant of the other factors.

9.2. Influence of G-loadings on Operating Conditions of Solid-Propellant Rocket Motors

G-loadings of various direction, to which a rocket is subjected in flight, can influence RDTT operating conditions through disturbances of various kinds, the principal disturbances among which are the following:

change in rate of fuel burning;

change in burning surface as a consequence of formation of cracks and disruption of charge-case adhesion;

change in thrust chamber flow passage cross sectional areas as a consequence of charge deformation;

change in nozzle flow rate coefficient.

9.2.1. Change in Propellant Burning Rate Under G-loadings

As experiment indicates, the burning rate of solid propellant increases in a stressed state.

R. Ye. Sorkin [24] links this with stress tensor influence on the rate of condensed phase breakdown, equating this phenomenon with dispersion of propellant microparticles from the surface into the gaseous phase. It is possible that an increase in the propellant burning rate in a stressed state is caused by the appearance of a network of microcracks, that is, increase in the effective propellant burning surface.

It is proposed that the influence of charge deformation on burning rate be taken into account by means of introducing into the law governing TRT combustion a correction factor [24]:

$$k_\varepsilon = 1 + \eta \varepsilon^n,$$

where ε -- deformation of elongation; η -- experimental coefficient; n -- exponent.

In calculating disturbances of RDTT operating conditions one should assume the following:

$$\delta u_{1\varepsilon} = \eta \varepsilon^n.$$

Change in burning rate from centrifugal G-loadings was discovered in developing rockets and missiles with RDTT which turn in flight on their longitudinal axis. Studies of TRT combustion in motors mounted on a centrifuge or on a rotating test bench indicated that all types of rocket propellants are subjected to the influence of centrifugal G-loadings on rate of burning, but this influence is stronger on propellants with metal additives and begins to be manifested at a low level of G-loading [12].

Change in the burning rate during rotation is caused by the thermal effect of condensate particles on the charge burning surface. Craters are formed on this surface, at the peaks of which globules of condensate are located. Formation of craters leads to increased effective charge surface and consequently to increase in the mass burning rate. At the same time there is an increase in the linear rate of propellant burning.

This takes place as a consequence of the fact that combustion of metal particles takes place near the surface, which leads to an increase in heat flow toward the surface. Intensification of heat transfer from gases to propellant is also achieved due to the heat conductivity of the contacting condensate particles. In the final analysis the effective burning rate (that is, in relation to flat burning surface) increases. A similar mechanism of interaction between condensate and combustion surface is manifested not only in metallized composite propellants but also in propellants of any composition, including ballistite, since the combustion products of any TRT contain a certain quantity of solid particles.

The authors of [23] propose that the coefficient of increase of propellant burning rate with centrifugal G-loadings k_Ω be determined from analytically obtained equation

$$k_\Omega(k_\Omega - 1) + \frac{D_1}{\sqrt{N}}\sqrt{k_\Omega}(k_\Omega - 1) = D_2,$$

where $D_2 = \lambda_k/\lambda_r$ -- ratio of coefficients of heat conductivity of propellant combustion particles and gaseous products; D_1 -- dimensionless parameter constituting a complex aggregate of physicochemical characteristics of propellant and combustion products, which is determined experimentally; N -- G-loading factor.

Change in burning rate under G-loadings is determined by the magnitude and orientation of the acceleration vector relative to the burning surface; maximum change occurs when the centrifugal force vector is directed perpendicular to the burning surface and into the charge. With an increase in G-loading the burning rate increases, asymptotically approaching its upper limit:

$$k_{\Omega_{np}} = \lim_{N\to\infty} k_\Omega = \frac{1}{2}\left(1 + \sqrt{4D_2 + 1}\right).$$

When calculating RDTT operating condition disturbances one should assume

$$\delta u_{1\Omega} = k_\Omega - 1.$$

9.2.2. Change in Charge Burning Surface Under G-loadings As a Consequence of Formation of Cracks

In the process of operation a rocket propellant charge is affected by loads of various kind, which begins during manufacture and is continued at subsequent stages of utilization during transport, storage under variable temperature conditions, loading, etc. Accumulation of the influence of applied loads can lead to the formation of cracks. Significant defects in charge structure occurring in the process of manufacturing and storage can be discovered by means of crack detection inspections and can serve as a reason for removing a motor from use. However, detection of small defects is difficult.

Rapid pressure-loading of a charge during engine ignition and imposition on the charge of various-directed G-loadings during flight can lead to the growth of prior-formed small cracks and the appearance of new cracks at points where the mechanical structure of the charge weakens. Crack formation in bonded charges of composite propellant is connected with the existence of tensile stresses. For inserted charges the occurrence of cracks is possible when the charge strikes the diaphragm with a sharp increase in axial loadings.

It would be erroneous to assume that the surface of any crack constitutes a direct addition to the total charge burning surface. The conditions of flame propagation in narrow cracks and channels were the subject of special experimental studies [11]. It was established that there exists a certain threshold crack width below which flame propagation deep into the crack becomes impossible, and consequently inclusion of the crack surface in the overall burning surface as well. Following are the principal factors determining threshold crack width: composition of the propellant, its burning rate, pressure, initial charge temperature. Threshold crack width decreases with an increase in pressure and propellant burning rate as well as with an increase in oxidizer content. It increases with an increase in oxidizer average particle diameter.

If flame penetrates into a crack, the crack may continue to develop as a consequence of the development of overpressure within the crack, as well as from stresses applied to the propellant caused by G-loadings. Tensile stresses acting in a direction crosswise to the crack are the most dangerous for crack growth.

In determining deviations of engine operating conditions caused by the occurrence of cracks in a TRT charge, one must take into consideration crack existence time, figured from the moment the crack is opened by the combustion front to complete burnup of the propellant layer in which the crack is located. If during this time engine pressure reaches a new level corresponding to the increased burning surface, consideration of the influence of a crack, manifested in the form of disturbance δS, is effected on the basis of the relations in Chapter 8. If crack existence time is significantly less than transient process time, investigation of such disturbances passes into the area of RDTT dynamic characteristics examined in the second part of this study.

9.2.3. Change in Thrust Chamber Flow Passage Cross Sectional Areas With Axial G-loading

A composite propellant charge bonded to the case seeks to displace toward the nozzle under the effect of pressure drop forces along its length $\Delta p_{\text{камк}}$ and axial G-loadings. This is hindered by forces of adhesion between propellant and case, as well as internal propellant cohesion forces. With considerable charge length and G-loadings there occurs an appreciable axial creep by the propellant mass, which leads to change in engine flow passage cross sectional areas. Change in cross sectional area varies

along the length of the charge. The consequences of this change also differ. An increase in flow passage cross sectional areas in the forward part of the charge, where gas velocities are significantly below the erosion combustion threshold, does not produce substantial changes in conditions of propellant burning. On the contrary, a decrease in flow passage cross sectional areas in that portion of the charge adjacent to the nozzle, where erosion combustion occurs, leads to intensification of the erosion effect and can have a substantial influence on engine operating characteristics.

In other words, when calculating disturbances of RDTT operating conditions, in this instance one can proceed from change in cross sectional area of gas-dynamic passage δF_k, estimated from charge deformation in the lower portion, facing the nozzle.

Change in nozzle flow rate coefficient with centrifugal G-loadings is due to nonuniformity of distribution of pressure of the slowed flow in the nozzle inlet section. This effect is observed at high rpm, and its consideration becomes substantial only for spin-stabilized projectiles.

9.3. Nozzle erosion

In an RDTT the nozzle is the most heat-stressed structural assembly. The critical section region -- the nozzle throat -- is particularly heavy and is the most subjected to erosion.

Heat erosion of the nozzle throat area results in decreased engine pressure as well as thrust and specific thrust impulse. A decrease in P and I_y takes place both as a consequence of a drop in pressure and a decrease in the d_a/d_{kp} ratio, since heat erosion of the nozzle exit section is usually insignificant in comparison with F_{kp} erosion.

Following are the principal factors determining the magnitude of nozzle erosion:

1) gas flow parameters (gas temperature and density, composition of combustion products);

2) thermal state of nozzle surface;

3) nozzle material;

4) duration of engine operation.

In estimating expected nozzle throat area erosion, one must differentiate among the following principal events.

1. Nozzles on motors with brief charge burning time, operating under transient heating conditions, fabricated of metals with a melting point below the propellant burning temperature ($T_{пл} < T_k$);

2. Nozzle inserts of heat-resistant materials (various forms of graphite, tungsten, molybdenum) with a melting point (sublimation) above the propellant burning temperature ($T_{пл} > T_к$).

We shall initially examine the first case.

As is indicated by an analysis of experimental data on erosion of nozzles fabricated of metals with a relatively low melting point (stainless and chrome steel, heat-resistant steel, etc), significant nozzle erosion is observed in those cases when temperature on the interior surface of the nozzle throat reaches a certain critical level $T^*_{с.в}$, close to the metal's melting point.

Duration of nozzle operation without significant erosion of the throat area will be determined by the time required to reach temperature $T^*_{с.в}$. The method of estimating quantity $\tau_{пр}$ is presented in [22]. Here we shall limit ourselves to an overall approximate relation for $\tau_{пр}$, obtained on the basis of the specified method:

$$\tau_{пр} = 1{,}42\,(\ln \theta^*_{с.в})^{2{,}3}\,\frac{\lambda c \rho}{\alpha^2}. \qquad (9.1)$$

Here

$$\theta^*_{с.в} = \frac{T_к - T^*_{с.в}}{T_к - T_н};$$

$T_н$ -- initial temperature of nozzle material; λ, c, ρ -- coefficients of heat conductivity, heat capacity and density of nozzle material respectively; α -- heat transfer coefficient.

The formula is valid for the region of Biot criterion values Bi=0.4-4.0.

It follows from the formula that nozzle erosionless operating time decreases sharply with an increase in propellant burning temperature $T_к$ and heat transfer coefficient α, which in turn is determined by the level of working pressure in the engine. Time $\tau_{пр}$ increases with an increase in set $\lambda c \rho$ -- thermal activity of the material. As a consequence of this, low-carbon steel is a preferable material for nozzles of this type, with a coefficient of thermal conductivity several times greater than for heat-resistant steels.

Let us proceed to the second case. When utilizing nozzle inserts of heat-resistant materials with a melting (sublimation) point higher than the temperature of the propellant combustion products, chemical erosion is the main cause of nozzle throat erosion. Solid propellant combustion products contain a number of compounds and elements which at high temperatures can enter into chemical reaction with the nozzle insert material, forming oxides of carbon or metals. As is indicated by studies, under conditions of an RDTT, water vapor and carbon dioxide possess a high degree of chemical activity [2]. For example, the following reactions with graphite are possible:

$$C + CO_2 \rightarrow 2CO; \quad C + H_2O \rightarrow CO + H_2.$$

The linear rate of chemical erosion is determined by the following relation [22]:

$$u_s = \frac{\varphi \alpha_к}{\bar{c}_p \rho_s} \sum_i \frac{C_{ei} M_{si}}{M_{gi} K}, \qquad (9.2)$$

where $\alpha_к$ -- coefficient of convective heat emission; $\bar{c}_p$ -- mean thermal capacity of combustion products in the region of the boundary layer; C_{ei} -- concentration of i oxidizing component of combustion products at the core of the flow; M_{si}, M_{gi} -- molecular masses of the oxidized and oxidizing components (elements); K -- stoichiometric coefficient in the equation of oxidizer reaction with an oxidizing component; ρ_s -- density of insert material; φ -- coefficient taking into account the state of the insert surface and the structure of its material.

In view of the fact that at the present time coefficient φ is determined only experimentally, this relation does not enable one to obtain reliable calculated figures. Establishing a direct relationship between rate of erosion and coefficient of convective heat emission, however, it opens up the way to modeling of erosion processes. Since according to the Bartz relation $\alpha_к \sim p^{0.8} d_{kp}^{-0.2}$, the rate of nozzle erosion on a full-scale specimen can be determined from the test figures on a model version as

$$u_s = u_{s\,мод} \left(\frac{p_к}{p_{к.\,мод}}\right)^{0,8} \left(\frac{d_{кр.\,мод}}{d_{кр}}\right)^{0,2},$$

where $p_{к.\,мод}$, $d_{кр.\,мод}$ -- pressure and throat area diameter for the model.

During nozzle erosion considerable surface roughness may occur as a consequence of nonuniform removal of material. This leads to additional losses of specific thrust impulse due to friction. According to experimental data [33], these losses may comprise 0.5-1.0% of nominal value.

Total drop in specific impulse due to nozzle erosion as a consequence of drop in pressure, decrease in expansion ratio and development of roughness can constitute a considerable quantity from its initial value, corresponding to initiation of engine operation.

In some cases in the process of engine operation there occurs a decrease in nozzle throat area (nozzle obliteration) as a consequence of deposition of condensed phase on the nozzle surface. This process can be cyclic. Periods of deposition of condensate can alternate with periods of condensate removal, when the force of gas-dynamic resistance exceeds the force of its cohesion with the nozzle wall.

Methods of calculating condensate deposition on nozzle walls have been little elaborated up to the present time.

9.4. Disturbances of Operating Conditions of a Solid-Propellant Rocket Motor and Its Output Characteristics Connected With Removal of Thermal Protection Materials

Active thermal protection of the motor structure is extensively utilized in RDTT with extended operating time, protection based on absorption of a substantial percentage of the heat transferred to the surface with breakdown and removal of heat shielding material. Polymer-based heat shielding materials (TZM), most frequently reinforced plastics, are employed for this purpose. Under the effect of heat there takes place breakdown of the organic bond (rubber, epoxy or phenolic resins, etc), with the formation of gases and coke residue. The latter forms, together with a filler, a porous carbonized layer, which subsequently, interacting with the stream of propellant combustion products, is carried away from the surface of the protective coating. Thus as a result of the thermal action of the main flow of gases on the protective coating, there occurs complete removal of a certain layer of the coating and formation of a carbonized layer, which retains solid pyrolysis products and filler. The relationship between thickness of the removed and carbonized layers is determined by the characteristics of the material and the concrete conditions of protective coating operation.

Following are the principal consequences of breakdown and removal of the protective coating:

1) change in the composition and temperature of propellant combustion products at nozzle throat section inlet;

2) change in flow rate of gases emerging from the thrust chamber and at nozzle exit;

3) change in passive weight of the structure.

In chemical composition protective coating components subjected to thermal destruction are close to the fuel-binder of composite fuels. One can assume that the decomposition products of these coating components will affect the equilibrium composition of the gaseous phase of TRT combustion products in a first approximation just as change in the content of fuel-binder in the composition of propellant, which can be expressed by the following relation:

$$\delta (RT_к)_г = \frac{d}{d\tilde{m}_г} (RT_к) \frac{1}{RT_к} \delta \tilde{m}_г, \qquad (9.3)$$

where $\tilde{m}_г$ -- relative content of fuel-binder in the propellant; $\delta \tilde{m}_г$ -- change in this percentage due to TZM [heat protection coating].

Since all rocket propellants known from the literature are compositions with a negative oxygen balance, quantity $\delta (RT_k)$ is negative.

The degree of influence of the examined factor depends on the degree to which the composition of a given propellant differs from stoichiometric, since quantity

$\frac{d}{d\tilde{m}_r}(RT_к)$ increases in a direction away from stoichiometry toward excessive binder.

This also determines the contradictory nature of data in the literature on the influence of removal of protective coating on quantity RT_k and specific thrust impulse.

The influence of the filler, which proceeds together with products of decomposition from the removed coating layer, is different. Alongside a given thermal effect of reactions taking place in the flow core, as a rule its entry will be accompanied by an increase in condensed phase content:

$$\delta(RT_к)_н = \frac{d}{d\tilde{m}_к}(RT_к)\frac{1}{RT_к}\delta\tilde{m}_н, \qquad (9.4)$$

where $\tilde{m}_H$ -- relative percentage share of condensed phase; $\delta\tilde{m}_H$ -- increase in this share due to inflow of condensed coating removal products.

Relative change $\delta(RT_к)_п = \delta(RT_к)_т + \delta(RT_к)_н$ will be manifested in change in pressure in the engine, thrust and specific thrust impulse.

The simplest thing is to take into consideration the influence of additional mass TZP removal products in prior-derived relations by means of variation $\delta\rho_T$, which, applied to this problem, we can present in the form

$$\delta\rho_т = \delta\rho_{т_0} + \delta\dot{m}_п p_к^{\nu}, \qquad (9.5)$$

where $\delta\rho_{T_0}$ -- variation of density of the principal propellant; $\delta\dot{m}_п = \dot{m}_п/\dot{m}_T$ -- coating mass protection in relation to consumption of principal propellant at operating pressure p_k.

Let us examine how RDTT principal characteristics for a zero-dimensional solution change due to removal of in-chamber heat protection coating.

According to relations (8.4), (8.5), and (8.9), we obtain

$$\left.\begin{aligned}
(\delta p_к)_{у.\,п} &= \frac{1}{1-\nu}\left[\delta\dot{m}_п p_к^{\nu} + \frac{1}{2}\delta(RT_к)_п\right];\\
(\delta\dot{m}_c)_{у.\,п} &= \frac{1}{1-\nu}\left[\delta\dot{m}_п p_к^{\nu} + \frac{\nu}{2}\delta(RT_к)_п\right];\\
(\delta I_у)_{у.\,п} &= \frac{\gamma_р}{1-\nu}\delta\dot{m}_п p_к^{\nu} + \frac{1+\gamma_р-\nu}{2(1-\nu)}\delta(RT_к)_п.
\end{aligned}\right\} \qquad (9.6)$$

A number of investigators have endeavored to introduce an independent specific impulse of TZP and burned nonpropellant materials, determining it from losses of RDTT specific impulse. However, the values of this characteristic obtained by them range within broad limits from 50 to 200 s, varying in relation to the propellant oxygen balance [19, 35]. For example, for a spacecraft RDTT burning a propellant with I_y=290, and with TZP removal comprising 0.5-1.5% of propellant mass, independent specific coating impulse comprised ~50 s [35]. Consequently, such a TZP characteristic is not universal and is of limited, purely cognitive interest.

9.5. Figuring Heat Losses and Incomplete Fuel Combustion

Losses from heat transfer into the motor case and from incomplete combustion are figured, in determining RFTT operating characteristics, with correction factor χ to fuel force RT_k, determined experimentally by calorimetric method or on the basis of thermodynamic calculations.

A general expression for determining coefficient of heat losses in an RDTT has the form

$$\chi = 1 - \frac{\sum^{S_{BH}} \alpha (T_K - T_{c.B}) \Delta S}{\dot{m}_T H_0},$$

where $\dot{m}_T$ -- quantity of fuel burning per unit of time; H_0 -- total enthalpy of a unit of mass of combustion products; $T_{c.B}$ -- temperature of thrust chamber interior surface contiguous to gases; α -- coefficient of heat trasnfer; S_{BH} -- thrust chamber interior surface area.

Parameters α and $T_{c.B}$ change both along the chamber surface contiguous to the gases and in time, causing change in coefficient χ on a time axis.

The magnitude of the coefficient of thermal losses and the relations determining it are quite different for a motor without insulation with an insert charge and for a motor with interior-insulated case. Therefore these two instances are examined separately.

9.5.1. Determination of Heat Losses for RDTT Without Heat Insulation

This instance is characterized by the transient nature of heat losses throughout the extent of the entire operating period, as well as the significant magnitude of these losses, caused by the large surface in contact with the gases. The bulk of heat losses (from 70 to 90%) usually occurs on the cylindrical surface of the thrust chamber. Proceeding from the determining role of convective heat exchange in an RDTT, the heat transfer coefficient can be represented as

$$\alpha = K_\alpha \frac{\dot{m}^{0,8}}{d_r^{0,2}},$$

where $\bar{m}=\dot{m}/F_k$ -- mass flow of gas per unit of charge flow passage cross sectional area; d_r -- effective thermal section diameter; K_α -- a coefficient taking into account the thermophysical properties of the gas.

Change in charge flow passage cross sectional area in time can be expressed with the relation

$$F_к = F_{к0}(1 + b\psi),$$

where F_{k0} -- initial flow passage cross sectional area; ψ -- relative percentage share of burned fuel;

$$b = \frac{\varepsilon}{1-\varepsilon}; \quad \varepsilon = \frac{S_{т0}}{F_{кон}}.$$

We shall assume change in mass flow of gas along the length of the charge to be linear

$$\dot{m}_x = \dot{m}_c \frac{x}{L}.$$

We shall also assume $d_r \sim F_к^{0,5}$.

An expanded expression for determining thermal losses in the cylindrical section of the chamber assumes the form

$$\chi = 1 - \frac{K_т \pi D_к}{F_{к0}^{0,9} \dot{m}_c^{0,2} L^{0,8} H_0} \frac{\int_0^L [T_к - T_{с.в}(x, t)]\, x^{0,8} dx}{[1 + b\psi(t)]^{0,9}}, \qquad (9.7)$$

where quantity $T_{c.B}$ (x, t) is determined for each chamber zone with coordinate x by solving the problem of wall transient heat conductivity with a variable value α. In view of the unwieldiness of solution, the practical value of equation (9.7) for obtaining quantitative results is very limited. However, it enables one analytically to establish the character of change in time of thermal losses in the engine.

If we assume $T_{c.B}$ (x, t) for the present point in time to be the average value $\bar{T}_{c.B}$ along the length of the chamber, and if we apply a power of 1 with the binomial in the denominator, we obtain the relation

$$\chi = 1 - A \frac{T_к - \bar{T}_{с.в}}{1 + b\psi}. \qquad (9.8)$$

Ya. M. Shapiro [26], performing calorimetric measurements of heat losses on a model motor with interruption of combustion, obtained the experimental relation

$$\chi = 1 - \frac{B}{1 + b_1\psi}. \qquad (9.9)$$

He obtained the following for the conditions of the performed experiments: B=0.30; b_1=5. Consequently the experiment confirms analytical relation (9.8). In formula (9.9) change $T_k - \bar{T}_{c.B}$ in time is taken into consideration indirectly -- by selection of coefficient b_1 which is not equal to

the value $b=\varepsilon/(1-\varepsilon)$ in formula (9.8), but is somewhat higher, as could be expected. Thus according to (9.9) when B=0.30; b=5, the value of χ in the process of engine operation varies from 0.7 to 0.95, and correspondingly heat losses, initially comprising 30%, decline to 5% by the end of RDTT operation.

Since initiation of steady-state conditions for such motors takes place when $\psi \leq 0.1$, the magnitude of thermal losses and their variance in the initial period of operation may exert a substantial influence on the stability of working characteristics and particularly on quantity $p_{k\ max}$.

Following are the principal causes of variance of thermal losses in the initial period:

random changes in the character of pressure increase in the chamber when entering conditions leading to a sharp dispersion of the time-average coefficient of thermal transfer by change in quantity $\dot{m}$;

change in the state of the chamber surface due to deposition of condensate (soot, metal oxides), gummy deposit residues, etc.

9.5.2. Determination of Thermal Losses for an RDTT With Removable Heat Protection Coating

Heat losses for a motor with a bonded charge burning on the cavity surface and on the end, with a heat protection coating on the nozzle-adjacent portion of the case and on the upper end plate, decrease sharply in comparison with uninsulated RDTT and comprise fractions of a percent in steady-state mode. We should also note that removal of coating material is accompanied by regeneration of the heat transferred into the coating, minus that percentage absorbed during endothermic pyrolysis reactions. These phenomena are taken into account in determining disturbances connected with removal of TZP in conformity with the method described in 9.4.

Processes taking place in the coating at the initiation of engine operation require special examination. During heating in a reinforced plastic, a clearly-marked pyrolysis front is formed, which leaves behind a carbonized layer. Initially there occurs displacement of the pyrolysis front deep into the material. Subsequently, when carbonized material comes into contact with high-temperature gases on the surface, material begins to be carried away from the surface. The rates of displacement of the pyrolysis front u_{ζ} and the surface of coating removal $u_{c.B}$ equalize with time. After this the thickness of the carbonized layer contained between these surfaces remains constant in time. Consequently the quantity of heat accumulated in the coating also remains constant. However, as long as u_s remains greater than $u_{c.B}$, the thickness of the carbonized layer increases.

The quantity of heat accumulated in a carbonized layer per unit of area will total

$$Q_{ak} = \int_0^{L_{o6}} \rho_{o6} c_{o6} (T - T_н)\, dx,$$

where ρ_{o6} and c_{o6} -- density and heat capacity of the carbonized material; T -- local material temperature; L_{o6} -- thickness of carbonized layer.

Irreversible thermal losses connected with accumulation of heat in the carbonized layer in the initial period, per unit of time per unit of coating area, will be as follows:

$$\frac{dQ_{ak}}{dt} \cong \frac{1}{2} \rho_{o6} c_{o6} (T_{c.в} + T_s) \frac{dL_{o6}}{dt},$$

where $T_{c.B}$ -- temperature of removal surface; T_s -- temperature on pyrolysis front.

With the passage of time dL_{o6}/dt approaches zero, causing quantity dQ_{ak}/dt also to approach zero.

One should bear in mind that with some charge shapes, such as a slotted charge, new sections of coating involved in heat and mass exchange with the hot flow of gases are continuously being exposed during burning in the area of the slots, as a consequence of which thermal losses connected with accumulation of heat in the carbonized coating layer accompany the entire period of charge combustion.

In view of the triviality of heat losses in RDTT with removed heat protection coating, it is expedient to effect consideration of this factor in the form of $\delta(RT_k)$.

9.5.3. Consideration of Incompleteness of Solid Propellant Combustion

Following are the most typical causes of incomplete propellant combustion in an RDTT:

incompleteness of the chemical reactions taking place in the gaseous phase;

incomplete combustion of metal particles in the thrust chamber;

ejection of charge particles through the nozzles.

Incomplete combustion in the gaseous phase usually occurs with low engine pressures. The following flame zone reactions, characteristic of combustion of ballistite propellants, are highly sensitive to decreased pressure in the engine:

$$2CO + 2NO = 2CO_2 + N_2;$$
$$2H_2 + 2NO = 2H_2O + N_2.$$

The rate of these reactions is governed by a dependence which is common to bimolecular reactions:

$$\frac{dC_3}{dt} = -K_r C_1 C_2,$$

where C_1 and C_2 -- concentrations of reacting substances; C_3 -- concentration of substance forming during reaction.

Proceeding to relative concentrations $\bar{C}=C/\rho$, we obtain

$$\frac{dC_3}{dt} = -K_p p^2 \bar{C}_1 \bar{C}_2. \qquad (9.10)$$

Since these reactions produce a substantial quantity of the heat released during combustion (up to 50% in the case of ballistite propellants of average caloricity), their incompleteness can have a substantial effect on quantity RT_k.

For reactions which take place in the gaseous phase and possess a differing order of magnitude, on the whole completeness of combustion is determined by exponential relation

$$\chi_{cr} = 1 - e^{-kt}, \qquad (9.11)$$

where t -- time.

When utilizing relation (9.11), one must substitute in it the total time in the thrust chamber of each separate forming gas portion

$$t_{np} = \int_{x_i}^{L} \frac{dx}{v},$$

where x_i -- distance from the area of specific gas generation to the forward end; L -- total chamber length (from end plate to nozzle throat area); v -- local axial velocity of gas flow in the specified section.

For the motor as a whole we obtain

$$\chi_{cr} = 1 - \bar{f}_r \sum g_i \exp\left(-K \int_{x_i}^{L} \frac{dx}{v}\right),$$

where $\bar{f}_r$ -- relative change in quantity RT_k due to flame zone reaction; g_i -- mass attraction of i formation in total combustion products discharge; K -- coefficient of chemical reaction, determined by pressure and temperature.

The same approach can be utilized in determining incompleteness of combustion of metal particles. In this case the chemical constant should take into account influence of particle diameter, concentration of

oxidizing components in the gaseous medium, and the metal's ability to be chemically activated. In conformity with the figures on combustion rate of aluminum contained in [38], one can represent in an approximate fashion component χ_M, resulting from incomplete aluminum combustion:

$$\chi_M = \bar{f}_M \sum g_i K \int_0^L \frac{dx}{v},$$

where $K=3\cdot10^3 \frac{c_{ok}^{0,9}}{d_T^{1,5}}$; C_{ok} -- relative concentration of oxidizing reagents in propellant combustion products; d_T -- average diameter of aluminum particles, in microns; $\bar{f}_M$ -- relative change in quantity RT_k due to combustion of aluminum.

Ejection of particles of unburned propellant is usually connected with breakdown of charge elements in the final stage of combustion. It is manifested most strongly during utilization of thin-webbed charges.

Chapter 10. INFLUENCE OF CHARGE INITIAL TEMPERATURE ON CHARACTERISTICS OF A SOLID-PROPELLANT ROCKET MOTOR, MOTOR TUNING AND ADJUSTMENT

Among the factors disrupting RDTT operating conditions, change in initial charge temperature in the process of rocket operation occupies a special place. Greater attention to the temperature factor is dictated by the fact that in practice it produces the most profound changes in engine operating conditions, which go far beyond the bounds of individual random deviations from the specified conditions. At the same time in most cases it is possible to take into account in advance the consequences of this factor and to limit its influence by means of special measures: by adjustment or thermostatic control of the motor prior to launch.

In examining the question of the effect of charge initial temperature on engine operating characteristics, one should emphasize two instances:

1) initial charge temperature is practically constant throughout the entire thickness of the burning web;

2) initial charge temperature varies within significant limits through the thickness of the web.

Each of these instances is examined in this chapter.

Problems connected with RDTT tuning and adjustment are examined applicable to the first case. However, the obtained relations can also be applied to the case of temperature varying through the thickness of the web with utilization of the concept of effective charge temperature, which is separately selected for each temperature field realization.

10.1. Relationship Between Characteristics of a Solid-Propellant Rocket Motor And Charge Initial Temperature

Chapter 7 contained various expressions of the empirical relationship between TRT burning rate and charge temperature. In order to simplify the mathematical calculations connected with determining RDTT operating parameters at different charge temperatures, it is more convenient to utilize exponential relation

$$u_{1T_H} = u_{1T_N} e^{D(T-T_N)}. \qquad (10.1)$$

Henceforth we shall omit subscript "H" in this chapter with the current charge temperature value, for the purpose of symbol simplification.

Selection of temperature T_N, adopted as standard, is determined by the specific features of the motor being designed. For a motor designed for use across a broad range of temperatures, temperature $T_{H\ min}$ can be adopted as T_N, corresponding to the lower limit of motor utilization under the most adverse conditions of propellant combustion, that is, a case designated as standard for ensuring stability of charge burning.

In this chapter, for simplification of mathematical calculations, we have also assumed $T_N = T_{H\ min}$.

The difference in selection of standard temperature has no effect on the magnitude of power D, but leads to a disparity of values u_{1N}. If we assume that standard temperature T^I_N corresponds to u^I_{1N}, then, adopting T^{II}_N as standard temperature, one must adopt in formula (10.1) the following as coefficient of burning rate:

$$u^{II}_{1N} = u^{II}_{1N} e^{D(T^{II}_N - T^I_N)}.$$

Initial charge temperature also affects propellant burning temperature. For ballistite propellants of average caloricity, the heat capacity of which is approximately equal to that of the combustion products, change in combustion temperature is numerically equal to change in initial charge temperature [26]:

$$T_{к(T)} = T_{к(N)} + T_н - T_N.$$

With a change of T_N from -50 to +50°C, product RT_k will change by 3.5-4.5%. For composite propellants with a higher combustion temperature, relative change RT_k with temperature will be smaller. According to experimental data obtained for a spacecraft RDTT [35], this change will comprise only 2%. Consequently the dependence of propellant force RT_k on initial charge temperature is relatively slight. On analogy with relation (10.1) we can write

$$RT_{к(T)} = RT_{к(N)} \cdot e^{2m(T-T_N)}. \qquad (10.2)$$

The value of coefficient m in the exponent varies in relation to the propellant's energy characteristics, comprising approximately 0.0003 for ballistite propellants with low caloricity, and approaching 0.0002 for composite propellants [35, 26].

We shall initially determine how RDTT operating characteristics vary with charge initial temperature in the absence of adjustment and control.

Utilizing formulas (7.15) and (7.40) and substituting in them the dependences of combustion rate (10.1) and propellant force (10.2) on initial charge temperature, we obtain for engine working pressure at temperature T

$$p_T = \left(\frac{u_{1N}\rho_T S K_u \sqrt{\chi R T_{к(N)}}}{\varphi_c A F_{кр}}\right)^{\frac{1}{1-\nu}} e^{\frac{m+D}{1-\nu}(T-T_N)}. \qquad (10.3)$$

The first factor expresses the magnitude of combustion chamber pressure p_N at standard (nominal) temperature T_N.

Consequently, relative pressure change in a noncontrollable motor with change in charge temperature will comprise

$$\frac{p_T}{p_N} = e^{\frac{m+D}{1-\nu}(T-T_N)}. \qquad (10.3a)$$

It follows from formula (10.3) that the relative pressure change with an increase in charge temperature is independent of charge loading parameters but is determined by temperature differential and constants D, m, ν. We shall note that with a specified value of constants D and m, chamber pressure at small values of ν is less dependent on charge temperature and, on the contrary, high values of ν increase the temperature dependence. The results of calculations of p_T/p_N for two propellants are contained in Table 10.1.

Table 10.1.

1 Характеристика топлива		p_T/p_N	P_T/P_N	$1+X$	τ_T/τ_N
D	ν				
Нерегулируемый РДТТ 2					
0,0038	0,69	3,19	3,31	1	0,318
0,0014	0,4	1,27	1,28	1	0,800
РДТТ, регулируемый на постоянство давления 3					
0,0038	0,69	1	1,395	1,432	0,710
0,0014	0,4	1	1,135	1,155	0,883
РДТТ, регулируемый на постоянство тяги 4					
0,0038	0,69	0,638	1	1,379	0,982
0,0014	0,4	0,756	1	1,363	0,982

Key:
1. Propellant characteristic
2. Noncontrollable RDTT
3. RDTT controlled for constant pressure
4. RDTT controlled for constant thrust

Note: T_N=-40°C; T=+50°C.

Relative change in thrust due to temperature will comprise

$$\frac{P_T}{P_N} = \frac{p_T}{p_N} \frac{\sigma_c f(\lambda_a) - p_H/p_T}{\sigma_c f(\lambda_a) - p_H/p_N}. \qquad (10.4)$$

Considering the smallness of the second term of the difference, one can in a first approximation assume

$$\frac{P_T}{p_N} \sim \frac{p_T}{p_N} = e^{\frac{m+D}{1-\nu}(T-T_N)}.$$

The linear rate of fuel combustion at temperature T is determined as

$$u_T = u_{1T} p_T^{\nu} = u_{1N} e^{\frac{D+m\nu}{1-\nu}(T-T_N)}.$$

Charge burning time at temperature T: $\tau_T = e_1/u_T$.

Relative change in burning time will be

$$\frac{\tau_T}{\tau_N} = \frac{u_N}{u_T} = e^{-\frac{D+m\nu}{1-\nu}(T-T_N)}. \qquad (10.5)$$

Let us determine how specific thrust impulse changes with initial charge temperature. Substituting in formula (7.20) dependences on temperature for propellant force (10.2) and for working pressure (10.3), we obtain

$$I_{y(T)} = \sqrt{\frac{k+1}{2k}} \chi \sqrt{(RT_K)_N}\, e^{m(T-T_N)} \left[2\chi_c Z(\lambda_a) - \right.$$
$$\left. - \left(\frac{k+1}{2}\right)^{\frac{1}{k-1}} \frac{F_a}{\varphi_c F_{KP}} \frac{p_H}{p_{KN}} e^{-\frac{m+D}{1-\nu}(T-T_N)} \right], \qquad (10.6)$$

where p_{kN} and $(RT_k)_N$ -- pressure and propellant force at standard temperature T_N.

10.2. Objectives and Means of Tuning and Adjustment of a Solid-Propellant Rocket Motor

Prelaunch adjustment of an RDTT is at the present time the principal procedure employed in regulating the thrust parameters of this motor. Tuning and adjustment eliminates to a significant degree the influence of the main causes of instability of an RDTT -- the dependence of TRT combustion rate on charge temperature and difference in burning rates of charges produced from different batches of propellants.

Depending on the stated objective, one distinguishes motor adjustment for constant pressure, constant thrust, and constant flow rate. Adjustment for constant flow rate is characteristic for RDTT utilized for auxiliary purposes as a gas generator. When utilizing an RDTT as a main propulsion unit,

adjustment for constant pressure and thrust is most typical. RDTT adjustment for constant pressure throughout the entire specified range of engine utilization temperatures makes it possible substantially to reduce maximum pressure $(p_m)_{max}$, which is an input quantity in making engine strength calculations. This reduces engine mass characteristic α and achieves a decrease in rocket gross launching mass with specified range and payload.

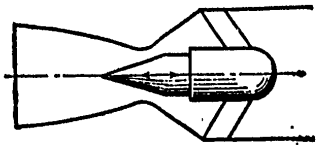

Figure 10.1. Diagram of Device for Smooth Change in Nozzle Throat Area

Adjustment of an RDTT for constant thrust makes it possible at all charge temperatures for ballistic-type rockets to ensure constant parameters of the powered segment of flight and thus to facilitate securement of a high degree of accuracy of target impact. For rockets with a flight mode close to cruise, thrust adjustment makes it possible to maintain the required flight conditions and to avoid speed going below or above the values specified by the flight program.

In the case of small motors, adjustment can be performed in conformity with ambient temperature. For large motors, however, due to the thermal inertia of the charge, its temperature can differ substantially from ambient temperature, and motor tuning and adjustment should be performed in conformity with the readings of the temperature sensors contained in the motor.

The simplest means of RDTT adjustment is change in nozzle throat area in conformity with initial charge temperature and propellant charge performance specifications -- unit burning rate specified for the given propellant batch. In some instances release valves can be employed.

The simplest device for changing nozzle throat area is a set of replaceable nozzles. Replaceable nozzle inserts can be used in place of replaceable nozzles in order to shorten the time required to ready a motor for launch. Sometimes multiple-nozzle units are employed, with alternate nozzles covered by diaphragms. When a certain pressure is exceeded the diaphragms are cut, total throat area increases, and further engine pressure increase is prevented.

Smooth adjustment of nozzle throat area in conformity with charge temperature is achieved with utilization of a throttle (Figure 10.1) which can displace along the axis of the nozzle. A throttle can be moved into place manually or with the aid of a mechanical drive. There are a number of self-adjusting nozzle designs, where the throttle is moved into position automatically, without intervention by servicing personnel. Some of them are described in [26].

The devices mentioned above make it possible to tune an engine not only on initial charge temperature but also on other parameters as well, deviations of which from nominal value are known prior to launch.

10.3. Tuning of a Solid-Propellant Rocket Motor Nozzle to Constant Pressure

Retaining in an RDTT constant pressure or pressure varying within small limits throughout the entire temperature range of engine utilization makes it possible to reduce standard pressure on the basis of which engine wall thickness is determined, and thus to improve its weight characteristics. The gain in structural weight achieved thereby will depend on the one hand on the characteristics of the propellant utilized, that is, on the possible pressure drop in the absence of control, and on the other hand on the weight of additional components and devices by means of which nozzle throat area is varied.

The throat area of one or several nozzles, in a multiple-nozzle variant, altered during tuning and adjustment, can be represented as the sum of a certain constant component $F_{кр\ N}$, equal to throat area at standard charge temperature T_N, and variable component $\tilde{F}_{кр}$. Designating $X=\tilde{F}_{кр}/F_{кр\ N}$, we obtain

$$F_{кр\,T} = F_{кр\,N}(1 + X). \qquad (10.7)$$

We shall first examine adjustment of nozzle throat area solely on initial propellant charge temperature.

Substituting (10.7) in formula (10.3), we obtain

$$p_T = p_N \left[\frac{e^{(D+m)(T-T_N)}}{1+X} \right]^{\frac{1}{1-\nu}}. \qquad (10.8)$$

In order to ensure constant pressure with varying propellant charge temperature, it is necessary to satisfy condition

$$1 + X = e^{(D+m)(T-T_N)}. \qquad (10.9)$$

With equation (10.9) one can find the nozzle throat area required with the given temperature

$$F_{кр\,T} = F_{кр\,N} e^{(D+m)(T-T_N)}. \qquad (10.10)$$

For a propellant with a low temperature dependence, expanding the exponential factor into a series and discarding terms of a second order of smallness, we obtain:

$$1 + X = 1 + (D + m)(T - T_N) \quad \text{or} \quad X \cong (D + m)(T - T_N).$$

If the nozzle throat area is simultaneously adjusted according to actually measured combustion rate deviation Δu_1 from the standard value for a given batch of propellant charges, one should substitute in formula (10.3) in place of u_{1N}

$$u_{1N}\left(1 \pm \frac{\Delta \tilde{u}_1}{u_{1N}}\right) = u_{1N}(1 \pm \delta \tilde{u}_1).$$

Required nozzle throat area will be determined as

$$F_{\text{кр}\,T} = F_{\text{кр}\,N}(1 + \delta\tilde{u}_1)\, e^{(D+m)(T-T_N)}. \qquad (10.11)$$

For small $\delta\tilde{u}$ values for propellants with a low temperature dependence:

$$X = \delta\tilde{u} + (D + m)\,\delta T.$$

Tuning and adjustment to any parameter with deviation known prior to launch is performed in like manner.

Relative change in operating time of a motor adjusted for constant pressure is equal to

$$\frac{\tau_T}{\tau_N} = \frac{u_N}{u_T} = e^{-D(T-T_N)}. \qquad (10.12)$$

It follows from a comparison of formulas (10.5) and (10.12) that in a motor with constant pressure maximum variance of time with change in propellant charge temperature is less than in an uncontrolled motor.

Let us see how engine thrust varies in relation to temperature when maintaining constant pressure if the discharge area remains constant.

Utilizing relation (7.18), we obtain

$$\frac{P_T}{P_N} = \frac{\sigma_{cT} f(\lambda_{aT}) - p_H/p_K}{\sigma_{cN} f(\lambda_{aN}) - p_H/p_K}. \qquad (10.13)$$

In order to utilize this relation, one must establish a link between quantity X and change in gas-dynamic function f (λ_a).

Since

$$q(\lambda_{aN}) = \frac{F_{\text{кр}\,N}}{F_a};$$

$$q(\lambda_{aT}) = \frac{F_{\text{кр}\,T}}{F_a};$$

$$q(\lambda_{aT}) = q(\lambda_{aN})(1 + X). \qquad (10.14)$$

Since quantity q (λ_{aN}) is assumed specified, relation (10.14) makes it possible to determine value q (λ_{aT}) from quantity X, after which one can determine f (λ_{aT}).

Table 10.1 contains calculation figures for two propellants, which indicate that maintaining constant engine pressure by adjusting F_{kp} involves significant thrust variation. Prelaunch thermostatic engine control is the only possible method of motor adjustment whereby conditions of constant pressure and thrust coincide.

In some cases, for rockets of the simplest design, in place of adjustment for constant pressure it is sufficient to restrict pressure variation within certain limits, so that on the one hand it never drops below the level

p_{min}, guaranteeing stable propellant combustion, and on the other hand does not rise above p_{max}, tolerated by structural strength. This can be achieved by graduated adjustment of F_{kp} with a set of interchangeable nozzles, nozzle inserts or nozzle plugs (with a multiple-nozzle version).

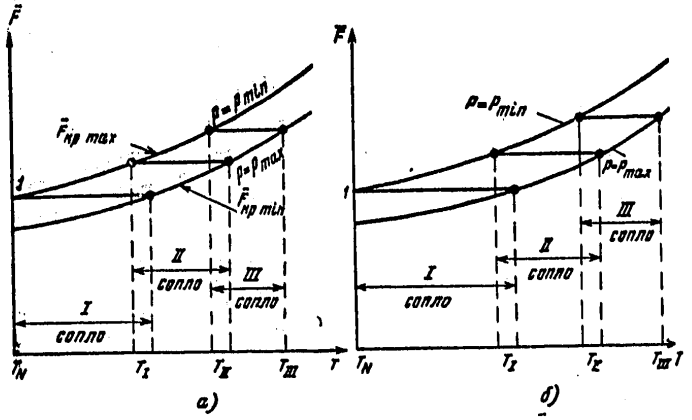

Figure 10.2. Diagram of Selection of Throat Areas of Interchangeable Nozzles

Key:

a.--When adjusting RDTT to constant pressure (p_k=const)

b. When adjusting RDTT to constant thrust (P=const)

1. Nozzle

A diagram of a selection of throat areas of interchangeable nozzle devices and establishment of an operating range of temperatures for each of them is contained in Figure 10.2. We shall adopt as a figuring unit a nozzle throat area providing maximum pressure p_{min} at temperature T_N. In order to ensure that this pressure remains constant with temperature, with continuous adjustment, the nozzle throat area should follow relation (10.9). The curve of relative increase in throat area $\overline{F}_{kp\ max}$ was plotted in conformity with this relation. Now we shall plot a curve of variation in $\overline{F}_{kp\ min}$ in order to ensure constant pressure p_{max} in a motor with continuous corrective adjustment. The curve is constructed on the same relation (10.9), but the starting-point value $(\overline{F}_{kpN})_{min}$ at temperature T_N will be that which is determined by ratio

$$(\overline{F}_{кр\,N})_{min} = \left(\frac{p_{min}}{p_{max}}\right)^{1-\nu}.$$

We shall run from a point on the upper curve corresponding to $p=p_{min}$ with $T=T_N$, horizontal segment $\overline{F}_{kp}$=const=1 to the point of intersection with the lower curve. The point of intersection will determine the upper temperature boundary of employment of the first interchangeable device (nozzle) T_I. We begin the horizontal segment for the second nozzle with a curve corresponding to p_{min}, but not from a point with coordinate T_I but rather a point lying

5-10°C to the left of it, in order to ensure overlap of temperature ranges of employment of interchangeable nozzles.

From the relative values $\bar{F}_{kp}$ determined from the curve, the absolute throat area values are obtained by multiplying $\bar{F}_{kp}$ by $(F_{kp\ N})$, calculated for preselected engine characteristics at temperature T_N and with the adopted value p_{min}.

10.4. Tuning a Solid-Propellant Rocket Motor Nozzle to Constant Thrust

We shall first examine the case where tuning and adjustment is performed by changing the nozzle throat area with a constant nozzle exit area.

Utilizing relation (7.18), the condition of constant thrust at various propellant charge temperatures can be written in the form

$$\sigma_{cT} f(\lambda_{aT}) p_T = \sigma_{cN} f(\lambda_{aN}) p_N,$$

whence

$$\frac{p_T}{p_N} = \frac{\sigma_{cN} f(\lambda_{aN})}{\sigma_{cT} f(\lambda_{aT})}. \qquad (10.15)$$

Substituting p_T/p_N from (10.8), we obtain

$$e^{\frac{D+m}{1-\nu}(T-T_N)} = (1+X)^{\frac{1}{1-\nu}} \frac{\sigma_{cN} f(\lambda_{aN})}{\sigma_{cT} f(\lambda_{aT})}. \qquad (10.16)$$

The obtained equation can be solved by two methods.

The first method consists in utilizing the relation for T obtained by means of logarithmic operation (10.15):

$$T = T_N + \frac{1}{D+m} \ln(1+X) + \frac{1-\nu}{D+m} \ln\left[\frac{\sigma_{cN} f(\lambda_{aN})}{\sigma_{cT} f(\lambda_{aT})}\right].$$

Specifying values X for a propellant with known characteristics D, m and ν, one can construct relation T=f (X).

A second method of solution is based on the fact that there exists a relationship between the values of gas-dynamic functions f (λ) and q (λ) in the region λ =1.8-2.5, expressed by an approximating relation of the type

$$f(\lambda) = k_f [q(\lambda)]^n.$$

With proper selection of k_f and n, approximation error does not exceed 1%. In the range λ_a=1.8-2.5 when k=1.15-1.25, exponent n is close to 0.9.

From the approximating relation we obtain

$$\frac{f(\lambda_{aN})}{f(\lambda_{aT})} = \left[\frac{q(\lambda_{aN})}{q(\lambda_{aT})}\right]^n = \frac{1}{(1+X)^n}. \qquad (10.17)$$

Substituting the obtained result in (10.16), we obtain

$$1+X = e^{\frac{(D+m)(T-T_N)}{1-n(1-\nu)}} \left(\frac{\sigma_{cT}}{\sigma_{cN}}\right)^{\frac{1-\nu}{1-n(1-\nu)}}. \qquad (10.18)$$

If in the first assumption we assume $\sigma_{cT} = \sigma_{cN}$, then

$$1+X = e^{\frac{(D+m)(T-T_N)}{1-n(1-\nu)}}. \qquad (10.18a)$$

Relative engine pressure change when tuning a nozzle to constant thrust is determined by the relation obtained from formulas (10.16), (10.17) and (10.18a):

$$\frac{p_T}{p_N} = e^{-\frac{n(D+m)(T-T_N)}{1-n(1-\nu)}}. \qquad (10.19)$$

Listed below are the results of calculations for a motor tuned for constant thrust in the range T=-40... +60°C. The following were assumed in the calculation: $\nu = 0{,}4$; $D = 0{,}0014$; $m = 0{,}0002$; $T_N = -40°$ C; $F_a/F_{kp} = 6{,}25$; $\sigma_{cT} = \sigma_{cN}$.

Table 10.2.

T, °C	−40	−12,4	+12,9	+33,3	+55
X	0	0,1	0,2	0,3	0,4
p_T/p_N	1	0,92	0,85	0,79	0,74

It is evident from tables 10.1 and 10.2 that working pressure in a motor tuned for constant thrust increases with a decrease in initial propellant charge temperature in the degree to which this is necessary in order to compensate for a decrease in rate of propellant combustion with temperature. It follows from a comparison of lines 1 and 3 in Table 10.1 that relative pressure change in a motor with constant thrust, when ν =0.4 is approximately the same as in an uncontrolled motor, but the maximum pressure values in these motors are located at the opposite ends of the operating temperature range.

For propellants with a high temperature relation (high values of D), when tuning a nozzle for constant thrust the throat area must be varied within broad limits. With an increase in D, there is also an increase in pressure differential p_N/p_T in the preselected temperature range. A high value of

exponent γ in the given case is a favorable factor which ensures the requisite effect of adjustment with small changes in nozzle flow passage cross sectional area and working pressure in the motor (see figures in Table 10.1 for γ =0.4 and 0.69).

When interchangeable nozzle inserts or nozzles are employed in place of continuous variation of nozzle throat area for the purpose of tuning, the method of selecting inserts and the range of their utilization proves analogous to that which was examined in chapter section 10.3.

In the case of employment of interchangeable inserts, specifying allowable thrust variation limits P_{max}-P_{min}, one plots for these limits curves of continuous change in nozzle throat area within the preselected temperature range according to relation (10.18), and then one establishes, in conformity with the diagram in 10.2), the temperature interval of utilization of the individual inserts.

With utilization of interchangeable nozzles, if the ratio F_{κ}/F_{kp} remains constant for them, f (λ_a)=const and equations (10.18) and (10.19) assume the form

$$1 + X = e^{\frac{(D+m)(T-T_N)}{\nu}};$$

$$\frac{p_T}{p_N} = e^{-\frac{D+m}{\nu}(T-T_N)}.$$

Relative change in propellant charge burning time

$$\frac{\tau_T}{\tau_N} = \frac{u_N}{u_T} = e^{-m(T-T_N)}.$$

10.5. Tuning a Solid-Propellant Rocket Motor to Constant Flow Rate

At the present time an RDTT in rocket equipment is extensively employed as a generator for gas utilized in the most diversified systems, such as auxiliary propulsion units, servodrives, hot-gas gyrosystems, as well as supercharging, additional gas feed, stage separation, and buoyant rescue equipment inflation systems. Solid-propellant gas generators are frequently employed to drive turbines powering on-board electric generators [9]. Many of these gas-using devices impose rigid requirements on constancy of flow rate. We shall examine possible ways of solving this problem.

Substituting in the flow rate formula (7.13) dependences of pressure in an uncontrolled motor and propellant force on propellant charge temperature, we obtain a formula which indicates how propellant consumption varies with initial charge temperature in the absence of tuning:

$$\frac{\dot{m}_T}{\dot{m}_N} = e^{\frac{D+vm}{1-v}(T-T_N)}.$$

If a constancy of gas flow to the gas-driven device is achieved by dumping gas from a receiver in the line in which pressure is maintained constant, relative gas losses in relation to initial temperature are as follows:

$$K_{m_1} = \frac{\dot{m}_T - \dot{m}_N}{\dot{m}_N} = e^{\frac{D+vm}{1-v}(T-T_N)} - 1.$$

Consequently, with this method of regulating gas flow, the store of fuel in the generator must be increased by K_{m1} times over the minimum requisite quantity calculated for temperature T_N.

Dumping of gas directly from the gas generator through a constant-pressure valve ensures propellant charge combustion at the same pressure at all temperatures. With an unknown throat area of the nozzle through which gas enters the line to the driven device, gas flow fluctuates within the limits of variation with temperature of quantity $\sqrt{RT_k}$, that is,

$$\left(\frac{\dot{m}_T}{\dot{m}_N}\right)_{\text{раб}} = e^{-m(T-T_N)}.$$

In view of the small value of constant m for rocket propellants, gas flow can be considered practically constant. However, actual propellant consumption, taking into account dumping into the atmosphere, will vary as

$$K_{m_2} = \frac{\dot{m}_T}{\dot{m}_N} = e^{D(T-T_N)}.$$

Relative dumped gas flow will be

$$\frac{\dot{m}_{\text{стр}}}{\dot{m}_N} = e^{D(T-T_N)} - 1,$$

increasing with an increase in initial propellant charge temperature. Burning time will decrease simultaneously with an increase in propellant charge temperature.

Consequently selection of thickness of burning web with this mode of tuning should be performed for the preselected gas generator operation time for the highest propellant charge temperature, while the required burning surface should be selected according to the preselected consumption for the lowest charge temperature.

Thus the charge burns incompletely at minimum temperature during operation of the gas-driven device; at maximum temperature the charge burns completely, but a substantial portion of the generator gases will be discharged into the atmosphere. The actual propellant supply should be specified at K_{m2} times the quantity required by the gas-driven device.

Unproductive propellant consumption can be avoided when tuning the gas generator nozzle to constant set $\frac{pF_{kp}}{V\sqrt{RT_k}}$. Performing the substitutions which we have employed in the preceding chapter subdivisions, we shall obtain a relation of the requisite change with temperature of the gas generator relative throat area

$$1+X=e^{\frac{D+mv}{v}(T-T_N)}.$$

Gas flow rate and charge combustion time remain strictly constant with any initial charge temperature.

10.6. Causes of Nonuniformity of Charge Temperature Field and Its Equalizing Time

During rocket operation it is possible that initial charge temperature T_H will differ significantly from ambient temperature T_A. Such a difference in temperatures may occur, for example, as a result of airlifting rockets large distances from one climate zone to another. With a large-size propellant charge and initial temperature drop of several dozen degrees, from several hours to several days are required to reach equal charge and air temperatures. Therefore in practice there is the possibility that an RDTT will be fired prior to establishment of a temperature equilibrium between propellant charge and environment, with a substantial nonuniformity of propellant charge temperature field.

When a rocket is continuously sited at a launch position or on a launcher en route, not in a container, under atmospheric conditions, nonuniformity of propellant charge temperature can be caused by the daily fluctuations in ambient temperature. The magnitude of these fluctuations depends on the time of year and climatic conditions. For large propellant charges thermal relaxation time may prove to be greater than the period of air temperature fluctuations, which lead to the occurrence of a temperature gradient through the thickness of the charge.

Nonuniformity of propellant charge temperature field, a direct consequence of which is change in unit burning rate through the thickness of the charge, leads to deformation of the burning surface in the process of motor operation. In other words the position and shape of the combustion surface as well as its total area with a nonuniform charge temperature field, considered for any given point in time, may differ substantially from that which is determined by geometric calculations performed on the basis of the hypothesis of propellant burning in parallel layers. First of all this affects both the magnitude of mean values of RDTT thrust parameters and their extremal values, which determine maximum rocket G-loading and motor case strength. It is difficult to foresee in advance what temperature conditions are the most difficult.

With a uniform temperature field of a propellant charge in an uncontrolled RDTT, maximum pressure is achieved at maximum charge temperature. With a nonuniform temperature field an additional factor appears -- increase in burning surface as a consequence of its deformation during combustion; a factor determined by temperature differential through the thickness of the propellant charge but not by the mean temperature value. It is not known in advance which of these factors -- change in combustion rate averaged on the propellant charge volume or change in burning surface area -- exerts a stronger influence and whether pressure determined by maximum surface is greater than pressure determined by maximum temperature.

Possible change in RDTT ballistic and thrust parameters with temperature differentials in the propellant charge should also be taken into consideration during RDTT tuning (prelaunch adjustment) [26].

In view of this fact it seems advisable first of all to examine estimate relations which determine propellant charge temperature field equalization time and which limit the region where the nonuniformity of this field must be taken into account.

Then the most typical instances of deformation of burning surface and the influence of this factor on RDTT static characteristics will be examined.

As studies indicate, duration of change in rocket propellant charge temperature field with constant ambient temperature T_A and heat transfer coefficient α is determined primarily by the regular mode stage. At this stage change in temperature for all points in a propellant charge on a time axis follows a simple exponential relation, that is, temperature simplex natural logarithm

$$\theta = \frac{T - T_A}{T_H - T_A}$$

for any point in a propellant charge with temperature T will change according to the linear law. Quantity

$$m_\tau = \frac{d}{dt}(\ln \theta),$$

called cooling (heating) rate, will be the same for all points in a charge, as well as for its mean mass temperature $\overline{T}$.

Then the time to reach charge average temperature $\overline{T}_p$ will be specified as

$$\tau_p = \frac{1}{m_\tau} \ln \frac{T_A - T_H}{T_A - \overline{T}_p}. \qquad (10.20)$$

Relation (10.20) enables one to determine the time required to reach average charge temperature $\overline{T}_p$, close to T_A and assumed equilibrium. It also enables one to solve the inverse problem: from the specified charge time under given temperature conditions, to determine the average charge temperature reached by this time, and from its comparison with T_A, to estimate the degree of nonuniformity of the charge's temperature field.

Heating (cooling) rate m_τ is determined with the formula

$$m_\tau = \frac{\alpha}{c\rho_T}\frac{F}{W}\psi, \qquad (10.21)$$

where α -- coefficient of heat transfer from the environment to the motor surface; c -- propellant specific heat; $\psi = \frac{T_A - T_n}{T_A - \bar{T}}$ -- criterion of nonuniformity of propellant charge temperature field; F -- exterior lateral motor surface; W -- volume of propellant charge.

For charges of tubular shape, which includes slotted charges,

$$\frac{W}{F} = \frac{(1 - M^2)R_H}{2}, \qquad (10.22)$$

where R_H -- outer charge radius; R_{BH} -- cavity radius;

$$M = R_{BH}/R_H.$$

Criterion ψ is determined by the Biot criterion $Bi = \alpha R_H/\lambda_T$ and the geometric shape of the propellant charge, but is not dependent on its absolute dimensions, which makes it possible to obtain from an experiment on a model or from temperature field calculations value ψ for all geometrically similar propellant charges.

On the basis of temperature field calculations for charges of tubular shape, we determined the values of criterion ψ for variants with different coefficients M (Figure 10.3).

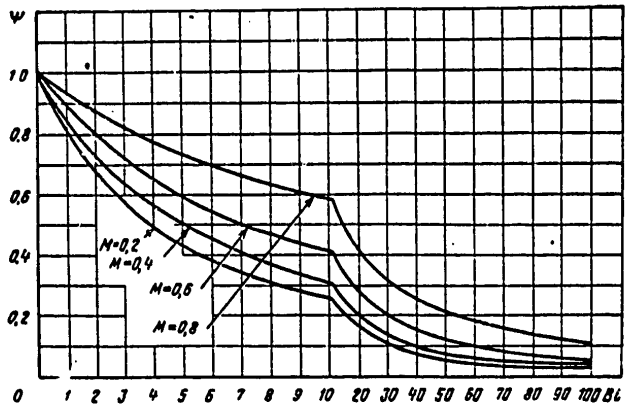

Figure 10.3. Dependence of Criterion of Nonuniformity of Temperature Field ψ for a Propellant Charge With a Cylindrical Cavity on Biot's Criterion

Calculating Biot's criterion with prespecified conditions of heat exchange between motor and environment, we can obtain from the graph corresponding value ψ, and then from formula (10.21) obtain, taking into account relation (10.22), m_τ, requisite for estimating temperature equalization time.

A major advantage of the above-examined relations is the fact that they enable one to obtain an estimate of temperature field nonuniformity, avoiding excessively unwieldy calculations connected with determining the temperature field proper in the dynamics of its change.

10.7. Influence of Nonuniformity of Charge Temperature Field on Solid-Propellant Rocket Motor Operating Conditions

Since with a nonuniform temperature field the burning rate varies from one section of the propellant charge surface to another, in order to calculate pressure in formula (7.15), in place of product $u_1 S$, one must substitute the following integral gas formation characteristic:

$$\Gamma = \sum \Delta S u_1 (r, x, \varphi),$$

where u_1 (r, x, φ) -- a relation characterizing change in unit combustion rate by cylindrical coordinates r, x, φ. In those cases where temperature drop on the propellant charge radius is determining, it would seem possible to limit oneself to taking into account change in velocity in this direction. Then, taking into account relation (10.1), one can write

$$\Gamma = \sum^{s} \Delta S u_{1N} e^{D \Delta T (r)},$$

where Δ T (r) -- a function expressing change in temperature difference $T-T_N$ on the charge radius.

For a relative pressure change in the process of propellant charge combustion we obtain

$$\frac{p_{ki}}{p_{k0}} = \left(\frac{\Gamma_i}{\Gamma_0}\right)^{\frac{1}{1-\nu}} = \left[\frac{\left(\sum^{s} \Delta S e^{D \Delta T (r)}\right)_i}{\left(\sum \Delta S e^{D \Delta T (r)}\right)_0}\right]^{\frac{1}{1-\nu}},$$

where Γ_0 and Γ_i -- values of gas formation characteristic for the initial and i points in time.

Thus calculation of RDTT characteristics with a nonuniform propellant charge temperature field is complicated by the fact that for each point in time the combustion surface must be broken down into sections, within which the combustion rate can be assumed constant, corresponding, according to (10.1), to the average propellant temperature in that section. Displacement of the combustion front in each of these sections in the course of a short time interval is assumed to occur at a constant pressure. Distortion of the combustion front is taken into account according to relation (7.10). A new engine pressure value is determined for the end of the time interval, in conformity with the reached magnitude of combustion surface and with new

distribution of burning rates on the surface. Time interval (charge thickness interval) is selected so that change in propellant charge temperature within the interval of combustion surface displacement does not exceed 3-5°C.

Examining the influence of propellant charge temperature field nonuniformity on RDTT operating conditions, one can specify three typical cases:

1) end-burning charges, with axial direction of burning normal to the plane of the maximum temperature gradient;

2) radial burning charges on which the combustion front at any point in time coincides with the isotherm (telescopic charge, cylindrical single-cavity grain);

3) radial-burning charges with a combustion front which does not coincide with the isotherms in the charge (star, slotted charge).

10.7.1. End-Burning Charge

We shall first examine a charge of the simplest shape -- a cylinder coated on the lateral surface and burning on the end facing the nozzle. We shall assume that the temperature field is symmetrical and that temperature changes only on the charge radius. To avoid ambiguity, we shall consider an exterior-cooled charge. For simplicity of calculations we shall assume that temperature T_N has been reached on the exterior surface of the charge, and temperature T_1 is maintained on the charge axis. Analysis of temperature fields on the basis of [26] indicates that in the majority of cases, corresponding to maximum temperature differential on the propellant charge radius, the temperature profile is close to parabolic, that is, one can assume:

$$\Delta T(r) = T - T_N = (T_1 - T_N)\left(1 - \frac{r^2}{R_H^2}\right), \qquad (10.23)$$

where r -- radius of a random point; T -- temperature at this point (Figure 10.4).

Distribution of rates of propellant combustion on the radius will be expressed by the relation

$$u = u_{1N} e^{M(1-\bar{r}^2)} p^\nu,$$

where

$$M = D(T_1 - T_N); \quad \bar{r} = r/R_H.$$

A higher burning rate on the axis of the charge will in time lead to deformation of the combustion front, which is initially flat, into a crater.

If a crater is present the local axial burning rate at that point in the profile at a distance r from the axis of the charge will be expressed, taking into account relation (7.10), as

$$u_x = u_{1N} e^{M(1-\bar{r}^2)} p^\nu \sqrt{1 + \left(\frac{\partial r}{\partial x}\right)^2} \frac{1}{\partial r/\partial x}. \qquad (10.24)$$

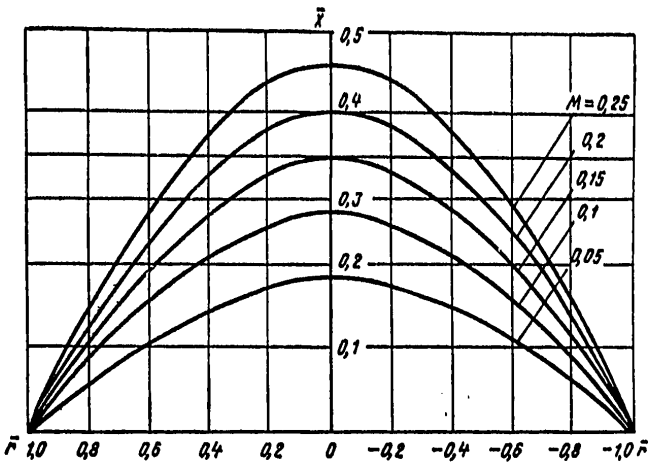

Figure 10.4. Stable Crater Profiles in an End-Burning Charge with Nonuniform Temperature Field

Gas generation from the burning surface per unit of time will be expressed as

$$\dot{m}_T = \int_0^F \rho_T u_x \, dF, \qquad (10.25)$$

where $dF=2\pi r\,dr$ -- projection of burning surface element onto a plane perpendicular to the axis of the charge.

Substituting (10.24), (10.25) and (7.15) into material balance equation (7.11), we obtain an expression determining the current engine pressure value:

$$p_к = \left[\frac{2\pi R_н^2 \rho_T \sqrt{\chi R T_к}\, u_{1N}}{\varphi_c A F_{кр}} \int_0^1 e^{M(1-\bar{r}^2)}\bar{r}\sqrt{1+\left(\frac{dx}{dr}\right)^2}\,d\bar{r}\right]^{\frac{1}{1-\nu}}. \qquad (10.26)$$

With a charge of considerable length, there occurs stabilization of the crater profile in the process of combustion. The condition of stability of crater profile is expressed by constancy of the axial component of burning rate on the charge radius u_x (r)=const.

$$e^{-M\bar{r}^2} = \frac{d\bar{r}/d\bar{x}}{\sqrt{1+(d\bar{r}/d\bar{x})^2}}, \qquad (10.27)$$

where $\bar{x}=x/R_н$.

Solving equation (10.27), we obtain a relation which determines combustion profile

$$\bar{x} = -\int_{1}^{\bar{r}} (e^{2M\bar{r}^2} - 1)^{1/2}\, d\bar{r}. \qquad (10.28)$$

Since for a stabilized combustion profile u_x=const for the entire surface, we obtain

$$\dot{m}_T = \rho_T u_{T_1} S_T,$$

where u_{T1} -- burning rate on the axis of the propellant charge.

10.7.2. Radial-Burning Charge With Isothermal Orientation of Burning Surface

As an illustration we shall examine a propellant charge consisting of one end-coated cylindrical grain with initial cavity radius r_0 and initial exterior radius $R_н$. We shall assume temperature distribution on the radius corresponding to relation (10.23). Then the gas formation function for any point in time will assume the form

$$\Gamma = 2\pi L u_{1N} [re^{M(1-\bar{r}^2)} + Re^{M(1-\bar{R}^2)}],$$

where r -- current cavity radius value; L -- grain length; R -- current value of exterior grain radius;

$$\bar{r} = r/R; \quad \bar{R} = R/R_н.$$

Relative pressure change in the process of charge combustion will be

$$\frac{p_{\kappa t}}{p_{\kappa 0}} = \left[\frac{\bar{r}_t e^{M(1-\bar{r}_t^2)} + \bar{R}_t e^{M(1-\bar{R}_t^2)}}{1 + \bar{r}_0 e^{M(1-\bar{r}_0^2)}}\right]^{\frac{1}{1-\nu}}, \qquad (10.29)$$

where $\bar{r}_t = \bar{r}_{t-1} + \Delta\bar{r}$; $\bar{R}_t = \bar{R}_{t-1} - \Delta\bar{R}$.

In view of a difference in rates of displacement of the outer and inner surfaces, intervals Δr and ΔR are not equal to one another. Change in interior radius Δr for a certain time interval Δt will be

$$\Delta r = \Delta\bar{r} R_н = u_{1N} e^{M(1-\bar{r}^2)} p^\nu \Delta t.$$

During this same time the exterior radius will decrease by amount

$$\Delta R = \Delta\bar{R} \cdot R_н = u_{1N} e^{M(1-\bar{R}^2)} p^\nu \Delta t,$$

consequently,

$$\frac{\Delta\bar{r}_t}{\Delta\bar{R}_t} = e^{M(\bar{R}_t^2 - \bar{r}_t^2)}. \qquad (10.30)$$

Specifying a given displacement interval for one of the surfaces, such as $\Delta\bar{r}$, the displacement interval of the second surface should be determined from formula (10.30).

The time interval corresponding to an independent surface displacement interval will be

$$\Delta t = \frac{\Delta r_i R_н}{u_{1N} e^{M(1-\bar{r}_i)} p_{кi}^{\nu}}.$$

A charge of this shape, representing with a homogeneous temperature field a classic example of a neutral combustion charge, will display a degressive character of combustion if temperature increases toward the outer surface, and progressive if it decreases in that direction.

10.7.3. Radial-Burning Charges With a Combustion Front Intersecting the Isotherms

The simplest variant for this case is a slotted charge in which in the area of the slot the combustion front is initially orthogonal to the isotherms, while in the cylindrical section it always has an isothermal orientation. Distribution of temperatures on the radius in both sections can be assumed identical, since the slots, in view of their radial orientation and narrow width, do not cause a substantial temperature field distortion.

The gas formation function for a given point in time will consist of four components:

$$\Gamma = \Gamma_ц + \Gamma_ш + \Gamma_т + \Gamma_с,$$

characterizing gas formation;

$\Gamma_ц$ -- on the surface of the cylindrical cavity; $\Gamma_ш$ -- on the surface of the slots; $\Gamma_т$ -- on the surface of the burning end (or ends); $\Gamma_с$ -- on the surface of the slot web.

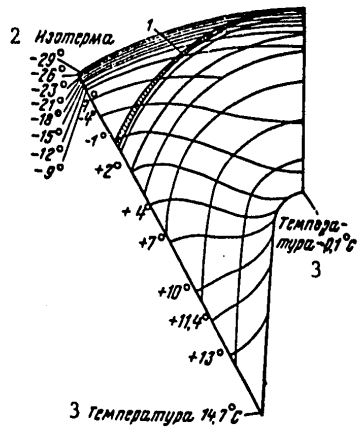

Figure 10.5. Temperature Field of Charge With Star-Shaped Cavity With Maximum Temperature Differential Through the Thickness of the Web

Key to Figure 10.5 on preceding page:

1. Decrease in percentage of unburned propellant particles with a negative temperature jump
2. Isotherm
3. Temperature

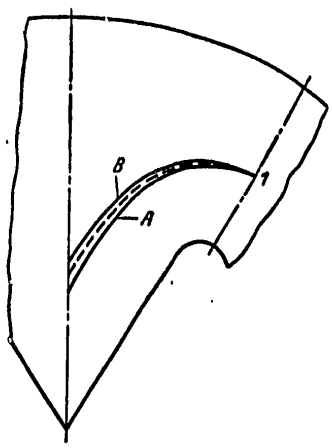

Figure 10.6. Change in Combustion Front With Nonuniform Temperature Field of Charge With Star-Shaped Cavity

If we include the slot web area in the end area and figure the web perimeter with correction factor $\lambda \cong 0.6$, with the above temperature distribution on the radius of the charge, the function of gas formation in a first approximation will be expressed as

$$\frac{\Gamma}{u_{1N}} = 2\pi (r_0 + e)\, e^{M(1-\bar{r}^2)} \left[L - L_{\text{ш}} - \lambda e + 2n (r_0 + e)\left(\frac{\pi}{4} - \varphi\right) L_{\text{ш}}\right] + \\ + 2\pi L_{\text{ш}} \int_r^R e^{M(1-\bar{r}^2)} \cos(dl \cdot r)\, dr + 2\pi \int_r^R r e^{M(1-\bar{r}^2)}\, dr,$$

where L -- total length of charge; $L_{\text{ш}}$ -- length of slot section;

$$r = r_0 + e;$$

e -- thickness of burned layer of propellant determined for the cylindrical section; dl·r -- local angle between combustion front and direction of radius run through slot sector angle point.

Calculation for a charge with star-shaped cavity and its modifications proves to be more complex. Figure 10.5 gives an idea of the character of the temperature field of such a charge. In this case one must consider

temperature change both on radius r and by coordinate angle φ. Nonuniformity of the temperature field of a charge with a star-shaped cavity leads to change in its progressiveness characteristics and percentage of degressive residue, as is shown by the diagram in Figure 10.6. The dashed-line curve corresponds to the position of the combustion front at a temperature which is constant through the entire charge section.

With a temperature diminishing from the periphery to the center of the charge, as a consequence of lag in burning rate on the axis of a star point, the combustion front will assume position A on reaching point 1. The burning surface in this instance will be greater than with uniform temperature distribution, and the percentage of degressive residue will increase.

On the other hand, at a temperature which increases toward the center of the charge, burning on the axis of a star point will run ahead of burning in the middle of a projection, as a consequence of which when the combustion front passes through point 1 it will occupy position B, which corresponds to a smaller surface quantity. We include below calculated figures for a star-cavity charge with a diameter of 152 mm [25] with maximum possible temperature drop.

	$T_A = -29°$ C; $T_н = +21°$ C	$T_A = +21°$ C; $T_н = -29°$ C
Change in percentage of degressive charge residue, %	+7,96	−6,36
Change in burning time, %	+41,5	−39,2

Section III. STATIC CHARACTERISTICS OF HYBRID ROCKET MOTORS

Chapter 11. DESIGNS AND FEATURES OF OPERATION OF HYBRID ROCKET MOTORS

11.1. Designs of Hybrid Rocket Motors

A hybrid rocket motor burning a two-component propellant contains the following:

combustion chamber containing solid component charge;

tank with liquid component;

equipment of system for feeding liquid propellant component into the combustion chamber;

automatic control elements, with the aid of which motor operation is controlled (launch, shutdown, transition from one mode to another, control, etc).

Classification of GRD [hybrid rocket motors], just as of other types of rocket motors, can be performed according to various attributes -- they can be differentiated, for example, by function, magnitude of thrust, potential number of firings and shutdowns, etc. These classification attributes are insignificant, however, for analysis of static characteristics. More important in this regard are differences among GRD in features of the devices of the system for feeding liquid component to the combustion chamber.

Practically all types of corresponding systems of liquid-propellant rocket motors can be used to feed liquid propellant component into the combustion chamber of a GRD. In conformity with this, one can designate the following GRD by type of liquid component supply system:

with a gas pressurization supply system;

with a pump supply system.

GRD with a gas pressurization liquid component supply system in turn can be classified by type of device boosting pressure in the tank during motor

operation (pressure accumulator). On analogy with ZhRD, one can consider possible utilization of the following in hybrid motors:

air (gas) pressure accumulator (VAD);

cartridge pressure accumulator (PAD);

hybrid pressure accumulator (GAD).

Bottled compressed gas is used to force propellant from the tank with an air pressure accumulator. If a motor employs a cartridge or hybrid pressure accumulator, fuel combustion products are fed into the tank (solid propellant in the first instance and liquid-solid in the second).

Figure 11.1 contains a diagram of a GRD with a gas pressurization system of feeding liquid component and an air pressure accumulator.

When the motor is ignited, valve 2 opens, and compressed gas is fed through a pressure reducer to diaphragm 4. After penetrating the diaphragm, gas fills the free space in the tank. Diaphragm 6 bursts under the increased pressure of the liquid component; the component passes through open valve 7 to the combustion chamber and them into the charge cavity. The components ignite (either self-ignition or, if the pair of components do not spontaneously combust -- they are ignited by an outside source), and the motor enters the required operating mode. The motor is shut down by closing valve 7, as a result of which liquid component is no longer fed to the combustion chamber.

Figure 11.1. Diagram of GRD With Gas Pressurization Liquid Propellant Component Supply System

Key:

1. Compressed gas tank
2, 7. Valve
3. Pressure reducer
4, 6. Diaphragms
5. Tank with liquid propellant component
8. Combustion chamber

Figure 11.2. Diagram of Hybrid Pressure Accumulator

Key:
1. Bottled gas
2. Valve
3. Pressure reducer
4, 6, 9. Diaphragms
5. Pressure accumulator tank
7. Valve
8. Pressure accumulator chamber
10. Liquid propellant tank

A GRD cartridge pressure accumulator may not differ in design and operating features from analogous devices used by liquid-propellant rocket motors and therefore will not be discussed.

Figure 11.2 contains a diagram of a typical hybrid pressure accumulator. As is evident from a comparison of figures 11.1 and 11.2, in this instance the pressure accumulator essentially comprises a small hybrid motor from the combustion chamber of which combustion products enter the main engine's liquid-propellant component tank. This type of pressure accumulator is more complex in arrangement than a VAD, but its utilization makes it possible in principle to improve engine mass characteristics by reducing the mass of the compressed-gas tank.

A GRD with a pumped liquid component supply system can incorporate the following arrangements:

closed;

open.

In the first instance gas, after passing through the turbine, is fed into the combustion chamber and is subsequently ejected from the main exhaust nozzle together with the combustion products. In the second arrangement gas, after passing through the turbine, is ejected into the atmosphere through special exhaust nozzles.

A GRD, just as liquid-propellant motors, can employ various types of turbine gas generators. On the basis of this attribute, GRD with a pumped liquid propellant component supply system are subdivided into motors:

with a single-component gas generator (hydrogen peroxide, hydrazine, etc);

with gas tapped from the main combustion chamber;

with turbine-driving gas formed in a special chamber in which a two-component propellant burns (for example, the same components as in the main combustion chamber).

One should expect GRD turbopump units to be simpler than those of a ZhRD, since they must supply only one liquid component.

Just as in liquid-propellant rocket motors, a somewhat elevated tank pressure must be provided for GRD with a pumped supply system, in order to ensure stability and to maintain cavitation-free pump operation. Practically all those types of devices which are employed for the same purpose in liquid-propellant rocket motors can be used to boost tank pressure.

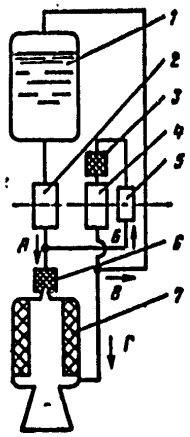

Figure 11.3. Closed GRD Arrangement

Key:

1. Tank
2. Pump
3. Gas generator reactor
4. Turbine
5. Gas generator pump
6. Combustion chamber reactor
7. Combustion chamber
А. Peroxide feed to chamber
Б. Peroxide feed to gas generator
В. Steam-gas feed to tank
Г. Steam-gas feed to chamber

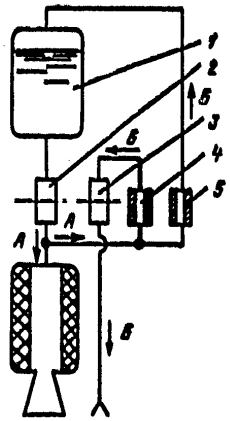

Figure 11.4. Open GRD Arrangement

Key:
1. Tank
2. Pump
3. Turbine
4. Turbine gas generator
5. Tank pressurization gas generator
А. Movement of liquid component
Б. Gas movement

Figures 11.3 and 11.4 present two layouts as examples of possible GRD arrangements with a pumped liquid component supply system, differing in the principle of utilization of spent turbine gas and type of gas generator employed. Figure 11.3 contains a diagram of a GRD with a closed liquid component feed system and a gas generator employing a single substance, which is also a propellant component. This arrangement can be utilized, for example, when hydrogen peroxide is the liquid component.

The diagram does not indicate the automatic control devices which control motor operation, and in particular motor ignition, in the process of which additional measures must be taken to accelerate turbine buildup to the required operating conditions, to provide preliminary tank pressurization, etc.

Figure 11.4 contains an open GRD arrangement with a gas generator employing hybrid (solid-liquid) propellant consisting of the same components as the motor propellant. As in the preceding instance, the diagram does not show automatic control devices.

Specific thrust impulse of a GRD with a pump liquid component supply system, just as for ZhRD of similar arrangements, depends on the type of supply system. In an open-arrangement motor thrust $P=P_k+P_{o.c}$,

where P_k -- thrust generated by the combustion chamber; $P_{o.c}$ -- thrust generated by the turbine exhaust nozzle.

If we designate flow through the combustion chamber nozzle and turbine exhaust nozzles with $\dot{m}_k$ and $\dot{m}_{o.c}$ respectively, specific engine impulse

$$I_y = \frac{P}{\dot{m}_\Sigma} = \frac{P_k + P_{o.c}}{\dot{m}_\Sigma} = \frac{I_{y.k}\dot{m}_k + I_{y.o.c}\dot{m}_{o.c}}{\dot{m}_\Sigma}.$$

Here $I_{y.k}$ and $I_{y.o.c}$ -- specific thrust impulses of combustion chamber and turbine nozzles; $\dot{m}_\Sigma = \dot{m}_k + \dot{m}_{o.c}$.

Designating coefficient of specific thrust impulse losses in a supply system with

$$\varepsilon_I = \frac{\dot{m}_{o.c}}{\dot{m}_\Sigma}\left(1 - \frac{I_{y.o.c}}{I_y}\right)$$

we can obtain $I_y = I_{y.k}(1 - \varepsilon_I)$.

As was shown earlier, quanty ε_I is connected with the magnitude of combustion chamber pressure p_k; the higher this pressure, the greater is ε_I, that is, the greater the loss to the turbine nozzles. Taking into consideration the fact that specific chamber impulse increases with an increase in pressure p_k, one can establish that function I_y (p_k) has for ZhRD a maximum in the region of pressures $p_k > 100 \cdot 10^5$ Pa. For GRD increase in mass with an increase in chamber pressure should be considerably more appreciable than for liquid-propellant motors, since the chamber is substantially larger (it contains a solid propellant component charge). Therefore a move to closed designs, that is, into the area of high chamber pressures, for GRD should produce less gain in total characteristics (energy, mass), in connection with which employment of closed designs is less efficient here.

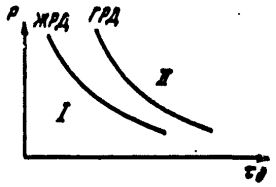

Figure 11.5. Regions of Efficient Employment of Various Types of Supply Systems

Key:
1. Region of gas pressurization systems
II. Region of pump systems

One can evaluate in approximately the same manner the correlation between regions of efficient employment of gas pressurization and pump liquid

propellant component supply systems. For liquid-propellant rocket motors it is expedient to employ gas pressurization systems with low thrust impulse values $I=P\tau_{\text{д}}$ ($\tau_{\text{д}}$ -- motor burning time), since with an increase in impulse I there is an increase in tank volume and the influence of their mass on overall mass characteristics. This also applies to GRD, but since in a GRD the tank contains only a portion of the propellant, the percentage share of the supply system mass in total engine mass will be less than for a ZhRD, and the region of efficient utilization of gas pressurization systems should be broader for a GRD than for liquid-propellant motors (Figure 11.5).

Certain differences in GRD layouts may also be caused by the specific design features of their combustion chambers. The chambers in the above GRD diagrams are of the simplest type -- uncooled, and with liquid propellant component fed only through the head of the chamber. Obviously the fact of a liquid propellant component makes it possible to cool the chamber in the same manner as is performed in ZhRD chambers. Since that portion of the chamber in which the solid propellant component charge is placed can be shielded from heating by the propellant layer and the dimensions of a GRD chamber are considerably greater than those of a ZhRD chamber (with equal thrust), one can assume that cooling only the unprotected portion of the chamber and nozzle is reasonable or possible (Figure 11.6).

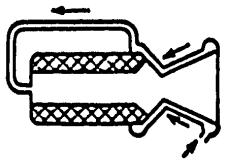

Figure 11.6. GRD Chamber Cooling Diagram

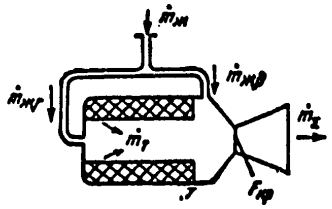

Figure 11.7. Diagram of GRD Chamber With Afterburning

The liquid propellant component can be fed into the chamber not only through the head of the chamber but also into the region forward of the nozzle, that is, beyond the charge (Figure 11.7). In this case propellant combustion takes place in two stages. The first stage takes place in the charge cavity, followed by "afterburning" in the nozzle-adjacent cavity of

the combustion products formed in the charge cavity. In conformity with this, the chamber design diagrammed in Figure 11.7 is sometimes called a design with afterburning.

Henceforth we shall employ the following designation for such a chamber:

$\dot{m}_т$ -- per-second consumption of solid propellant component;

$\dot{m}_ж$ -- per-second consumption of liquid component;

$\dot{m}_{ж.г}$ -- that part of the per-second liquid component flow entering the head of the chamber;

$\dot{m}_{ж.д}$ -- that portion of the per-second liquid component flow entering the afterburner.

$$\dot{m}_ж = \dot{m}_{ж.г} + \dot{m}_{ж.д}.$$

Total propellant consumption $\dot{m}_Σ = \dot{m}_ж + \dot{m}_т.$

Propellant consumption relation: $K = \dot{m}_ж/\dot{m}_т.$

Just as for ZhRD, specific thrust impulse is determined by the ratio of components and pressure differential between chamber and nozzle exit:

$$I_y = I\left(K, \frac{p_к}{p_а}\right).$$

Various propellant pairs can be employed in GRD.* Many possible compositions have been proposed. Practically all corresponding components of propellants used in modern ZhRD can be employed as liquid oxidizers or fuels. Nitrates or perchlorates of some elements (sodium, potassium, lithium, etc) or groups (ammonium, hydrazine, nitronium, etc), for example, can be employed as solid oxidizers. A wide range of substances can be employed as solid fuels -- polymeric compounds, rubber, hydrides of metals, (aluminum, lithium, beryllium), etc [7]. GRD based on a liquid oxidizer and solid fuel are considered preferable in a number of indices. Such GRD are sometimes called straight-design motors.

* Employment of two components in a GRD is the most typical. Foreign sources, however, have contained reports of GRD designs employing a three-component propellant; two liquid components (oxidizer and liquid hydrogen, for example) would be fed into the combustion chamber in order to improve a motor's energy characteristics.

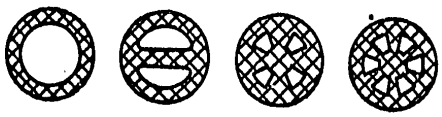

Figure 11.8. Possible Shapes of GRD Propellant Charge Cross Sections

In addition to other factors, the characteristics of a GRD are determined by the shape and dimensions of the solid component charge. Publications have discussed employment of charges of various shape. The simplest is the cylindrical charge with a single cavity (Figure 11.8). A charge of this shape, however, possesses a relatively small combustion surface and, in addition, does not ensure (and this may prove to be essential) constancy of surface during motor operation. Figure 11.8 also shows other possible charge cavity cross sectional shapes.

The principal characteristics of GRD, just as other types of rocket motors, are thrust, specific thrust impulse, and duration of operation. With a given propellant and engine design, these characteristics are determined by per-second component flow and consumption rates, which in turn are determined by the degree to which the values of the motor's numerous design parameters and operating conditions correspond to the design or rated values.

The most important factors in this respect, which influence GRD characteristics, are the following:

deviations from rated values of design parameters of the liquid component supply system;

deviations of combustion chamber dimensions, and particularly the nozzle throat area;

deviations of dimensions (length, cavity cross sections) of the solid component charge;

deviations of solid component burning rate;

deviations of propellant component temperature.

These factors should be primarily considered in analyzing the static characteristics of a GRD.

11.2. Propellant Combustion in a Hybrid Rocket Motor

The processes of combustion of a solid-liquid propellant in the conditions of a GRD chamber are extremely complex and unique. It is the features precisely of these processes which distinguish hybrid rocket motors to the

greatest degree from ZhRD and RDTT. In order to evaluate and calculate the characteristics of a GRD, just as the characteristics of motors operating on a solid propellant, one must know the relations determining the linear rate of combustion of the solid propellant component, that is, the rate of displacement of the combustion front into the charge in a direction perpendicular to its surface. These relations are distinguished from those which are utilized to determine the combustion rate of RDTT propellants, which is connected with the features of the process of combustion of GRD propellants and the composition of these propellants. As was noted above, RDTT propellants contain both fuel and oxidizing elements in a ratio ensuring at all times independent (without the participation of additional components) combustion of these propellants. In connection with this, combustion terminates entirely in the layer directly adjacent to the surface of the charge. Therefore in the majority of cases the state and parameters of the environment adjacent to the burning surface does not exert significant influence on the rate of burning of RDTT propellant. Processes take place differently under conditions of combustion of a GRD hybrid propellant. The solid component contains a large surplus of fuel or oxidizing elements and frequently is incapable of independent combustion. Requisite for combustion, that is, reactions of oxidation of fuel elements with release of heat, is contact between the substance of which the solid component consists and the substance of the liquid component. Usually this contact and the following oxidation reactions take place in a zone above the surface of the solid component. This zone is the combustion zone proper. But in order for steady-state combustion to be maintained, it is essential that new doses of components continuously enter this zone.

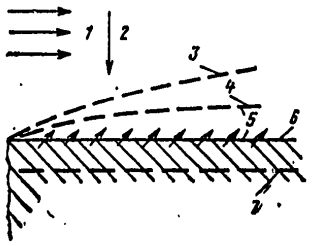

Figure 11.9. Diagram of Combustion of Hybrid Propellant

Key:

1. Direction of movement of liquid component
2. Heat flow
3. Zone of termination of reactions and equalization of composition
4. Zone of chemical reactions
5. Mixing zone
6. Surface of gasification
7. Zone of solid component heating

Figure 11.9 contains a diagram of steady-state conditions of hybrid propellant. Heat flows from the combustion zone proper to the surface of the solid component, as a result of which this component becomes heated. When the surface of the component reaches a certain temperature, gasification begins. The process of gasification can take place in a varying manner, depending on the composition of the solid component. It can involve melting with subsequent vaporization of a liquid film, sublimation (transition of a solid substance to a gaseous substance without intermediate transformation into a liquid) or pyrolysis (chemical decomposition with formation of a gaseous substance). Gasification products proceed from the surface into the combustion zone.

Upon entering the combustion chamber, the liquid component is broken up into fine droplets by injectors. The droplets are heated and vaporized by the heat released in the combustion zone. Thus fuel and oxidizer enter oxidation reactions in gaseous form. These reactions begin at certain local component ratio values which differ from the average. Then, in the process of movement by combustion products through the charge cavity toward the nozzle-adjacent space, these reactions terminate and there occurs equalization of the composition of the gas mixture to the computed value, corresponding to the selected propellant ratio.

As follows from what we have stated about the character of combustion of a hybrid propellant, this combustion constitutes an aggregate of complex physicochemical processes. It is therefore more correct to apply to the solid component not the terms "combustion" and "rate of combustion" but rather the terms "gasification" and "rate of gasification." In addition one can conclude that the determining factors for rate of gasification are primarily those factors which influence intensity of delivery of heat to the surface of the solid component. The rate of gasification should also be determined by the thermophysical properties of the component proper (for example, melting and evaporation heat and temperature, heat conductivity, etc). Heat is transferred to the surface of the solid component from the combustion zone by means of radiation and convection. The process of heat transfer is highly complex, but the factors which primarily determine its intensity are obvious. They include the properties (pressure and density) of the gas flowing over the surface of the solid component, the rate of gas movement along the surface, as well as temperature in the combustion zone, which in turn is determined by the composition of the propellant pair employed.

There have been numerous studies of the processes of combustion of hybrid propellant, aimed at establishing relationships for determining the rate of gasification of the solid component. Most frequently these relations are in the following form:

$$u = \bar{u}_1 p_к^{\nu} (\rho v)^{\beta} A^{\alpha}, \qquad (11.1)$$

where $\bar{u}_1$ -- coefficient taking into account the properties of the propellant component, including their temperature: for a given pair of components $\bar{u}_1 = \bar{u}_1(T)$; p_k, ρ, v -- pressure, density and velocity of gases over the

surface of the solid components; A -- coefficient taking into account other properties of the combustion products; ν, β, α - coefficients.

Designating $\bar{u}_1$ (T) $A^{\alpha}=u_1$ (T), we obtain

$$u = u_1(T)\, p_к^{\nu} (\rho v)^{\beta}. \qquad (11.2)$$

Usually for practical needs relation (11.2) is established experimentally. Coefficients ν and β and function u_1 (T) are determined thereby from experience. We shall note that if we disregard the influence of velocity of gas movement on the rate of gasification, that is, if we assume β =0, then relation (11.2) assumes the form

$$u = u_1(T)\, p_к^{\nu},$$

which corresponds to one of the most common types of solid propellant combustion rate formula. Taking into account that according to the gas flow continuity equation $\rho v = \dot{m}/F$, where $\dot{m}$ -- per-second gas flow rate through the section; F -- cross sectional area, we obtain from formula (11.2)

$$u = u_1 p_к^{\nu} \left(\frac{\dot{m}}{F}\right)^{\beta}. \qquad (11.3)$$

From this follows a number of conclusions which are important for analysis of the operating process in a GRD combustion chamber. Per-second rate of gas flow through a cross section of the cavity increases with progression along the charge as a consequence of the generation of additional mass during gasification of the solid component. Consequently, with utilization of a charge initially containing a cavity of constant (lengthwise) section, the rate of gasification also increases in the direction of gas movement, which should lead to nonuniform gasification along the charge and to change from the initial shape of the cavity.

Calculation of GRD static characteristics taking into account change in rate of gasification along the length of the charge is difficult. At the same time sufficient accuracy of solution for a number of problems can be obtained by utilizing average rate of gasification, which is defined as the rate of gasification which produces the same total (along the entire cavity surface) gas formation as actually occurs, that is, taking into account change in rate.

Let us determine the average rate for the case of employment of a cylindrical cavity.

If cavity diameter is D, charge length L, density of the solid component $\rho_т$, then gas formation of the entire charge will be

$$\dot{m}_т = \pi D \rho_т \int_0^L u\, dl, \text{ где } u = u(l).$$

By determination of average rate, gas formation can also be determined in the form

$$\dot{m}_т = \pi D L \rho_т u_{ср}.$$

Consequently,

$$u_{ср} = \frac{1}{L}\int_0^L u\,dl. \qquad (11.4)$$

The rate of gasification in the initial cross section of the charge cavity, where rate of gas flow is equal to liquid component flow rate $\dot{m}_ж$ according to relation (11.3), is determined as

$$u_0 = u_1 p_к^ν \left(\frac{\dot{m}_ж}{F}\right)^β.$$

We shall designate

$$\psi = \frac{\dot{m}_т}{\dot{m}_т + \dot{m}_ж}.$$

Utilizing these relations from (11.4), we can obtain [7] the following expression for average rate:

$$u_{ср} = u_0 \frac{\psi}{1-\psi}(1-\beta)\frac{1}{\left(\frac{1}{1-\psi}\right)^{1-\beta} - 1}. \qquad (11.5)$$

Or, designating

$$K(\psi, \beta) = \frac{\psi}{1-\psi}\frac{(1-\beta)}{\left(\frac{1}{1-\psi}\right)^{1-\beta} - 1}, \qquad (11.6)$$

we find that

$$u_{ср} = u_0 K(\psi, \beta). \qquad (11.7)$$

Following are typical for GRD: $\beta = 0{,}3 \cdots 0{,}6$; $\psi = 0{,}2 \cdots 0{,}3$.

$K(\psi, \beta) = 1{,}1 \cdots 1{,}2$ and, consequently, the average rate of gasification differs from the least (on entry into the charge cavity) by (10... 20)%. We must note that in the process of operation of a GRD the propellant charge in which initially had a constant cavity cross section, there occurs "equalization" of rates. The further the section from the beginning of the cavity, the higher the rate in that section and the greater the degree to which its area grows, which in conformity with (11.3) should cause a decrease in rate with an increase in time. Therefore the above-established correlation between average and minimum rates of gasification is maximum and decreases with continued motor operation.*

* We should draw attention to the fact that cavity shape also changes at the same time -- from cylindrical it becomes conical with a complex profile.

The basic possibility of one of the methods of GRD control also follows from formula (11.3). If a motor employs a combustion chamber with liquid component fed both through the chamber head into the charge cavity and into the nozzle-adjacent space beyond the cavity (see Figure 11.7), obviously not the entire flow rate of the liquid component is determining for rate of gasification, but only that part of the flow which goes through the chamber ahead. Therefore, altering the distribution of liquid component flow rate between the two above-stated components, one can affect charge gas formation to a certain degree and thus influence such principal motor characteristics as propellant consumption and composition (ratio of components), which in turn determine motor thrust and specific thrust impulse.

The above-noted feature of a GRD with a chamber in which liquid propellant component is fed not only into the charge cavity but also bypassing it -- into the nozzle-adjacent space, should be considered when determining the static characteristics of a GRD of this design.

11.3. Hybrid Rocket Motor Combustion Chamber Equations

The system of equations describing the relationship between the characteristics of a hybrid rocket motor under steady-state operating conditions contains, in the general form, equations of:

combustion chamber;

liquid component supply system equipment;

motor thrust characteristics.

Systems of linearized motor equipment equations, which make it possible to determine deviations of parameters from their nominal values, can be utilized to solve the majority of problems pertaining to examination and determination of the static characteristics of GRD, just as in the case of solving analogous problems pertaining to ZhRD.

GRD Combustion Chamber Equations

GRD combustion chamber equations should interrelate deviations in chamber pressure and fuel component flow and consumption rates with deviations of the principal factors influencing these parameters, that is, with deviations of charge dimensions, density of solid component, temperature of the components, etc.

Let us examine a combustion chamber of the most general design, with combustion product afterburning (see Figure 11.7).

We shall designate in addition: $T_{ж}$ and T_T -- temperatures of the liquid and solid components; K_{cT} -- stoichiometric ratio of rates of component consumption; α -- excess liquid component ratio; $\varphi = \dot{m}_{ж.г}/\dot{m}_{ж}$ -- ratio

of liquid component rate of flow through the head of the combustion chamber to its total flow rate; R and T_k -- gas constant and temperature of combustion products on entry into the nozzle; n -- polytropic expansion exponent; φ_c -- coefficient of losses during gas movement through the nozzle.

Operation in the combustion chamber under motor steady-state operating conditions is described by the following system of relations:

conservation of matter equation:

$$\dot{m}_\Sigma = \dot{m}_\tau + \dot{m}_{ж.г} + \dot{m}_{ж.к}; \qquad (11.8)$$

equation of gas flow rate through the nozzle:

$$\dot{m}_\Sigma = \frac{\varphi_c b(n) p_к F_{кр}}{\sqrt{RT_к}}; \qquad (11.9)$$

equations of flow rate-consumption ratios:

$$K = \alpha K_{ст} = \frac{\dot{m}_ж}{\dot{m}_\tau}; \qquad (11.10)$$

$$\varphi = \frac{\dot{m}_{ж.г}}{\dot{m}_ж}; \qquad (11.11)$$

equation of charge gas formation for a single-cavity grain:

$$\dot{m}_\tau = \int_0^L \pi D \rho_\tau u_l \, dl = \int_0^L \pi D \rho_\tau u_1 p_к^\nu \left(\frac{\dot{m}_l 4}{\pi D^2}\right)^\beta dl, \qquad (11.12)$$

where $\dot{m}_l$ -- gas flow rate in a given section;

$$\dot{m}_{ж.г} \leqslant \dot{m}_l \leqslant (\dot{m}_{ж.г} + \dot{m}_\tau).$$

From (11.12) one can obtain

$$\dot{m}_\tau = [4^\beta \pi^{(1-\beta)} (1-\beta) u_1 \rho_\tau L D^{1-2\beta} p_к^\nu + \dot{m}_{ж.г}^{(1-\beta)}]^{\frac{1}{1-\beta}} - \dot{m}_{ж.г}; \qquad (11.13)$$

equation of influence of temperature of propellant components and the ratio of their flow rates-consumption on parameters of the gas mixture:

$$RT_к = RT_к(\alpha, T_ж, T_\tau); \qquad (11.14)$$

equation of the influence of temperature of the solid component on the rate of its gasification: $u_1 = u_1(T_T)$.

Concurrently solving equations (11.9), (11.10) and (11.14), linearized in the environs of nominal conditions, we obtain the first of GRD chamber equations:

$$a_{\kappa}^{p_{\kappa}}\delta p_{\kappa} + a_{\kappa}^{\dot{m}_{\kappa}}\delta\dot{m}_{\kappa} + a_{\kappa}^{\dot{m}_{\tau}}\delta\dot{m}_{\tau} + b_{\kappa}^{F_{\kappa p}}\delta F_{\kappa p} + \\ + b_{\kappa}^{\varphi_c}\delta\varphi_c + c_{\kappa}^{T_{\kappa}}\delta T_{\kappa} + c_{\kappa}^{T_{\tau}}\delta T_{\tau} = 0, \qquad (11.15)$$

where dimensionless coefficients:*

$$a_{\kappa}^{p_{\kappa}} = b_{\kappa}^{F_{\kappa p}} = b_{\kappa}^{\varphi_c} = -1; \quad a_{\kappa}^{\dot{m}_{\kappa}} = \frac{\bar{K}}{1-\bar{K}} - \frac{1}{2}\frac{\bar{\alpha}}{R\bar{T}_{\kappa}}\frac{\partial(RT_{\kappa})}{\partial\alpha};$$

$$c_{\kappa}^{T_{\kappa}} = \frac{1}{2}\frac{\bar{T}_{\kappa}}{R\bar{T}_{\kappa}}\frac{\partial(RT_{\kappa})}{\partial T_{\kappa}}; \quad a_{\kappa}^{\dot{m}_{\tau}} = \frac{1}{1+\bar{K}} + \\ + \frac{1}{2}\frac{\bar{\alpha}}{R\bar{T}_{\kappa}}\frac{\partial(RT_{\kappa})}{\partial\alpha}; \quad c_{\kappa}^{T_{\tau}} = \frac{1}{2}\frac{\bar{T}_{\tau}}{R\bar{T}_{\kappa}}\frac{\partial(RT_{\kappa})}{\partial T_{\tau}}.$$

From equations (11.12) and relation $u_1=u_1(T_T)$ we obtain the second GRD chamber equation (gas formation equation):

$$a_{r}^{\dot{m}_{\tau}}\delta\dot{m}_{\tau} + a_{r}^{\dot{m}_{\kappa.r}}\delta\dot{m}_{\kappa.r} + a_{r}^{p_{\kappa}}\delta p_{\kappa} + b_{r}^{u_1}\delta u_1 + \\ + b_{r}^{\rho_{\tau}}\delta\rho_{\tau} + b_{r}^{L}\delta L + b_{r}^{D}\delta D + c_{r}^{T_{\tau}}\delta T_{\tau} = 0, \qquad (11.16)$$

where coefficients

$$a_{r}^{\dot{m}_{\tau}} = -1; \quad a_{r}^{\dot{m}_{\kappa.r}} = 1 - f(\bar{\varphi}, \bar{K}); \quad a_{r}^{p_{\kappa}} = \frac{\nu}{1-\beta}f(\bar{\varphi}, \bar{K});$$

$$b_{r}^{L} = b_{r}^{\rho_{\tau}} = b_{r}^{u_1} = \frac{1}{1-\beta}f(\bar{\varphi}, \bar{K}); \quad b_{r}^{D} = \frac{1-2\beta}{1-\beta}f(\bar{\varphi}, \bar{K});$$

$$c_{r}^{T_{\tau}} = \frac{\bar{T}_{\tau}}{\bar{u}_1}\frac{\partial u_1}{\partial T_{\tau}}\frac{1}{1-\beta}f(\bar{\varphi}, \bar{K}).$$

In expressions for coefficients function

$$f(\bar{\varphi}, \bar{K}) = (1+\bar{\varphi}\bar{K})\left[1 - \left(\frac{\bar{\varphi}\bar{K}}{1+\bar{\varphi}\bar{K}}\right)^{1-\beta}\right]. \qquad (11.17)$$

From GRD chamber equations (11.15) and (11.16), as a particular case corresponding to $\bar{K}=0$, $\bar{\alpha}=0$ and $\beta=0$, one easily obtains solid propellant thrust chamber equations:

---

* Designations a have been adopted for coefficients with deviations in operating parameters and process characteristics, b -- for coefficients with deviations in structural dimensions and characteristics, c -- for coefficients with deviations in environmental factors affecting the process.

$$\left.\begin{aligned}\delta p_к - \delta\dot{m}_т + \delta F_{кр} + \delta\varphi_c - \frac{1}{2}\frac{\bar{T}_т}{R\bar{T}_к}\frac{\partial(RT_к)}{\partial T_т}\delta T_т = 0;\\ \nu\delta p_к - \delta\dot{m}_т + \delta u_1 + \delta\rho_т + \delta D + \delta L + \frac{T_т}{u_1}\frac{\partial u_1}{\partial T_т}\delta T_т = 0.\end{aligned}\right\} \quad (11.18)$$

11.4. Equations of Liquid Component Supply System Equipment

These include the following equations: turbine; pumps; turbine gas generator; pressure accumulator; propellant and gas lines; etc.

One can expect that all these components and elements of a GRD liquid propellant component supply system will be similar to corresponding equipment of liquid-propellant rocket motor supply systems, which should also be reflected in similarity of the corresponding equations. Transforming previous equations, taking into account this equation of ZhRD equipment, to a form which is more convenient and more frequently utilized for hybrid motor equipment, we obtain the following equations.

Turbine Equations

As already noted, the most probable in a GRD is employment of liquid component supply system open layouts, the turbines of which can operate with large pressure differentials and in connection with this can be designed as constant-pressure turbines.

In this case the basic turbine equation which relates deviations in turbine output with deviations in working medium flow rate and other parameters influencing output has the form

$$a_т^N\delta N_т + a_т^{m_{тг}}\delta\dot{m}_{тг} + a_т^n\delta n + a_т^{RT_г}\delta(RT_г) + \\ + b_т^{F_{кр.т}}\delta F_{кр.т} + b_т^{F_{а.г}}\delta F_{а.г} + b_т^{\eta_e}\delta\eta_e = 0, \quad (11.19)$$

where

$$a_т^{m_{тг}} = -a_т^N = b_т^{\eta_e} = 1;\quad a_т^n = A_т;\quad a_т^{RT_г} = 1 - \frac{A_т}{2};$$

$$b_т^{F_{кр.г}} = -b_т^{F_{а.г}} = \frac{2(1-n_а)}{2\pi_т^{\frac{n_а-1}{n_а}} - 1};$$

$$A_т = 1 - \mu_т x\frac{\mu_т + \frac{\psi_т\cos\beta_2}{B_т}(\varphi_т\sqrt{1-\rho_т}\cos\alpha_1 - \mu_т^2 x)}{\varphi_т\sqrt{1-\rho_т}\cos\alpha_1 - \mu_т^2 x + \mu_т\psi_т\cos\beta_2 B_т};$$

$$B_т = \sqrt{\varphi_т^2 - 2x\varphi_т\cos\alpha_1 + x^2}.$$

Pump Equations

Pump equations determine the relationship between deviations in pump output and pressure and various factors affecting these principal pump parameters:

$$a_{\text{н}}^{\Delta p_{\text{н}}}\delta\,\Delta p_{\text{н}} + a_{\text{н}}^{m_{\text{н}}}\delta\dot{m}_{\text{н}} + a_{\text{н}}^{n}\delta n + b_{\text{н}}^{H_0}\delta H_0 + c_{\text{н}}^{\rho_{\text{ж}}}\delta\rho_{\text{ж}} = 0; \quad (11.20)$$

$$a_{N}^{N_{\text{н}}}\delta N_{\text{н}} + a_{N}^{m_{\text{н}}}\delta\dot{m}_{\text{н}} + a_{N}^{n}\delta n + b_{N}^{H_0}\delta H_0 + b_{N}^{\eta}\delta\eta_{\text{н}} + c_{N}^{\rho_{\text{ж}}}\delta\rho_{\text{ж}} = 0, \quad (11.21)$$

where coefficients

$$a_{\text{н}}^{\Delta p_{\text{н}}} = -b_{\text{н}}^{H_0} = -1; \quad a_{\text{н}}^{m_{\text{н}}} = \frac{\operatorname{tg}\beta_{\text{н}}}{\operatorname{tg}\alpha_{\text{н}}}; \quad a_{\text{н}}^{n} = 2 - \frac{\operatorname{tg}\beta_{\text{н}}}{\operatorname{tg}\alpha_{\text{н}}};$$

$$c_{\text{н}}^{\rho_{\text{ж}}} = 1 - \frac{\operatorname{tg}\beta_{\text{н}}}{\operatorname{tg}\alpha_{\text{н}}}; \quad a_{N}^{N_{\text{н}}} = b_{N}^{\eta} = -b_{N}^{H_0} = -1;$$

$$a_{N}^{m_{\text{н}}} = 1 + \frac{\operatorname{tg}\beta_{\text{н}}}{\operatorname{tg}\alpha_{\text{н}}} - \frac{\operatorname{tg}\beta_{\eta}}{\operatorname{tg}\alpha_{\eta}};$$

$$a_{N}^{n} = 2 + \frac{\operatorname{tg}\beta_{\eta}}{\operatorname{tg}\alpha_{\eta}} - \frac{\operatorname{tg}\beta_{\text{н}}}{\operatorname{tg}\alpha_{\text{н}}}; \quad c_{N}^{\rho_{\text{ж}}} = \frac{\operatorname{tg}\beta_{\eta}}{\operatorname{tg}\alpha_{\eta}} - \frac{\operatorname{tg}\beta_{\text{н}}}{\operatorname{tg}\alpha_{\text{н}}};$$

δH_0 -- pump manufacturing error as regards pressure (determined during pump tests under nominal operating conditions).

The quantities controlled in the pump equations and the coefficients of these equations are linked with experimental pump pressure characteristics (Figure 11.10) plotted in coordinates

$$\frac{Q_{\text{н}}}{n} \div \frac{H}{n^2},$$

where $Q_{\text{н}}$ -- volumetric per-second liquid flow rate and H^{n} -- pressure generated by the pump

$$(Q_{\text{н}} = \dot{m}_{\text{н}}/\rho_{\text{ж}};\ H = \Delta P_{\text{н}}/\rho_{\text{ж}}).$$

Points A (on the pressure characteristic curve) and B (on the efficiency line) correspond to nominal conditions.

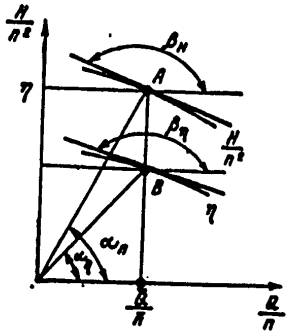

Figure 11.10. Pump Pressure Characteristic Curve

Line Equations

The hydraulic line equation links deviations in flow rate and line pressure drop with deviations in density of the liquid and dimensions (and shape) of the hydraulic line:

$$a_M^{\dot m_M}\delta\dot m_M + a_M^{\Delta p_M}\delta\Delta p_M + b_M^{\xi_M}\delta\xi_M + c_M^{\rho_{\text{ж}}}\delta\rho_{\text{ж}} = 0, \qquad (11.22)$$

where

$$a_M^{\dot m_M} = 2;\quad a_M^{\Delta p_M} = -b_M^{\xi_M} = c_M^{\rho_{\text{ж}}} = -1.$$

In the line equation we designate with ξ_M a synthesized line resistance coefficient which takes into account all resistances throughout the line.

GRD gas lines should be figured with special equations only in those cases where gas flow rates and pressure losses in these lines are sufficiently large, which occurs, for example, in closed-layout motors. Since such designs are little probable in GRD applications, henceforth gas line equations will not be separately considered.

Pressure Accumulator Equations

Pressure accumulator equations should make it possible to determine tank pressure change.

A gas pressure accumulator equation is written on analogy with the equation for a ZhRD gas pressure accumulator, in the form

$$a_a^{p_б}\delta p_б + b_a^{p_{г.н}}\delta p_{г.н} + b_a^{p_р}\delta p_р = 0, \qquad (11.23)$$

where $p_б$ -- pressure in the propellant component tank; $p_{г.н}$ -- initial pressure in the accumulator tank; $p_р$ -- pressure at reducer outlet.

The values of coefficients in equation (11.23) can be determined just as for equation (3.40), which describes the operation of a ZhRD gas pressure accumulator (see 3.5).

The type of cartridge pressure accumulator equation depends on the operating mode of the PAD [cartridge pressure accumulator]. If the accumulator is designed for supercritical gas flow from the chamber, PAD equations are written in the form of an RDTT equation, that is, in the form of equations (11.18). From these equations one obtains gas flow rate deviation, which can be utilized for determining deviation in pressure $p_б$ with the tank gas mass state equation.

If pressure in the PAD can be assumed equal to pressure in the tank, PAD equations are written in the form of (3.41).

And finally, if a hybrid pressure accumulator is employed, its operation is described by its own system of equations, which makes it possible to determine

the flow rate and parameters of gas entering the motor tank. This system includes chamber equations in the form (11.15) and (11.16). Pressure change in the tank is connected with change in gas flow rate through an equation of state.

Turbine Gas Generator Equations

When examining motor characteristics, changes in rate of gas flow into the turbine and motor efficiency should be obtained from gas generator equations.

For a generator operating on a solid-component propellant, the equations are in the form of PAD equations with supercritical gas flow, that is, the form (11.18).

Everything stated above for an analogous pressure accumulator applies to a generator operating on a hybrid propellant.

If a GRD design employs a liquid monopropellant generator, hydrogen peroxide, for example, change in gas flow rate to the turbine is equal to change in propellant (peroxide) flow rate,

$$\delta\dot{m}_{\Gamma\Gamma} = \delta\dot{m}_{H_2O_2}.$$

Equations of peroxide feed into the reactor should be written to determine $\delta m_{H_2O_2}$.

Change in gas capability to perform work is caused by changes in peroxide concentration and temperature, and can be obtained with the relation

$$\delta(RT)_{\Gamma\Gamma} = f(\delta K_{H_2O_2},\ \delta T_{H_2O_2}).$$

Equations of Thrust Characteristics

Deviations in motor thrust and specific thrust impulse are obtained from equations of thrust characteristics. These equations can be borrowed from ZhRD theory in the form of equations (3.45) and (3.46).

Considering that for GRD, which as a rule have only one propellant pump and relatively low combustion chamber pressure, required gas flow rate to the turbine will be substantially less than for a ZhRD of equal thrust, in these equations one can disregard terms which take into account deviations in thrust and thrust impulse of the turbine exhaust nozzles.* In this instance deviation in thrust is equal to deviation of combustion chamber pressure.

* Chapter subsection 1.2 stated that for a ZhRD without afterburning relative gas flow rate through the turbine exhaust nozzles comprises (2-8)% of total flow rate. Taking this into account, one can expect that in hybrid motors this consumption rate will be in the order of 1%, which results in extremely little influence of change in the thrust characteristics of the turbine exhaust nozzles on change in thrust characteristics of the motor as a whole.

Chapter 12. STATIC CHARACTERISTICS OF HYBRID ROCKET MOTORS

12.1. Influence of External and Internal Factors (Disturbances) on Operating Parameters of Hybrid Rocket Motors

Just as for liquid or solid propellant rocket motors, GRD operating conditions depend on quite a number of factors. Determination of deviations of operation parameters with change in these factors (or, as they say, with the occurrence of disturbances) constitutes one of the principal tasks of investigation of motor static characteristics.

In the majority of practical cases this task can be accomplished with utilization of a system of static equations of GRD equipment in the small deviations specified above.

We shall examine two examples of estimate of the influence of various disturbances on the operating conditions (parameters) of a hybrid rocket motor.*

1. Influence of Disturbances on Operating Conditions of a GRD With a Gas Pressurization Liquid Propellant Component Supply System

Figure 12.1 contains a diagram of a GRD. This motor employs a combustion chamber of the most general type, with liquid component being fed both into the charge cavity and into the nozzle-adjacent space (afterburner). Division of the flow of liquid component (flow rate $\dot{m}_{ж}$) into two parts ($\dot{m}_{ж.р}$ and $\dot{m}_{ж.д}$) takes place at point N. Ignoring pressure losses in the charge cavity, that is, assuming that pressure in the afterburner is equal to pressure at the head of the combustion chamber, and designating this pressure by p_k, we determine that pressure drops in the line branches from N to the afterburner and head of the combustion chamber are equal, that is,

* The material for these examples was borrowed from a book by Ye. B. Volkov, G. Yu. Mazin, and Yu. A. Shishkin, "Raketnyye dvigateli na kombinirovannom toplive" [Combined Propellant Rocket Motors], Mashinostroyeniye, 1973.

$$(\Delta p_{N-k})_{\dot{m}_{ж.г}} = (\Delta p_{N-k})_{\dot{m}_{ж.д}} = \Delta p_{N-k}. \qquad (12.1)$$

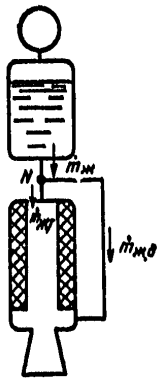

Figure 12.1. Diagram of GRD With Gas Pressurization Liquid Fuel Component Supply System

The pressure accumulator, which forces propellant component from the tank, is designated in Figure 12.1 in general form. In order not to complicate analysis of GRD characteristics by including in them accumulator characteristcs, we shall place tank pressure deviation $\delta p_б$ among the disturbing factors specified for calculating deviations in motor parameters. In this case the system of equations for the GRD in the diagram will be as follows:

$$\left.\begin{aligned}
&1.\ a_к^{p_к}\delta p_к + a_к^{\dot{m}_ж}\delta\dot{m}_ж + a_ж^{\dot{m}_т}\delta\dot{m}_т + b_к^{F_{кр}}\delta F_{кр} + b_к^{\varphi_c}\delta\varphi_c = 0;\\
&2.\ a_т^{\dot{m}_т}\delta\dot{m}_т + a_т^{\dot{m}_{ж.г}}\delta\dot{m}_{ж.г} + a_т^{p_к}\delta p_к + b_т^{L}\delta L + b_т^{u_1}\delta u_1 +\\
&+ b_т^{\rho_т}\delta\rho_т + b_т^{D}\delta D = 0;\\
&3.\ a_{\dot{m}_ж}^{\dot{m}_ж}\delta\dot{m}_ж + a_{\dot{m}_ж}^{\dot{m}_{ж.г}}\delta\dot{m}_{ж.г} + a_{\dot{m}_ж}^{\dot{m}_{ж.д}}\delta\dot{m}_{ж.д} = 0;\\
&4.\ a_M^{\dot{m}_ж}\delta\dot{m}_ж + a_M^{\Delta p_б - N}\delta\Delta p_{б-N} + b_M^{\xi_б - N}\delta\xi_{б-N} + c_M^{\rho_ж}\delta\rho_ж = 0,\\
&5.\ a_M^{\dot{m}_{ж.г}}\delta\dot{m}_{ж.г} + a_M^{\Delta p_{N-k}}\delta\Delta p_{N-k} + b_M^{\xi_{N-к.г}}\delta\xi_{N-к.г} +\\
&+ c_M^{\rho_ж}\delta\rho_ж = 0;\\
&6.\ a_M^{\dot{m}_{ж.д}}\delta\dot{m}_{ж.д} + a_M^{\Delta p_{N-k}}\delta\Delta p_{N-k} + b_M^{\xi_{N-к.д}}\delta\xi_{N-к.д} +\\
&+ c_M^{\rho_ж}\delta\rho_ж = 0;
\end{aligned}\right\} \qquad (12.2)$$

$$
\left.
\begin{aligned}
&7.\ a_{\delta-N}^{\Delta p_{\delta-N}}\Delta p_{\delta-N}+a_{\delta-N}^{p_N}\delta p_N+b_{\delta-N}^{p_\delta}\delta p_\delta=0;\\
&8.\ a_{N-k}^{\Delta p_{N-k}}\delta\Delta p_{N-k}+a_{N-k}^{p_N}\delta p_N+a_{N-k}^{p_k}\delta p_k=0;\\
&9.\ a_k^K\delta K+a_k^{m_т}\delta\dot m_т+a_k^{m_ж}\delta\dot m_ж=0;\\
&10.\ a_I^{I_y}\delta I_y+a_I^K\delta K=0;\\
&11.\ a_т^P\delta P+a_т^{p_k}\delta p_k=0.
\end{aligned}
\right| \quad (12.2)
$$

In system of equations (12.2):

equations (1) and (2) are equations of GRD chamber with component fed to the head of the chamber and afterburner, written in the form (11.15) and (11.16);

equation (3) was obtained from relation $\dot m_ж=\dot m_{ж.т}+\dot m_{ж.д}$ and is a liquid component flow rate balance equation. In this equation

$$a_{m_ж}^{m_ж}=-1;\ a_{m_ж}^{m_{ж.т}}=\bar\varphi;\ a_{m_ж}^{m_{ж.д}}=1-\bar\varphi,$$

where $\bar\varphi=\bar{\dot m}_{ж.т}/\bar{\dot m}_ж$.

equations (4)-(6) are propellant line equations; the first of them applies to line segment "tank-point N," the second -- to line segment "point N-chamber head," and the third -- to segment "point N-afterburner";

equations (7) and (8) are equations of pressure balance on these same line segments taking into account (12.1); in these equations p_N -- pressure at point N; the coefficients comprise:

$$a_{\delta-N}^{\Delta p_{\delta-N}}=a_{N-k}^{\Delta p_{N-k}}=-1;\ b_{\delta-N}^{p_\delta}=\frac{\bar p_\delta}{\Delta\bar p_{\delta-N}};$$

$$a_{\delta-N}^{p_N}=-\frac{\bar p_N}{\Delta\bar p_{\delta-N}};\ a_{N-k}^{p_N}=\frac{\bar p_N}{\Delta\bar p_{N-k}};$$

$$a_{N-k}^{p_k}=-\frac{\bar p_k}{\Delta\bar p_{N-k}};$$

equation (9) was obtained from ratio $K=\dot m_ж/\dot m_1$;

$$a_k^k=a_k^{m_т}=-a_k^{m_ж}=1;$$

equations (10) and (11) are equations of thrust characteristics; in these equations:

$$a_I^{I_y}=a_т^P=-a_т^{p_k}=1;\ a_I^k=-\left(\frac{\partial I_y}{\partial K}\right)\frac{\bar K}{\bar I_y}.$$

As is evident from system of equations (12.2), operation of a GRD, even of the extremely simple arrangement taken for analysis, and with a number of simplifying assumptions (pressure accumulator equations are not considered; it is assumed that there are no pressure changes along the solid propellant charge cavity, there is no control or adjustment, etc), is described by a system of equations which is significantly more complex than solid-propellant motor equations and which approximately corresponds in complexity to a system of equations for a ZhRD with a similar propellant supply system.*

System of equations (12.2) is a closed system, which contains 11 unknown deviations of GRD operating conditions parameters from their nominal values:

$$\delta p_к,\ \delta \dot{m}_ж,\ \delta \dot{m}_т,\ \delta \dot{m}_{ж.г},\ \delta \dot{m}_{ж.д},$$
$$\delta p_N,\ \delta \Delta p_{б-N},\ \delta \Delta p_{N-к},\ \delta K,\ \delta I_y,\ \delta P.$$

The following deviations are examined in this instance as disturbances which cause change in motor operating conditions:

deviation in dimensions of solid component charge δL, δD, and coefficient in the law of its rate of gasification δu_1;

deviation in size of nozzle throat area and coefficient of losses $\delta F_{кр}$, $\delta \varphi_c$;

deviation in propellant component densities $\delta \rho_т$, $\delta \rho_ж$;

deviation in tank pressure $\delta p_б$, due to error in accumulator operation or change in G-loads acting on the liquid component during rocket flight;

deviation in coefficients of hydraulic losses in the liquid component supply lines

$$\delta \xi_{б-N};\ \delta \xi_{N-кг};\ \delta \xi_{N-кд}.$$

The values of the coefficients in the equations of system (12.2) are determined primarily by the values of the following dimensionless coefficients, indices and ratios specified for rated (nominal) motor operating conditions:

$$\overline{K},\ \nu,\ \beta,\ \overline{\varphi},\ \frac{\bar{p}_б}{\Delta \bar{p}_{б-N}},\ \frac{\bar{p}_к}{\Delta \bar{p}_{N-к}}.$$

* The system of equations for a ZhRD with a gas pressurization propellant supply system would be more complex than system (12.2) by inclusion of additional equations which describe operation of the feed line for the second liquid component, but on the other hand it would be distinguished by greater simplicity of combustion chamber equations.

In addition, the values of some coefficients are determined by the value of derivative functions RT_k ($T_{ж}$, T_T) and I_y (K) at points corresponding to nominal GRD operating conditions.

Solution of system (12.2) with preselected values of parameters of nominal operating conditions and adopted disturbance values makes it possible to determine all deviations of motor characteristics. As an illustration, Table 12.1 contains the results of calculation of coefficients of influence of various disturbances on principal GRD parameters.*

Table 12.1.

№ по пор.	1 Возмущения	2 Коэффициенты влияния для параметров				
		$\delta p_к$	$\delta \dot{m}_ж$	$\delta \dot{m}_т$	δK	δI_y
1	$\delta F_{кр}$	—0,410	+0,630	+0,394	+0,236	—0,047
2	$\delta \varphi_c$	—0,410	+0,630	+0,394	+0,236	—0,047
3	δu_1	+0,073	—0,113	+1,000	—1,113	—0,222
4	$\delta \rho_т$	+0,073	—0,113	+1,000	—1,113	—0,222
5	δL	+0,073	—0,113	+1,000	—1,113	—0,222
6	δD	—0,22	+0,034	—0,300	+0,334	—0,067
7	$\delta \rho_ж$	+0,192	+0,205	+0,128	+0,077	—0,015
8	$\delta \rho_б$	+0,782	+0,835	+0,522	+0,313	—0,062
9	$\delta \xi_{бб-N}$	—0,044	—0,048	—0,030	—0,018	—0,004
10	$\delta \xi_{бN-к.д}$	—0,025	—0,038	+0,039	—0,077	—0,015
11	$\delta \xi_{бN-к.г}$	—0,122	—0,119	—0,137	+0,018	—0,004

Key:
1. Disturbances
2. Coefficients of influence for parameters

* Coefficient of influence is defined as a number which indicates the magnitude of motor parameter deviation caused by a single disturbance, that is quantity $\delta p_к/\delta F_{кр}$; $\delta \dot{m}_ж/\delta F_{кр}$, etc.

For calculations we have assumed

$$\bar{p}_K = 40 \cdot 10^5 \text{ Па}; \quad \bar{K} = 5; \quad \beta = 0{,}65; \quad \nu = 0; \quad \bar{\varphi} = 0{,}8;$$
$$\Delta\bar{p}_{G-N} = 3 \cdot 10^5 \text{ Па}; \quad \Delta\bar{p}_{N-k} = 10 \cdot 10^5 \text{ Па};$$
$$\frac{\bar{K}}{I_y}\frac{\partial I_y}{\partial K} = 0{,}2; \quad \frac{\partial (RT_K)}{\partial K} = \frac{\partial (RT_K)}{\partial T_{\text{ж}}} = \frac{\partial (RT_K)}{\partial T_{\text{т}}} = 0.$$

In calculating deviations in specific thrust impulse δI_y it was assumed that a deviation in the coefficient of ratio of components K in either direction from nominal value results in an impulse decrease; this is equivalent to the assumption that nominal conditions correspond to maximum value I_y.

The calculation results contained in Table 12.1 enable one to draw certain conclusions on the characteristics of a GRD laid out as specified.

An increase in nozzle throat area causes, just as in an RDTT, a decrease in chamber pressure, but to a lesser degree, which is due to an increase in liquid component flow rate with a decrease p_k, that is, the presence of an additional factor opposing change in chamber pressure.

In the cited example gas formation of the charge also increases together with an increase in the rate of consumption of the liquid propellant component. This occurs because we have adopted a law of gasification whereby the rate of gas formation is independent of pressure ($\nu = 0$) and at the same time depends significantly on liquid component flow rate ($\beta = 0.65$).

An increase in charge length, density of the solid component, or its rate of gasification (coefficient u_1) leads to one and the same consequences: the rate of consumption of the solid component increases, which leads in turn to increased combustion chamber pressure and, as a consequence, to a certain decrease in liquid component flow into the chamber. Differing-sign changes in consumption of propellant components produce significant change in the coefficient of consumption ratio and corresponding change in specific thrust impulse.

Deviation in charge cavity diameter differently affects motor parameters. An increase in diameter causes a reduced rate of gasification which is more appreciable than the increase in gas formation surface, and therefore solid component consumption decreases. This results in a combustion chamber pressure drop, but to a lesser degree than decrease in charge gas formation.

An increase in tank pressure quite appreciably affects motor parameters. It causes an increase in liquid component flow rate, which leads to increased charge gas formation and combustion chamber pressure.

Changes in the coefficients of line hydraulic resistances produce in most cases opposite-sign changes in all operation parameters. An exception is the case of change in hydraulic resistance in the line through which liquid component is fed to the afterburner. With an increase in this resistance there can be an increase (that is, a like-sign change) in charge gas formation. This is due to the fact that in this case, in spite of a decrease in overall liquid component flow rate ($\delta \dot{m}_{ж} < 0$), its flow into the charge cavity may increase, which leads to an increase in the solid component gasification rate. This feature of a GRD of the design under discussion can be utilized to perform motor tuning and adjustment.

2. Maximum Burning Time

It follows from Table 12.1 that consumption of GRD propellant components is determined by the density of the liquid component. A density increase by 1% in our illustration produces an increase in the mass consumption of both components: liquid by approximately 0.2%, and solid by 0.13%. The density of the liquid component is determined by its temperature, and therefore propellant component consumptions are dependent on temperature. This produces change in other motor parameters, including maximum burning time.

We shall designate with M_T and $M_{ж}$ masses of solid and liquid propellant components in a motor prior to ignition (mass of the solid component charge and mass of liquid propellant on board). Component burnup time with consumption rates $\dot{m}_{ж}$ and $\dot{m}_T$ will be

$$\tau_т = \frac{M_т}{\dot{m}_т} \qquad \text{and} \qquad \tau_{ж} = \frac{M_{ж}}{\dot{m}_{ж}},$$

and their deviations with consumption deviations

$$\delta\tau_т = \delta M_т - \delta\dot{m}_т; \quad \delta\tau_{ж} = \delta M_{ж} - \delta\dot{m}_{ж}.$$

An analysis of the influence of various factors on engine burning time can be performed on the basis of these relations.

In the case we are examining, that is, when only the temperature of the liquid component can change (in the process of motor storage),

$$\delta M_т = \delta M_ж = 0$$

and $$\delta\tau_т = -\delta\dot{m}_т; \quad \delta\tau_ж = -\delta\dot{m}_ж.$$

With an increase in the temperature of the liquid component, its density decreases, as do mass flow and consumption rates, in conformity with Table 12.1. Consequently, a temperature increase increases component consumption time, and the increase is more rapid for the liquid component (0.2%) than for the solid (0.13%). Change in maximum motor burning time for our example is illustrated in Figure 12.2.

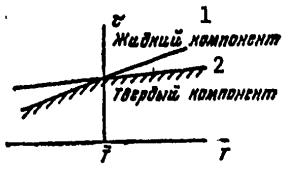

Figure 12.2. Relationship Between GRD Propellant Component Consumption Time and Temperature of the Liquid Component

Key:
1. Liquid component
2. Solid component

If the motor is designed to operate at a temperature $T=\bar{T}$ it is natural to assume that for this temperature: $\tau_т = \tau_ж$.

When $T \geq \bar{T}$ $\tau_ж > \tau_т$, and when $T < \bar{T}$ $\tau_ж < \tau_т$.

Under these conditions liquid component consumption time will be the time limiting normal (with utilization of both components) motor operation at temperatures below the rated figures, while at temperatures above the rated figure it will be charge consumption time.

3. Influence of Disturbances on Operating Conditions of a GRD With a Pumped Liquid Component Supply System

As an example we have specified deviations in the operating parameters of an open-arrangement GRD with a hybrid propellant turbine gas generator

(Figure 12.3). Motor control capability is not figured in. Liquid component flow from the tank through the pump ($\dot{m}_{\text{Н}}$) at point 2 is distributed into the following components: flow to the gas generator $\dot{m}_{\text{ж.гг}}$ and flow to the combustion chamber $\dot{m}_{\text{ж}}$. At point 1 flow $\dot{m}_{\text{ж}}$ in turn divides into two flows -- to the chamber head $\dot{m}_{\text{ж.г}}$ and to the afterburner $\dot{m}_{\text{ж.А}}$. As in the preceding example, it is assumed that pressure remains unchanged along the length of the charge cavity, that is,

$$\Delta p_{1\text{-к.г}} = \Delta p_{1\text{-к.А}} = \Delta p_{1\text{-к}}.$$

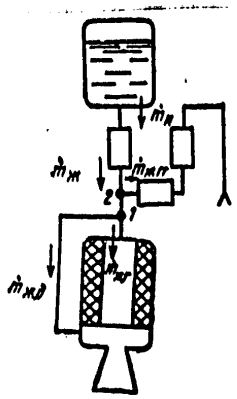

Figure 12.3. Diagram of GRD With a Pumped Liquid Propellant Component Supply System

Key:

1. Point of division of flow of liquid component to combustion chamber
2. Takeoff point where liquid component is fed to gas generator

Table 12.2 contains the results of calculation of coefficients of influence of various disturbances on the principal parameters of the motor under discussion.

For calculations we have assumed the following:

$$\bar{p}_{\text{к}} = 100 \cdot 10^5 \text{ Па};\ \bar{p}_{\text{г}} = 70 \cdot 10^5 \text{ Па};\ \bar{p}_{\text{б}} = 5{,}5 \cdot 10^5 \text{ Па};$$

$$\Delta\bar{p}_{\text{б-}N} = 0{,}5 \cdot 10^5 \text{ Па};\ \Delta\bar{p}_{N\text{-}2} = 20 \cdot 10^5 \text{ Па};\ \Delta\bar{p}_{1\text{-к}} = 10 \cdot 10^5 \text{ Па};$$

$$\bar{K} = 5;\ \bar{K}_{\text{гг}} = 40;\ \bar{\alpha}_{\text{к}} = 0{,}97;\ \nu = 0;\ \varphi = 0{,}8;\ \beta = 0{,}65;\ A_{\text{т}} = 0{,}75;$$

$$\frac{\operatorname{tg}\beta_{\text{н}}}{\operatorname{tg}\alpha_{\text{н}}} = -0{,}25;\ \frac{\operatorname{tg}\beta_{\eta}}{\operatorname{tg}\alpha_{\eta}} = 0;\ \frac{\bar{K}}{\bar{I}_{\text{y}}}\frac{\partial I_{\text{y}}}{\partial K} = 0{,}2.$$

Table 12.2.

№ по пор.	1 Возмущения	2 Коэффициенты влияния				
		$\delta p_к$	$\delta \dot{m}_ж$	$\delta \dot{m}_т$	δK	$\delta I_у$
1	$\delta F_{кр}$	−1,000	−0,018	0	−0,018	−0,004
2	$\delta \varphi_с$	−1,000	−0,018	0	−0,018	−0,004
3	δL	+0,178	+0,003	+1,066	−1,063	−0,212
4	δu_1	+0,178	+0,003	+1,066	−1,063	−0,212
5	$\delta \rho_т$	+0,178	+0,003	+1,066	−1,063	−0,212
6	δD	−0,053	−0,001	−0,321	+0,320	−0,064
7	$\delta F_{кр.г}$	+0,100	+0,118	+0,067	+0,041	−0,008
8	$\delta F_{ат}$	+0,307	+0,325	+0,205	+0,120	−0,024
9	$\delta \varphi_{сг}$	+0,100	+0,118	+0,067	+0,041	−0,008
10	$\delta L_г$	+0,016	+0,017	+0,011	+0,006	−0,001
11	$\delta u_{1г}$	+0,016	+0,017	+0,011	+0,006	−0,001
12	$\delta \rho_{т.г}$	+0,016	+0,017	+0,011	+0,006	−0,001
13	$\delta D_г$	−0,005	−0,005	−0,003	−0,002	0
14	δH_0	−0,341	−0,363	−0,227	−0,136	−0,027
15	$\delta \eta_к$	+1,023	+1,084	+0,685	+0,409	−0,082
16	$\delta \eta_т$	+1,023	+1,084	+0,685	+0,409	−0,082
17	$\delta \rho_б$	+0,030	+0,032	+0,020	+0,012	−0,002
18	$\delta \xi_{б-М}$	−0,003	−0,003	−0,002	−0,001	0
19	$\delta \xi_{М-з}$	−0,012	−0,012	−0,008	−0,004	−0,001
20	$\delta \xi_{з-1}$	0	+0,002	+0,001	+0,001	0
21	$\delta \xi_{1-к.г}$	−0,010	+0,001	−0,062	+0,062	−0,012
22	$\delta \xi_{1-к.д}$	+0,002	0	+0,012	−0,012	−0,002
23	$\delta \xi_{з-тг}$	−0,145	−0,155	−0,097	−0,058	−0,012
24	$\delta \rho_ж$	+0,974	+1,041	+0,65	+0,390	−0,078

Key:
1. Disturbances
2. Coefficients of influence

The reaction of a GRD with liquid component pumped supply to the effect of various disturbances differs from that which occurred in a motor with a gas pressurization system. For example, change in nozzle throat area in a GRD with a pump system produces practically the same combustion chamber pressure change, while in the preceding example the corresponding influence factor was only 0.41. In a motor with a pump supply system component consumption rates change little, while they increased quite appreciably for a motor with a gas pressurization system. These differences are connected with the fact that combustion chamber pressure changes in the motor arrangements we have examined differently influence the liquid component consumption rate -- in the first of the arrangements being compared this influence was significantly greater. For this same reason one also observes a difference in the reaction of motors to identical changes in a number of other factors, such as the dimensions of the solid propellant charge in the thrust chamber and coefficient u_1 for this charge.

For GRD with a pumped supply system the influence of tank pressure change on motor parameters is much less than for a motor with a gas pressurization system, since in this case this pressure is of itself small and plays a minor role in producing the overall pressure which determines the flow rate of the liquid component.

Changes in densities of the propellant components exert qualitatively identical influences on the operating parameters of motors of both types, although quantitatively the coefficients of influence differ.

Influences which are characteristic only of GRD with a liquid component pumped supply system include deviations in characteristics and dimensions of turbine, pump, gas generator and hydraulic line which feeds liquid component to the generator (numbers 7-16, 19 in Table 12.2). Motor parameters are most strongly influenced by deviations in pump and turbine efficiency. Changes in efficiency produce changes in output expended on pumping liquid component, which produces a change in rate of flow, and as a consequence also in all other motor operation parameters.

One's attention is drawn by the relatively little influence on motor parameters by changes in the dimensions of the gas generator solid component charge. This feature of the motor under discussion is connected with the fact that consumption of solid component in the gas generator comprises a very small part of total gas consumed on the turbine

$$K_{rr} = \frac{\dot{m}_{grr}}{\dot{m}_{trr}} = 40.$$

Among deviations in coefficients of hydraulic resistances, the greatest influence on motor operation parameters is exerted by deviation in the coefficient of resistance of the line through which liquid component is fed to the gas generator. An increase in this resistance leads to a decrease in flow of gas into the turbine, a decrease in turbine output and, as a consequence, decreased propellant component flow and consumption rate as well as combustion chamber pressure.

Deviations in flow and consumption rates of liquid and solid components depend on the density of the liquid component unequally. Therefore in the given GRD arrangement change in temperature of the liquid component may lead to burnup of the propellant components at different times.

Nonsimultaneous burnup of the propellant components can also occur in the remaining cases, where under the influence of any disturbances there occur appreciable deviations in the coefficient of ratio of consumption rates with constant charge mass. As is evident from Table 12.2, such values of δK occur under the effect of deviations δu_1, $\delta \rho_T$, $\delta \eta_H$, $\delta \eta_T$, etc.

The existence of substantial deviations in the coefficient of consumption rate ratios is also undesirable because it causes a reduction in specific thrust impulse.

12.2. Tuning and Adjustment of a Hybrid Rocket Motor

General statement of the problem of tuning and adjusting a GRD does not differ from its statement as applied to liquid or solid-propellant rocket

motors. Control devices can be utilized to correct some deviations of motor operating conditions from the rated figures. But even for controllable motors it is extremely desirable to reduce the variance in parameters which would occur without control. This is connected with the fact that introduction of a control system complicates a motor, as well as the fact that control cannot eliminate all harmful deviations of motor characteristics and is easier to effect with less variance in characteristics. In connection with this it is always desirable to reduce to a minimum variance in principal motor parameters, which is also the principal objective of motor tuning and adjustment. Depending on the function, design features and conditions of employment of a GRD, tuning and adjustment can have the purpose of minimizing the spread of various parameters. They include first and foremost the coefficient of ratio of propellant component consumption rates. Deviations in this parameter not only reduce specific thrust impulse but also lead, as was indicated above, to nonsimultaneous exhaustion of the propellant components, that is, essentially lead to a decrease in the quantity of propellant which can be productively utilized.

Combustion chamber pressure is a second parameter a decreased spread of which can be achieved by tuning and adjustment. If tuning also minimizes variances in the coefficient of propellant consumption rate ratio and combustion chamber pressure, this is also achieved by decreasing variance in thrust, which is simultaneously dependent on combustion chamber pressure (propellant consumption) and specific impulse (ratio of propellant components).

For a GRD with a pumped liquid component supply system and a two-component gas generator, on analogy with a ZhRD, it is highly desirable to reduce the variance in the coefficient of propellant component consumption rate ratio in the gas generator. Deviations in this coefficient from the rated value not only change turbine output but can also have an adverse effect on operating conditions of the gas generator proper, and particularly the turbine blades.

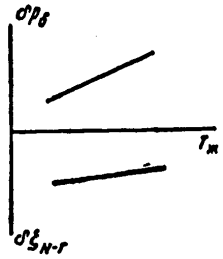

Figure 12.4. Relations for GRD Tuning and Adjustment

Deviations in characteristics of various motor components can be selected as influences with the aid of which tuning and adjustment is performed,

depending on the motor design. It is important that these deviations can be adjusted fairly easily and precisely during tuning and that the coefficients of their influence on the target motor parameters possess the requisite magnitude.

A system of GRD static equations of the type presented above is adopted as the basis of tuning calculations. The system is solved relative to quantities adopted as the influences adjusted in the tuning process. Then one introduces into this solution the values of those disturbances which should be compensated for during tuning, and then one figures the requisite values of the controlled influences.

Let us consider as an example tuning and adjustment of a GRD with a gas pressurization liquid component supply system, a diagram of which is contained in Figure 12.1. We shall adopt as tuning and adjustment tasks elimination of deviations of combustion chamber pressure and coefficient of propellant component ratio, that is, we shall state that as a result of tuning and adjustment we should achieve the following: $\delta p_k = \delta K = 0$.

Since motor tuning and adjustment should be performed on two parameters, it is also necessary to have two influencing characteristics. Let us adopt as such characteristics deviation in tank pressure and deviation in hydraulic resistance on the line through which the liquid component is fed to the combustion chamber head, that is, deviations $\delta p_{\text{г}}$ and $\delta_{N-\text{г}}$. As is evident from Table 12.2, precisely these influences have relatively large coefficients of influence on principal motor parameters, and at the same time they can be easily achieved from an engineering standpoint.

Assuming in system (12.1) $\delta p_k = 0$; $\delta K = 0$ and considering $\delta p_{\text{г}}$ and $\delta \xi_{N-\text{г}}$ unknown, we obtain a system of 19 equations with an equal number of unknowns. In order to solve the system, the values of those deviations of external and internal factors which must be compensated for as a result of tuning and adjustment should be prespecified. Just as when applied to a ZhRD, the problem can be solved either with utilization of statistical data or with employment of the results of tests on individual motor components. For GRD which are designed to be employed under different temperature conditions, tuning and adjustment can be performed in two stages.

Deviations in design parameters and characteristics of solid propellant charge ($\delta F_{\text{кр}}$, δu_1, $\delta \xi_{N-\text{кз}}$, etc) are established at the plant where the motor is manufactured. These quantities are put into the system of equations and, solving this system, one obtains

$$\left.\begin{aligned} \delta p_{\text{б}} &= f_{p_{\text{б}}}(\delta \rho_{\text{ж}}) = f'_{p_{\text{б}}}(T_{\text{ж}}); \\ \delta \Delta \xi_{N-\text{г}} &= f_{\xi}(\delta \rho_{\text{ж}}) = f'_{\xi}(T_{\text{ж}}). \end{aligned}\right\} \qquad (12.3)$$

These relations determine the values of the parameters of tuning and adjustment in the function of liquid component temperature with those deviations of other disturbances which occur in the given motor (Figure 12.4). If the component temperature prior to motor ignition is known, then determining from (12.3) the requisite values for tank pressure (reducer adjustment) and hydraulic losses (adjustment of controllable hydraulic resistance), one can also reduce to a minimum deviations in the coefficient of component consumption rate ratio and combustion chamber pressure and, together with these, as indicated above, motor thrust as well.

BIBLIOGRAPHY

1. Alemasov, V. V.; Dregalin, A. F.; and Tishin, A. P. "Teoreiya raketnykh dvigateley" [Theory of Rocket Motors], Moscow, Mashinostroyeniye, 1968, 547 pages.

2. Barintsev, B. I., and Zvyagin, Yu. V. "Turbulentnyy pogranichnyy sloy na reagiruyushchey poverkhnosti" [Turbulent Boundary Layer on a Reactive Surface], Moscow, Nauka, 1975, pp 48-60.

3. Botvin, R. "Flight Tests of the Propulsion Units of the Apollo Lunar Module," VRT, No 3, 1970, pp 31-40.

4. Varfolomeyev, V. I.; Kopytov, M. I., et al. "Proyektirovaniye i ispytaniya ballisticheskikh raket" [Designing and Testing Ballistic Missiles], Moscow, Voyenizdat, 1970, 391 pages.

5. Volkov, Ye. B.; Golovkov, L. G.; and Syritsyn, T. A. "Zhidkostnyye raketnyye dvigateli" [Liquid-Propellant Rocket Motors], Moscow, Voyenizdat, 1970, 590 pages.

6. Volkov, Ye. B.; Sudakov, R. S.; and Syritsyn, T. A. "Osnovy teorii nadezhnosti raketnykh dvigateley" [Fundamentals of Theory of Reliability of Rocket Motors], Moscow, Mashinostroyeniye, 1974, 400 pages.

7. Volkov, Ye. B.; Mazing, G. Yu.; and Shishkin, Yu. N. "Raketnyye dvigateli na kombinirovannom toplive" [Combined-Propellant Rocket Motors], Moscow, Mashinostroyeniye, 1973, 184 pages.

8. Volodin, V. A. "Konstruktsiya i proyektirovaniye raketnykh dvigateley" [Construction and Design of Rocket Motors], Moscow, Mashinostroyeniye, 1971, 336 pages.

9. "Vspomogatel'nyye sistemy raketno-kosmicheskoy tekhniki" [Auxiliary Space-Rocket Hardware Systems], translated from English, I. V. Tishchukin, editor, Moscow, Mir, 1970, 168 pages.

10. Glikman, B. F. "Avtomaticheskoye regulirovaniye zhidkostnykh raketnykh dvigateley" [Automatic Control of Liquid-Propellant Rocket Motors], Moscow, Mashinostroyeniye, 1974, 396 pages.

11. Godai, T. "Flame Propagation in a Crack in a Rocket Motor Solid-Propellant Charge," VRT, No 6, 1970, pp 27-30.

12. "Charge Combustion in an Acceleration Field," VRT, No 4, 1974, pp 31-41.

13. "Two-Phase Flows in Rocket Motor Nozzles," VRT, No 7, 1974, pp 37-41.

14. Dobrovol'skiy, M. V. "Zhidkostnyye raketnyye dvigateli" [Liquid-Propellant Rocket Motors], Moscow, Mashinostroyeniye, 1968, 396 pages.

15. Dunin-Barkovskiy, I. V., and Smirnov, N. V. "Teoriya veroyatnostey i matematicheskaya statistika v tekhnike" [Probability Theory and Mathematical Statistics in Technology], Moscow, GITTL, 1955, 556 pages.

16. Makhin, V. A.; Prisnyakov, V. F.; and Belik, N. P. "Dinamika zhidkostnykh raketnykh dvigateley" [Dynamics of Liquid-Propellant Rocket Motors], Moscow, Mashinostroyeniye, 1969, 384 pages.

17. Makhin, V. A.; Milenko, N. P.; and Pron', L. V. "Teoreticheskiye osnovy eksperimental'noy otrabotki ZhRD" [Theoretical Principles of Experimental Development of Liquid-Propellant Rocket Motors], Moscow, Mashinostroyeniye, 1973, 282 pages.

18. Mitropol'skiy, A. K. "Tekhnika statisticheskikh vychisleniy" [Techniques of Statistical Calculations], Moscow, Nauka, 1971, 576 pages.

19. Miller, V. G., and Barrington, D. K. "Modern Methods of Calculating Interior Ballistic Characteristics of a Solid-Propellant Rocket Motor," VRT, No 1, 1970, pp 47-68.

20. Mayros, Dzh., and Sarlat, I. M. "Control of the Aftereffect Impulse of a Solid-Propellant Rocket Motor," VRT, No 6, 1976, pp 53-67.

21. Ovsyannikov, B. V., and Borovskiy, V. I. "Teoriya agregatov pitaniya zhidkostnykn raketnykh dvigateley" [Theory of Liquid-Propellant Rocket Motor Supply Systems], Moscow, Mashinostroyeniye, 1971, 540 pages.

22. Orlov, B. V., and Mazing, G. Yu. "Termodinamicheskiye i ballisticheskiye osnovy proyektirovaniya raketnykh dvigateley na tverdom toplive" [Thermodynamic and Ballistic Principles of Designing Solid-Propellant Rocket Motors], Moscow, Mashinostroyeniye, 1968, 298 pages.

23. Rayzberg, B. A.; Yerokhin, B. T.; and Samsonov, K. P. "Osnovy teorii rabochikh protsessov v raketnyykh sistemakh na tverdom toplive" [Fundamentals of Theory of Operating Processes in Solid-Propellant Rocket Systems], Moscow, Mashinostroyeniye, 1972, 367 pages.

24. Sorkin, R. Ye. "Gazotermodinamika raketnykh dvigateley na tverdom toplive" [Gas and Thermodynamics of Solid-Propellant Rocket Motors], Moscow, Nauka, 1967, 372 pages.

25. Fillips, B., and Tendzher, G. "Influence of Nonuniform Propellant Charge Temperature on the Ballistic Characteristics of a Solid-Propellant Rocket Motor," in the volume "Raketnaya tekhnika" [Rocket Technology], No 6, 1962, pp 49-68.

26. Shapiro, M. Ya.; Mazing, G. Yu.; and Prudnikov, N. Ye. "Teoriya raketnogo dvigatelya na tverdom toplive" [Theory of Solid-Propellant Rocket Motors], Moscow, Voyenizdat, 1966, 312 pages.

27. Shapiro, Ya. M.; Mazing, G. Yu.; and Prudnikov, N. Ye. "Osnovy proyektirovaniya raket na tverdom toplive" [Fundamentals of Solid-Propellant Rocket Design], Moscow, Voyenizdat, 1968, 364 pages.

28. Sharakshane, A. S., and Zheleznov, I. G. "Ispytaniya slozhnykh sistem" [Testing Complex Systems], Moscow, Vysshaya shkola, 1974, 184 pages.

29. Shishkov, A. A. "Gazodinamika porokhovykh raketnykh dvigateley" [Gas Dynamics of Solid-Propellant Rocket Motors], Moscow, Mashinostroyeniye, 1974, 262 pages.

30. ASTRONAUTIK, No 3, 1973, pp 199-204.

31. AJAA PAP, No 1143, 1972, pp 8-17.

32. AJAA PAP, No 1144, 1972, pp 6-12.

33. Baetz, J. G. "Advanced Carbon-Carbon Materials for Solid Rocket Nozzles," AJAA PAP, No 1057, 1974.

34. JOURNAL OF SPACECRAFT AND ROCKETS, No 6, 1974, pp 447-448.

35. Landsbaum, Ellis M. "Solid Motor/Spacecraft Interfaces," AJAA PAP, No 1051, 1974.

36. RAUMFAHRTFORSCHUNG, No 17, 1973, pp 225-230.

37. RAUMFAHRTFORSCHUNG, No 19, 1975, pp 27-39.

3024
CSO: 8144/1234 - END -